

Structure and Dynamics of Plumbing Systems  
of Oceanic Shield Volcanoes:  
An Example from Réunion Island

Dissertation  
zur Erlangung des Doktorgrades  
der Mathematisch-Naturwissenschaftlichen Fakultäten  
der Georg-August-Universität zu Göttingen

vorgelegt von

Ludovic Letourneur

aus Annecy (Haute-Savoie) – Frankreich

Göttingen 2008

D 7

Referentin: Jr. Prof. Dr. Sonja Philipp

Geowissenschaftliches Zentrum der Universität Göttingen

Korreferent: Prof. Dr. Agust Gudmundsson

Department of Earth Sciences, Royal Holloway, University of London

Tag der mündlichen Prüfung: 8 Juli 2008

## Acknowledgements

---

During this thesis, there have been interactions with a lot of people, and not only the co-authors of my papers, but people in Réunion, in France and in Germany. Before I started here in Germany, there have also been the people who gave me the desire to pursue a PhD.

I would like to start by acknowledging the person at the origin of this thesis, Agust Gudmundsson, who gave me the chance (and the money!!) to accomplish this work. In the first place, I must acknowledge the confidence that he has shown, by taking me on, and then, allowing a certain freedom in the way the thesis was dealt with. I am very grateful that I didn't have an overlooking supervisor. There have been discussions between us, a few disagreements, but in the end, only constructive talks. His experience in volcano-tectonics was of great value, and allowed me to extend my knowledge in this area. It was also a great benefit to have a supervisor that had not already made his own ideas about the island of Réunion, allowing fresh comments about its evolution.

I then would like to thank Sonja Philipp, with the help she provided at the end of the thesis, by taking me under her official supervision after Agust left. She has spent time and effort on this thesis for which I am thankful. She also interacted in the early part of my work by introducing me to the mysteries of numerical modelling or at least mysteries to me at that time. Your course was very helpful.

A PhD starts only by having completed your studies before. I must acknowledge the supervision of Laurent Michon during my Master in Réunion and his participation all along my thesis with helpful discussions and comparison of point of views. But he is not the only person in Réunion that must be thanked. Aline, thank you for your company in the field, discussions, data and providing a roof above my head in my first fieldtrip (congrats on your position in Paris!!). I must not forget the staff from the Observatory and its director Thomas Staudacher, for the little helicopter ride, and the fun in the field during the eruptions and the lava sampling. Thank you Anthony for welcoming me in your flat during my second fieldtrip, and with him, the other roommates and friends, Snej and Bou. Then, I wish to thank the staff from the University of Réunion, Vincent, Patrick, Franky, Olivier, Stefan, Jean-Lambert and of course, mon petit Ben, for various help in the field, and talks about work and more. Mon petit Ben, it's whenever you want that we go sampling lava bombs on the cone of a future eruption. A special thought goes to the car rental guy that gave me the best news ever on my arrival in 2006, the start of an eruption the night before. I also thank all the people that I have forgotten above and that were with me in the field, all the people that I met during my trekking/fieldwork, with a

special thought to my rasta friend and his indecent proposal... Finally, everybody on this little paradise that is Réunion is thanked.

I cannot continue without expressing my gratitude towards all the staff from the LMV in Clermont-Ferrand who managed to transmit their passion for volcanoes to a large number of people like me. A thought goes also to all students of Clermont that share a same passion: volcanoes. A special thought goes towards the Master students of 2004-2005.

I cannot also ignore the people from Göttingen, who helped at several levels. Thank to Ines with whom it was interesting to compare our respective islands, Marie-France for her help in administrative papers, even if part of it was not related to the university. Thank to Nadine for her help when I arrived in Göttingen, and thank to the whole department of structural geology.

My final thoughts go to my friends, spread around, from Clermont or elsewhere.

And of course my final thoughts go to Ruth, who shared my life for the last two years...

## Abstract

---

This study focuses on the volcano-tectonic evolution of the two main volcanoes that constitute Réunion Island. This island, located in the south-western part of the Indian Ocean, hosts two main shield volcanoes: the dormant Piton des Neiges, and the active Piton de la Fournaise. Due to the tropical climate of the island, combined with the presence of volcano-tectonic structures (caldera, landslides scarps), it is deeply eroded. This study is divided in two parts. The first part deals with the intrusive system of the eroded Piton des Neiges, the second with the relationship between the active plumbing system of Piton de la Fournaise and the deformation of the edifice. Piton des Neiges has three main rift zones, trending N30°, N120° and N160°, located in the western half of the edifice. The field data show that the rift zones evolved under different stress fields. Magma-generated stress field played a major role close to the central conduit, but its influence decreases with distance. In the N120° and N160° rift zones, the maximum compressive principal stress is vertical and controls the injection of magma. Here it is proposed that this stress field results in the repeated injection of magma along a N120° direction, that of crustal structures. By contrast, in the N30° rift zone, magma injection has been partly influenced by surface stresses leading to the injection of sills and shallow-dipping sheets. The field studies suggest that the many sill clusters in the N30° rift zone and in the Salazie cirque, are related to tough plastic breccia that acted as a mechanical barriers to dyke propagation. Despite these differences, blade-like dyke injections were common in all the three rift zones, with the denser magmas being injected at greater depths and the lighter magmas at shallower depths. The field data also indicate that the N120° rift zone generated mechanical instabilities resulting in landslides, in agreement with the common, debris avalanche deposits observed in the Cilaos and Salazie cirques.

Similar dyke-injection mechanisms were previously proposed for Piton de la Fournaise. Intrusive events in this volcano, however, are commonly accompanied by an asymmetrical pattern of ground deformation. This pattern was previously interpreted as reflecting the dip of the intrusions. However, the field results presented here suggest that the rift zones are close in style to the N120° and N160° rift zones of Piton des Neiges. The results also suggest that the deformation asymmetry is related both to a curved magma path and to the presence of stiff heterogeneities in the edifice, inherited from the past eruptive centre. It is also shown that the steep flanks of the summit cone are related to (1) the past eruptive history and (2) the concentration of deformation on the eastern side of the summit cone. This preferential deformation of the eastern side of the cone also explains the presence of tectonic fractures observed.

## **Kurzfassung**

---

Diese Arbeit beschäftigt sich vor allem mit der vulkanotektonischen Entwicklung der beiden Vulkane, die La Réunion aufbauen. Diese Insel liegt im südwestlichen Indischen Ozean und beherbergt zwei große Schildvulkane: den erloschenen Piton des Neiges sowie den aktiven Piton de la Fournaise. Wegen der Verbindung des tropischen Klimas der Insel und vulkanotektonischen Strukturen (Caldera, Rutschungsflächen), ist die Morphologie tief erodiert. Basierend auf den beiden Vulkanen wurden in dieser Arbeit zwei Themen bearbeitet, die auch diese Dissertation in zwei Teile gliedern: der erste Teil beschäftigt sich mit der Untersuchung des intrusiven Systems des erodierten Piton des Neiges, der zweite mit der Beziehung zwischen dem aktiven Vulkansystem des Piton de la Fournaise und der Deformation dessen Vulkangebäudes.

Piton des Neiges weist im westlichen Teil des Vulkangebäudes drei große Riftstrukturen auf, die  $30^\circ$ ,  $120^\circ$  und  $160^\circ$  streichen. Geländebeobachtungen zeigen, dass diese Riftzonen sich in verschiedenen Spannungsfeldern entwickelt haben. Das durch Magma hervorgerufene Spannungsfeld spielte in der Nähe des zentralen Förderkanals eine große Rolle, sein Einfluss nimmt jedoch mit der Entfernung ab. In den  $120^\circ$ - und  $160^\circ$ -streichenden Riftzonen ist die maximale Hauptnormalspannung vertikal orientiert und kontrolliert die Magmeninjektion. Hier wird vorgeschlagen, dass dieses Spannungsfeld durch die wiederholte Magmeninjektion entlang der  $120^\circ$ -Richtung krustaler Strukturen hervorgerufen wird. Im Gegensatz dazu wurde die Magmeninjektion in der  $30^\circ$  Riftzone teilweise von oberflächennahen Spannungen beeinflusst, die zur Injektion von Lagergängen und flacheinfallenden Gängen führte. Die Geländebeobachtungen lassen vermuten, dass viele Lagerganghäufungen in der  $30^\circ$ -Riftzone und dem Salazie Cirque mit zähen plastischen Brekzien zusammenhängen, die als mechanische Barrieren für die Gangausbreitung fungierten. Trotz dieser Unterschiede treten messerschneidenartige Ganginjektionen in allen drei Riftzonen häufig auf, wobei die dichteren Magmen in größerer Tiefe injiziert wurden, die leichteren in geringerer Tiefe. Die Geländedaten weisen ebenso darauf hin, dass die  $120^\circ$ -Riftzone zu mechanischen Instabilitäten führte, die Rutschungen hervorrufen, wie beispielsweise die Schuttlawinenablagerungen im Cilaos und Salazie Cirques.

Ähnliche Ganginjektionsmechanismen wurden bereits für Piton de la Fournaise vorgeschlagen. Intrusive Ereignisse in diesem Vulkan werden jedoch normalerweise von einer asymmetrischen Verteilung der Landdeformation begleitet. Diese Verteilung wurde bisher so gedeutet, dass sie

das Einfallen der Intrusionen widerspiegelt. Die Geländeergebnisse dieser Arbeit weisen jedoch darauf hin, dass die Riftzonen in ihrem Aufbau denen der 120°- und 160°-streichenden Riftzonen des Piton des Neiges ähneln. Die Ergebnisse weisen auch darauf hin, dass die Asymmetrie der Deformation sowohl mit einem bogenförmigen Magmenaufstiegsweg sowie der Existenz steifer Heterogenitäten im Vulkangebäude, die noch vom früheren eruptiven Zentrum resultieren, in Zusammenhang stehen. Es wird ebenso gezeigt, dass die steilen Flanken des Gipfelkegels zum einen mit der früheren eruptiven Geschichte, zum anderen mit der Konzentration der Deformation auf der Ostseite des Gipfelkegels zusammenhängen. Diese bevorzugte Deformation der Ostseite des Kegels erklärt auch die Existenz der beobachteten tektonischen Brüche.

*Table of Contents*



---

<b>GENERAL INTRODUCTION</b>	<b>- 1 -</b>
<i>1 Structure and Dynamics of Shield Volcanoes: A Review</i>	<i>- 4 -</i>
<b>1.1 Different types of volcanism</b>	<b>- 6 -</b>
<b>1.2 Intra-oceanic volcanism</b>	<b>- 7 -</b>
<b>1.3 Structure and Dynamics of oceanic-shield volcanoes</b>	<b>- 11 -</b>
1.3.1 Organisation of the feeding system	- 11 -
1.3.2 Origin of dykes and sills: mechanisms of magma injection	- 12 -
1.3.3 Origin of rift zones	- 14 -
1.3.4 Deformation of volcanoes	- 15 -
<b>1.4 The modelling tool: a short introduction to numerical modelling</b>	<b>- 16 -</b>
<i>2 The Island of Réunion</i>	<i>- 18 -</i>
<b>2.1 Geodynamics</b>	<b>- 20 -</b>
<b>2.2 Volcanism of La Réunion</b>	<b>- 22 -</b>
2.2.1 Piton des Neiges	- 24 -
2.2.2 Piton de la Fournaise	- 27 -
2.2.2.1 General evolution	- 27 -
2.2.2.2 The origin of the volcano-tectonic events	- 28 -
2.2.2.3 The recent dynamics – insights on the plumbing system	- 29 -
<b>2.3 What geophysics tell us: insights on the internal structure of the Island</b>	<b>- 30 -</b>
2.3.1 Seismic data	- 30 -
2.3.2 Magnetic data	- 31 -
2.3.3 Gravimetric data	- 32 -
2.3.4 Electrical data	- 33 -
<i>3 Structure and Dynamics of an Oceanic Shield: the example of Piton des Neiges</i>	<i>- 34 -</i>
<b>3.1 Introduction</b>	<b>- 36 -</b>
<b>3.2 Structure and dynamics of Piton des Neiges volcano: Paper 1</b>	<b>- 36 -</b>
3.2.1 Introduction	- 37 -
3.2.2 Geological context	- 39 -

---

3.2.3	The structure of Piton des Neiges intrusive system	- 41 -
3.2.4	Dynamics of Piton des Neiges intrusive system	- 46 -
3.2.5	Comparison with Piton de la Fournaise	- 50 -
3.2.6	Conclusions	- 51 -
<b>3.3</b>	<b>A specific aspect of Piton des Neiges structure: the occurrence of sills: Paper 2</b>	<b>- 52 -</b>
3.3.1	Introduction	- 54 -
3.3.2	Geological context	- 55 -
3.3.3	Field data	- 57 -
3.3.4	Origin of sills	- 62 -
3.3.4.1	<i>Mechanics of fluid-filled fractures</i>	- 62 -
3.3.4.2	<i>Models for the origin of sills</i>	- 64 -
3.3.5	Discussion	- 68 -
3.3.6	Conclusions	- 71 -
<b>3.4</b>	<b>Sills at Piton de la Fournaise</b>	<b>- 72 -</b>
<b>3.5</b>	<b>Summary and conclusions</b>	<b>- 75 -</b>
<b>4</b>	<b><i>Growth and Deformation: Relationship with the Rift zones</i></b>	<b>- 77 -</b>

---

<b>4.1</b>	<b>Introduction</b>	<b>- 79 -</b>
<b>4.2</b>	<b>Influence of heterogeneities on the deformation: Paper 3</b>	<b>- 79 -</b>
4.2.1	Introduction	- 80 -
4.2.2	Geological settings	- 82 -
4.2.3	Field results	- 85 -
4.2.3.1	<i>General description</i>	- 85 -
4.2.3.2	<i>Dyke studies</i>	- 86 -
4.2.3.3	<i>Application to the recent activity</i>	- 87 -
4.2.4	Modelling	- 90 -
4.2.4.1	<i>Influence of the superficial fracturing</i>	- 90 -
4.2.4.2	<i>Influence of the rift zone system</i>	- 92 -
4.2.5	Discussion	- 93 -
4.2.5.1	<i>A complex plumbing system</i>	- 93 -
4.2.5.2	<i>Rift zone, fractures and structural control</i>	- 96 -
4.2.5.3	<i>Influence of rift system on deformation</i>	- 98 -

4.2.6	Conclusions	- 99 -
4.2.7	Lava pile characterisation	- 101 -
<b>4.3</b>	<b>Growth and deformation of Piton de la Fournaise summit cone: Paper 4</b>	<b>- 101 -</b>
4.3.1	Introduction	- 102 -
4.3.2	Morphology and inner structure of the central cone of PdF	- 104 -
4.3.3	Fractures of the central cone	- 109 -
4.3.4	Co-intrusive deformation	- 114 -
4.3.4.1	<i>Types of eruptions and the related magmatic paths</i>	- 114 -
4.3.4.2	<i>The co-intrusive displacements inferred from GPS</i>	- 114 -
4.3.5	Discussion	- 117 -
4.3.5.1	<i>Origin of the general steep slopes of the central cone</i>	- 117 -
4.3.5.2	<i>Tectonic structures, co-intrusive deformation and rift zones</i>	- 118 -
4.3.6	Conclusion	- 123 -
<b>4.4</b>	<b>Conclusions</b>	<b>- 124 -</b>
<b>5</b>	<b>General conclusions</b>	<b>- 125 -</b>
<hr/>		
	<b>BIBLIOGRAPHY</b>	<b>- 129 -</b>

Figure 1.1-1: Map of the main hot spots, and the main on-land active volcanic areas.	- 6 -
Figure 1.2-1: Topographic profiles for two stratovolcanoes and a shield volcano,	- 8 -
Figure 1.2-2: Model of evolution for a Hawaiian shield volcano.	- 9 -
Figure 1.2-3: Digital Elevation Model (DEM) of the Galapagos and of Hawaii.	- 10 -
Figure 1.3-1: Schematic representation of the three principal modes of fractures.	- 12 -
Figure 1.3-2: Models for the origin of rift zones in oceanic shield volcanoes.	- 15 -
Figure 2.1-1: Surface representation of the south-western part of the Indian Ocean.	- 21 -
Figure 2.1-2: Structure of the oceanic crust in the surroundings of Réunion Island.	- 21 -
Figure 2.1-3: Trace of the Réunion Hot Spot.	- 21 -
Figure 2.2-1: The Island of Réunion.	- 22 -
Figure 2.2-2: Map of the debris avalanche deposits on the flanks of Réunion Island.	- 23 -
Figure 2.2-3: Geological map of Réunion Island (modified from Nehlig et al., 2006).	- 24 -
Figure 2.2-4: Chronology of the subaerial activity of Piton des Neiges	- 26 -
Figure 2.2-5: Magmatic feeding system of Piton de la Fournaise.	- 28 -
Figure 2.2-6: Duration of the eruptions since 1981.	- 29 -
Figure 2.2-7: Volume and cumulative volume emitted during the eruptions since 1972.	- 29 -
Figure 2.3-1: 2-D P velocity section along a SW-NE profile across the island of Réunion.	- 31 -
Figure 2.3-2: Maps of magnetic anomalies.	- 32 -
Figure 2.3-3: Bouguer anomaly maps of Réunion.	- 33 -
Figure 3.2-1: Location of Réunion Island in the Indian Ocean.	- 39 -
Figure 3.2-2: Dip, thickness and strike of all measured intrusions in Piton des Neiges.	- 41 -
Figure 3.2-3: Strike distribution of intrusions within each cirque.	- 42 -
Figure 3.2-4: Dip, thickness and distance of intrusions in Cilaos.	- 43 -
Figure 3.2-5: Dip, thickness and distance of intrusions in Mafate.	- 44 -
Figure 3.2-6: Lithology abundance in the various rift zones of Cilaos and Mafate.	- 45 -
Figure 3.2-7: Strike distribution within the Cilaos cirque.	- 45 -
Figure 3.2-8: Relationship between intrusion characteristics in Cilaos.	- 46 -
Figure 3.2-9: Strike distribution within the Mafate cirque.	- 48 -
Figure 3.2-10: Dip of intrusions in a transect perpendicular to the N120 rift zone.	- 48 -
Figure 3.2-11: Relationship between intrusion characteristics in Mafate.	- 49 -
Figure 3.3-1: DEM of the submarine and subaerial part of Réunion Island.	- 55 -
Figure 3.3-2: Location of measured intrusions (triangle), and area studied (line).	- 56 -
Figure 3.3-3: Histograms for dip, thicknesses and distance of dykes and sills.	- 57 -
Figure 3.3-4: Strike distribution for dykes and sills.	- 58 -
Figure 3.3-5: Example of dykes within the preferential intrusion path in Mafate.	- 59 -
Figure 3.3-6: Strike of sills with dip $< 15^\circ$ and $> 15^\circ$ in Cilaos and Mafate.	- 59 -
Figure 3.3-7: Example of scattered sills within the lava pile.	- 60 -
Figure 3.3-8: Example of a sill cluster intruded at a contact below a breccia unit.	- 61 -
Figure 3.3-9: Close up photograph of a sill cluster in Cilaos in the axis of the rift zone.	- 62 -
Figure 3.3-10: Evolution of overpressure in a vertical dyke, for 3 different magmas.	- 65 -
Figure 3.3-11: $\sigma_3$ values induced by an overpressure of 5 MPa in a propagating dyke.	- 66 -
Figure 3.3-12: $\sigma_3$ values induced by an overpressure of 5 MPa in a propagating dyke.	- 67 -
Figure 3.3-13: Overpressure in a vertical dyke in a homogeneous medium.	- 68 -
Figure 3.4-1: Sill intruded in the northern cliff of Bory pit-crater.	- 73 -
Figure 3.4-2: Example of a sill intruding at a contact.	- 74 -

Figure 3.4-3: Laccolith intruded in the cliff surrounding of the Enclos Fouqué caldera.	- 75 -
Figure 4.2-1: (A) Location of Réunion Island, (B) main volcanoes of the island, (C) and main structures of Piton de la Fournaise.	- 83 -
Figure 4.2-2: Eruptive fissures and cones visible on aerial photographs from August 2003	- 84 -
Figure 4.2-3: Cumulative displacements recorded from September 2004 to January 2006.	- 84 -
Figure 4.2-4: Location of the study areas.	- 85 -
Figure 4.2-5: Photograph of the internal structure of the northern branch of the rift zone.	- 86 -
Figure 4.2-6: Strike direction and pole plot of dykes in the Bellecombe scarp and Plaine des Osmondes.	- 87 -
Figure 4.2-7: Histogram of dip distribution for the Bellecombe scarp and the NE rift zone.	- 87 -
Figure 4.2-8: Eruptive fissures since 1998.	- 88 -
Figure 4.2-9: Gravity-generated state of stress within the volcano.	- 89 -
Figure 4.2-10: Comparison of the deformation induced by a vertical dyke.	- 91 -
Figure 4.2-11: Location of the rift zone within the model (dashed line), and limit of the computed area (thin black line) using Ansys.	- 92 -
Figure 4.2-12: Models for the injection of a planar dyke in a homogeneous medium.	- 93 -
Figure 4.2-13: Deformation resulting from the injection of dykes along the rift zones.	- 94 -
Figure 4.2-14: Models considering the overpressure in a shallow magma chamber.	- 95 -
Figure 4.2-15: A) Location of the April 1977 and the post-1997 eruptive fissures.	- 95 -
Figure 4.2-16: Schematic representation of the plumbing system of Piton de la Fournaise.	- 97 -
Figure 4.2-17: Characteristic lava piles in Piton de la Fournaise	- 101 -
Figure 4.3-1: Slope maps of characteristic shield volcanoes.	- 104 -
Figure 4.3-2: 25 m step Digital Elevation Model of Piton de la Fournaise.	- 105 -
Figure 4.3-3: a- Slope map of the central cone calculated from the 25 m step DEM.	- 107 -
Figure 4.3-4: Panoramas and interpretations of the scarps of the April 2007 caldera.	- 108 -
Figure 4.3-5: Distribution of the eruptive fissures.	- 110 -
Figure 4.3-6: Picture of the concentric fractures and of the flank fractures.	- 111 -
Figure 4.3-7: Spatial distribution of the flank fractures.	- 113 -
Table 4.3-1: Displacements measured by GPS.	- 115 -
Figure 4.3-8: Horizontal and vertical co-intrusive displacements recorded by GPS.	- 116 -
Figure 4.3-9: Synthesis of the co-intrusive deformation related to summit and proximal intrusions.	- 120 -
Figure 4.3-10: Interpretation of the short, narrow N120° rift zone.	- 122 -

## *General Introduction*

The mechanisms of magma injection are a key to the understanding of volcanic eruptions. Eruptions correspond to the arrival at the surface of magma that has often been stored in a shallow magma chamber. However, magmatic injections do not always intrude into a volcanic edifice in similar ways. As magma injections are ruled by the state of stress within the volcano, they mark the regional extensive direction of the stress field.

In oceanic shield volcanoes, descriptions of plumbing systems include various examples from the Canary Islands (Marinoni and Gudmundsson, 2000; Fernández et al., 2002; Ancochea et al., 2003), the Samoan Islands (Walker and Eyre, 1995), Hawaii (Walker, 1987), and Madeira (Schwarz et al., 2005), to name a few. These studies give insights on the internal structure of the respective volcanoes, the evolution of the edifice and an overview of the stress field. They commonly show that shield volcanoes are organised along rift zones, which represent the places of maximum extension within the volcano, and can find their origins in several processes (Carracedo, 1994; Walter et al., 2006).

In Réunion, the set up of the island offers an exceptional opportunity to study both the dormant and the active volcanoes located on the island. Rapid erosion has uncovered the deepest structures of the dormant volcano, Piton des Neiges, while volcano-tectonic events at Piton de la Fournaise cut across the past rift zones, offering an overview of their internal structure. Despite these conditions of observation, no extensive structural studies have been undertaken in the recent years, and results of previous ones on Piton des Neiges appear discordant with one another (Chevallier, 1979; Maillot, 1999). At Piton de la Fournaise, recent eruptions have cleared parts of the scarp of the most recent volcano-tectonic event, along the axis of one of the rift zones. More recently, the collapse of Dolomieu pit-crater offers an overview of the upper 300 metres of the central part of the plumbing system.

The first part of this study has been focused on Piton des Neiges volcano, using mostly field work and numerical modelling, it aims to:

- Propose a model for the dynamics of the intrusive system
- Find an appropriate model for the origin of sills
- Hypothesise the origin of the intrusive system according to the evolution observed in the field

The second part of this study aims at answering or providing information on:

- The origin of the morphology of the cone
- The process of deformation of the summit cone
- The internal structure and dynamics of Piton de la Fournaise rift system
- The origin of the systematic asymmetric deformation observed.

This work is here presented as a compilation of four papers. At the time of writing, one paper is published (Letourneur et al., 2008; Section 4.2), one is accepted with minor revisions (Michon et al., in press; Section 4.3) and two have been accepted with major revisions in the *Journal of Volcanology and Geothermal Research* (Letourneur and Gudmundsson, Section 3.2 and Letourneur et al., Section 3.3).



*1 Structure and Dynamics of Shield Volcanoes:  
A Review*

---

## **Objectives:**

- Summarise the knowledge gathered on the processes of construction of shield volcanoes as well as their structure.
  
- Provide basic information on the understanding of mechanisms of magma injection.
  
- Introduce the methods of numerical modelling used in this thesis.

## 1.1 Different types of volcanism

Active volcanoes are spread over the continents and the oceans. It has long been identified that volcanoes are usually gathered along specific features. For example, most of the volcanism is not observable, occurring at the bottom of the oceans, along oceanic ridges, that constitute a long relief along which sea-floor spreading occurs (Francis, 1993). One exception to that is Iceland, where the oceanic ridge is superimposed on a mantle plume. Other concentrations of volcanoes exist, and are more spectacular due to (1) their activity on-land and (2) their eruptive processes mostly characterised by explosive activity. These are the volcanoes of active margins, where the oceanic crust is recycled into the mantle (*Figure 1.1-1*).

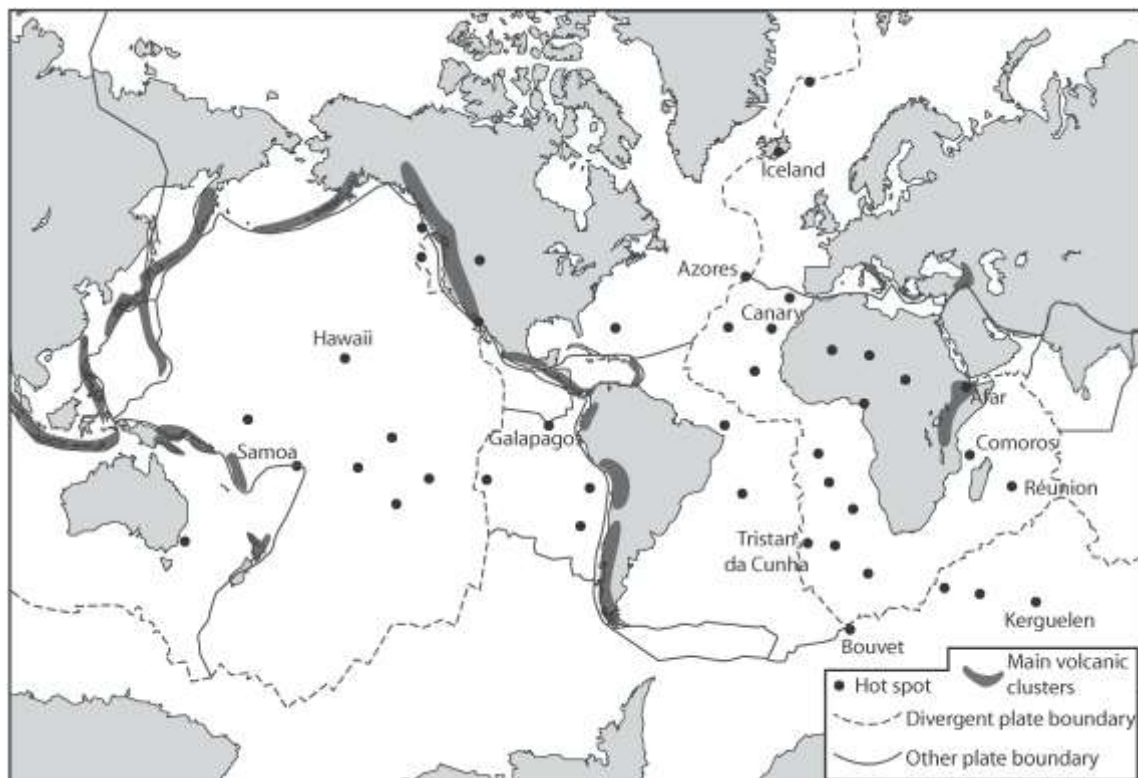


**Figure 1.1-1: Map of the main hot spots, and the main on-land active volcanic areas (modified after Duncan and Richards, 1991 and Global Volcanism Program website: [www.volcano.si.edu](http://www.volcano.si.edu)).**

However, to be complete, we need to add a third type of volcanism, located in intra-plate domains; either continental or oceanic (*Figure 1.1-1*). They form stand-alone volcanoes in areas where volcanism is not expected. They can be classified into various categories:

- Continental hot spots, mostly located in Africa, that occur as a result of the stability of the plate over the plume.
- Continental rifting, such as the East African Rift, which is partly linked with the activity of a large mantle plume (active rift in the north), combined with the extension of the lithosphere (passive rift in the south).

- Continental flood basalts and oceanic plateaus, which correspond to the emergence of the mantle plume head at the surface, creating a large amount of magma in a ‘short’ period of time.
- Intra-oceanic hot spots which are the expression of the tail of a mantle plume, under a thin oceanic crust.

## 1.2 Intra-oceanic volcanism

Intra-oceanic volcanoes are often characterised by shallow slopes that lead people to refer to them as shield volcanoes, due to their resemblance to warrior shields. The term shield was used to describe the monogenetic shallow-sloped volcano, resulting from a long-lived eruption, commonly found in Iceland and in some continental flood basalt provinces. More recently, the term has been used to describe all volcanoes with a shallow slope (usually  $< 10^\circ$ , locally reaching higher values), and mostly issued from the accumulation of fluid lava flows. This is in opposition to stratovolcanoes and scoria cones that have much steeper slopes (*Figure 1.2-1*), and result from the accumulation of pyroclastic deposits as well as lava flows. It appears that most of the shield volcanoes are located in intra-oceanic domain, and are related to mantle plumes. Due to the displacement of the oceanic plate over the supposedly fixed mantle plume, we usually observe chains of seamounts or islands, such as the Emperor – Hawaii chain.

The ascent of a large quantity of hot material (the definition of a mantle plume) in the upper part of the mantle leads to the creation, mostly by adiabatic decompression, of a large amount of magma. This magma is either intruded through the crust and can subsequently be erupted or stored at shallower level; or alternatively accumulated at the mantle-crust interface, creating underplating (Wolfe et al., 1994; Bonneville et al., 1997; Charvis et al., 1999; Gallart et al., 1999; Klugel et al., 2005). However, each mantle plume is different, and the amount of magma produced varies from one another. The general characteristics of these magmas are that they are poor in gas content and are tholeiitic or alkalic (Best, 2002). These variations reflect the origin of the material submitted to fusion (depleted mantle corresponding to the upper mantle material or enriched mantle, brought by the mantle plume, of a deeper origin), as well as the degree of fusion depending on the position in relation to the hot spot (Watson and McKenzie, 1991).

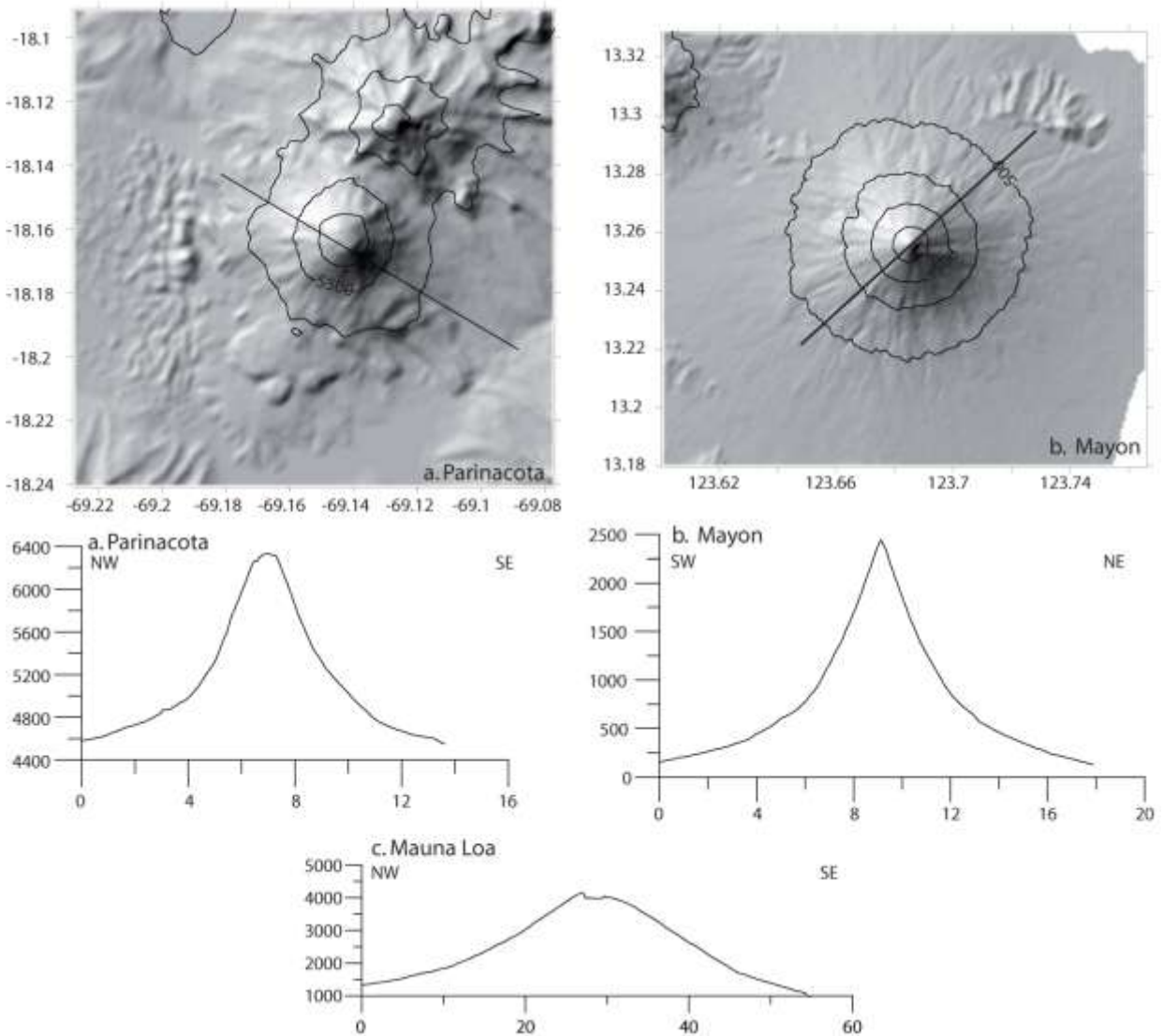


**Figure 1.2-1: Topographic profiles for two stratovolcanoes, a. Parinacota and b. Mayon; and comparison with a shield volcano, c. Mauna Loa.** Heights on the profiles are in metres, distances in kilometres. See Figure 1.2-3 for the location of the profile of Mauna Loa. Digital Elevation Model (DEM) from the SRTM mission (Jarvis et al., 2006). Geographic coordinates on the DEM.

Due to both the temperatures of the magmas, and their composition, magmas emitted are usually fluid. However, with the evolution of the edifice, magma may get trapped in shallow magma chambers (Pinel and Jaupart, 2000; 2004), and evolve as suggested by the appearance of more differentiated terms, and the increased proportion of explosive deposits in the latter stage of activity (e.g. Deniel et al., 1992; Huertas et al., 2002). The amount of lava emitted can be in the order of several hundreds to thousands of km<sup>3</sup>. The larger shields emerge above the sea level to create islands such as the Hawaiian archipelago, Réunion, and Galapagos archipelago. Their evolution has been described, and a general model, based on the evolution of Hawaii, is commonly accepted, with submarine and subaerial stage of growth (Figure 1.2-2).

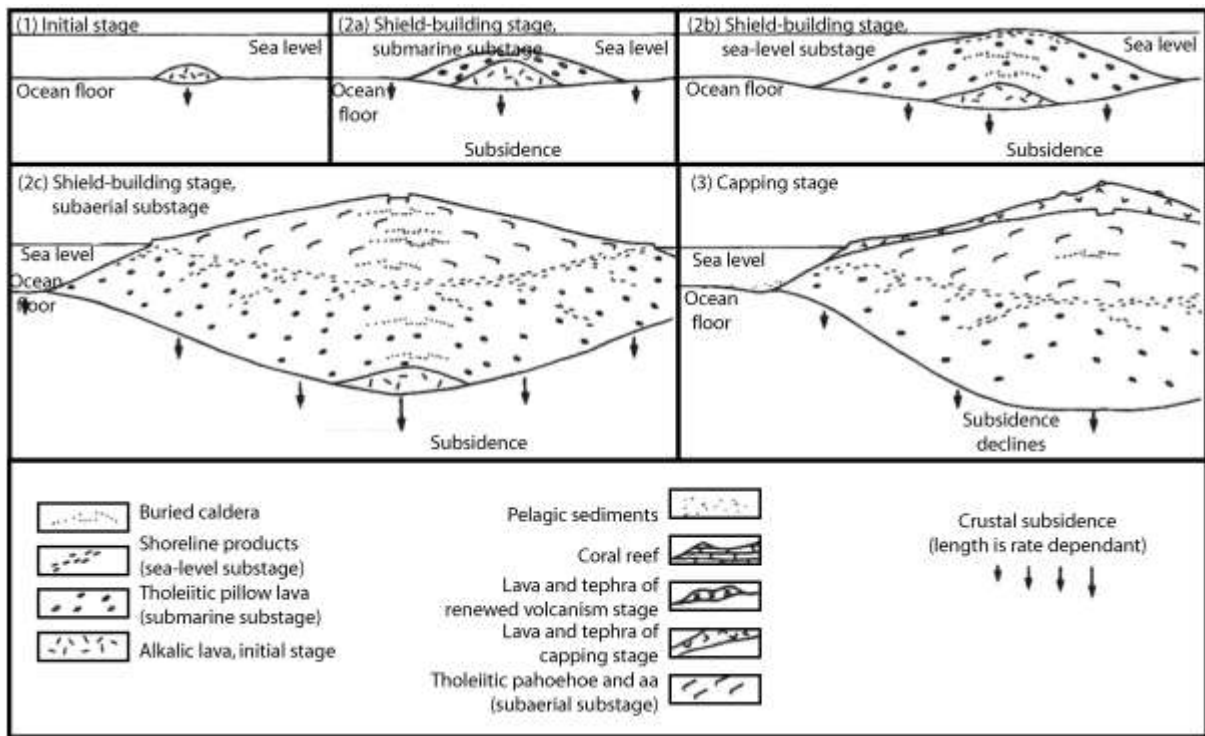


**Figure 1.2-2: Model of evolution for a Hawaiian shield volcano.** The capping stage is the latest stage observed in Réunion, later stages are not shown here (modified from Peterson and Moore, 1987).

However, despite this common evolution, each island, or more specifically, each volcano presents its own morphology. For example, the shields in the Hawaiian archipelago usually display a ridge-like shape, affected or not by summit collapsed calderas (*Figure 1.2-3*). By comparison, the shields from the Galapagos present sub-circular shapes, with steep slopes and flat tops, their summit areas being usually affected by collapsed calderas. As suggested in *Figure 1.2-3*, the calderas observed are dissimilar in the Galapagos and Hawaii. The former is characterised by deep calderas, rather large in comparison to the size of the edifice, while the latter present shallow, coalesced calderas, rather small in comparison to the edifice. In Hawaii, pit-craters are also common in both the summit area and along the rift zones, a feature that is absent in the Galapagos.

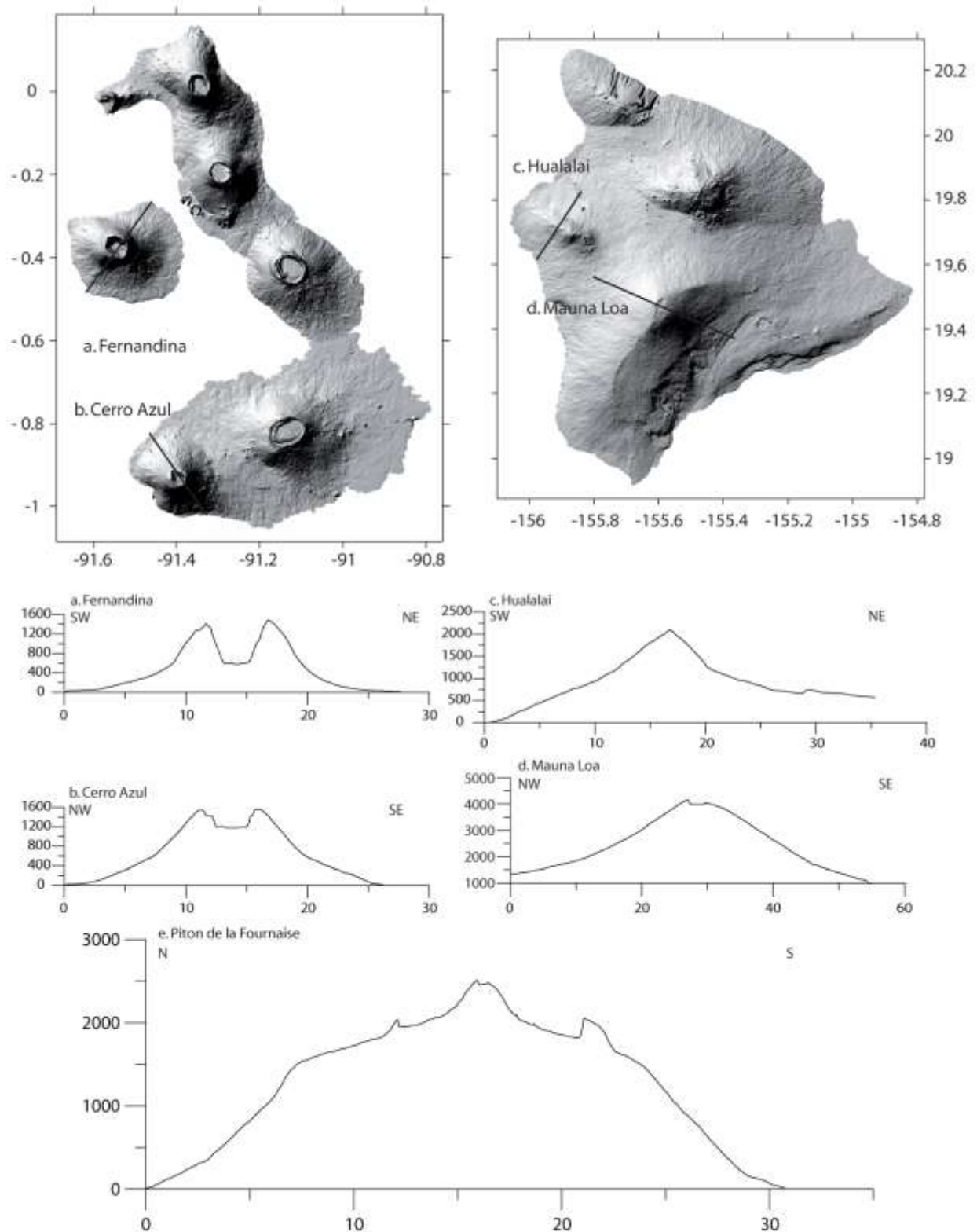


**Figure 1.2-3: Digital Elevation Model (DEM) of the western islands of the Galapagos archipelago (a, b) and of Hawaii (c, d).** The lines correspond to the profiles presented below. In addition there is a N-S profile of Piton de la Fournaise (Réunion Island, e) for comparison. Heights are in metres while the horizontal distances are in kilometres. DEM in geographic coordinates – decimal degrees. DEM from SRTM mission, geographic coordinates (Jarvis et al., 2006).

Other processes act to modify the shape of volcanoes. It has been discovered that the growth of such edifices is often interrupted by processes of dismantlement (Moore et al., 1989; 1994).

This is a gravity-related process, and corresponds to the slow spreading of the flank of a volcano over the sea floor (known as slumps, the best example being the Hilina slump on Hawaii) (Smith et al., 1999; Okubo, 2004), or the fast dismantlement of a flank of the edifice under horizontal pressure applied in the inner part of the volcano, such as repeated dyke injection along a rift zone (e.g. McGuire et al., 1990; Elsworth and Voight, 1995; Carracedo, 1999; Elsworth and Day, 1999). Most of the time, the two processes are related, the flank collapse or debris avalanche concluding a period of flank spreading. Usually, weak cohesion planes tend to favour these events (Oehler et al., 2005). Mapping around the major oceanic islands has shown that these processes can be repeated over time, and constitute the major hazard at the scale of the island and the oceanic basin (Moore et al., 1989; Carracedo, 1999; Carracedo et al., 1999a; Carracedo et al., 1999b; Oehler et al., 2004; Oehler, 2005).

### **1.3 Structure and Dynamics of oceanic-shield volcanoes**

#### **1.3.1 Organisation of the feeding system**

An eruption implies that an amount of magma, usually stored at shallow or intermediate depth, reaches the surface. Stratovolcanoes are usually characterised by summit eruptions (e.g. Merapi, Mayon, Pinatubo, Unzen), associated with a sub-vertical conduit. However, on shield volcanoes, eruptions are more often than not characterised by fissure eruptions that may or may not open at the summit of the volcano (e.g. Dvorak and Okamura, 1985; Froger et al., 2004). These eruptive fissures are related to elongated feeding structures, i.e. dykes that can propagate significant distances from their point of origin, as suggested by the extent of eruptive fissures. The systematic mapping of eruptive vents reveals the organisation along preferential, linear or curved, structures named rift zones. They are characterised by a combination of dry extension fractures and eruptive fissures, spatter and scoria cones, and also pit-craters. They present a wide range of lengths and widths, in relation with the type of volcanic edifice (Walker, 1992). Rift zones, as preferential sites for eruptions, constitute specific reliefs on a volcano and can affect its morphology. For example, some volcanoes in Hawaii display a ridge-like morphology (*Figure 1.2-3*), the crest being the area of maximum vent density, marking the emplacement of the rift zone axis. Inversely, shields in the Galapagos, with their sub-circular shapes, are characterised by a combination of radial rift zones and circumferential eruptive fissures in the summit area (Chadwick and Howard, 1991).

At depth, rift zones correspond to intrusive sheet complexes. The density of these swarms can vary from only few percent of dykes, to up to 60-70% of dykes. Such variations depend mostly on the tectonic settings and the intrusive rates. Studies of intrusive swarms reveal the



common occurrence of dykes, sills being less common (Walker, 1987; Walker and Eyre, 1995; Marinoni and Gudmundsson, 2000; Marinoni, 2001). Studies in well exposed edifices have shown that dyke swarms usually display a ‘wedge structure’, the rift zones narrowing both upward and downrift (Walker, 1992).

### 1.3.2 Origin of dykes and sills: mechanisms of magma injection

Magma is transported through fractures usually opened under the magma pressure. As such, they usually correspond to mode I fractures (*Figure 1.3-1*), with pure opening and without any shear components. However, in some cases, shear can be present leading to a mix-mode fractures (Rubin, 1995).

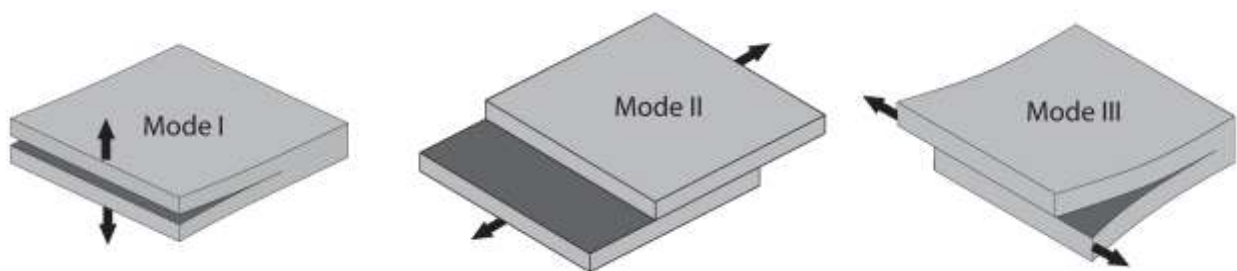


**Figure 1.3-1: Schematic representation of the three principal modes of fractures.** *Black arrows indicate direction of opening.*

In order to propagate, the magma must be able to fracture the host rocks, and inject into the newly created fracture. Two main models for fracture mechanics have been developed, and consider two different aspects. The first model, using the notion of fracture toughness, based on the theory of *linear elastic fracture mechanics* (Lawn and Wilshaw, 1975; Kanninen and Popelar, 1986), has been developed by combining two ideas, the first idea based on thermodynamics (Griffith, 1920; 1924); the second idea is based on the notion of *stress intensity factors* (Irwin, 1958). The first idea states that, for a pre-existing crack under tension, the growth of a crack will only be possible if the total energy in the rock decreases with the growth of the crack (a system tends to reach the state of lower energy). The total energy is dependent on the elastic strain energy, the surface energy of the crack and the gravitational potential of the rock. The Griffith criterion can be written as (Griffith, 1920; 1924):

$$T = \sqrt{\frac{2\gamma E}{\pi l}} \quad (1)$$

Here,  $T$  is the tensile stress applied to the system,  $\gamma$  the surface energy per unit area,  $E$  is the Young's modulus of the rock, and  $l$  is the initial half-length of the crack. This criterion is combined with the notion of stress intensity factor (Irwin, 1958), that studies the state of stress in the vicinity of a crack tip. It can be written as:

$$K_I = T\sqrt{\pi l} \quad (2)$$

Here  $K_I$  is the stress intensity factor for mode I fractures,  $T$  is the tensile stress applied (in the case of a fluid filled fracture, it corresponds to the overpressure within the fracture), and  $l$  is the half length of the crack (in the case of a blade-like dyke, its half height).

The *linear elastic fracture mechanics* theory (Lawn and Wilshaw, 1975; Kanninen and Popelar, 1986) states that a critical stress intensity factor or a critical energy release rate is required in order for the fracture to propagate:

$$K_{Ic} = \sqrt{2\gamma E}; G_c = \frac{K_{Ic}^2}{E} = 2\gamma \quad (3)$$

Typical values for  $K_{Ic}$  for basalts or intrusive rocks, in the brittle domain, are in the range of 1-3 MPa m<sup>-1/2</sup> (Pollard and Fletcher, 2005). However, these values are much higher in plastic material, due to the energy necessary to accommodate plastic deformation (Ashby and Jones, 1998), such as shale, in the range of 30-100 MPa m<sup>-1/2</sup> (Delaney and Pollard, 1981).

The second model, based on the work of Griffith (1924), and using a critical stress, rather than a critical energy, as criterion for crack propagation can be used. It proposes that the magma pressure must be sufficient, reaching a critical value, above which the fluid-filled crack will propagate (Anderson, 1937):

$$p = \sigma_3 + T_0 \quad (4)$$

Here  $p$  is the total magmatic pressure,  $T_0$  the tensile stress of the host rock and  $\sigma_3$  the minimum principal compressive stress. The propagation of magma will depend on the local stress field, as the crack will open perpendicularly to  $\sigma_3$ . In the case of a volcanic edifice associated with a magma chamber, the total pressure of magma corresponds to at least the burden of the column of overlying rocks (of height  $h = \rho gh$ ), usually associated with an excess pressure  $P_e$  in the magma chamber (e.g. input of magma, fractional crystallisation). Once the pressure reaches the critical value, a crack initiates and the magma starts its propagation. Two cases can be established, (1) for a vertical propagation suggesting that  $\sigma_1$  (maximum principal compressive stress) is vertical and  $\sigma_3$  horizontal, and (2) for a horizontal propagation suggesting that  $\sigma_1$  is horizontal and  $\sigma_3$  vertical. The driving pressure,  $\Delta P$ , of the magma, that is the difference between the magma pressure and the stress applied perpendicularly to the margin of the intrusion, must equal the tensile strength of the rock in order for the dyke to propagate. It can be expressed as a function of the stress difference  $\sigma_d$  ( $\sigma_1 - \sigma_3$ ), the buoyancy of the magma, and the magma chamber excess pressure, as follows:

$$\Delta P = \sigma_d + P_e + (\rho_r - \rho_m)gh_d > T_0 \quad (5)$$

Here,  $h_d$  is the height of the dyke above the magma chamber,  $\rho_r$  and  $\rho_m$  the density of the host rock and the magma, respectively, and  $g$  the gravitational acceleration.

These two models present each interesting aspects, the first, with the aspect of plasticity and fracture propagation through plastic material, the second relating directly the magmatic pressure, tensile strength and crack propagation. In any case, propagation of magma will be, at a large scale, ruled by the stress field within the edifice, which is ruled by the gravitational stress field, the magmatic stress field, and in some cases the tectonic stress field. In most of the cases, the result is a vertical or lateral propagation of magma that leads to dykes. However, as suggested by the notion of fracture toughness, magma might be influenced in its propagation by heterogeneities such as contacts that present low to null toughness (Rubin and Pollard, 1987).

### 1.3.3 Origin of rift zones

As shown in the previous section, magma propagation is linked with the stress field, and magma will preferentially inject in a domain where there is the highest relative tension (the lowest  $\sigma_3$ ). The existence of rift zones indicates the existence of a heterogeneous stress field within a volcanic edifice. The variation of shapes (width and length) (Walker, 1999) indicates a variation of the extension of these heterogeneities. A narrow rift zone suggests that the favourable stress field is concentrated along a narrow linear feature, while a broad rift zone suggests a diffused stress field. These differences are usually a result of the origin of the rift zone.

Several origins have been identified as to why rift zones exist in an oceanic context (*Figure 1.3-2*):

- The existence of a regional extensive stress. An example of this is Iceland, located on top of the Mid-Atlantic ridge. This case is limited to the proximity of an oceanic ridge, or an active rift (e.g. Carracedo, 1994).
- Presence of tectonic features on the oceanic plate favours the ascent of magma through the crust and the subsequent creation of a rift zone. Transform faults are among these tectonic features that can efficiently control the magma, leading to the creation of elongated islands (e.g. Azores) (e.g. Carracedo, 1994).
- The superposition of volcanic edifices leads to instabilities within the overlying volcano. In this case, the gravitational instability favours extension and the injection of magma. Examples include Kilauea and several of the Hawaiian volcanoes (e.g. Walter et al., 2006).
- The pressure applied to the crust by the plume, in a homogeneous crust leads to the creation of a tri-axial rift zone with branches at  $120^\circ$  from each other (e.g. Carracedo, 1994).

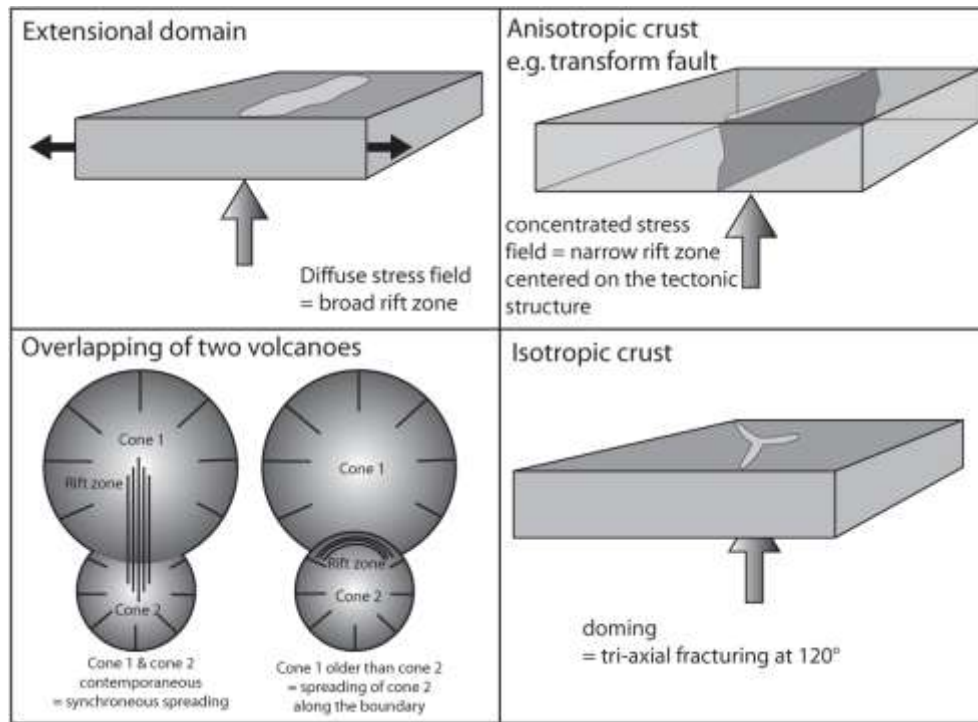


**Figure 1.3-2: Models for the origin of rift zones in oceanic shield volcanoes (after Carracedo, 1994 and Walter et al., 2006).** The black arrows indicate extension while the grey arrows correspond to the mantle plume pressure underneath the crust.

### 1.3.4 Deformation of volcanoes

Injections of magma in a volcanic edifice, aside from triggering eruptions, also perturb the stress field. Changes in the stress field suggest that deformations will occur. Indeed, deformation on volcanic edifices have been recorded for a long time (e.g. Murray et al., 1977). Methods of measuring their deformation have evolved with time, from levelling to satellite radar interferometry, with a wide range of intermediate solutions (Electronic Distance Measurements – EDM, tiltmeter, extensometer, GPS).

Observations through time have resulted in the conclusion that volcanoes undergo deformation, of multiple origins. The most common deformations are temporarily linked with magmatic activity, resulting from the deformation of the magma chamber under internal pressure (e.g. Lu et al., 2002; Lundgren et al., 2003; Chadwick Jr. et al., 2006; Dzurisin et al., 2006; Froger et al., 2007); the injection of magma from the magma chamber in the edifice (e.g. Tryggvason, 1994; Bonforte et al., 2004; Froger et al., 2004; Pagli et al., 2007); or the contraction (deflation) of a magma chamber (e.g. Owen et al., 2000; Pagli et al., 2006; Sturkell et al., 2006). Deformation of another origin can also be observed. Hydrothermal activity can be responsible for large uplift in the caldera complex (Battaglia et al., 2006; Hurwitz et al., 2007). Large-scale deformation, affecting usually a whole flank of a volcano, can also be observed (Owen et al., 2000; Froger et al., 2001; Lundgren et al., 2003; Lundgren et al., 2004). Such

deformations are usually related to the movement of a flank under repeated dyke injections, and are known as slumps (e.g. Moore et al., 1989; Moore et al., 1994; Smith et al., 1999; Lipman and Coombs, 2006).

Magmatic-linked deformations are usually characterised by an occurrence restricted in time. They are constrained to an area, centred on the feeding dyke and the magma chamber. The surface of the area affected will vary from one eruption to another, depending on the depth and pressure within the source of deformation (Mogi, 1958). This field of deformation has long been used to define as closely as possible the source of deformation. It gives information on the depth of the magma chamber as well as the organisation of the feeding system. The first model which assumed a homogeneous half-space and a point source was proposed by Mogi (1958). While this model is extremely simplistic, it allows, in a first approach, a good estimation. Similarly, a solution in an elastic half-space, was developed to calculate the deformation linked with a fault, either in tension or shear (Okada, 1985). Moreover, these models assume flat topography, while it has been demonstrated that topography will modify the field of deformation (e.g. Cayol and Cornet, 1998a). With the development of numerical tools, more efficient reconstruction of pressure sources can be done by the inverse method. Any type of deformation data can be used, GPS and radar interferometry (e.g. Bonforte et al., 2004; Froger et al., 2004; Lundgren et al., 2004; Houlié et al., 2006; Pagli et al., 2006), being the more common, but reconstruction can also be performed with tiltmeter and extensometer data (Peltier et al., 2006b).

As a result of deformation, the volcano will undergo modifications in its morphology. An increase in slope is usually associated with dyke injections (e.g. Annen et al., 2001; Fukushima, 2005; Michon et al., Paper 4). In the Galapagos, intrusions are thought to be partly responsible of the unusual morphology of the edifices (Chadwick and Howard, 1991).

#### **1.4 The modelling tool: a short introduction to numerical modelling**

In Earth sciences, most of the structures that we observe are developed over thousands, hundreds of thousands and often millions of years, with processes that often occur at depth, meaning they cannot easily be witnessed. With the development of geophysics, geochemistry and other tools available, geologists are able to better describe an event. However, to actually understand the process behind, theories and models need to be developed. The aim of modelling is to reproduce and interpret structures that can be observed in the field. Models are used to investigate potential mechanisms for the creation of a structure, and integrate available data.

Several types of models exist, from geometrical ones, such as geological cross-sections, to

kinematic models that predict, for example, the plate displacement. These two types of models actually describe more than explain their origin. To understand the origin of process, we need to account for the physical properties of the material considered, including rheology, mechanical behaviour etc. For this purpose, two types of models have been developed, analogue and mathematical. Analogue modelling requires a set of parameters that will allow scaling down the object but preserving the mutual relationship of various parameters (e.g. Merle and Borgia, 1996). The main element that needs to be scaled down is time, and thus requires the use of material of similar properties to rocks, but which react over a much shorter time scale. For example, deformation and spreading of a volcano, in nature, takes hundreds of thousands of years, and involves the viscous deformation of material. Analogue models will use viscous analogous materials that will have viscosity much lower than the actual viscosity of rocks (Merle and Borgia, 1996).

Mathematical modelling proposes to resolve the problems accounting for the physical behaviour of the material. Considering the laws of physics (commonly the laws of continuum mechanics – where no drastic changes occur within the material), equations can be resolved, and result in the understanding of deformation and stress distribution within an object submitted to a specific stress field. These models are ruled by equations describing the behaviour of the constituting materials (i.e. elastic or plastic) as well as the conservation laws (mass and momentum), that create a set of partial differential equations, and must then be solved.

Two processes for solving mathematical models are available; either analytically (by hand) or numerically. The obvious limit of the first is the time consuming process leading to the resolution of the model. Numerical resolution allows the resolution of much larger, and much more complex models, using the calculation potential of a computer. Due to the complexity of the models and the fast resolution, the finite-element method (FEM) (Logan, 2002), was used in this thesis. The FEM is a differential method that requires the creation of simple differential equations that approximate the partial differential or integral equations. This method is preferred in more complex geometries, such as the ones dealt with during this thesis. The resolution is calculated for nodes that correspond to the intersections of elements.

Modelling creates a result that will vary depending on the input data. Similarly, the same result can be reached using different geometries and material properties. For that reason, field data is important because it brings constraint to the model. However, a result does not correspond to the only answer, as the complexity of Nature cannot be fully taken into account, thus all modelling results are a best fit given the data available. Modelling allows an approach for an understanding of a mechanism at the origin of a structure.

## *2 The Island of Réunion*

---

**Objectives:**

- Summarise the work that has been previously done on the island, aiming to understand its geodynamic context, internal structure and volcanic dynamism.



## 2.1 Geodynamics

The volcanic island of Réunion is located in the South-West of the Indian Ocean, about 750 km east of Madagascar. The island, located in the eastern margin of the Mascarene Basin, is one of the Mascarene Islands, with Mauritius and Rodrigues (*Figure 2.1-1*). The island is located on a 68 Ma (late Cretaceous) oceanic crust, the structure of which is complex. Its topography is characterised by the presence of several palaeo-ridges segments, of NW-SE trend, offset by several SW-NE trending fracture zones, both structures active during the spreading of the Mascarene Basin between magnetic anomalies 34 (84 Ma) to 27 (62 Ma) (*Figure 2.1-2*) (Dyment, 1991). At about 60 Ma, the spreading was shifted to the still active Carlsberg Ridge, which limits the Indian and African plates (Dyment, 1998). WSW-ENE trending topographic ridges, of unknown origin, can also be observed south-west of Réunion.

The island of Réunion is located at the south-western end of the Mascarene Plateau and south-west of Mauritius, from which it constitutes a distinctive relief. The origin of the volcanic ridge that is the Mascarene Plateau has been attributed to the presence of a mantle plume, which is actually located in the surroundings of Réunion Island (*Figure 2.1-3*; Bonneville et al., 1997). The trace of this mantle plume can be followed from Réunion towards India and the Deccan Traps, with several islands and archipelagos found along its trace. The first activity of the mantle plume has been dated at about 65-66 Ma in the Deccan province. Subsequent activity includes the Laccadives ridge (58 Ma), the Maldives (55 Ma), and Chagos (49 Ma) on the Indian plate; and the Mascarene Plateau (45 Ma), the Nazareth Bank (31 Ma), Mauritius (1-7 Ma) and Réunion (0-2 Ma) on the African plate (*Figure 2.1-3*) (Mahoney et al., 2002; O'Neill et al., 2003). At ~ 30 Ma, the separation of the Chagos - Laccadives ridge from the Mascarene Plateau is initiated.

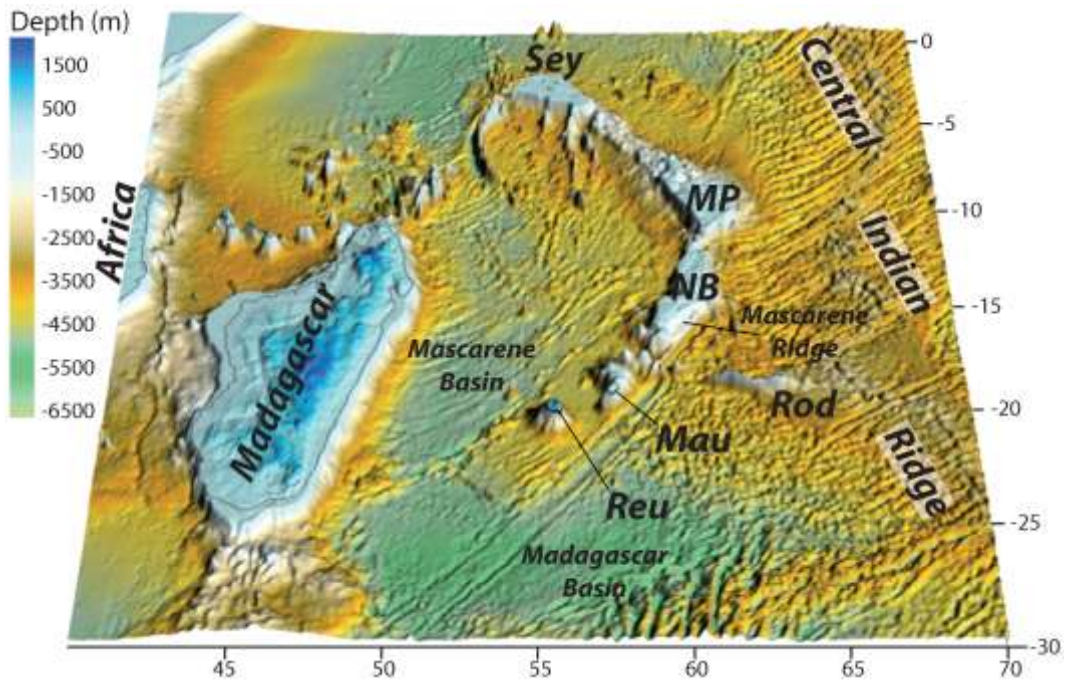


**Figure 2.1-1: Surface representation of the south-western part of the Indian Ocean.** *Reu: Réunion Island, Mau: Mauritius, Rod: Rodrigues, NB: Nazareth Bank, MP: Mascarene Plateau, Sey: Seychelles Archipelago.* The island of Réunion is separated from the rest of the Mascarene Ridge. Geographic coordinates (bathymetry from Smith and Sandwell, 1997).

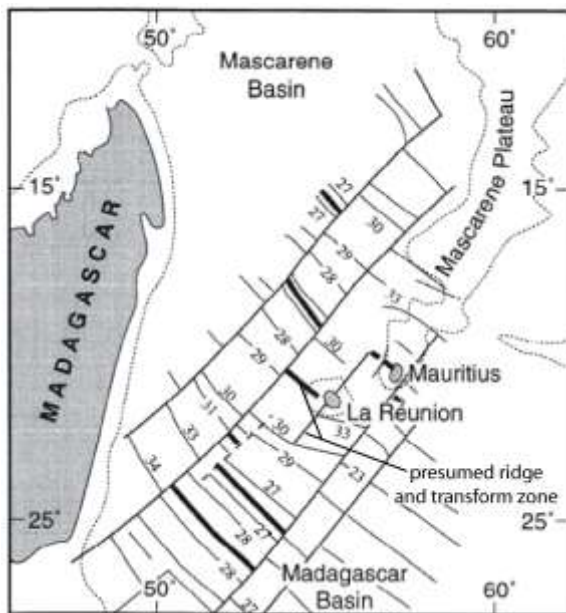


**Figure 2.1-2: Structure of the oceanic crust in the surroundings of Réunion Island.** *The thick lines correspond to the palaeo-ridges while the thin lines perpendicular to the ridge segments are the palaeo-transform zones. The magnetic anomalies are annotated. Geographic coordinates (modified from Dymont, 1991).*

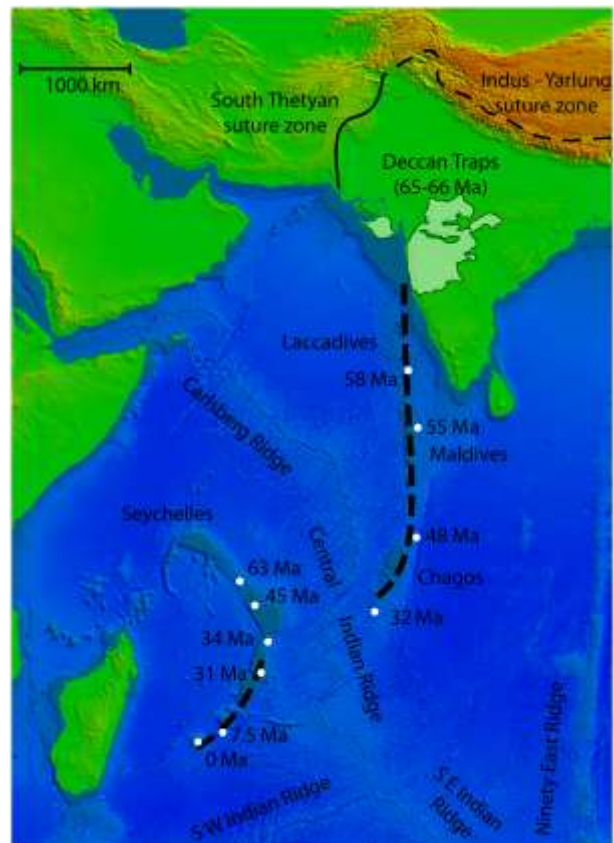


**Figure 2.1-3: Trace of the Réunion Hot Spot.** *The main archipelagos and islands are noted. The white dot and number associated corresponds to the radiometric ages obtained in the ODP Legs 115 (adapted from Mahoney et al., 2002; O'Neill et al., 2003).*

## 2.2 Volcanism of La Réunion

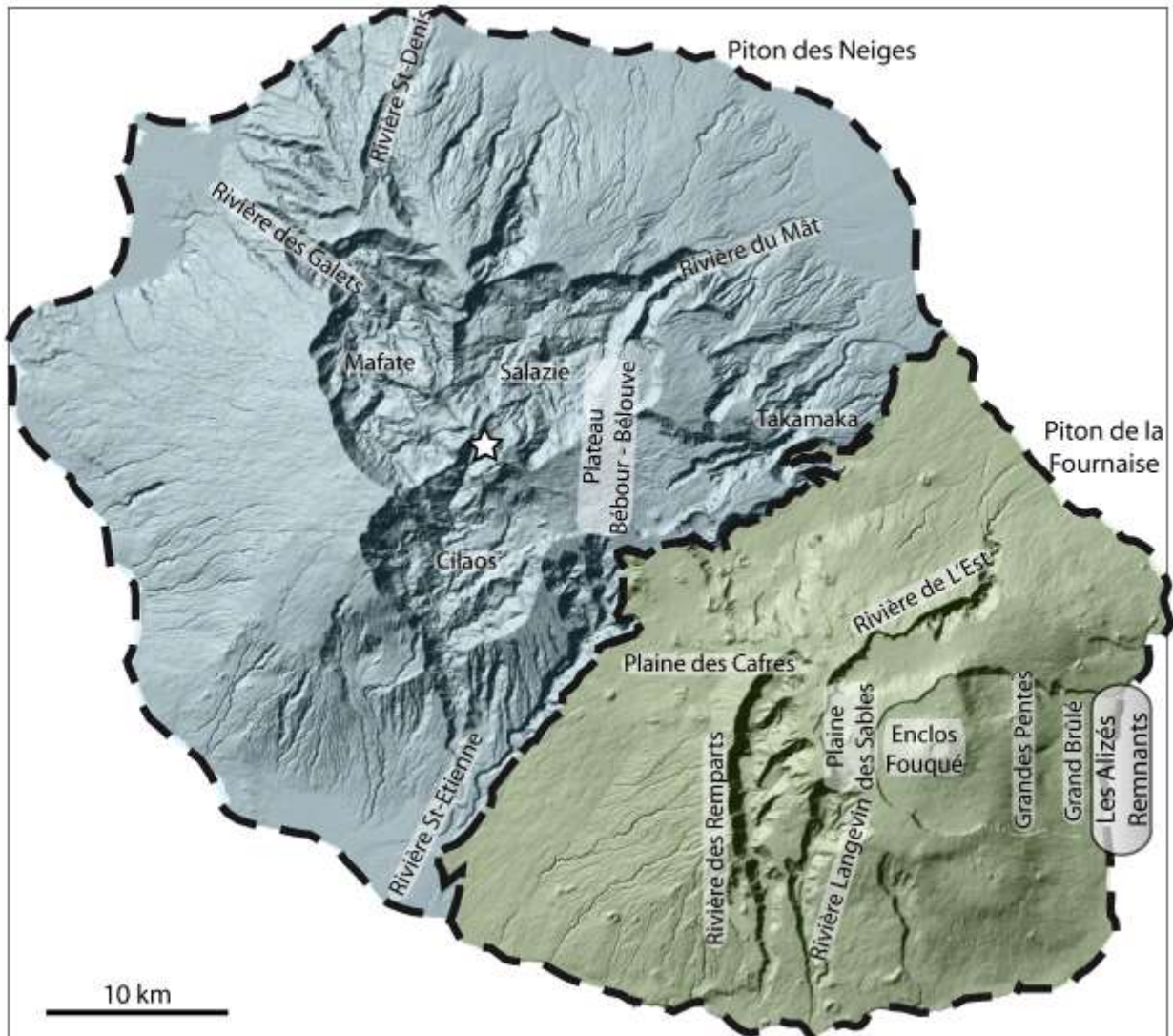


**Figure 2.2-1: The Island of Réunion.** The deposits of Piton de la Fournaise and Piton des Neiges are marked. The emplacement of the palaeo magma chamber associated with Les Alizés volcano is marked. The names of the main morphological features are given on this shaded relief map of the 25m-DEM (from the IGN). The star marks the inferred eruptive centre of Piton des Neiges.

Réunion Island itself constitutes a ~7500 m high edifice, from seafloor to summit. The base of the island rests at about 4000-4500 m b.s.l., on a sedimentary layer which has been estimated as being about 500-700 m thick, with thickness locally reaching up to 1000 m (de Voogd et al., 1999). The island results from the growth of three separate volcanoes, Piton des Neiges, Les Alizés and Piton de la Fournaise (Malengreau et al., 1999; Lénat et al., 2001). The two first edifices are both inactive and located in the north-western and south-eastern extremities of the island respectively (*Figure 2.2-1*). All the volcanoes have undergone several flank collapses, the deposits of which have been identified both on land and on the submarine flanks of the edifice (Bachèlery et al., 2003; Oehler et al., 2004; Oehler, 2005) (*Figure 2.2-2*). As a result, Les Alizés does not actually crop out at the surface. Its presence is inferred from the presence of

a shallow, solidified magma chamber in the eastern part of the island, and is now covered by the still active Piton de la Fournaise (Rançon et al., 1989; Lénat et al., 2001). The eruptive products observed are mostly of basaltic nature, but more differentiated products cover Piton des Neiges (*Figure 2.2-3*).

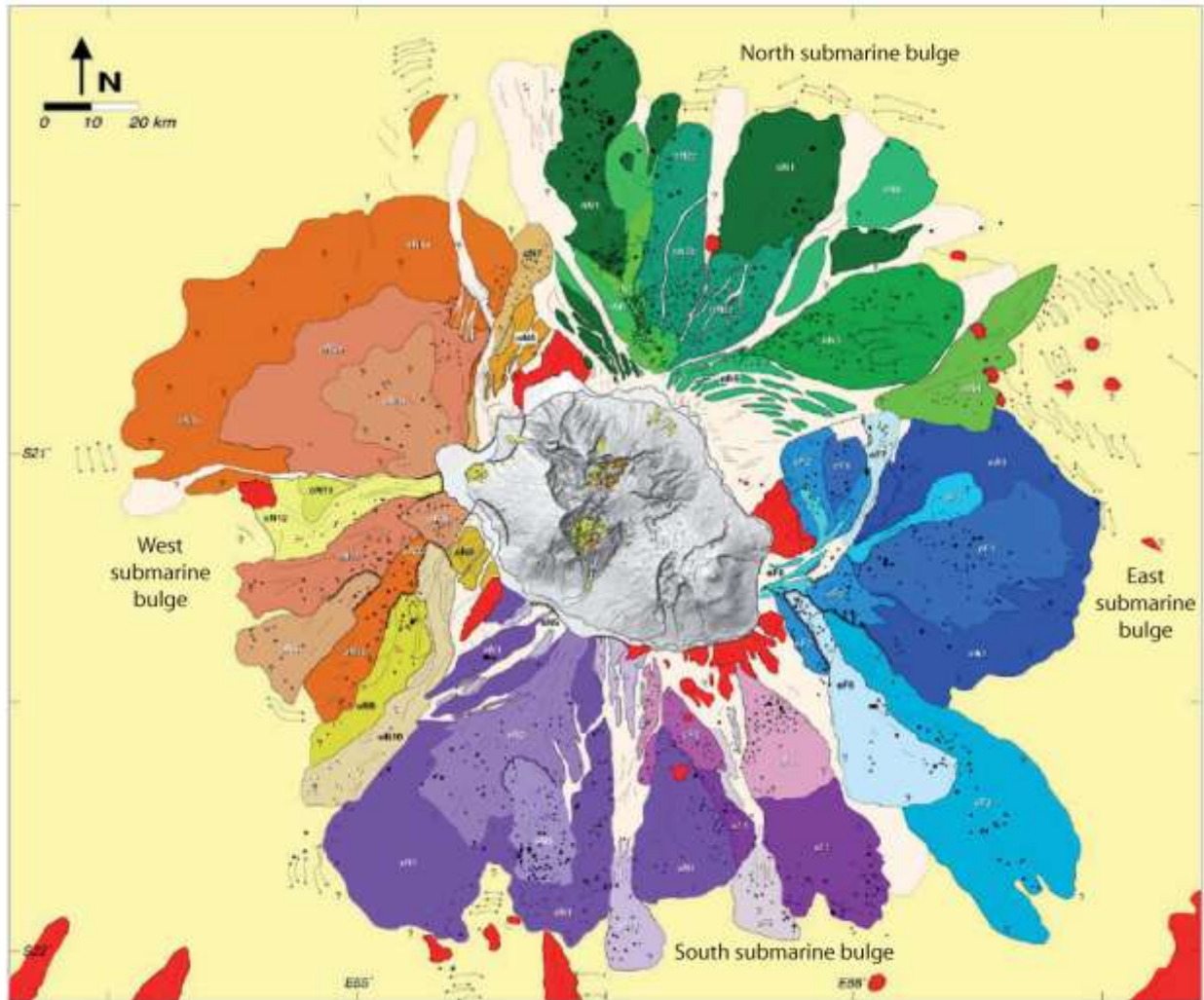


**Figure 2.2-2: Map of the debris avalanche deposits identified on the submarine flanks of Réunion Island** (modified from Oehler, 2005). Each bulge is identified in a family of colours; each colour corresponds to a single debris avalanche. In red are the pre-existing reliefs, the arrows represent axis of sedimentary ridges, and on-land deposits are identified in yellow.

The topography of the island is marked by deeply eroded valleys. The tropical climate associated with various volcano-tectonic structures, has led to their creation (Louvat and Allègre, 1997; Bret et al., 2003). The most spectacular features of the island are the three amphitheatre headed valleys entailing Piton des Neiges and constituting the three cirques of Mafate, Salazie and Cilaos. In Piton de la Fournaise, the younger age of deposits leads to the observation of only less developed structures such as la Rivière des Remparts and Rivière Langevin.

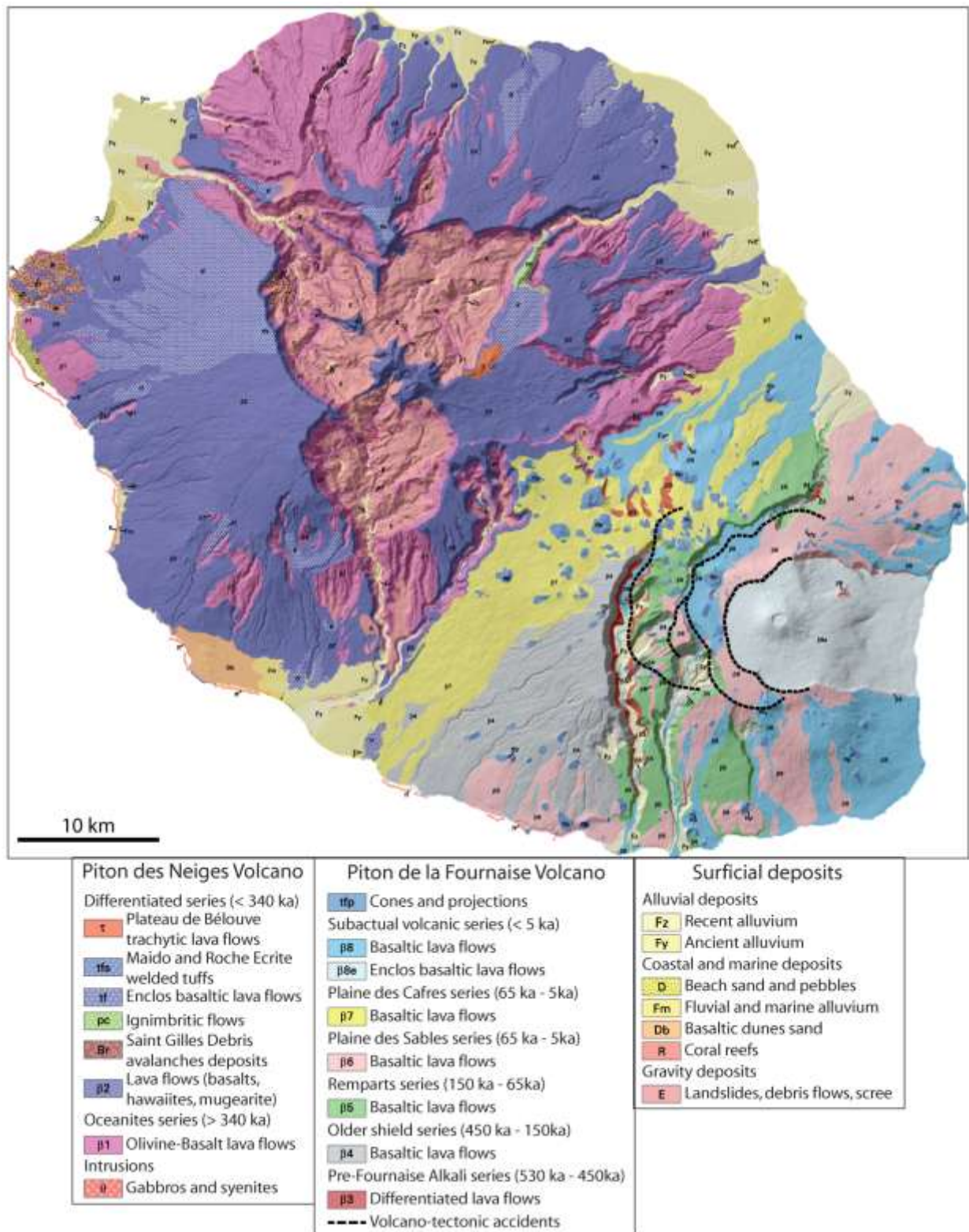


Figure 2.2-3: Geological map of Réunion Island (modified from Nehlig et al., 2006).

### 2.2.1 Piton des Neiges

Piton des Neiges volcano occupies the 2/3 of the island in the North-West (*Figure 2.2-1*). It culminates at 3070 m and is the highest point of the island. It is considered as inactive, but not extinct as the last signs of activity are no older than 12 ka. The initiation of sub-aerial activity

has been dated at about 2.1 Ma, this being the age of the oldest aerial lava flows observed, in the north-western part of the edifice. The activity and growth of the volcano has been characterised by several stages, each characterized by typical petrographies (*Figure 2.2-4*) (Deniel et al., 1992; Bret et al., 2003):

- The subaerial shield stage can be subdivided in two series:
  - The lower basaltic series that corresponds to submarine breccias outcropping at the bottom of the Cirques, and is older than 2.1 Ma.
  - The upper basaltic series, from 2.1 Ma to 0.45 Ma, is characterised by picritic basalts (locally named oceanites), olivine basalts and aphyric basalts, as well as the intrusion of their plutonic equivalent. Datings define 3 periods of effusion from 2.1 Ma to 1.9 Ma, 1.2 Ma to 1.0 Ma, and finally 0.57 Ma to 0.43 Ma.
- A period of inactivity during which major erosion occurred lasted from 0.45 Ma to 0.34 Ma.
- The capping stage is characterised by alkalic and more evolved terms that are distributed in time:
  - 0.35 – 0.17 Ma: a period of effusive activity is characterised by basalts to mugearites. The basalts present a liquid composition close to the aphyric basalts from the shield stage. However, the presence of a high quantity of plagioclase macrocrystals (named in Réunion ‘roche Pintade’) gives a bulk composition of hawaiites.
  - 0.17 – 0.13 Ma: a period of erosion with an increasing explosive activity is characterised by the emplacement of evolved terms such as mugearites and trachytes.
  - 0.13 – 0.05 Ma: a period of effusive activity with the eruption of evolved terms from mugearites to trachytes.
  - 0.05 – 0.012 Ma: the final period of activity that sees a decreasing effusive activity, accompanied by an increase of explosive activity.

Few studies of the structure and organisation of the intrusive system have been done. Earlier studies suggested that the volcano had two distinct types of organisation. First, during its shield stage, a system of rift zones trending N10°, N45°, N120° and N160°, radiating from the eruptive centre (Chevallier, 1979). These rift zones became inactive during the alkali capping stage, the feeding system being mainly organised around a summit feeding system, with few intrusions propagating away from the summit (Chevallier, 1979). The presence of shallow dipping intrusions and sills was also noted, and was attributed to caldera collapse events, with a

mode of emplacement similar to that of a cauldron (Chevallier, 1979). Sills have also been noted by Maillot (1999), and while the author gave arguments as to the origin of sills, no real model was proposed.

Absolute Ages	Series	Activity	Chemistry	Petrography	Stage
0.012 Ma	Serie	Erosion	Cirques erosion Silica saturated and oversaturated alkaline, sodic	Trachytes	Stage
0.05 - 0.07 Ma		Explosive		Effusive	
0.13 - 0.15 Ma	Differentiated	Effusive	Silica undersaturated alkaline, sodic	Mugearites to Benmoreites	
0.17 - 0.19 Ma		Explosive		Caldera collapse	
0.22 Ma	Erosion Period	Erosion	Paleo-cirques erosion	Mugearites	Capping
0.35 Ma		Explosive		Effusive	
0.43 Ma	Upper Oceanites Serie	Effusive	Silica saturated and oversaturated alkaline, sodic	Basalts to Mugearites	Alkalic
> 2.1 Ma				Lower Oceanites Serie	
				Aphyric Basalts	Subaerial Shield Stage
				Olivine Basalts	
				Oceanites	Submarine Shield Stage

Figure 2.2-4: Chronology of the subaerial activity of Piton des Neiges (adapted from Deniel et al., 1992).

## 2.2.2 Piton de la Fournaise

### 2.2.2.1 General evolution

Piton de la Fournaise volcano, whose summit culminates at 2631 m, is the only active volcano on the island, and is amongst the most active volcanoes in the world. The average rate of eruption in the historic time, before 1998, was about of an eruption every 14 months (Bachèlery, 1999). Since 1998, however, this eruptive rate increased to an eruption every 4 months. The eruptive activity at Piton de la Fournaise started ~530 ka ago, the products of which are located in the deeply incised valleys of La Rivière des Remparts and La Rivière de l'Est (e.g. Bachèlery and Mairine, 1990). It appears that Piton des Neiges and Piton de la Fournaise shared a common period of activity, mostly differentiated at the former, and basaltic at the latter.

The growth of Piton de la Fournaise is complex, though an age evolution can be observed from west to east (*Figure 2.2-5*). A model for the structural evolution of Piton de la Fournaise was proposed by Bachèlery and Mairine (1990). According to the age evolution, they proposed that the growth of the volcano was interrupted by volcano-tectonic events. This results in the distinction between:

- An older shield, whose activity spanned between 530 ka and 150 ka. This centre has been affected by at least two major volcano-tectonic events (flank landslide or caldera collapse), in the Rivière des Remparts (290 ka) and Morne Langevin (150 ka). The activity was organised along a NE-trending, N110° and N240° rift zones centred on the Plaine des Sables and its western part (*Figure 2.2-5*). In this early stage, 'roche Pintade' (see description for Piton des Neiges above) and Pl-Ol-Px basalts are emitted. With time, the proportion of these basalts decreased in favour of olivine basalts. In the second part of this period, oceanites, olivine basalts and aphyric basalts become the dominant products. The presence of an evolution from alkalic terms towards tholeiitic terms can be seen. This period ends with the Morne Langevin volcano-tectonic event.

- The younger shield whose activity started at 150 ka and continues to the present. This period coincides with the cessation of activity of the previous eruptive centre of the older shield, in the western part of the volcano, to concentrate on the Plaine des Sables. The growth has been affected by two collapsed structures, the Plaine des Sables event (65 ka), and the Enclos Fouqué collapse (5 ka) (*Figure 2.2-5*). The first has been thought to be associated with the migration of the eruptive centre towards the west of the actual Enclos Fouqué, while the



second is associated with the migration of the eruptive centre towards its current position. The products erupted during this recent shield stage have similar characteristics to those erupted in the late older shield stage (oceanites, olivine basalts and aphyric basalts).

The eruptive centres have always been associated with a range of rift zones. A NE trending, N110° and N240° rift system is thought to have been active during the older shield period. With the migration and the concentration of the activity in the eastern part, the rift system has been reorganised along NE-SE trending and N120° rift zones. The NE-SE trending system is highly active, while the N120° between Piton de la Fournaise and Piton des Neiges has not been active historically. East of the cone, a rift zone, trending N120° is periodically active (Michon et al., 2007a).

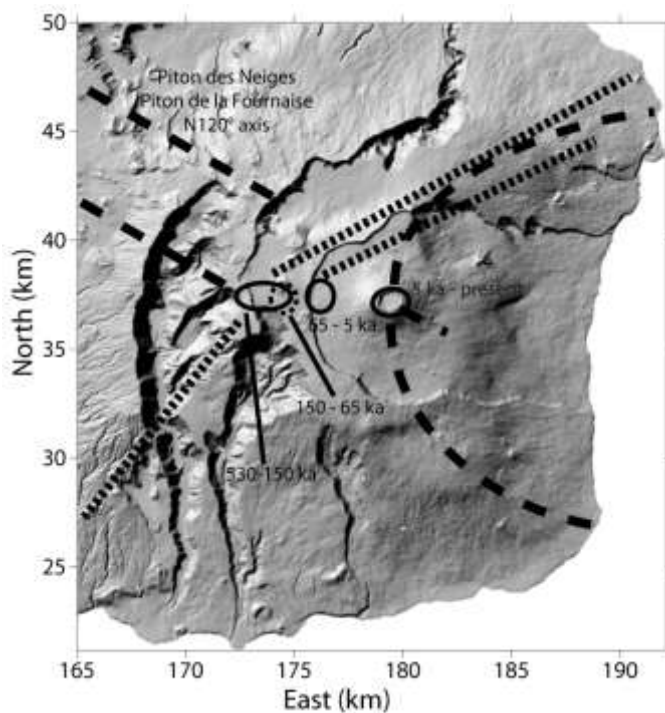


**Figure 2.2-5: Magmatic feeding system of Piton de la Fournaise.** The circles correspond to the location of the eruptive centres. Short dashed lines correspond to the presumed location of the previous rift zones, long dashed line correspond to the present rift zones, inferred from the model of evolution proposed by Bachèlery and Mairine, 1990. Coordinates Gauss-Laborde Réunion (in kilometres).

### 2.2.2.2 The origin of the volcano-tectonic events

The origin and dynamics of the several volcano-tectonic events that have affected Piton de la Fournaise are still debated. A common assumption is that all the events are based on the same dynamics, best represented by the most recent event; the Enclos Fouqué collapse. Several models have been proposed for its origin, and they can be classified in four main types:

- A polylobate caldera in the upper area, combined with a landslide in the lower part of the edifice (Bachèlery, 1981; Bachèlery and Mairine, 1990). This implies, considering the size of the collapsed structure, the associated magma storage will be of sill type, over a large area.
- A landslide that affected a large part of the flank (Labazuy, 1996).
- A mixed model, suggesting that deformation over a hydrothermal core can lead to the

creation of a landslide and a caldera-like depression at the summit (Merle and Lénat, 2003; Barde-Cabusson, 2007; Barde-Cabusson and Merle, 2007).

- A vertical collapse (Michon and Saint-Ange, 2008).

### 2.2.2.3 The recent dynamics – insights on the plumbing system

Since the creation of the Observatory of Piton de la Fournaise (Observatoire Volcanologique du Piton de la Fournaise – OVPF), over 50 eruptions have occurred. Most of these eruptions are characterised by rather small volumes, in the order of few  $10^6 \text{ m}^3$  (data from the OVPF). The mathematical average duration of an eruption, since 1981, is about 3 weeks. However, one third of the eruptions have lasted less than 5 days (Figure 2.2-6). These eruptions account for only a small amount of the total volume erupted, indeed, they usually emit less than  $1 \times 10^6 \text{ m}^3$  (Figure 2.2-7). The erupted volume is emitted during two types of eruptions:

- Long-lived eruptions such as 1998, characterised by aphyric basalts
- Short to medium-lived eruptions (less than 4 weeks) that have a high emission rate, usually characterised by olivine-rich magma.

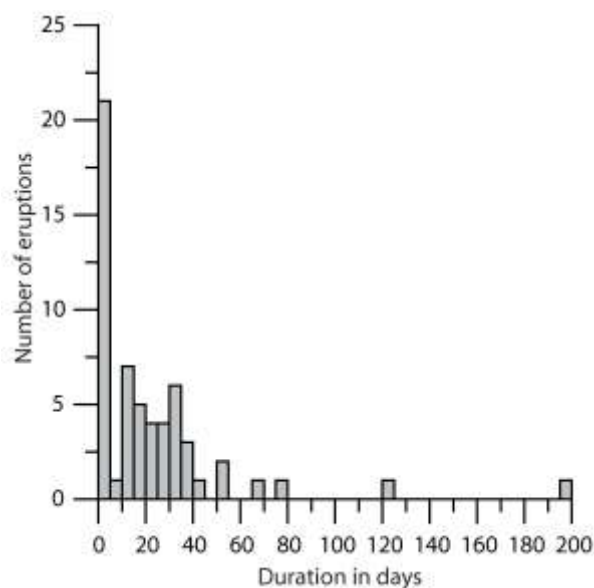


Figure 2.2-6: Duration of the eruptions since 1981 (data from the OVPF; Peltier, 2007).

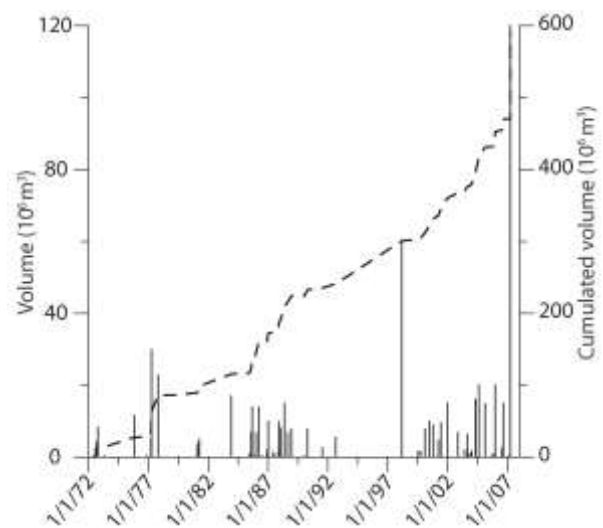


Figure 2.2-7: Volume and cumulative volume emitted during the eruptions since 1972 (data from the OVPF; Peltier, 2007).

This mode of lava emission leads to a step-like distribution of the cumulative volume, the increase characterised by large volume or an increased eruptive rate, with eruptions of small volume (few  $10^6 \text{ m}^3$ ). The steps correspond to periods with few small eruptions, or quiet periods, recurrent in the historical evolution of the volcano (1966-1972 and 1992-1998).

The most commonly emitted products are aphyric basalts, while oceanitic eruptions, associated with an increased emission rate are less frequent. The petrographic differences are

also associated with geographical repartitions. Oceanites are common in the eruptions occurring at distance from the summit, along the active rift system identified (e.g. Peltier, 2007).

The rift system is part of the feeding system. Its structure has been deduced from the location of eruptive fissures, deformation, seismic and other geophysical data (Lénat and Bachèlery, 1990; Michel and Zlotnicki, 1998; Michon et al., 2007a). A main shallow storage system is located underneath the current summit craters. Initially, the storage system was thought to be composed of sills (e.g. Lénat and Bachèlery, 1990). However, according to seismic studies, and more recent work, the presence of a shallow magma chamber at sea level is now thought to be the main storage system (Sapin et al., 1996; Fukushima, 2005; Peltier, 2007). Other arguments, such as the volumes of eruptions do not support the sill-like storage system, as in such condition an evolution of volume would be expected with time (*Figure 2.2-7*).

This shallow magma storage is refilled during deep injections, scattered in time. Initially believed to be associated to oceanitic eruptions (e.g. Bachèlery, 1999), the only refilling event monitored, with a magma of deep origin (-6 km) (Battaglia and Bachèlery, 2003), in 1998, was not accompanied with the emission of oceanites, but typical aphyric basalts with an abnormal geochemical signature issued from fractionation at depth (Vlastélic et al., 2005). Recent oceanitic eruptions have not been accompanied by deep seismicity, similar to that of the one from 1998. It has been recently suggested that the oceanites could be initiated from the lower level of the shallow magma chamber, or that since 1998, a continued income of magma from greater depth was feeding the shallow magma chamber (Peltier, 2007).

The shallow processes of injection are usually separated in two processes:

- A vertical injection from the shallow magma level towards the summit crater (Nercessian et al., 1996; Peltier et al., 2005).
- A lateral injection of magma at shallow level (mostly aphyric magma) or deeper (for oceanites) along the rift zones (Fukushima, 2005; Peltier et al., 2005; Peltier, 2007). This lateral injection occurs usually through eastward inclined dykes (e.g. Froger et al., 2004; Fukushima et al., 2005).

## **2.3 What geophysics tell us: insights on the internal structure of the Island**

### **2.3.1 Seismic data**

Seismic studies have revealed the general structure of the island, the distribution of material within the island and the base of the crust. The base of the crust, in the south-western part of the island is under-plated by up to 2 km of plume material that have been added to the crust (Charvis et al., 1999). It can be observed a slight depression, the centre of which would be

located at the vertical of the island (*Figure 2.3-1*). However, while the depression profile is observed on each part of the island, the crust is slightly domed along the vertical axis of the island (de Voogd et al., 1999). This has been interpreted as the result of the slow movement of the oceanic plate over the mantle plume (Michon et al., 2007a).

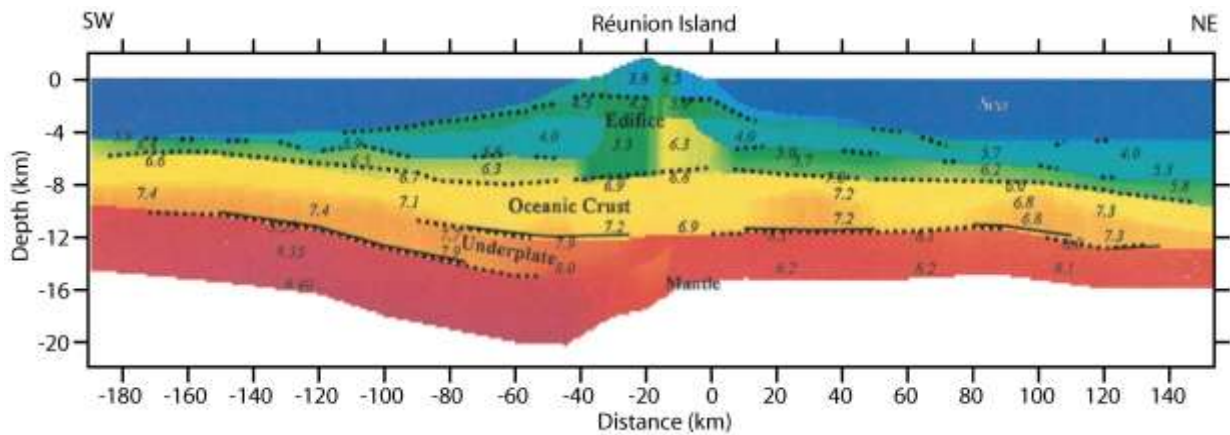


**Figure 2.3-1: 2-D P velocity section along a SW-NE profile across the island of Réunion.** Speeds are given in km/s on the figure. Note the presence of lateral speed variations within the edifice (modified from Gallart et al., 1999).

### 2.3.2 Magnetic data

The growth of Réunion, in its subaerial part, has been spread over 2.1 Ma. This period of time corresponds to two magnetic epochs; the first, mostly in reverse polarity, being the Matuyama epoch from 2.6 Ma to 0.78 Ma; followed by the Brunhes epoch, of normal polarity (Lénat et al., 2001). This limit at 0.78 Ma is highly convenient in the case of Réunion, as most of the shield building stage of Piton des Neiges and Les Alizés have been under reverse polarity, while its capping stage, as well as the growth of Piton de la Fournaise has been under normal polarity. A distinction between the structures associated with the growth of Piton des Neiges and Les Alizés or Piton de la Fournaise can be easily done.

The magnetic anomaly map (*Figure 2.3-2*; Lénat et al., 2001) shows that negative anomalies (corresponding to reversely magnetised materials) are present in the North, East and South of the island. These three anomalies are combined with two sharp and elongated structures, reversely magnetised in the East and South-West of the island. They are interpreted as rift zones, that have been dominantly active prior the Matuyama-Brunhes transition. Associated with these reverse anomalies, are two main positive anomalies, centred on the western flank of Piton des Neiges and on Piton de la Fournaise.

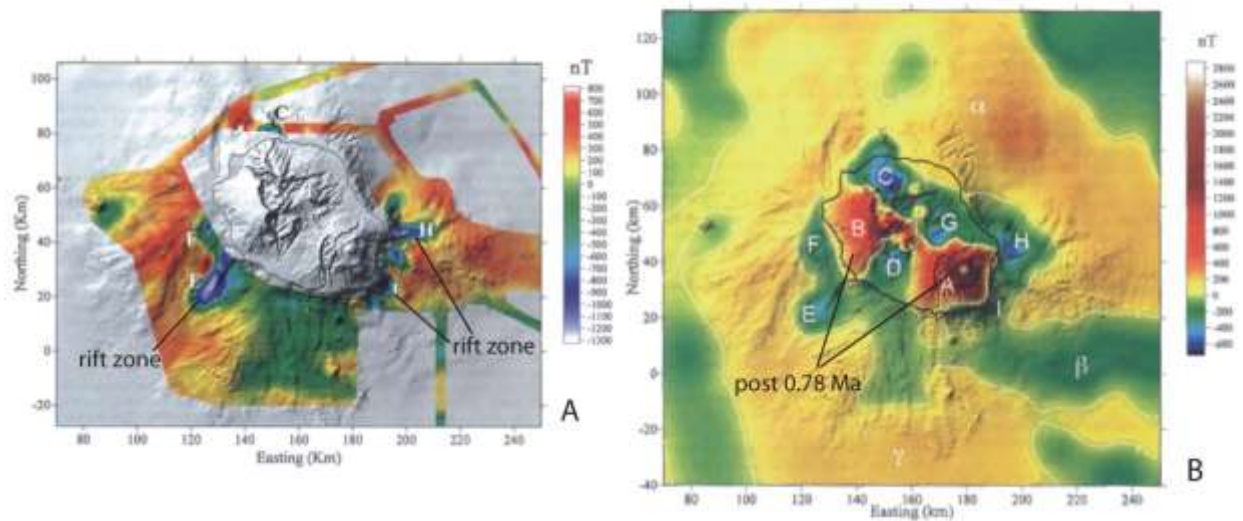


**Figure 2.3-2: Maps of magnetic anomalies.** A) pole reduction at sea level, B) pole reduction at 3500 m. Coordinates in Gauss-Laborde Réunion (modified from Lénat et al., 2001). Markings refer to the different anomalies discussed in Lénat et al., 2001.

The model of evolution proposed by Lénat et al. (2001), suggests that two volcanoes were active before 0.78 Ma, Piton des Neiges, and Les Alizés. Their activity was likely to have been organised along rift zones, remnants of which are shown by the two sharp and elongated anomalies. The magnetic anomaly map also shows that the western part of Piton des Neiges is mostly associated with rocks younger than 0.78 Ma. This has been interpreted as an accumulation of recent products in the scar of a dismantled flank, the products of which have been identified on-land (Bachèlery et al., 2003) and on the submarine flanks (Oehler, 2005). On the eastern part, the growth of Piton de la Fournaise took place over the remnants of Les Alizés volcano, previously dismantled during a flank collapse.

### 2.3.3 Gravimetric data

Several campaigns of gravimetric surveys have been done in Réunion. Most of them were centred on Piton de la Fournaise. They have revealed the presence of a large dense body underneath the eastern flank of Piton de la Fournaise (Figure 2.3-3). It has now long been attributed to a large fossil magma chamber, related to the now extinct Les Alizés volcano. They also revealed the presence of a dense body, of lesser extent underneath la Plaine des Sables and in the west of the Enclos Fouqué (Rousset et al., 1989; Malengreau et al., 1999).

At the scale of the island, gravimetric surveys also reveal the existence of a dense body, with a SW-NE trending elongation, and located underneath the massif of Piton des Neiges. In a lesser extent, denser rocks seem to be present in the Takamaka area (Malengreau et al., 1999). At a smaller scale, gravimetric studies have shown the existence of slightly denser bodies

underneath the rift zones of Piton de la Fournaise that were interpreted as the cooled dykes (Rousset et al., 1989; Lénat and Bachèlery, 1990).

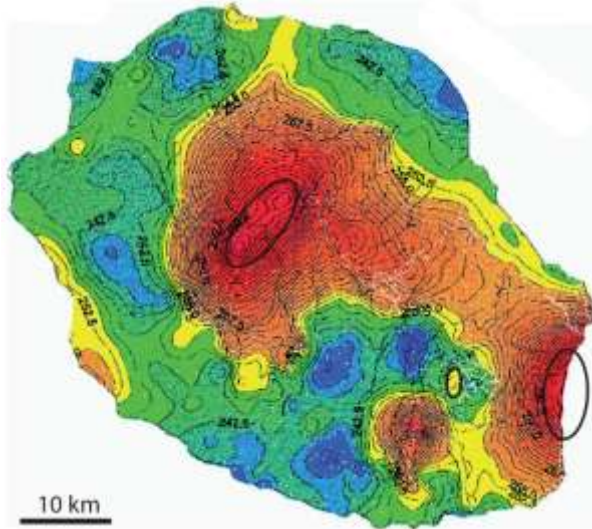


**Figure 2.3-3: Bouguer anomaly maps of Réunion.** The density correction is  $2.9 \times 10^3 \text{ kg/m}^3$ . Contour interval: 2.5 mGal. The black ellipses correspond to the inferred locations of main dense bodies. Red for the highest anomalies, blue for the lowest (modified from Malengreau et al., 1999).

### 2.3.4 Electrical data

Geoelectrical prospection has been used mainly on the active Piton de la Fournaise. Several methods have been used, Self-potential, Audio-Magnetotelluric, Transient Electro-magnetic, and Direct Current. Here the focus is on the studies that were used to better constrain the structure of the volcano and its dynamics. Self-potential surveys, in the Enclos Fouqué, revealed the existence of several anomalies around the summit as well as on the cone and within the Enclos Fouqué (Lénat and Bachèlery, 1990; Michel and Zlotnicki, 1998). These anomalies were interpreted as zones of fractures allowing the ascent of hydrothermal fluid. The major anomalies observed at the scale of the Enclos Fouqué are concordant with the existence of the rift zones (Michel and Zlotnicki, 1998).

Finally, the combination of Direct Current and Transient Electro-magnetic has shown the structure of the Enclos Fouqué. A large structure of low resistivity exists, centred on the summit cone, and covered by the highly resistive superficial rocks. This structure, interpreted as the hydrothermal system, becomes shallow in the central area, and deepens outside the central cone (Lénat et al., 2000).

*3 Structure and Dynamics of an Oceanic  
Shield: the example of Piton des Neiges*

---

### **Objectives:**

- Study the internal structure of the deeply eroded Piton des Neiges volcano.
  
- Propose a model of dynamics for the intrusive system.
  
- Propose a coherent model for the origin of sill clusters in volcanic domain.



### **3.1 Introduction**

Studies of the internal structure of eroded volcanoes are of major importance to understand the mechanisms of eruptions on active volcanoes. Such studies also allow the exploration of the origin of structures observed and the organisation of the stress field. On oceanic shields, similar studies allowed the proposal of a model of evolution of shield volcanoes (Walker, 1987), and reveal the stress field organisation (Marinoni and Gudmundsson, 2000; Marinoni, 2001), as well as the origin of rift zones (Walter and Schmincke, 2002). The historical evolution of the volcano can also be uncovered by the study of its internal structure (Ancochea et al., 2003; Rodriguez-Losada and Martinez-Frias, 2004).

Here a structural study of the island of Réunion is proposed, with a focus on the dormant and eroded Piton des Neiges volcano. The attention has been focused on the intrusion system, with characterisation of the various intrusions by their strike, dip, thickness, and petrology of both intrusion and host rock. The strike was systematically measured, with a compass corrected for the magnetic declination in Réunion Island ( $\sim 20^\circ$  W). The location of each intrusion was determined using a hand GPS receiver, with a precision of about 3-5 m in the best conditions. The use of map localisation was used when no location could be determined by GPS (e.g. in narrow gorges).

### **3.2 Structure and dynamics of Piton des Neiges volcano: Paper 1**

As suggested before, only few structural studies have been done in the dormant and eroded Piton des Neiges. Recent studies have been focused on only one sector of the volcano, and do not offer a general view of the volcano. Moreover, it appears that the few structural studies are contradictory concerning some aspect of the structure of the intrusive system. While a rift system, organised along four main rift zones, was described (Chevallier, 1979), at least one of the rift zone was later reconsidered (Maillot, 1999). Similarly, no models of evolution and origin of the rift zones were previously proposed.

A large set of data was gathered and is presented here, covering all the cirques as well as the deep valleys within the volcano. This allows the proposal of a model explaining the dynamics of the rift zone that fits our field data. Moreover, these data can be used to infer the dynamics of the feeding system of Piton de la Fournaise volcano. This work has been submitted for publication in the *Journal of Volcanology and Geothermal Research*.

## Structure and dynamics of the Piton des Neiges rift zone system

Ludovic Letourneur<sup>a</sup>, Agust Gudmundsson<sup>b</sup>

<sup>a</sup> University of Göttingen, Geoscience Centre, Department of Structural Geology and Geodynamics, Goldschmidtstrasse 3, 37077, Göttingen, Germany

<sup>b</sup> Department of Earth Sciences, Queens Building, Royal Holloway, University of London, Egham, Surrey, TW20 0EX, UK

### Abstract

Piton des Neiges, one of the volcanoes constituting the island of Réunion, is a deeply eroded oceanic shield volcano. It has evolved from an aerial shield to an alkalic capping stage and has been dormant for the last 12 ka. Previous structural studies proposed an organisation along rift zones, the location and dynamics of which were disputed. A field study within the volcano shows that it is organised along three main rift zones, N30°, N120° and N160°, distributed north, north-west and south of the eruptive centre. These rift zones display essentially rocks from the shield stage, which suggests that they have been mostly active during this stage of construction. Most of the intrusions are laterally injected from a central feeding path. A recurrent distribution can be observed, with aphyric basalts mainly located in the central part of the edifice, and occasionally observed further away. Olivine and picritic basalts are observed further away from the eruptive centre. This distribution indicates that dense magmas do not rise high in the edifice, and initiate a lateral propagation, feeding eruptions downrift. Meanwhile lighter magma rises in the central part and intrudes laterally. Olivine and picritic basalts, through deep intrusion conserve their overpressures, favourable to distal propagation, while aphyric basalts undergo a loss of pressure once they have reached the surface, preventing lateral injection.

The magma path is controlled at the scale of the edifice by several stress fields. In the central part, there is a predominantly magmatic inclined stress field that disappears in the distal parts of the rift zones, where another stress field controls the magma injections. In Mafate, this second stress field presents with a sub-horizontal  $\sigma_3$  (minimum principal compressive stress), while in Cilaos,  $\sigma_3$  is strongly dipping. We propose that the former is inherited from a deep, possibly crustal structure, while the latter is strongly influenced by surface stresses.

### 3.2.1 Introduction

Rift zones are common features of oceanic shield volcanoes. They are observed on most of the oceanic shield volcanoes such as in Hawaii (e.g. Rubin, 1990), the volcanoes of the Canary

Islands (e.g. Carracedo, 1994), Madeira (e.g. Schwarz et al., 2005), the Galapagos (e.g. Glass et al., 2007), Comoros (Bachèlery, 1999), and Réunion (e.g. Chevallier, 1979; Bachèlery, 1981). They correspond to preferential magma paths that are attributed to stress fields in relative extension. It is common to observe tension fractures within a rift zone. As preferential magma paths, they display a high concentration of eruptive features, either spatter or scoria cones, or eruptive fissures. Historical activity suggests that eruptions along rift zones actually initiate as a fissure, and later evolve to create localised points of activity, over which cones are created. However, when observing the morphology of oceanic shield volcanoes, it appears that a wide range of shapes are encountered, usually between two extremes, a ridge-like morphology (Hualalai), and a sub-circular one (Fernandina, the outline of Piton des Neiges). This suggests that rift zones have their own dynamics, and do not exert the same control on magma injection.

The sub-surface expression of an eruptive fissure is a dyke. The inner structure of volcanic rift zones in oceanic shields is usually comprised of a high density of steeply dipping intrusions (e.g. Walker, 1987; Marinoni and Gudmundsson, 2000). According to the model of Walker (1992), dykes inject laterally within the rift zone at the level of neutral buoyancy, and will either propagate at the margin of the rift zone, or alternatively along the weak core of previously intruded dykes. As a result of the accumulation of intrusions, the rift zone forms a structure that is broad at its base (large amount of intrusions) and gets thinner both upwards and downrift (fewer intrusions reach the surface or propagate away from the eruptive centre) (Walker, 1992).

The origin of these preferential magma paths can be found in various processes. Gravitational spreading of an edifice growing on the flank of a previous volcano, is the key factor leading to the creation of rift zone such as in Kilauea or Piton de la Fournaise (Walter, 2003; Walter et al., 2006). The common three-branches structure observed in several cases, including the Canary Islands (Carracedo, 1994), has led authors to propose that the bulging and fracturing of the crust under the pressure of the mantle plume led to the creation of tri-axial rift zones (e.g. Carracedo, 1994). In some other cases, the inheritance of crustal structures leads to the creation of elongated rift zones such as in the Azores (Nunes et al., 2006). However, these latter cases, are usually characterised by a strong structural control on the magma injection that leads to thin and elongated rift zones (Carracedo, 1994).

In Réunion, several structures defined as rift zones have been identified in all constituting volcanoes, and have been either recognised by morphological characteristics (presence of steep ridges) or intrusive characteristics (high density of intrusions). However, early studies are in disagreement with the few recent studies (Chevallier, 1979; Maillot, 1999). In this study, we

focus on the intrusive structures present in the deeply eroded Piton des Neiges volcano. We interpret the field data as regards to the dynamics and potential origin of the rift zones, and use the data collected to compare both edifices of Réunion Island.

### 3.2.2 Geological context

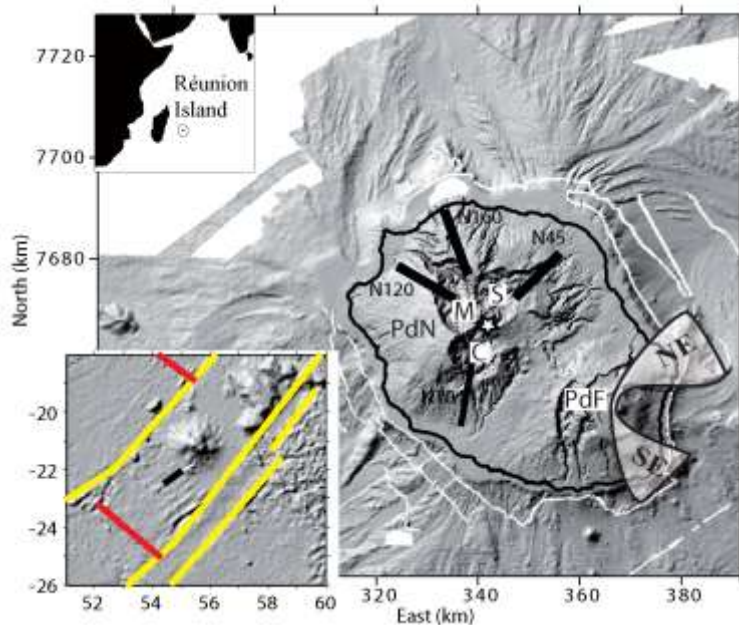


**Figure 3.2-1: Location of Réunion Island in the Indian Ocean, the crustal structures in the surrounding of the island (Dyment, 1991; Michon et al., 2007a), and the rift zones of Piton des Neiges previously described (Chevallier, 1979), and Piton de la Fournaise (Bachèlery, 1981). M: Mafate, C: Cilaos and S: Salazie. The coordinates are UTM (40 south) in km, except for the insert displaying the crustal structures, with coordinates in degrees.**

Piton des Neiges (PdN) and Piton de la Fournaise (PdF) are the two volcanoes creating the island of Réunion, in the south-western part of the Indian Ocean (*Figure 3.2-1*). The two volcanoes are the surface expression of a larger edifice of 220-240 km in diameter and about 7000-7500 m in height. It rests at ~ 4000 - 4500 m b.s.l., on a slightly uplifted oceanic crust (de Voogd et al., 1999; Michon et al., 2007a), of Late Cretaceous / Early Palaeocene age (Dyment, 1991). The crust is organised along two main regional trends (*Figure 3.2-1*): (1) N30° corresponding to the trend of the transform zones in this area of the Mascarene basin (Dyment, 1991), the closest located at about 130 km both north-west and south-east of the island, and (2) N120° corresponding to the direction of magnetic anomalies and paleo-ridges (Dyment, 1991), the closest ridge located at about 400 km south-west of the island. However, there are some anomalies in the immediate surroundings of the island, such as the reorientation of the magnetic anomalies in a N80° direction, east of the island, and the existence of several parallel topographic ridges, trending N55°-60°, south-south-west of the island (*Figure 3.2-1*, Lénat et al., 2001; Michon et al., 2007a), the origins of which remain unknown.

PdN covers two thirds of the island in the north-west, and PdF covers the remaining third in the south-east. The subaerial activity initiated at PdN ~2.1 Ma ago (McDougall, 1971) and lasted until 12 ka (Deniel et al., 1992), most of its deposits preceding the Brunhes-Matuyama magnetic reversal (0.78 Ma) (Lénat et al., 2001). The activity at PdF started ~530 ka ago (Gillot

and Nativel, 1989) and continues at the present time with a high eruptive rate. Drilling and geophysical studies provide insights on the remains of a third, extinct volcano, Les Alizés, located in the extreme south-eastern part of the island, underlying the young deposits of PdF (Rançon et al., 1989; Malengreau et al., 1999). The presence of mainly reversely magnetized rocks belonging to the Matuyama epoch suggest an age anterior to 0.78 Ma (Lénat et al., 2001).

Due to its high eruptive rate (over 25 eruptions in the last 10 years, and over 50 since the opening of the Volcanological Observatory in 1981), PdF has attracted much interest. The activity is organised around its summit area, from which two main NE and SE-trending rift zones radiate (Bachèlery, 1981), as well as a less active N120°-trending rift zone extending both towards PdN in the west and south-east of the summit (Michon et al., 2007a). The rift zones drain, through laterally injected dykes, most of the ascending magma injected from a shallow magma chamber (Necessian et al., 1996; Fukushima, 2005; Peltier et al., 2005). The common eruptive pattern suggests that the magma reaches the summit of the edifice, with opening of eruptive fissures in the summit craters, and then flows laterally within the summit cone, leading to eruptions on the flank or at the base of the summit cone (Fukushima, 2005; Peltier et al., 2005). However, a deep lateral propagation happens in some cases, most of which is related to high-density magma containing much olivine phenocrysts, in opposition to summit eruptions that are mostly supplied with olivine-free magma (Bachèlery, 1999; Peltier, 2007; Letourneur et al., 2008). The volcano has been affected by several volcano-tectonic events, the origin of which is discussed (Bachèlery and Mairine, 1990; Merle and Lénat, 2003; Michon and Saint-Ange, 2008), the most recent one leading to the creation of a horseshoe-shape collapse structure.

In comparison, the dormant PdN has not received much attention in recent years. Petrological studies show that the volcano has undergone a chemical evolution from periods with primarily basaltic magmas to periods with more evolved ones, following the model of evolution for shield volcanoes (Peterson and Moore, 1987), the main transition occurring between 0.43 Ma and 0.35 Ma, which corresponds to a rest period (Deniel et al., 1992). The rest period since the last activity, 12 ka ago, has allowed the erosion of the edifice in three deep cirques (Bret et al., 2003). This erosion has likely been directed by volcano-tectonic structures such as caldera collapses or landslides (Oehler et al., 2008), the deposits of which have been identified both on land and on the submarine flanks (Bachèlery et al., 2003; Oehler, 2005).

Geophysical studies suggest the presence of a large intrusive body, underlying the actual summit, the top of which is located between 1000 m b.s.l. and sea level (Demange et al., 1989; Malengreau et al., 1999). Numerous smaller intrusive bodies have been identified, and are

intruded as small plutons, dykes or sills. Structural studies have revealed the existence of several rift zones, radially organised, along four main directions; N10° in the south, N45° in the north-east, N120° in the north-west and N160° in the north. Note that all directions are given in azimuth from 0° to 180°. A detailed study has covered the Cilaos cirque, and shows contradictory results with the previous studies (Chevallier, 1979; Maillot, 1999). However, no recent studies have covered the whole volcano in detail. Here, we present the results of a detailed study of the three cirques and surrounding deep valleys that cut across over 2000 m of deposits, giving access to the deeper structure of the volcano. From the field data, we infer the structure and origin of the intrusive system that are then compared to the active PdF.

### 3.2.3 The structure of Piton des Neiges intrusive system

This study presents a large set of data on the intrusive system of PdN. The particular topography of the island, deeply marked by erosion (Bret et al., 2003) allows a good overview of the intrusive system. The various characteristics of intrusions, such as strike, dip, thickness and lithology, have been determined wherever possible.

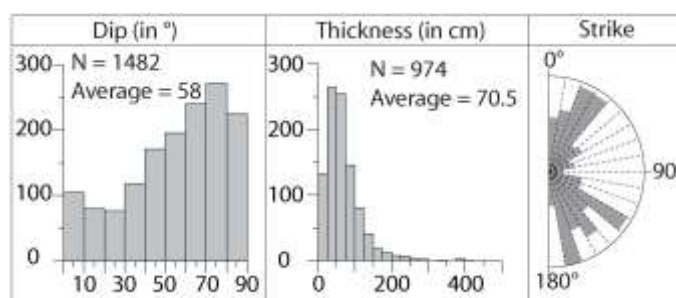


**Figure 3.2-2: Dip, thickness and strike of all measured intrusions in Piton des Neiges.**

As such, measurements do not represent all the intrusions, but the systematic measurements give statistical information, and provide data on the structural evolution of the intrusive system. For this purpose, the data have been studied at several levels, first at the volcano scale, secondly the cirque scale (Cilaos, Mafate and Salazie), and finally by sector of about 1-2 km in diameter. For each of these sectors, an average dip and thickness have been calculated, and compared with the average altitude and distance from the eruptive centre. This comparison allows the determination of an evolutionary trend for each lithology, within the same cirque. It appears that the trends of evolution followed for each lithology are similar to one another. As a result of this, we do not account for the petrology variation when considering this evolution intra-cirque. The absence of a dense set of data in Salazie, due to the prevalence of recent breccia deposits, prevents us giving any relationship between thickness and dip with distance from the eruptive centre, altitude or lithology.

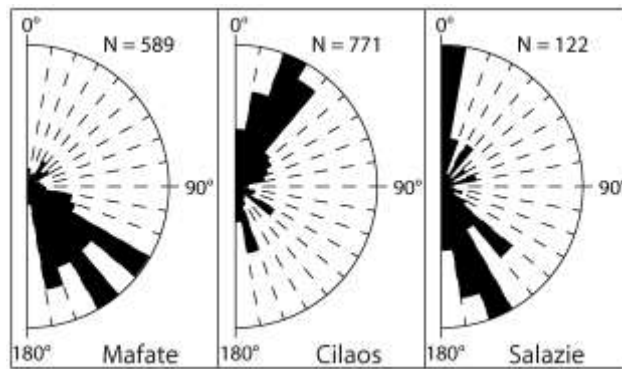


**Figure 3.2-3: Strike distribution of intrusions within each cirque.**

A varying range of rocks has been observed including plutonic and eruptive rocks covering a large range, from the most primitive (gabbro and picritic basalts), to highly differentiated (syenite and trachyte). However, the most common rocks observed are eruptive, including picritic basalts (locally called oceanites, > 30% olivine phenocrysts), olivine basalts (5-30% olivine phenocrysts), and aphyric basalts (< 5% olivine phenocrysts). At the scale of the volcano, contrary to what has been previously proposed (Chevallier, 1979), we identify 3 main rift zones N30°, N120° and N160° (Figure 3.2-2). These trends are partially constrained by the location of the three cirques. The intrusion zone trending N30° is observed mainly in Cilaos, while both rift zones trending N120° and N160° are observed in Mafate, Salazie displaying a N160° as well as a minor N0°-10° trend (Figure 3.2-3). Other trends might not be observed, due to the absence of erosion. However, the presence of surface structures (cones) suggests that no rift zone has been missed. The presence of cones on the ridge between PdN and PdF corresponds to the extension to the south-east of the N120° rift zone. Cones in the western part of PdN suggest the existence of a N30° rift zone, correlated by a submarine ridge (Lénat et al., 2001; Michon et al., 2007a), that is slightly offset from the main N30° rift zone observed in Cilaos.

The dips observed at PdN vary between sub-horizontal intrusions (sills) to sub-vertical (dykes) (Figure 3.2-2), while the mean intrusion thickness is ~0.7 m, similar to that observed in Hawaii (Figure 3.2-2; e.g. Walker, 1987). The mean thickness varies considering the three main lithologies, with a positive correlation between thickness and olivine phenocryst content (Figures 3.2-4; 3.2-5). However, the mean thickness of intrusions within Mafate is higher than in Cilaos. There is also a positive correlation between the lithological nature of an intrusion and the distance of the outcrop from the eruptive centre; olivine and oceanites intrusions are observed preferentially in the distal parts of the intrusive system, while aphyric basalts are the dominant type of intrusion at distance up to 12-13 km (Figures 3.2-4; 3.2-5). The few differentiated intrusions observed are restricted to the central part of the edifice and do not

appear further away than 4-5 km from the eruptive centre. Again, a difference appears between Mafate and Cilaos, with intrusions observed at greater distance from the eruptive centre in the former (*Figures 3.2-4; 3.2-5*). Finally, when considering the dip of intrusions, in relation to the lithology, a negative correlation appears, with a mean dip decreasing from aphyric basalts to oceanites (*Figures 3.2-4; 3.2-5*). Again, Mafate appears singular, with an average dip much higher than in Cilaos. The proportion of one lithology to another is common in both cirques, despite the variations observed above (*Figure 3.2-6*).

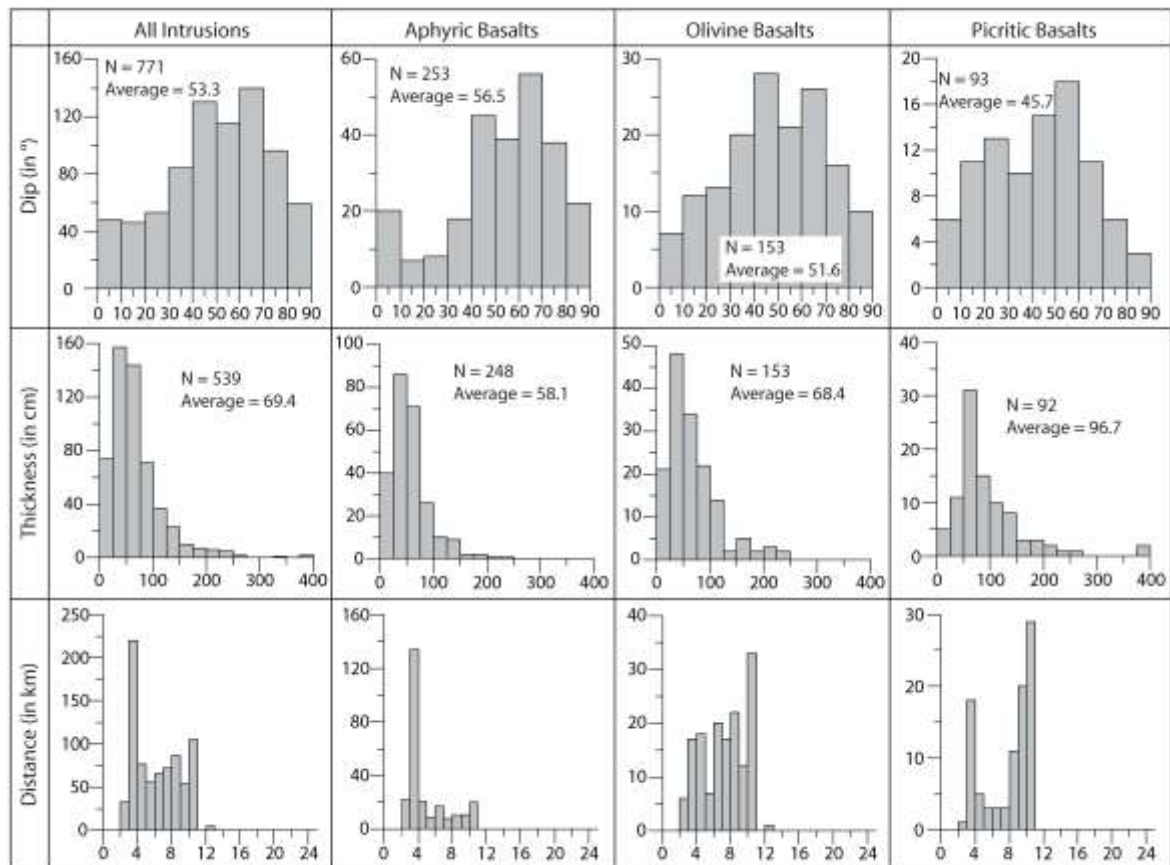


**Figure 3.2-4:** Dip, thickness and distance of all intrusions, aphyric, olivine and picritic basalts, in Cilaos. *The vertical axes correspond to the number of intrusions.*

### ➤ Cilaos

Intrusions measured in Cilaos strike in a majority between N10° and N40°. Two secondary directions are also present, N120° and N160° (*Figure 3.2-3*). The abundance of intrusions striking between N10° and N40° can be explained by the location, south of the eruptive centre. This main trend corresponds to both radial and non radial intrusions (*Figure 3.2-7*), while the secondary trends are non radial. A minor non radial trend, N70° also exists in a confined sector of Cilaos. It is noteworthy that the dip direction evolves within the cirque, with dominant westward dipping to the north-west and eastward dipping to the south-east (*Figure 3.2-7*), suggesting a structure similar to that proposed by Walker (1992). Most of the intrusions are observed up to 11 km.



When considering small sectors of the cirque, and the average dip, thickness, altitude and distance from the eruptive centre for each sector, we can determine an evolution. The average dips tend to decrease with the increase of the distance / decrease of altitude. A similar trend is observed for the evolution of the thickness (*Figure 3.2-8*).

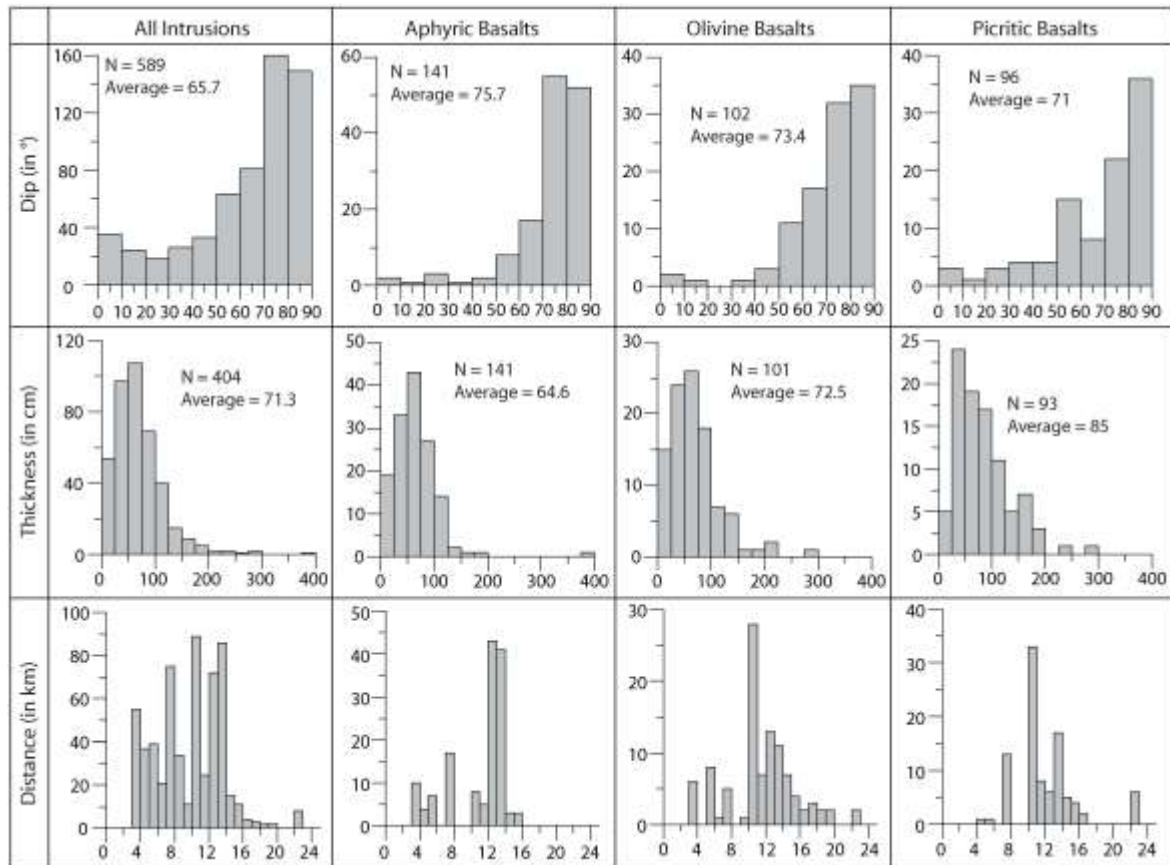


**Figure 3.2-5: Dip, thickness and distance of all intrusions, aphyric, olivine and picritic basalts, in Mafate.** The vertical axes correspond to the number of intrusions.

#### ➤ Mafate

Intrusions here are organised along several main trends, N120°, N145° and N160° (*Figure 3.2-3*). All trends appear to be both radial and non radial. A preferential dip distribution can also be observed, with mainly north-eastward dipping intrusions to the north of the cirque, and south-westward dipping one to the south (*Figures 3.2-9; 3.2-10*). Intrusions are observed at a distance of up to 24 km, and reach the coastline in the north-western part of the island. In contrast to Cilaos, both the average dip and altitude tend to increase with the distance from the eruptive centre / the decrease in altitude (*Figure 3.2-11*).

#### ➤ Salazie

Considering the few data available, and their geographic distribution, no real detailed study can be done. The intrusions observed are organised along three main directions, N0°-10°, N135° and N160° (with a range from N150° to N170°) (*Figure 3.2-3*). While

the  $N0^{\circ}$ - $10^{\circ}$  corresponds to mainly radial intrusions, the other two directions are in majority non radial. Salazie and Cilaos present in comparison to Mafate, a high density of sills, some of which appear as clusters.

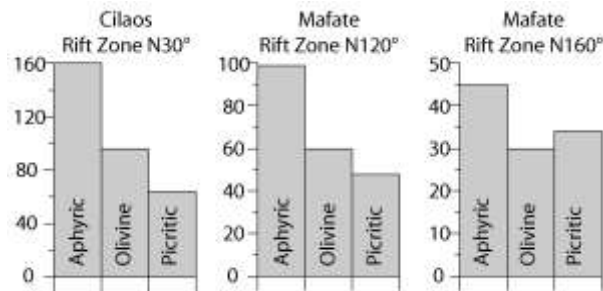


**Figure 3.2-6: Lithology abundance in the various rift zones of Cilaos and Mafate.**

From the field data, it appears that the intrusions in Mafate, Cilaos and Salazie have a distinct behaviour. While it is hard to comment on Salazie, a clear distinction, based on the evolution of parameters such as dip and thickness with distance to the eruptive centre or the altitude, can be done between Mafate and Cilaos. The opposing patterns of evolution suggest that both rift zones are related to specific stress fields, one for the  $N120^{\circ}$  and  $N160^{\circ}$  rift zone, mostly located in the northern and north-western parts of the edifice, and one related to the  $N30^{\circ}$  intrusions in the southern part.

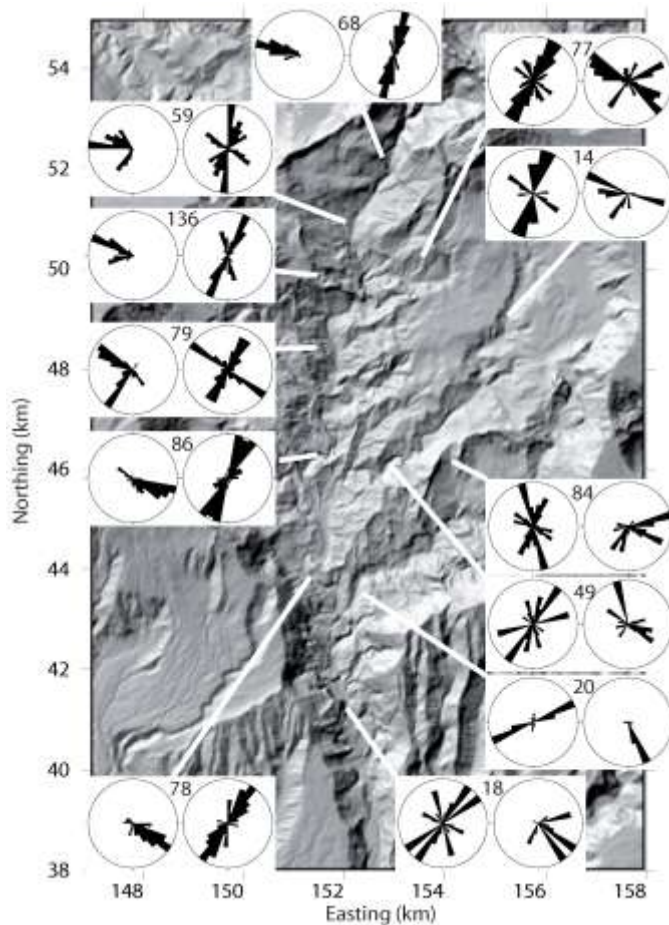


**Figure 3.2-7: Strike distribution within the Cilaos cirque.** The number of intrusions is indicated above each rose diagram. Strikes are represented on the symmetric rose diagram, the dip direction on the non-symmetric ones. Coordinates in Gauss-Laborde Réunion.

### 3.2.4 Dynamics of Piton des Neiges intrusive system

The field data suggests that a strong difference exists between (1) the N30° rift zone in Cilaos, and (2) the N120° and N160° rift zones mostly in Mafate. These differences are mostly characterised by the dip and thickness evolution with the distance to the eruptive centre / the altitude. However, similarities also exist between these rift zones. In each, aphyric basalts, olivine basalts and picritic basalts are observed in remarkably similar proportions (*Figure 3.2-6*). The slightly higher proportion of olivine and picritic basalts in the N120° and N160° rift zones could be a real variation, or be related to the location of outcrops, mainly in the distal part of the intrusive system, where these types of intrusions are more frequent (*Figures 3.2-4; 3.2-5*). Similarly, the absence of distal outcrops in Cilaos could lead to the underestimation of the proportion of both olivine and picritic basalts (*Figure 3.2-4*). Similarities in the lithology of the rift zones and the radial organisation seems to indicate that they are fed by the same batches of magma, most likely located at the junction of the rift zones, underneath the summit. Gravimetric evidence suggests a central magma chamber, underlying the central part of the volcano and slightly elongated in a NE-SW direction (Malengreau et al., 1999). However this trend could be due to the distribution of measurement points, no measurements having been made in Mafate.

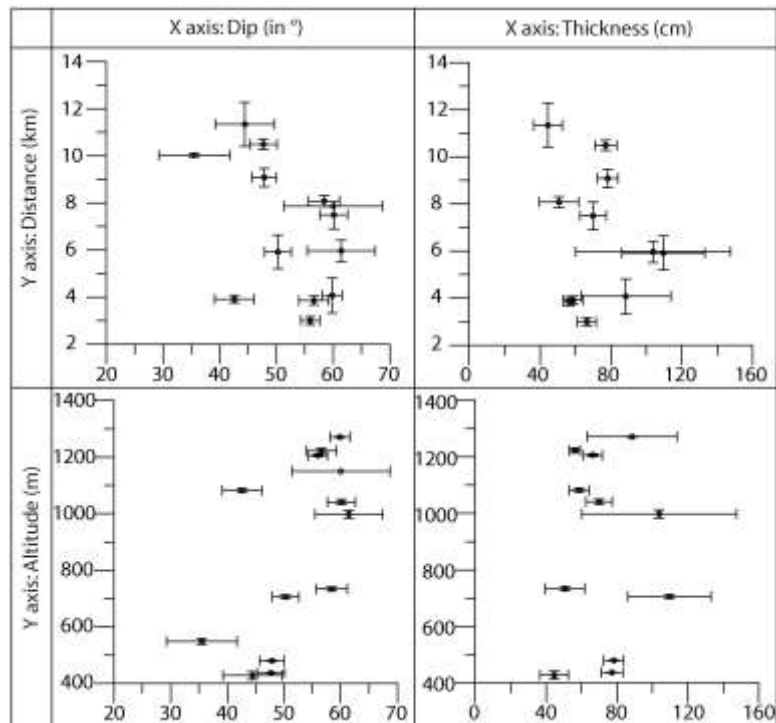


**Figure 3.2-8: Relationship between dip/distance from the eruptive centre, dip/altitude, thickness/distance from the eruptive centre, and thickness/altitude.** Each point corresponds to the averaged data for each of the sectors determined in Cilaos. The standard error is shown for altitude, thickness and dip, standard deviation is shown for the distance. Note that the average dips decrease with distance.

There is also a similar relationship between dip, thickness and the lithology, the only notable differences between Mafate and Cilaos being the average value for each, and intrusions being both thicker and steeper in Mafate. The thickness variation, both between one lithological type to another in the same cirque, and from one cirque to another can meet several explanations, likely combined. The thickness of an intrusion is linked to (1) its overpressure and (2) its length. For a similar overpressure, a large intrusion will be wider than a small one. Therefore, it appears logical that an intrusion propagating far from the eruptive centre will be larger than one propagating in the proximal part. The variation of overpressure can of course explain the difference of thickness. However, olivine rich magmas are denser than olivine free magmas. Hence, olivine rich magmas will be less buoyant than aphyric ones. Such a mechanism is in contradiction with the apparent thickness evolution. Two answers to this can be proposed. The olivine rich magmas are associated with different intrusive mechanisms, originating from a new magma input in the shallow magmatic system, similar to that proposed for the origin of olivine-rich magma in PdF (Bachèlery, 1999). Olivine-rich intrusions appear at lower level than aphyric ones, which tend to limit the buoyancy effect on these olivine-rich magmas, despite their higher density.

As mentioned above, oceanites and olivine basalts generally outcrop at lower altitudes than aphyric basalts, and thus appear further away from the eruptive centre (*Figures 3.2-4; 3.2-5*). This distribution can be interpreted in different ways. It could be argued that an age difference could explain the appearance of aphyric basalts being slightly more evolved than olivine and picritic basalts. However, aphyric basalts are usually associated with the shield construction stage, as are olivine and picritic basalts (Bret et al., 2003). Moreover, the association of olivine or picritic basalts with aphyric basalts and no other types of more evolved rocks suggest a similar age. In addition, at PdF, the same three lithologies are observed, and are all related to the shield stage, and were erupted simultaneously. Considering intrusions of similar age, the various depths of injections might be related to the density of the magma involved. Pinel and Jaupart (2004) propose that lateral injection of magma can occur under certain conditions. The depth of injection depends on several parameters, one of which is the density of the magma, the lighter magmas being laterally injected at higher altitude. Few field indicators such as bubble elongation suggest indeed that dyke propagate mainly laterally. Similar processes of lateral dyke injection are observed in several other cases (Rubin and Pollard, 1987; Fukushima et al., 2005; Peltier et al., 2005; Acocella et al., 2006).

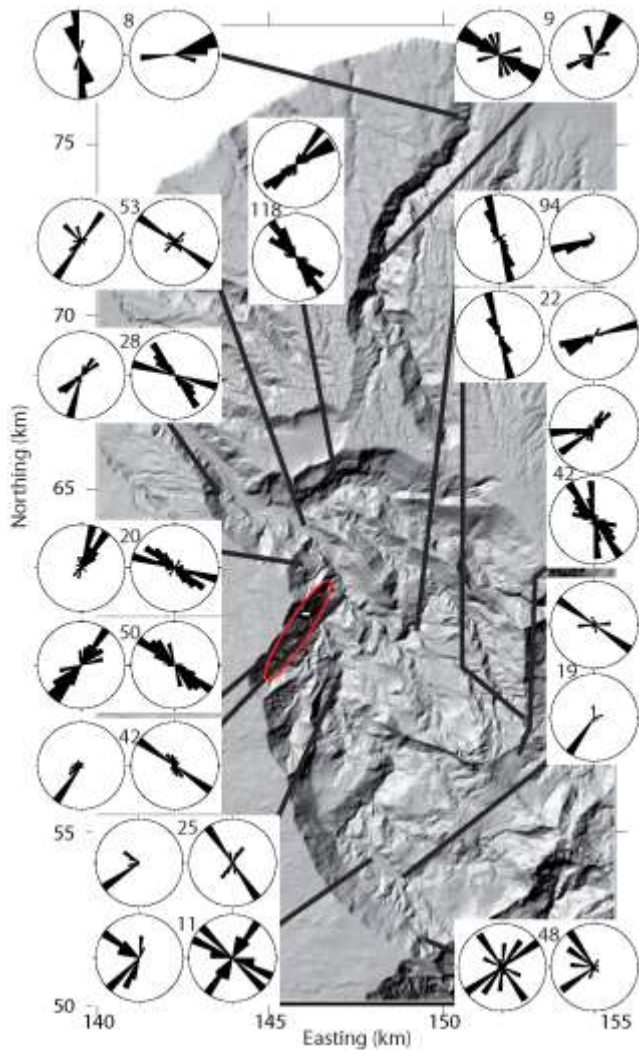
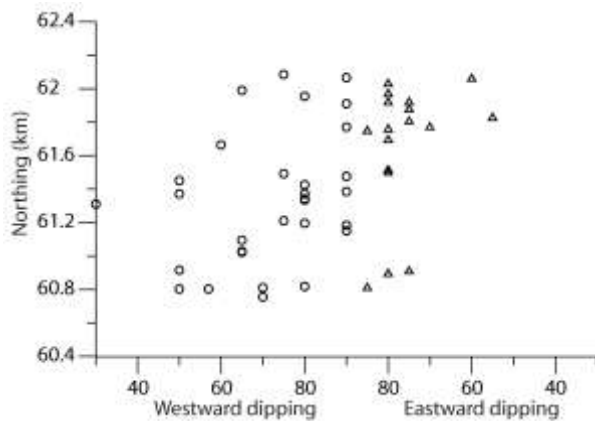


**Figure 3.2-9: Strike distribution within the Mafate cirque.** The number of intrusions is indicated above each rose diagram. Strikes are represented on the symmetric rose diagram, the dip direction on the non-symmetric ones. The red ellipse corresponds to the location of data used in Figure 3.2-10 Coordinates in Gauss-Laborde Réunion.



from westward (circle) to eastward (triangle) dipping intrusions can be observed, corresponding to a wedge structure.

**Figure 3.2-10: Dip of intrusions in a transect perpendicular to the N120 rift zone. A clear evolution**

Despite a common mechanism of lateral intrusion within the various rift zones, the state of stress varies from one to another as suggested by the different dip and thickness in Mafate and Cilaos (Figures 3.2-4; 3.2-5). The data suggest also that intrusions characteristics evolve in opposite ways, with a decrease of both thickness and dip with the increase of distance from the eruptive centre / decrease of altitude in Cilaos (Figure 3.2-8), and an increase of both dip and thickness with the increase of distance from the eruptive centre / the decrease of altitude in

Mafate (*Figure 3.2-11*). The intrusions are ruled by the state of stress within the edifice. The N30° rift zone in Cilaos shows a positive correlation between dip and altitude, or negative concerning dip and distance. The average dip observed in the central part is about 60° suggesting that  $\sigma_1$  was not vertical but rather inclined. The further away the intrusions propagate the shallower their dip becomes, similar to what has been observed in several places (Gautneb and Gudmundsson, 1992; Klausen, 2004; 2006). Such a change of the dip is also well known from hydraulic fracturing experiments (Valko and Economides, 1995). It is related to the decrease of the magmatic stress field, and the proportional increase of the influence of the gravitational stress field. At the free surface,  $\sigma_1$  is parallel to it (Cayol and Cornet, 1998b; Letourneur et al., 2008) which can explain the decrease of the dip. Similarly, the presence of landslide structures in the western part of the edifice (Lénat et al., 2001; Bachèlery et al., 2003; Oehler et al., 2004) might also perturb the stress field. The apparent contradiction between the thicknesses decreasing with the distance while thicker picritic are more abundant away from the eruptive centre (*Figures 3.2-4; 3.2-8*) is to be related with the relative abundance of aphyric intrusions, dominant in both proximal and distal parts of the cirque, reducing the effect linked with the lithological differences.

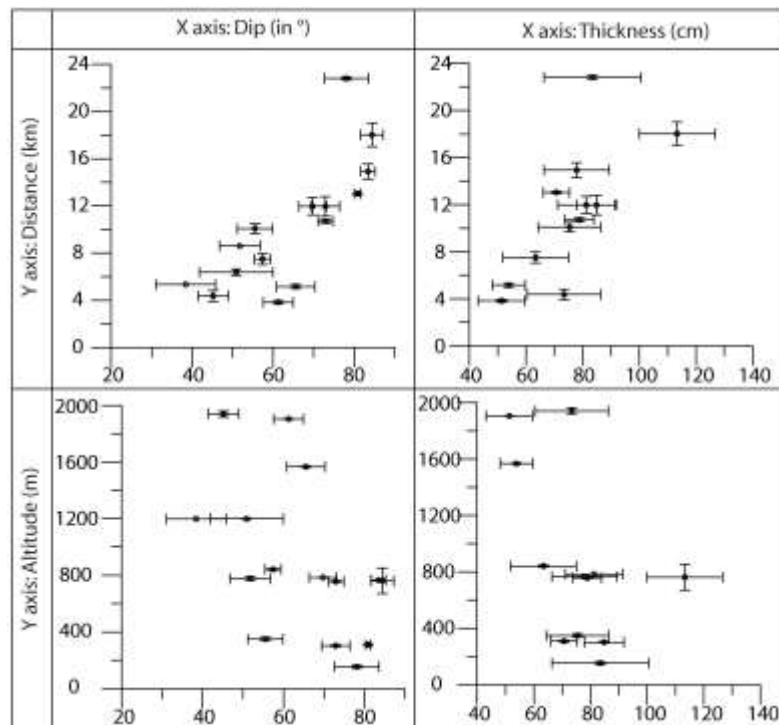


**Figure 3.2-11: Relationship between dip/distance from the eruptive centre, dip/altitude, thickness/distance from the eruptive centre, and thickness/altitude.** Each point corresponds to the averaged data for each of the sectors determined in Mafate. The standard error is shown for altitude, thickness and dip, standard deviation is shown for the distance. Note that the average dip increases with distance.

Observations in Mafate suggest that the evolution is opposite to that in Cilaos with an increase of both dip and thickness with the increase of distance / decrease of altitude (*Figure*

3.2-11). This is observed in both the N120° and N160° rift zones. Data along a profile at similar altitude show that the dip variation is mainly related to the distance from the eruptive centre, while at similar distances, variation of dip versus altitude is opposite to that observed at the cirque scale. The dip evolution suggests that the stress field in the central part presents a dip of about 50-60° and is more inclined than that in the rest of the rift zone. The magmatic stress field, while influential in the central part, will become ineffective further away in the rift zone, the dyke being 'captured' by the stress field of the rift zone. Similar processes happen at larger scales in Iceland, where the stress field of the central volcano has a limited impact in space (Gautneb and Gudmundsson, 1992; Klausen, 2004; 2006). In Cilaos, the stress field in the rift zone is strongly influenced by surface stresses (and thus shows shallow dips), while in Mafate the stress field presents a  $\sigma_1$  almost vertical.

We propose here that the stress field present within Mafate, affecting both N120° and N160° rift zone, is likely inherited from a deeper structure, as the N120° is a direction characteristic of the whole island (*Figure 3.2-1*; Michon et al., 2007a). Under the pressure of the mantle plume, the anisotropic crust will favour the injection of magma along the already existing weakness (Carracedo, 1994). In the crust, anisotropies are related with the dynamic of paleo-ridges that strike N120° in this area of the Indian Ocean. However, as the anisotropies are only diffused in the crust, their effect will only be limited, leading to the creation of a stress field favourable to magma injection over a wide area, and elongated in the N120° direction. Similarities between the N120° and N160° rift zones, and their geographical proximity, suggest that the latter is influenced by the stress field ruling the N120° rift zone, rather than corresponding to a deeper structure.

The origin of the N30° intrusion zone, with a stress field localised and superficial, can result from the existence of the N120° rift zone. Repeated injections of magma lead to an increase in the horizontal compression in the surrounding areas, especially in the case of an edifice hardly affected by any spreading. This increased compression can lead to a rotation of the stress field, favouring the injection in a direction perpendicular to that of the main rift zone (Michon et al., *in press*). Once a few injections have occurred, the path will be favoured for latter injection (e.g. Walker, 1999). The initiation of activity along the N120°-N160° complex, as the oldest intrusive system in Réunion (McDougall, 1971; Gillot et al., 1994) supports this model, that the N30° rift zone is a result of the repeated activity along the N120° and N160° rift zones.

### 3.2.5 Comparison with Piton de la Fournaise

PdF rift system dynamics is relatively well constrained, with a vertical flow of magma along a central conduit, which join a shallow magma chamber to the summit craters (Nercessian et al., 1996; Sapin et al., 1996; Peltier et al., 2005). This conduit is used during most of the eruptions that occur in the summit crater or on the flanks of the summit cone, for which magma injects laterally at shallow level along the rift zones (Fukushima, 2005; Peltier et al., 2005). These eruptions are represented mostly by aphyric magma, while eruptions occurring further away from the central cone, along the rift zones, are represented mostly by olivine and picritic basalts. This is observed in the recent activity as well as in the intrusions outcropping in the cliffs of the Enclos – Grand Brule structure (Peltier et al., 2006a; Letourneur et al., 2008). Present activity suggests that these olivine-rich injections do not rise high in the volcanic structure, but rather propagate at depth (Bachèlery, 1999; Peltier et al., 2006a), leading to a stratification similar to that observed in the rift zone of the neighbouring PdN. Seismic data also suggest that the rift zones extend laterally at both shallow and deeper levels (Brenquier et al., 2007).

The dip evolution across the NE-trending rift zone suggests that the dip range observed are similar to that of the N120° and N160° rift zone, suggesting that the stress field within the rift zone is not only of magmatic origin. The existence of an old rift zone striking in a similar direction, and related to the previous Les Alizés volcano (Lénat et al., 2001), can generate a local stress field leading the injection. In this case, it is possible that the present rift zones at PdF are partly inherited from a deeper structure.

### **3.2.6 Conclusions**

Field measurements of over 1400 intrusions in PdN lead us to reconsider the rift zones previously described in this volcano. We highlight the presence of at least three rifts zones striking N30°, N120°, N160°, in an organisation highly dissimilar to that of the traditional three branch rift zones observed in other locations (Carracedo, 1994). PdN rift zones appear to be fed by a common magma chamber, located at the junction of the rift zones, under the summit. The magma within the rift zones is injected laterally, at depths which are dependent on the density of the magma. Light magma, in similar dynamics to PdF, probably reached the surface in the central part, initiating a summit eruption that prevents long distance lateral propagation. Denser magmas, propagating at depth, conserve an overpressure sufficient allowing a distal propagation. The absence of evolved material in the outer part of the rift zones suggests that they have been active only during the basaltic stage, the differentiated stage characterised by central volcanism (Chevallier, 1979).



However, considering the evolution of intrusion properties, two groups can be defined as follows: (1) intrusions in Cilaos, striking mostly N30° and (2) intrusions in Mafate but appearing also in Salazie, striking N120° and N160°. These groups represent two different stress fields dictating the injection of magma within the island. We propose that both are ruled by the existence of two distinct stress fields; a magmatic one controlling the injection in the proximal part of the magmatic path and a gravitational or structural one influencing intrusions in the distal part. The differences observed between Cilaos and Mafate reflect the differences in the origin of this second stress field that is inherited from a crustal structure in Mafate, and is of gravitational origin, and strongly influenced by the surface stress field in the case of Cilaos.

The rift system at PdF suggests a similar injection mechanism with lateral injection of magma, the altitude of which is controlled by the magma density. It also appears that the rift zones at PdF might not only result from a gravitational process as previously suggested (Walter et al., 2006), but might be partially inherited from an older existing rift zone.

### **Acknowledgements**

The authors wish to thank Laurent Michon for comments on the data, and Ruth Andrew for helpful comments on the manuscript.

### **3.3 A specific aspect of Piton des Neiges structure: the occurrence of sills: Paper 2**

A study of the internal structure of Piton des Neiges has revealed the existence of a large amount of sills, outcropping either individually or at major contacts. Previous studies at Piton des Neiges had already mentioned the existence of sill complexes (Maillot, 1999). However, the analogue modelling done did not reproduce the sill injection despite the consideration of mechanical contrasts (Maillot, 1999). Similarly, several earlier studies explain the existence of sills, but at rigidity contrasts of a setup opposite to that observed in Piton des Neiges (e.g. Rivalta et al., 2005; Kavanagh et al., 2006). This study has been submitted to the *Journal of Volcanology and Geothermal Research*, and is presented below.

## **The origin of sill level at Piton des Neiges Volcano (Réunion Island): Field evidence and numerical modelling**

Ludovic Letourneur<sup>a</sup>, Laurent Michon<sup>b</sup>, Agust Gudmundsson<sup>c</sup>

<sup>a</sup> University of Göttingen, Geosciences Centre, Department of Structural Geology and Geodynamics, Goldschmidtstrasse 3, 37077, Göttingen, Germany

<sup>b</sup> Laboratoire GéoSciences Réunion, Université de la Réunion, Institut de Physique du Globe de Paris, CNRS, UMR 7154 – Géologie des Systèmes Volcaniques, 15 avenue René Cassin, 97715 Saint Denis, France.

<sup>c</sup> Department of Earth Sciences, Queens Building, Royal Holloway, University of London, Egham, Surrey, TW20 0EX, UK

### **Abstract**

Piton des Neiges volcano is a deeply eroded oceanic shield volcano on the island of Réunion. Extensive field work within the deep valleys and cirques revealed the existence of a well developed intrusive system with three dominant directions, N30°-40°, N120° and N160°. Alongside steeply dipping dykes, shallowly dipping and sub-horizontal sills are also present. These two main types of sills are observed in well defined settings; the first in the rift zone, at distance from the eruptive centre, while the second are mostly observed closer to the eruptive centre, within or close to the rift zones. They can both be characterised by their strike, parallel to that of the rift zone for the shallowly dipping sills and in the case of sub-horizontal sills, mostly perpendicular to the rift zone. Sub-horizontal sills are also characterised by the presence of clusters at preferential contacts between a comparatively stiff layers underneath (intrusive bodies or the lava pile), and overlaid by a comparatively soft layer (breccia). Here, models are presented to explain the origin of sills at Piton des Neiges. The results show that shallowly dipping sills find their origin in a combination of two effects, the decrease of magmatic influence (both overpressure and the magma chamber related stress field) and the comparative increase of the gravitational stress field, which can, close to the surface, be favourable to sill injection. Weak contacts, such as the ones between lava flows and scoria layers, favour the injection of sills under these conditions. Clusters of sub-horizontal sills, at contacts from stiff to soft layers, are in contradiction with previous models for origin of sills. We suggest that sill clusters occur at the base of a soft and partially plastic layer, such as landslides breccia. During periods of increased compression within the rift zone, such breccia might act again as a mechanical barrier and lead to the creation of a second generation of sills.

### 3.3.1 Introduction

Volcanic eruptions require the transport of magma from a magma chamber to the surface through, usually, sub-vertical dykes. However, it is well known that magma injections may become arrested at depth in the volcano or, alternatively, intrude sub-horizontally as sills (e.g. Lister and Kerr, 1991; Gudmundsson, 2006), concordant with the surrounding bedding, and usually fed by dykes (Lister and Kerr, 1991; Gouly, 2005). The magma migration is controlled by the state of stress within the volcanic edifice. Normally, the maximum principal compressive stress ( $\sigma_1$ ) is vertical, and the minimum principal compressive stress ( $\sigma_3$ ) horizontal, encouraging the vertical propagation of magma. The circumstances under which magma injects horizontally as sills are still not well understood. Holmes (1965) suggested that a level of neutral buoyancy (LNB) exists within the edifice which favours the arrest of vertical dyke propagation and the initiation of sills (Lister and Kerr, 1991). Further to this, field evidence from continental areas suggest that sills often occur in sedimentary rocks (Mudge, 1968; Johnson and Pollard, 1973; Pollard and Johnson, 1973; Barker, 2000) of a density less than that of the sill-forming magma.

A second model, mainly developed through numerical modelling using field data as boundary conditions, suggests that mechanical contrast (particularly as regards Young's modulus) at contacts can favour the reorientation of principal stresses, with  $\sigma_3$  becoming vertical and thereby favouring either the arrest of a dyke on meeting the contact or, alternatively, the horizontal injection along the contact whereby the dyke changes into a sill (Gudmundsson, 2006). Similar models have been suggested by several authors, using results from analogue and numerical modelling and field studies. A large favourable contrast in rigidity, that is a low-to-high rigidity contrast, is necessary to explain the existence of sills (Rivalta et al., 2005; Kavanagh et al., 2006).

In basaltic edifices, particularly oceanic islands, sills have not been widely reported. This might reflect the potential difficulty to distinguish sills from lava flows. Also, the difference between sills and low-dipping, inclined sheets is somewhat arbitrary, so that many sills may be referred to as inclined sheets. For example, shallow dipping intrusions are commonly described in an oceanic context as intrusive sheets (Walker, 1992) and related to slow spreading volcanoes with high injection rates. Other descriptions of low-dipping sheets or sills are, for example, from the islands of La Palma and La Gomera, in the Canary Islands (Staudigel et al., 1986; Fernández et al., 2002; Ancochea et al., 2006). In La Palma, sills are observed essentially in the basal complex, constituting the seamount series, and are older than the erosion

unconformity marking the transition between the seamount series and subaerial series (Staudigel et al., 1986; Fernández et al., 2002). In La Gomera, sills are mainly observed in the older part of the edifice within volcanic breccias and volcanic agglomerates (Ancochea et al., 2006).

Our field observations in the deeply eroded Piton des Neiges volcano (Réunion Island) suggest that its intrusive system is composed primarily of sub-vertical dykes and sub-horizontal sills. In this paper we combine the results of field studies of dykes and sills with numerical models in order to explain why sills are so abundant in the lava pile and the mechanics of emplacement. We focus on the effects of mechanical contrast between the geological units (breccias and lava flows) in the development of suitable conditions for the formation of sills within the edifice.

### 3.3.2 Geological context

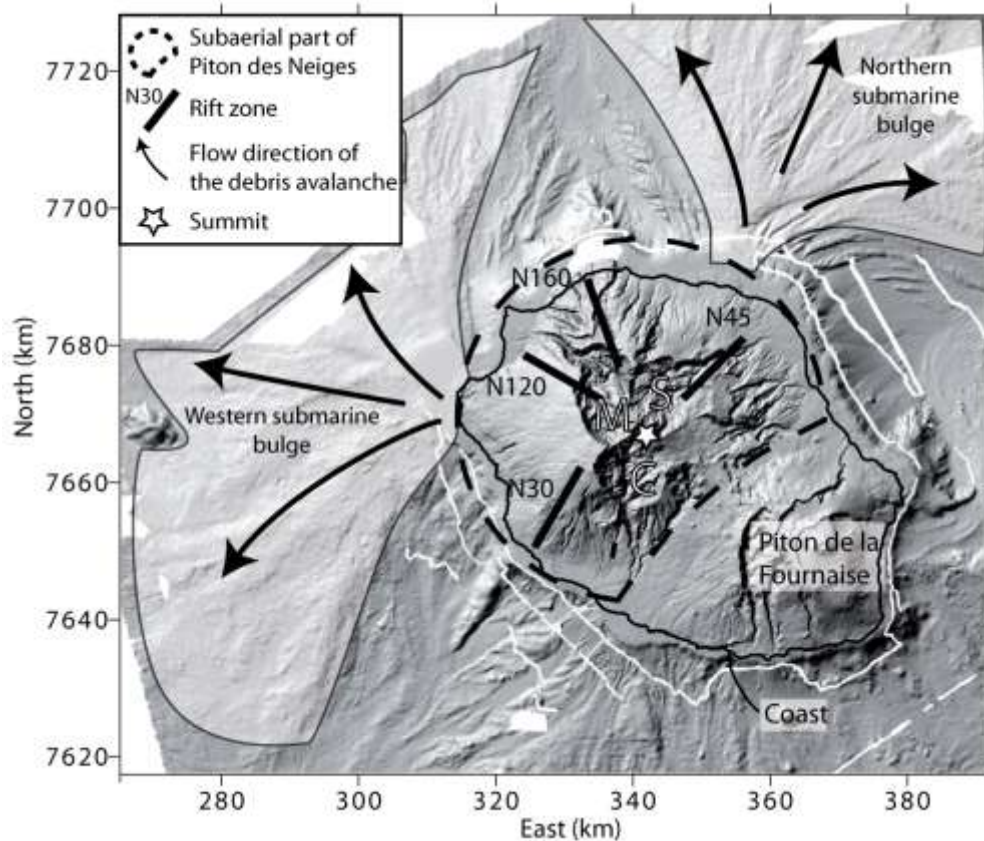


**Figure 3.3-1: DEM of the submarine and subaerial part of Réunion Island.** *M = Mafate Cirque, C = Cilaos Cirque, S = Salazie Cirque.* The main directions of intrusions as defined by Chevallier, (1979) are marked. The dashed line corresponds to N10 intrusion axis. The submarine bulges are determined according to Oehler et al., (2004). Coordinates in UTM zone 40S.

Réunion Island is composed of two subaerial volcanoes, Piton des Neiges and Piton de la Fournaise, lying at ~4000 m b.s.l. on an 80-Ma-old oceanic lithosphere, in the south-western part of the Indian Ocean (Figure 3.3-1). Piton des Neiges (PdN), which is currently inactive,

forms the north-eastern two-thirds of the island. It has a strongly dissected morphology due to powerful erosion. The extreme development of amphitheatre-headed valley erosion along potential volcano-tectonic structures has led to the formation of three large cirques, Cilaos, Mafate and Salazie, providing access to the interior of the upper 2500 m of the volcano (*Figure 3.3-1*). Geochronological data suggest that the subaerial stage of construction started at  $\sim 2.1$  Ma (McDougall, 1971). Combining dating and petrological studies, it has been shown that the magmas have evolved with time, from picritic and aphyric basalts to differentiated series composed of mugearite and a few trachytes (Upton and Wadsworth, 1965; McDougall, 1971). The transition between the initial basaltic and differentiated periods occurred between 0.43 and 0.35 Ma.

Gravimetric data (Malengreau et al., 1999) and a deep borehole cored in the central part of the massif (Demange et al., 1989) revealed the presence of a large solidified NE-SW trending intrusive complex underneath the present 3071 m-high summit. The intrusive body locally outcrops at 700-900 m a.s.l. where it corresponds to a layered gabbro (Upton and Wadsworth, 1972). Four rift zones trending  $N10^\circ$ ,  $N45^\circ$ ,  $N120^\circ$  and  $N160^\circ$  were initially described as connected to the intrusive complex (*Figure 3.3-1*; Chevallier and Vatin-Perignon, 1982). Additional structural (Maillot, 1999) and geophysical (Lénat et al., 2001) studies in the southern half of PdN do not support the existence of a  $N10^\circ$  rift zone but rather that of an old, narrow rift zone trending  $N30^\circ-40^\circ$  both in the southern subaerial and submarine parts of the edifice.

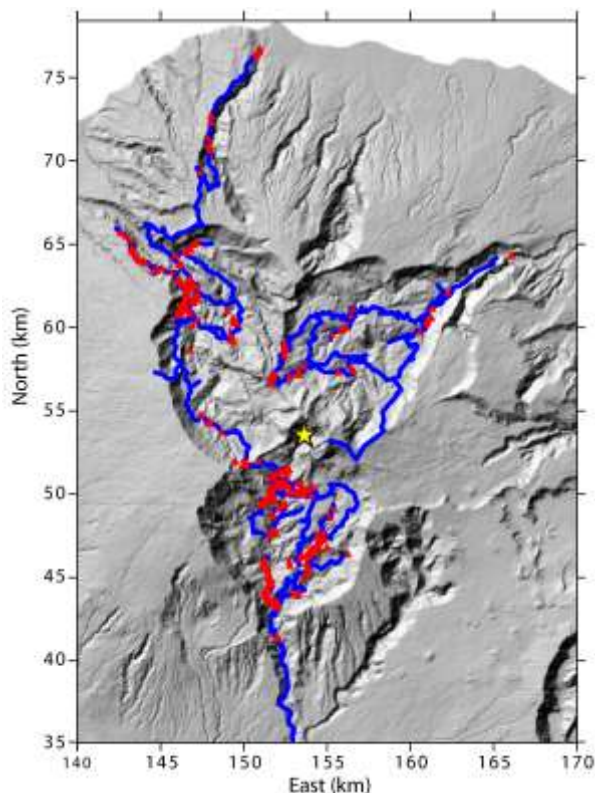


**Figure 3.3-2: Location of measured intrusions (triangle), and area studied (line). The star marks the supposed eruptive centre in Rond de Bras Rouge.**

As many volcanoes worldwide, PdN has undergone several massive flank collapses, the debris avalanche deposits of which were recognised both in the subaerial and submarine parts of the edifice (Bachèlery et al., 2003; Bret et al., 2003; Oehler et al., 2004). They develop from the central part toward the north and the west and have formed large submarine bulges on the flanks of the edifice (*Figure 3.3-1*; Oehler et al., 2004).

### 3.3.3 Field data

We present here a large set of field data which were collected in the three cirques and some of the deeply incised valleys (*Figure 3.3-2*). Field observations allow the distinction between two main types of intrusions. Plutons are relatively rare. They outcrop in Cilaos and Salazie at about 700-900 m a.s.l., and at a maximum distance of 5 km from the volcanic centre assumed to be located in Rond de Bras Rouge (*Figure 3.3-2*). They constitute essentially homogeneous bodies whose thicknesses vary between a few tens to a few hundreds of meters. They consist of gabbros and syenites that are related to the basaltic and differentiated magmatic periods.

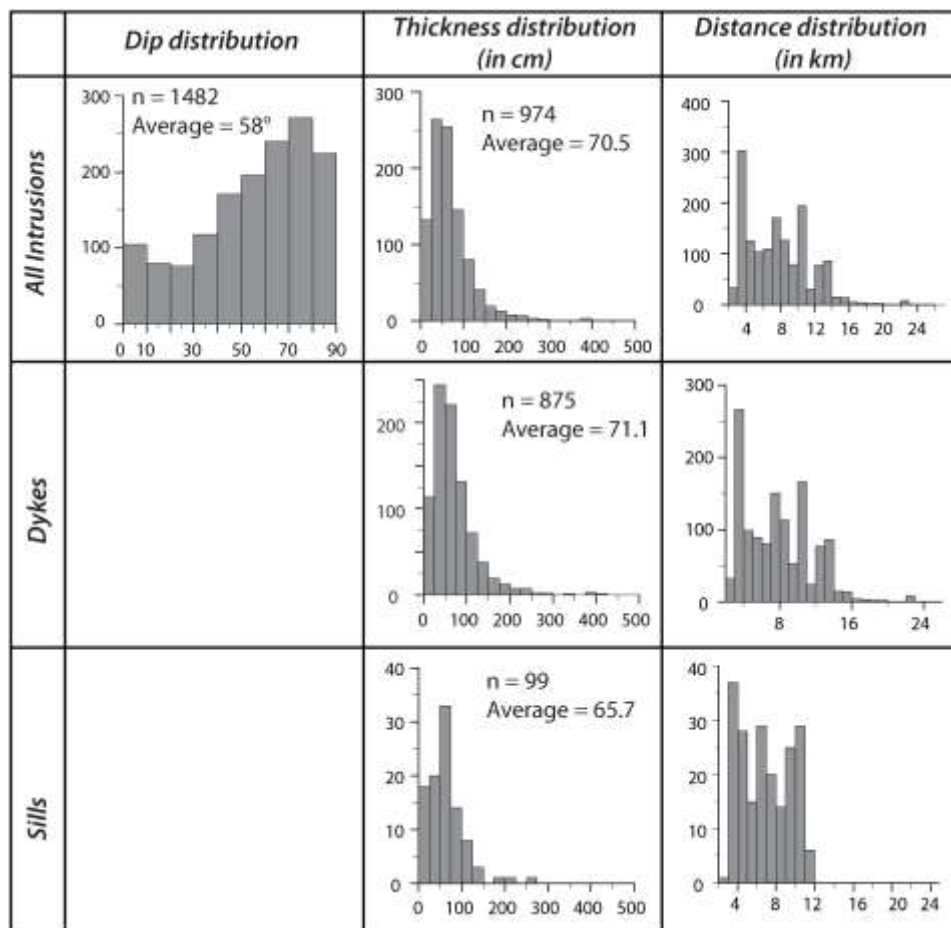


**Figure 3.3-3: Histograms for dip, thicknesses and distance from the eruptive centre of all intrusions, dykes and sills.** *The vertical axis corresponds to the number of intrusions.*

By contrast, thin sheet-like intrusions (< 5m, *Figure 3.3-3*) are very common and range from vertical dykes to sub-horizontal sills. The distinction between sills and dykes is here fixed from

the concordance or near-concordance with the lava pile. From field evidence, and considering the dip distribution of 1482 intrusions (*Figure 3.3-3*), we consider the bimodal dip distribution and the low frequency observed between 20°-30° to determine sills from dykes, intrusions with a dip lower than 30° are regarded as sills and those with a dip greater than 30° as dykes. The magma feeding the sills and dykes ranges from relatively primitive composition with more than 35% olivine phenocrysts to differentiated magmas such as benmoreite and trachyte (Upton and Wadsworth, 1965). The most common lithological types observed in the field are picritic basalt, olivine basalt, and aphyric basalt.

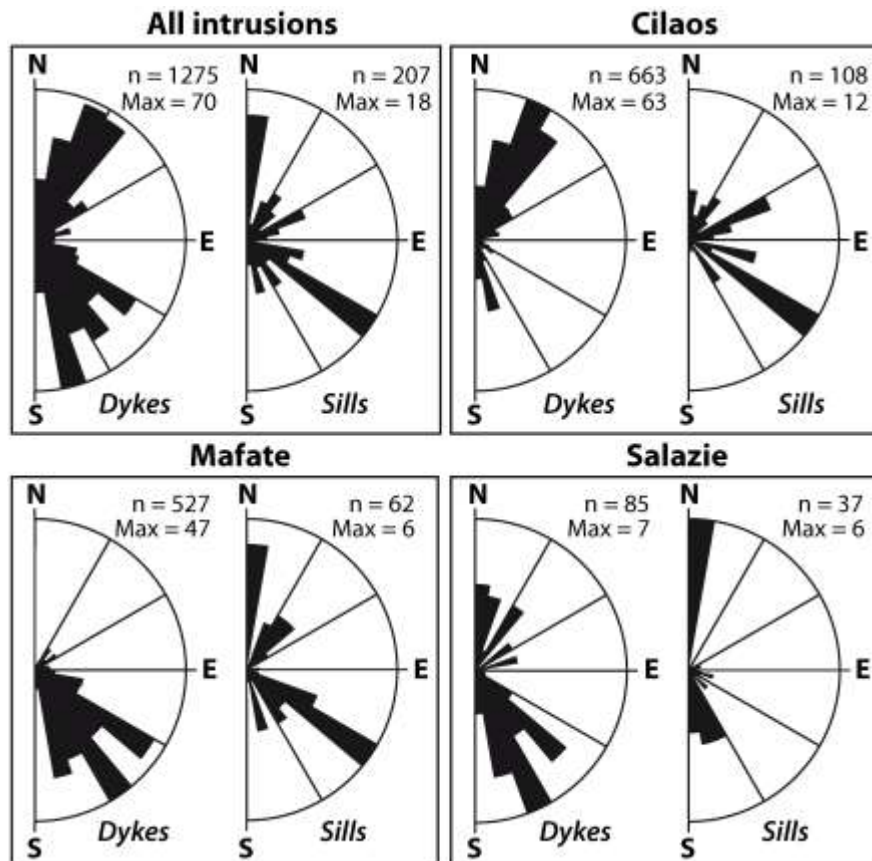


**Figure 3.3-4: Strike distribution for dykes (with dip higher than 30°), and sills (with dip lower than 30°) for all intrusions measured in Piton des Neiges, and according to their geographical distribution in the three main cirques Cilaos, Mafate and Salazie.**

The strike distribution of the various intrusions suggests the existence of preferential injection paths or intrusion zones (*Figures 3.3-2; 3.3-4*). In these zones, multiple or closely spaced parallel dykes are common, indicating that older dyke paths create weaknesses offering comparatively little resistance to new magma injections (*Figure 3.3-5 – Walker, 1992*). The strike of sills is mostly similar to that of dykes, although some sills strike perpendicular to adjacent dykes (*Figures 3.3-4; 3.3-6*).



**Figure 3.3-5:** Example of dykes and side-by-side dykes within the preferential intrusion path in Mafate. The outcrop is located at about 13 km from the eruptive centre and at about 250 m a.s.l.

The thickness of the dykes and sills is fairly uniform with a mean value of 70.5 cm (*Figure 3.3-3*). This is similar to the mean values of dykes (Walker, 1987) and sills (Ryan et al., 1983), thicknesses in Hawaii, but half the average dyke thicknesses in many other regions such as Iceland, the Canary Islands and Etna (Walker, 1987; Marinoni and Gudmundsson, 2000; Marinoni, 2001; Gudmundsson, 2002). It is noteworthy that sills are usually thinner than dykes (*Figure 3.3-3*), while examples from La Palma and other areas worldwide indicate that sills are commonly thicker than dykes (Staudigel et al., 1986). Dykes occur over a wide area, from the inner part of the volcano out to a distance of 24 km from its centre, whereas sills occur only within 11 km of the centre (*Figure 3.3-3*), and most are located close to the axis of the intrusion zone. The elevation of the measured outcrops is from 100 m a.s.l. to 2000 m a.s.l.

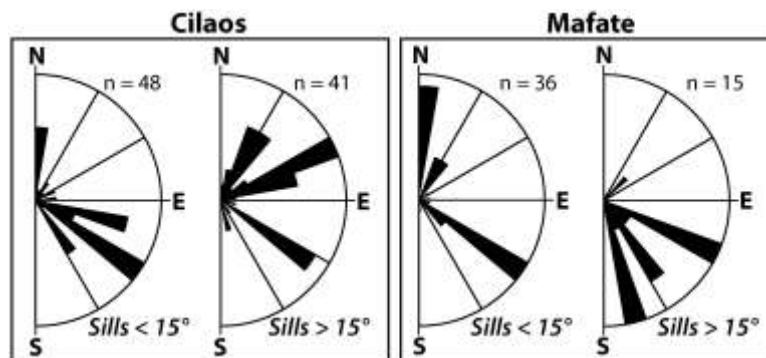


**Figure 3.3-6:** Strike of sills with dip lower than  $15^\circ$  and higher than  $15^\circ$  for Cilaos and Mafate. Compared to the strike of rift zone, it appears that shallow dipping sills (lower than  $15^\circ$ ) display strike almost perpendicular to that of the radial rift zones.



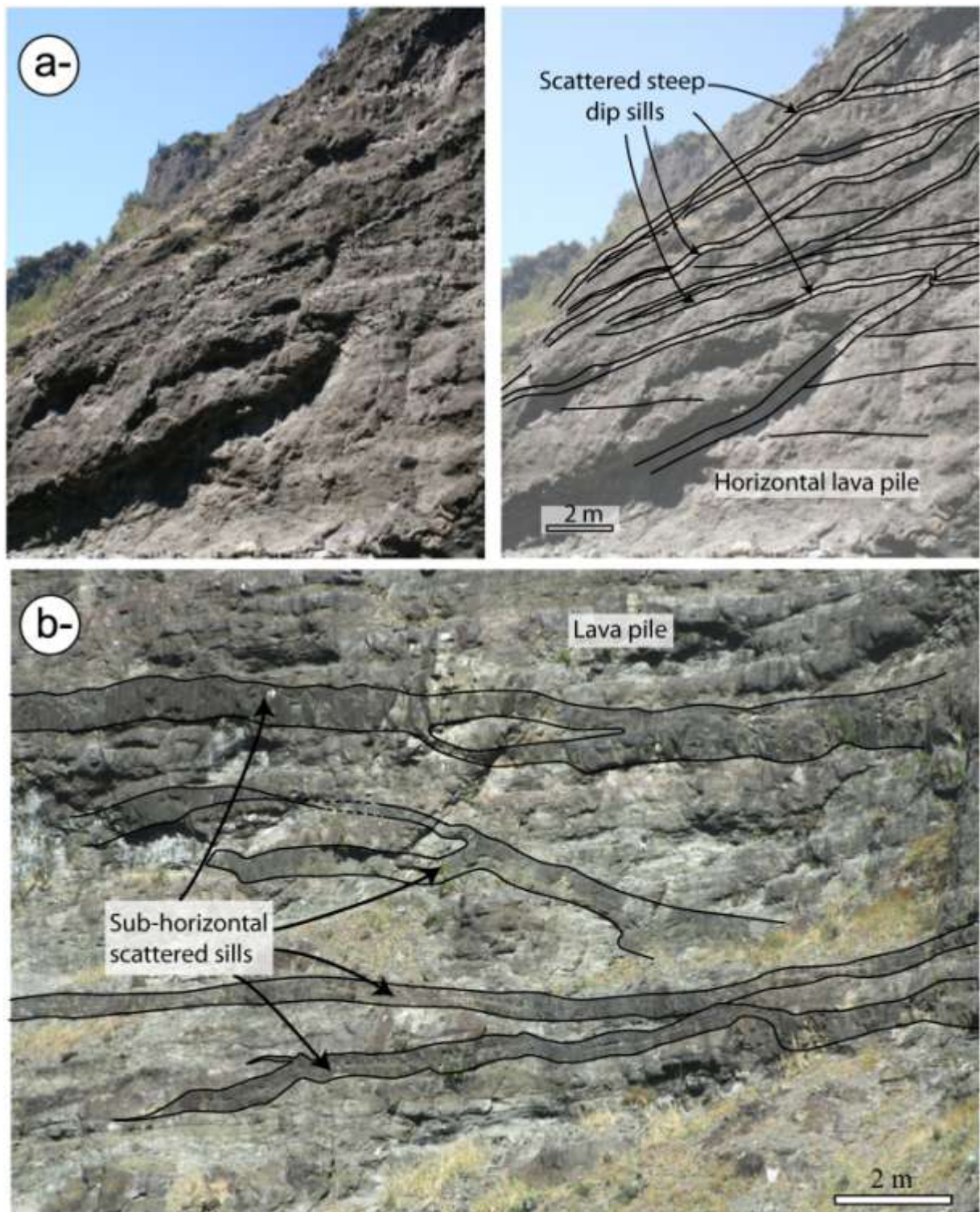


**Figure 3.3-7: Example of scattered sills within the lava pile.** A- The outcrop is located in Cilaos at about 10 km from the eruptive centre, and at about 400 m a.s.l. Here the intrusions are dipping at about 20°-25° and cross cut the lava pile. B- Scattered subhorizontal sill perpendicular to the contact between lava units.

Based on the outcrops, and relationship between sills, it is possible to differentiate between two main groups of sills. The first group (type A) consists of scattered sills, intruded within the lava pile or breccia units (*Figure 3.3-7*), while the second group (type B) consists of sills, grouped in clusters, and intruded along contacts (*Figures 3.3-8; 3.3-9*). Type A, while mostly

composed of single scattered sill units, can occasionally form clusters, normally with 5 or fewer sills. The sills dip up to  $30^\circ$ , strike parallel with the nearby rift zones, and occur primarily in the distal parts of the of the area containing sills. They usually outcrop within a pile of lava flows with a low to medium grade of compaction, and can be whether concordant to the lava pile or cross cut lava flows unit. However, in this case the difference of dip is usually low.

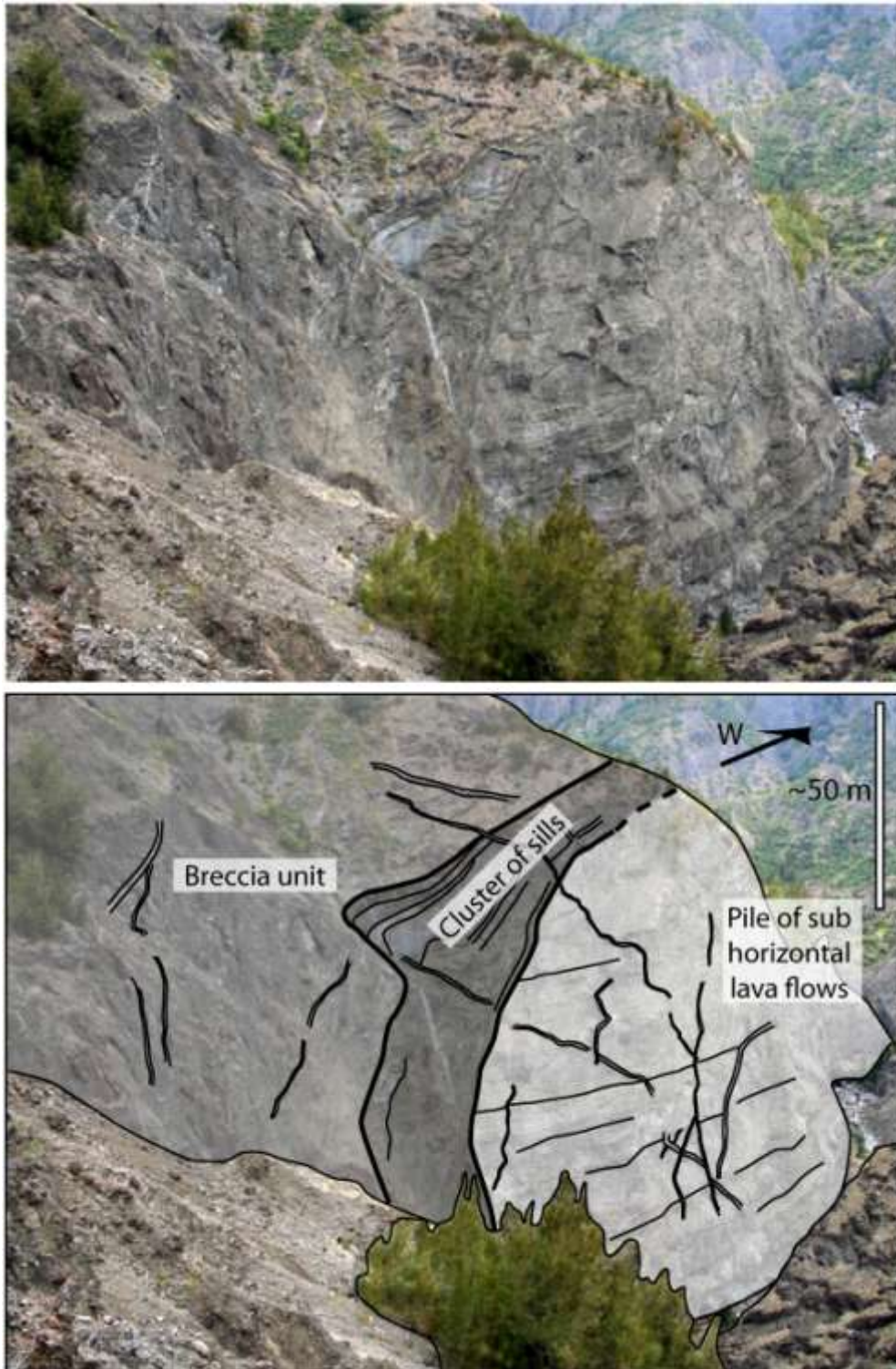


**Figure 3.3-8:** Example of a sill cluster intruded at a contact between a breccia unit overlying the lava pile. The outcrop is in Cilaos, at about 6-7 km from the eruptive centre and close to the axis of the rift zone  $N30^\circ-40^\circ$ .

The second type, B, is composed of sills that intrude at major contacts, the nature of which varies: some are between two breccia units; others are between a breccia unit overlying lava flows (*Figure 3.3-8*) or occasionally, a gabbroic body. The common feature of these contacts is the presence of a soft (low Young's modulus) layer overlying a stiffer (high Young's modulus) layer. The breccia units are usually thick (tens of meters) and constituted of angular elements. In some well exposed breccia, blocks display jigsaw cracks typical of debris avalanche deposits (DAD). The dip of the cluster of sills is subsequently dependent on the geometry of the contact. Observations reveal that they are usually characterized by shallow dip ( $<15^\circ$ , *Figure 3.3-8*), but they can exceptionally present higher dip values when the contact is oblique to the slope of the pre-existing formations (*Figure 3.3-9*). They usually tend to be confined to the central area of the volcano. According to the degree of alteration of sill units, several generations of sill might exist within a same cluster (*Figure 3.3-9*). However, the difference of alteration can also only reside in the difference of petrology.

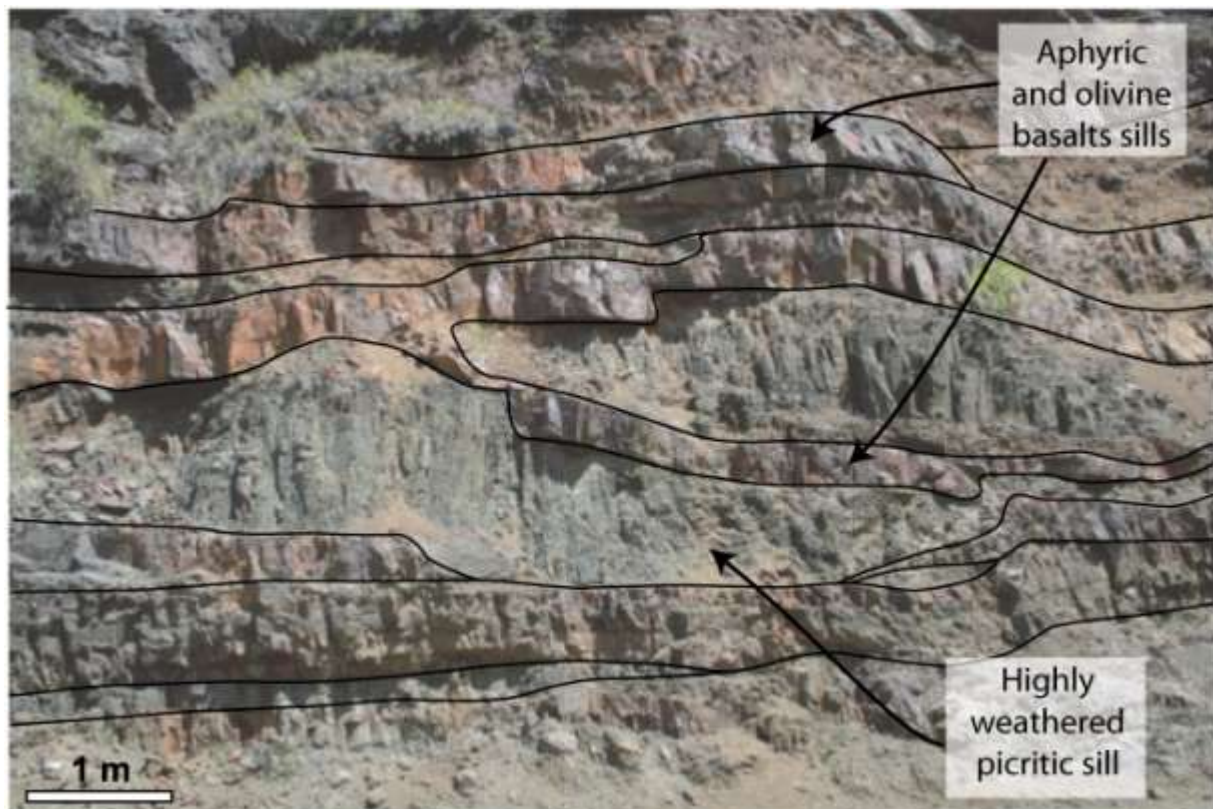


**Figure 3.3-9:** Close up photograph of a sill cluster in Cilaos in the axis of the rift zone. We can note the presence of several units of sill sub parallel displaying different grade of weathering suggesting an age difference.

### 3.3.4 Origin of sills

#### 3.3.4.1 Mechanics of fluid-filled fractures

To understand the processes leading to sill injection, it is necessary to review the mechanics of fluid-filled fracture emplacement. Sills form as extension fractures or, more specifically, as

fluid-driven fractures (hydrofractures) (Lister and Kerr, 1991). It follows that they propagate in the direction of the maximum principal compressive stress  $\sigma_1$ , and open up perpendicular to the direction of the minimum principal compressive (maximum tensile) stress  $\sigma_3$  (Anderson, 1951). The conditions for injection of a sheet (sill or dyke) from a magma chamber is given by (Anderson, 1951):

$$p > \sigma_3 + T_0 \quad (1)$$

Here  $p$  is the total magma pressure and corresponds to the sum of  $P_e$ , the excess fluid pressure in the magma chamber (in excess of  $\sigma_3$ ), and  $P_1$ , the lithostatic pressure in the chamber, normally equal to the vertical stress at the roof of the chamber.  $T_0$  is the tensile strength of the surrounding rocks. In the case of an isotropic state of stress ( $P_1 = \sigma_1 = \sigma_3$ ), sheet injection occurs when  $P_e$  becomes equal to, or slightly greater than  $T_0$ . The propagation of magma will also depend on the driving pressure within the sheet, defined, for a lithostatic state of stress, by:

$$\Delta P = P_e + (\rho_r - \rho_m)gh_d \quad (2)$$

Here,  $\rho_r$  and  $\rho_m$  are the densities of the host rock and the magma, respectively, while  $g$  is the gravitational acceleration, and  $h$  the height of the dyke above the magma chamber. However, the stress field, within an active volcanic edifice is unlikely to be isotropic. This follows from global gravitational instability, characterised by spreading, deformation and stresses associated with sheet injections. Generally, for a volcanic edifice under gravitational stress as the main loading,  $\sigma_1$  is normally vertical and  $\sigma_3$  horizontal (Cayol and Cornet, 1998b). For these stress conditions, the overpressure in a dyke becomes:

$$\Delta P = \sigma_d + P_e + (\rho_r - \rho_m)gh_d \quad (3)$$

Here  $\sigma_d$  is the stress difference  $\sigma_1 - \sigma_3$ . While the propagation of a sheet will normally be in the direction of  $\sigma_1$ , as it must be if the sheet is a pure extension fracture (Anderson, 1951), the propagation path depends also on other factors such as the tensile strength and the toughness of the material, which corresponds to the necessary energy required to reach the rupture of a material. In a brittle material, the crack will propagate if the strain release energy (dependent on both the length of the crack and the tension, or internal pressure applied) is equal or higher than the surface energy required for the creation of the new crack (Ashby and Jones, 1998; Jaeger et al., 2007). In most cases, in a brittle medium, this value is often of  $\sim 1\text{-}2 \text{ MPa}\cdot\text{m}^{-1/2}$  (Pollard and Fletcher, 2005), reached for cracks of few meters undergoing an overpressure of few MPa. However, for ductile material, the energy required to accommodate plastic deformation needs to be taken into account, leading to an increase of the energy required by several orders of magnitude (Ashby and Jones, 1998). As a result, magma might propagate along a path which is

not in agreement with the local stress field, but rather along a path characterised by extremely low tensile strength and material toughness, e.g. along a contact.

### **3.3.4.2 Models for the origin of sills**

Our field data show the existence of several sill clusters, in the central part of the volcano as well as individual scattered sills through the lava pile. The two main groups of sills, A and B, suggest at least two different mechanisms for sill injection. The scattered sills (type A) (*Figure 3.3-7*) generally strike in the direction of the rift zone (*Figure 3.3-6*), suggesting that the sill injection is controlled by the rift zone stress field, while the sills concordant with the lava pile present strikes mostly parallel to that of the geological formations, and subsequently to that of the slopes of the volcano. The origin of these sills may be partly attributable to the effects of the surface stress field where, indeed, the stress field may be reoriented so as to favour sill emplacement (Dieterich, 1988; Cayol and Cornet, 1998b). With distance, the magmatic influence (overpressure and magmatic stress field) decreases while the influence of the local stress field increases (Gautneb and Gudmundsson, 1992). This leads to a rotation of the intrusion from subvertical or inclined dykes to shallowly dipping intrusions. If close to the surface, the magma might propagate as a sill, favoured by the reorientation of the stress field, as well as the low degree of compaction of the lava pile, with contacts favouring the injection of magma. A similar phenomenon is equally observed for hydraulic fractures, for which the dip tends to decrease with the distance from the injection point (Valko and Economides, 1995).

Another process that can also favour the injection of sills, is a near-isotropic stress field, created, in the case of a volcanic edifice, by the increased compression due to repeated dyke injection (Dieterich, 1988; Cayol and Cornet, 1998b). In a near-isotropic stress field, there is almost no difference between the principal stresses. Under these circumstances, a weakness within the pile, such as a contact, might be sufficient to initiate a sill. Indeed, the energy required to open an already existing contact is almost non-existent. The toughness of a contact is relatively low. The magma will therefore follow the easiest path, which will be along a contact, non concordant with the principal stresses orientation.

Sill clusters are composed of several parallel sills intruded at a contact presenting a sharp lithological contrast, where a low-rigidity layer (breccia) overlies a comparatively stiff layer. The dip of the sills are that of the contact, which are usually shallow ( $< 15^\circ$ ), and strike mostly perpendicular to the rift zones, but can occasionally be steeper. Previous models suggested that level of neutral buoyancy was a requirement for the injection of sill. According to Eq. (3), the buoyancy term is only partly responsible for the propagation of magma; thus presence of low

density layers (or neutral buoyancy layer if its density is lower than that of the magma) cannot be the only condition for sill emplacement at certain contacts in the volcano. The presence of a low density layer tends to reduce the overpressure of magma, but abrupt changes do not occur at the contact (*Figure 3.3-10*).

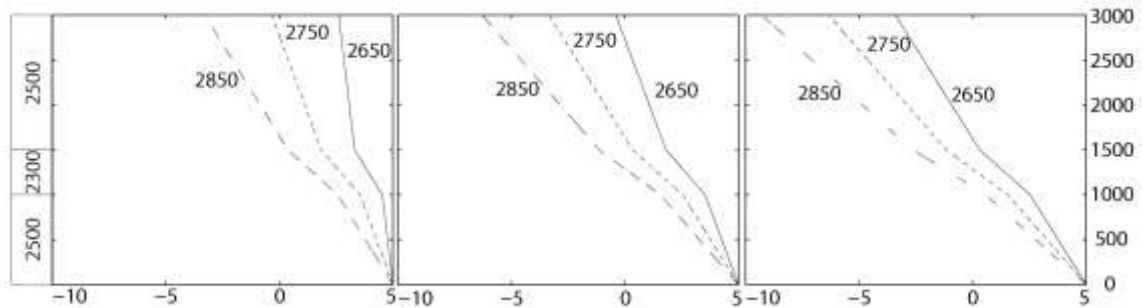


**Figure 3.3-10: Evolution of overpressure in a vertical dyke, for 3 different magmas (from aphyric – lower density – to picritic with 30% of olivine – higher density), in a heterogeneous lava pile.** The density ( $\text{kg/m}^3$ ) variation reflects the olivine content of the magma and has been calculated after the density of an aphyric liquid mixed with 30% of olivine. The altitude 0 corresponds to the top of the magma chamber, in which an overpressure of 5MPa exists. Left,  $\sigma_1$  is vertical and  $\sigma_d$  evolves linearly from 0 at the base to +3 MPa at the top. Middle, the stress field is lithostatic. Right,  $\sigma_3$  is vertical and  $\sigma_d$  evolves linearly from 0 at the base to -3 MPa at the top. The vertical scale corresponds to the altitude, while the horizontal scale corresponds to the overpressure in MPa. On the left, the density layering, with a density of  $2500 \text{ kg/m}^3$  for the lava pile and of  $2300 \text{ kg/m}^3$  for the breccia.

It has also been proposed that sill emplacement happens at rigidity contrasts usually involving layer pairing (high rigidity layer on top of a low-rigidity layer) (Dahm, 2000; Rivalta et al., 2005; Kavanagh et al., 2006). That is the opposite of what we observe, namely low-rigidity breccias are normally on top of high-rigidity layers such as lava flows or intrusions. We test the effect of mechanical contrast at contacts. However, we consider contacts at depth that have been, under the weight of the lava pile, sealed. We test different setups of contacts, with a low-to-high rigidity contrast, high-to-low rigidity contrast and high-to-high rigidity contrast. We also consider two cases, one in a stress field where a stress difference of 3 MPa exists, one in an isotropic stress field. Results show that high tensile stresses are concentrated at the tip of the propagating dyke when the model is in an anisotropic stress field, with a horizontal stress lower than the vertical stress by 3 MPa. However, the intensity reached varies depending on the stiffness of the overlying layer, the higher the stiffness, the higher the stress intensity. In an isotropic stress field, the stress concentration is much less efficient. However, the relationship between tensile stress values and stiffness of the overlying layers is similar to that observed previously, with relatively low tensile stresses observed in soft layers (*Figure 3.3-11*). The propagation of cracks within a medium will be dependent on its toughness. Basalts and intrusive rocks present usually values of a few  $\text{MPa m}^{-1/2}$ , while these value will decrease for breccia-like material (Pollard and Fletcher, 2005). For cracks of few metres long undergoing

overpressure in the range of that observed for dykes (few MPa), this critical value of toughness will be reached and allow the propagation of magma.

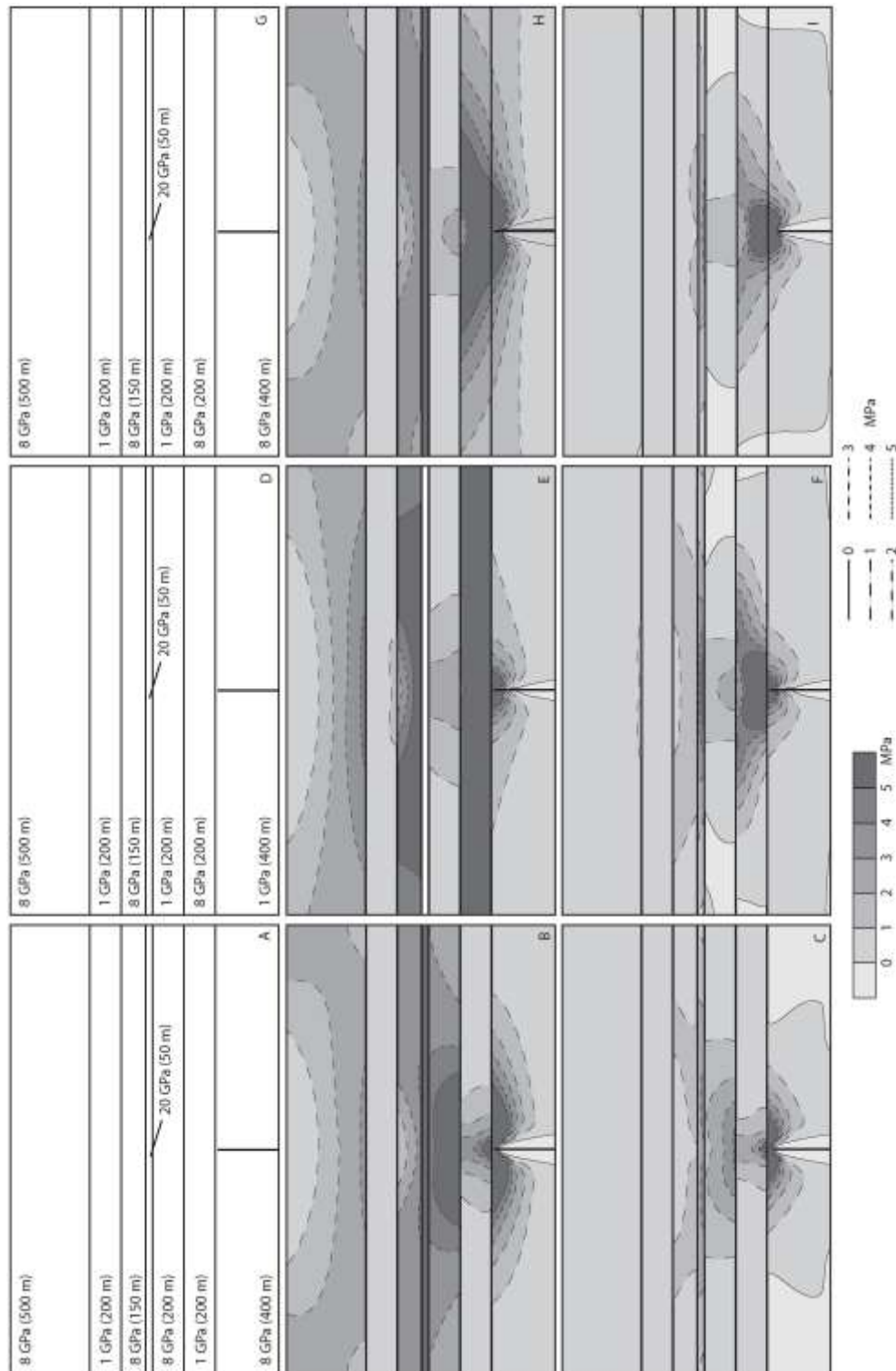


**Figure 3.3-11:**  $\sigma_3$  values induced by an overpressure of 5 MPa in a propagating dyke. A- Setup of the model with a contact stiff-soft. B- Model with a contact stiff-soft undergoing a horizontal tension of 3 MPa. C- Model with a contact stiff-soft in a lithostatic stress field. D- Setup of the model with a contact soft-stiff. E- Model with a contact soft-stiff undergoing a horizontal tension of 3 MPa. F- Model with a contact soft-stiff in a lithostatic stress field. G- Setup of the model with a contact stiff-stiff. H- Model with a contact stiff-stiff undergoing a horizontal tension of 3 MPa. I- Model with a contact stiff-stiff in a lithostatic stress field.

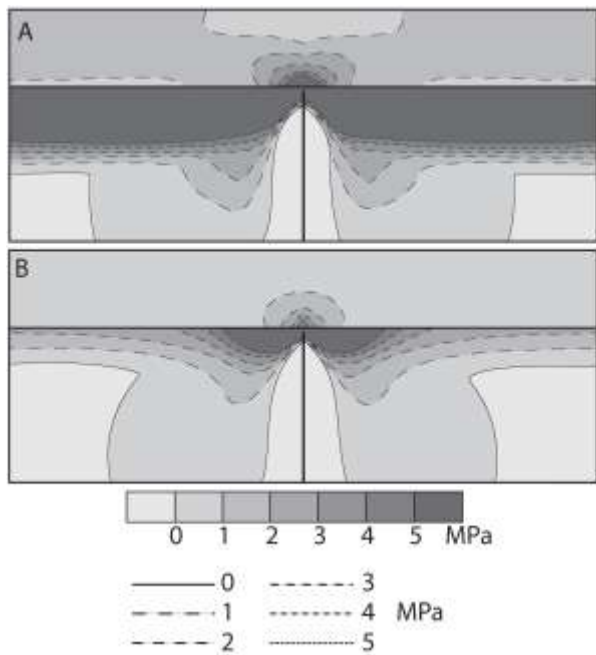


**Figure 3.3-12:  $\sigma_3$  values induced by an overpressure of 5 MPa in a propagating dyke.** The bottom layer has a Young's modulus of 8 GPa (lava pile) and a thickness of 400 m, while the top one has a Young's modulus of 0.5 GPa (breccia) and a thickness of 200 m. A- The model undergo a horizontal tension of 3 MPa (correspond to a stress difference of 3 MPa between  $\sigma_1$  and  $\sigma_3$ ). B- The stress field is lithostatic.

We test the role of soft and thick clay-rich layers of breccia on the propagation of magma. Indeed, most of the breccias observed at PdN contain a large quantity of clay, originating from the hydrothermal alteration of the inner core of the volcano. Clay, with sufficient water content might act as a plastic material. While propagating, a vertical dyke concentrates tensile stresses at its tip that allow the further propagation of a fracture. However, soft layers show little stress concentration, especially if the stress field is isotropic (*Figure 3.3-12*).

The presence of clay within the breccia layer, such as the breccias observed in PdN will strongly increase the toughness of the breccia (Ashby and Jones, 1998). Combining little tensile stress concentration at the tip of the dyke (*Figure 3.3-12*), within the soft material, and the high toughness of the partially plastic material, the vertical propagation of magma will be prevented, and may change into a sill. In particular, if the magma is still pressurised on meeting a contact or a layer with a local stress field unfavourable for further vertical dyke propagation, the dyke may change into a sill and propagate horizontally along the contact or layer. The requirement is that the total magma pressure is higher than the load normal to the contact at which magma intrudes. Applications of this in conditions reasonable for PdN (magma chamber at about sea level and a height of edifice of 3000 m, with a mean density of 2500 kg/m<sup>3</sup>) show that a positive overpressure (allowing horizontal propagation) exists at heights up to 1 to 2 km above the magma chamber, the variation depending on the density of the magma (*Figure 3.3-13*).



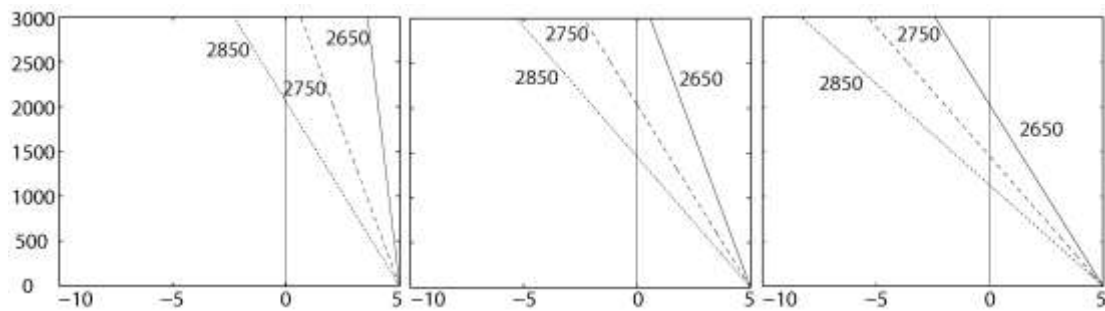


**Figure 3.3-13: Evolution of overpressure in a vertical dyke, for 3 different magmas, in a homogeneous medium of density equal to  $2500 \text{ kg/m}^3$ .** The density ( $\text{kg/m}^3$ ) variation reflects the composition, and the olivine content, of the magma. The altitude 0 corresponds to the top of the magma chamber, in which an overpressure of 5 MPa exists. Left,  $\sigma_1$  is vertical and  $\sigma_d$  evolves linearly from 0 at the base to +3 MPa at the top. Middle, the stress field is lithostatic. Right,  $\sigma_3$  is vertical and  $\sigma_d$  evolves linearly from 0 at the base to -3 MPa at the top. The vertical scale corresponds to the altitude, while the horizontal scale corresponds to the overpressure in MPa.

In this model, the sills will be intruded at the contact below the breccia, which, in the case of a flank collapse, corresponds to the landslide scarp. This will be exacerbated by the weakness of the contact if close to the surface, with little loading onto it.

Finally, repeated dyke injection, and accumulation of stresses, especially horizontal compression, due to the accumulation of intrusions might not only lead to an isotropic stress field, but favour a temporary pure horizontal compression. Under such circumstances, a dyke will intrude horizontally at a level concordant with the level of stress reorientation. Sills will therefore outcrop at any level within the volcano.

### 3.3.5 Discussion

The deep cirques that entailed PdN give a good view of the feeding system of this dormant basaltic shield volcano. Both eruptive and plutonic rocks, ranging in composition from basic to differentiated, marking the stages of the petrological evolution of the volcano (Upton and Wadsworth, 1965; McDougall, 1971), are exposed. However the most common rock types are picritic basalt, olivine basalt and aphyric basalt, mostly erupted during the basaltic stage of the volcano, plutonic rocks being rare. The intrusive system is organised along several intrusion zones trending  $\text{N}30^\circ\text{-}40^\circ$ ,  $\text{N}120^\circ$ , and  $\text{N}160^\circ$  (Figures 3.3-1; 3.3-2; 3.3-4). Within these intrusion zones, dip varies from sub-horizontal sills to sub-vertical dykes (Figure 3.3-3). However, sills are more common in Cilaos than in Mafate (Figure 3.3-6). While the dykes have similar characteristics as in other shield volcanoes (Figure 3.3-3; i.e. Walker, 1987), the sills show unusual characteristics such as their appearance in clusters (Figures 3.3-8; 3.3-9). Despite observation of sill clusters in other places (Burchardt, 2008), their origin can be related to the existence of mechanical contrast similar to what had already been studied previously (Rivalta et al., 2005; Kavanagh et al., 2006). As such it does not meet our model. Indeed, most of the sills,

outcropping as clusters in PdN are located at major contacts between breccia (above the contact) and lava flows or plutons (below the contact). The nature of the breccia is related to debris avalanches, with the presence of jigsaw cracks and important thickness.

We have discussed several mechanisms by which the sills could have been emplaced. The emplacement of sills of type A, with their dip varying from  $0^\circ$  to  $30^\circ$ , seems to be controlled by the rift zone stress field as well as the gravitational stress field. Field measurements suggest that in Cilaos, the dip of intrusions decreases with the distance from the centre of the volcano, resulting from the decrease of magmatic influence (overpressure and stress field) (Gautneb and Gudmundsson, 1992) and the relative increased influence of gravitational stresses. Close to the surface, or alternatively, away from the centre of the edifice, the stress field might reorientate to become favourable to sill injection (Dieterich, 1988; Cayol and Cornet, 1998b). With distance, the intrusions will see their dip decreasing, but with strike similar to that of the rift zone. Presence of weakness along a contact, and a near-isotropic stress field, will favour the injection of a sill concordant with the lava pile that will then present with strike similar to that of the lava flow. Similar evolutions have been observed for hydraulic fractures (Valko and Economides, 1995).

Repeated sill injections at specific levels within the volcano, however, suggest a different mechanism of intrusion. Here, several models are proposed to explain the formation of levels suitable for sill injections. In the first place, we emphasise the role of density contrast within an edifice. While no sharp changes of overpressure, explaining the existence of sill clusters, occur at contacts between two layers (*Figure 3.3-10*), the presence of low density layers tends to lead to a rapid decrease of the magma overpressure (*Figure 3.3-10*). Sill clusters cannot be directly related with a buoyancy effect. However, the decreased overpressure within dykes will favour their arrest, especially close to the surface, where the weaknesses, favouring the injection of magma, such as contacts, exist. While in a volcanic edifice this model is not applicable, it becomes an important mechanism for the emplacement of sills in sedimentary basins, where the density of the rocks is much lower than that of the magma. Indeed, large thickness of low density layers can be accumulated, leading to a rapid decrease of the magma overpressure, magma that will easily be stopped in its vertical propagation, and rather accumulate as a sill at the favour of contacts between two layers (Mudge, 1968; Johnson and Pollard, 1973).

A second model proposed here explores the influence of clay-rich layers of breccia. Field evidence suggests that debris avalanche deposits contain a certain fraction of clay, mostly in the matrix part of the deposits. When saturated, clays act as a plastic material, and increase their toughness (Ashby and Jones, 1998). The softness of the breccia also leads to the absence of

stress concentration at the tip of a propagating dyke close to an interface between the lava pile and the breccia (*Figure 3.3-12*). The two effects combined will prevent the fracturing of the breccia, and thus the arrest of the magma. The injection as a sill will occur only if the pressure of the magma is superior to the stress normal to the contact. Hence, a near-isotropic stress field will favour the injection of a sill, as well as a weak contact. In this model, the plastic nature of the breccia is likely to evolve with time. Field observations show that they act now, few hundred thousands of years after their emplacement, as a brittle material. Thus, this mechanism will be effective only during a certain amount of time following their emplacement. Observations by Mudge (1968) correlate with our observations and model. He suggested that the existence of a 'fluid barrier' was a requirement for the injection of sills.

A third model emphasises the influence of mechanical contrast at major contact within the lava pile. It was previously suggested that low-to-high mechanical contrasts were a requirement to the injection of sills (Rivalta et al., 2005; Kavanagh et al., 2006), as stiffer material present higher toughness than soft ones. Our numerical models show that, when the contact is sealed, soft layers present little stress accumulation, and are thus more likely to prevent dyke injection. Indeed little tensile stress concentration occurs in soft layers, in contrast with stiff layer (*Figure 3.3-11*). A fracture will propagate through a stiff layer, due to the high tensile stress present at the tip of a crack, while in a soft layer, the fracture might stop its propagation due to the absence of tensile stress. However, this model applies only if the soft material acts partially plastic, as brittle materials show usually low toughness (Pollard and Fletcher, 2005), this cannot explain the arrest of a propagating fracture. Alternatively, as the stress concentration, at the origin of the fracturing of the rocks, is dependent on the magma overpressure, low overpressure might favour the arrest of a dyke, when little stress concentration occurs. The magma can subsequently intrude as a sill if the magma pressure is not superior to the normal stress, condition favoured if we are in a near-isotropic stress field.

A combination of both models (plastic layers and stress field changes) can explain the origin of several generations of sills. While clay-rich and partially plastic breccia at the top of the pile might prevent the vertical propagation of magma, independently from the stress field, their evolution towards a more brittle behaviour with time (drier) will lead to their decreased influence as regard to the magma propagation. However, a change in the stress field, such as an increase of the horizontal compression will tend to reduce the stress concentration within these breccias, favouring the arrest of dyke at the same level, and create the second generation of sill. In these conditions, only dykes with low overpressure will be affected and turn into sills. Alternatively, the presence of an existing stiff sill level might also act as a stiff barrier. Sills are

usually stiffer than lava flows, for the same composition, and thus present higher toughness. If their toughness is high enough, it might prevent the injection of low-pressurised dyke through.

In all cases, the presence of a well defined plane and a near-isotropic stress field are two parameters that will highly increase the rate of injection of sills. The near-isotropic stress field, in a volcanic edifice such as PdN, results in the increased horizontal compression in connection with the high injection rate. A similar conceptual model was already suggested by Walker (1992), where slow spreading volcanoes were more likely to develop sill intrusions. If the injection rate is very high, and the stress accommodation almost inexistent, a pure horizontal compression might happen, and favour the injection of sills at any level within the volcano.

For both types of sills, field evidence suggest that sills are usually thinner than dykes, suggesting that they do not propagate in the exact direction of the most favourable stress field. Contacts influence the propagation of magma in a stress field where the stress normal to the intrusion is not the minimum compressive stress.

### **3.3.6 Conclusions**

The field data reveal that the PdN intrusive system is organised along three main radial intrusion axes. A wide range of intrusions have been observed, from large plutons, to dykes and sills. The sills are unusually common in the volcano and belong to two main types, A and B. The origin of various sill types can be explained as follows:

➤ Type A sills originate from the decrease of the magmatic stress field, and the relative increase of the gravitational stress field. With the increase of distance from the eruptive centre, the intrusions rotate and become sub-parallel to the near-surface stress field unfavourable to dyke injection. The presence of weak contacts is a factor that favours the injection of sills, as well as a near-isotropic stress field, created by repeated dyke injection.

➤ Type B sills are injected at contacts below breccia layers, the mechanical behaviour of which must be partially plastic, in relation to the clay content of these breccias. The injection of sills along the contact, which corresponds to the landslide base, is favoured while the breccias are 'fresh' (un-compacted and un-dried). Alternatively, an increased horizontal compressive loading (due to dyke injections) in the lava pile will favour sill injections at similar contacts under the condition that the breccia act still as a partially plastic material, or that the magma overpressure is low. The effect of an existing sill level might also act as a stiff barrier, and provoke the arrest of subsequent dykes, similar to the model previously proposed for the origin of sills (Rivalta et al., 2005; Kavanagh et al., 2006; Burchardt, 2008).

### **Acknowledgements**

The authors wish to thank Ruth Andrew for review and comments on an early version of the manuscript.

### **3.4 Sills at Piton de la Fournaise**

The previous section described and proposed a model as to the origin of sills at Piton des Neiges, both individual sills intruded in the lava pile at shallow level, or clusters of sill at major contacts, with a layer presenting high resistance to fracture propagation above the contact. Field work in Piton de la Fournaise also confirmed the model for the origin of single sill units. Indeed field evidences from Piton de la Fournaise show that in both the recent time, and earlier times, sills have been injected at shallow levels. The first example is that of a sill, observed in the northern cliff of the Bory pit-crater, which injected within the lava pile, along the planes defined by the existing lava flows, and as shallow as 20 metres below the surface (*Figure 3.4-1*). The presence of a step-like feature, cutting through the lava pile confirm its intrusive nature rather than extrusive.

As suggested above, the presence of relatively tough layers can limit the propagation of magma vertically. In Piton des Neiges, these tough layers are constituted of breccia that acts as plastic. However, there will also be a strong increase of toughness from a non-coherent material (scoria) to the lava pile. Examples at Piton de la Fournaise illustrate this mechanism, with dykes propagating vertically through a scoria cone and later propagating as a sill at the interface between scoria and lava flows along the contact (*Figure 3.4-2*).



**Figure 3.4-1: Sill intruded in the northern cliff of Bory pit-crater.** *The sill is about 70 cm thick, and is intruded parallel to the lava pile, except for two locations where it cut across the lava pile abruptly, conferring this apparent step-like structure. Absence of abundant gas vesicles suggests an intrusive origin.*

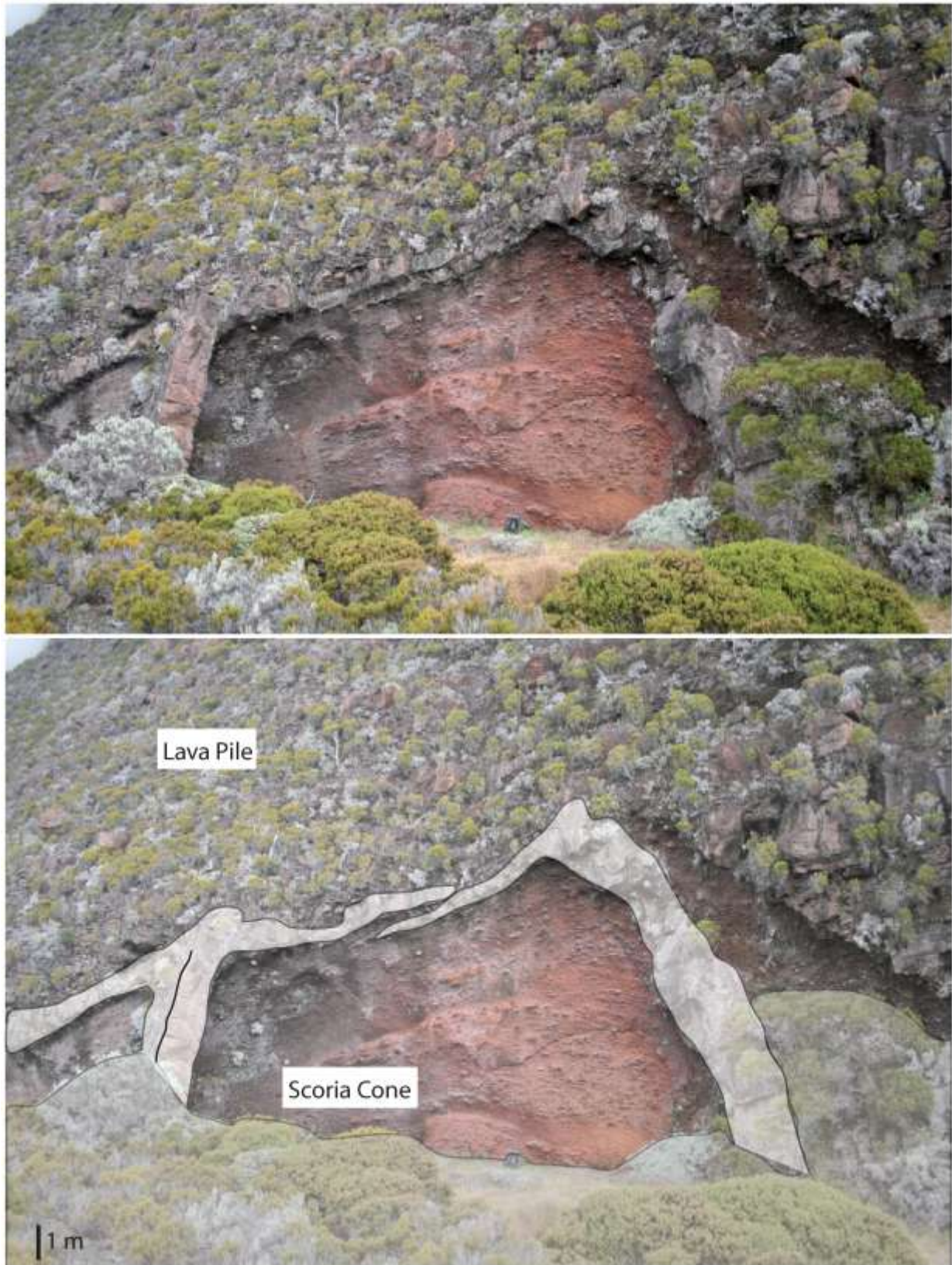


**Figure 3.4-2:** Example of a sill intruding at a contact between a granular material, and a tougher lava pile. The dyke sill on the left has propagated both up- and downward at the contact, while on the right, it intruded only downward. The outcrop is at the base of a ~200 m high cliff, indicating that the maximum depth of emplacement was 200 m.

Sills can, in the right conditions evolve to create a laccolith, and if fed, can evolve towards a magma chamber. Examples from Piton de la Fournaise show that magma has injected horizontally, and stored at really shallow depth, and created a small laccolith. The absence of a depression below the lava accumulation tends to suggest that this accumulation is not a tumulus. On the other hand, the apparent doming of the overlying rocks, to accommodate the magma suggests the intrusive origin (*Figure 3.4-3*). The presence of a dyke-like structure at the top of the laccolith suggest that the structure might have been a temporary storage of magma before its eruption, either during the same intrusive/eruptive event, or shortly after the arrival of magma at shallow depth.

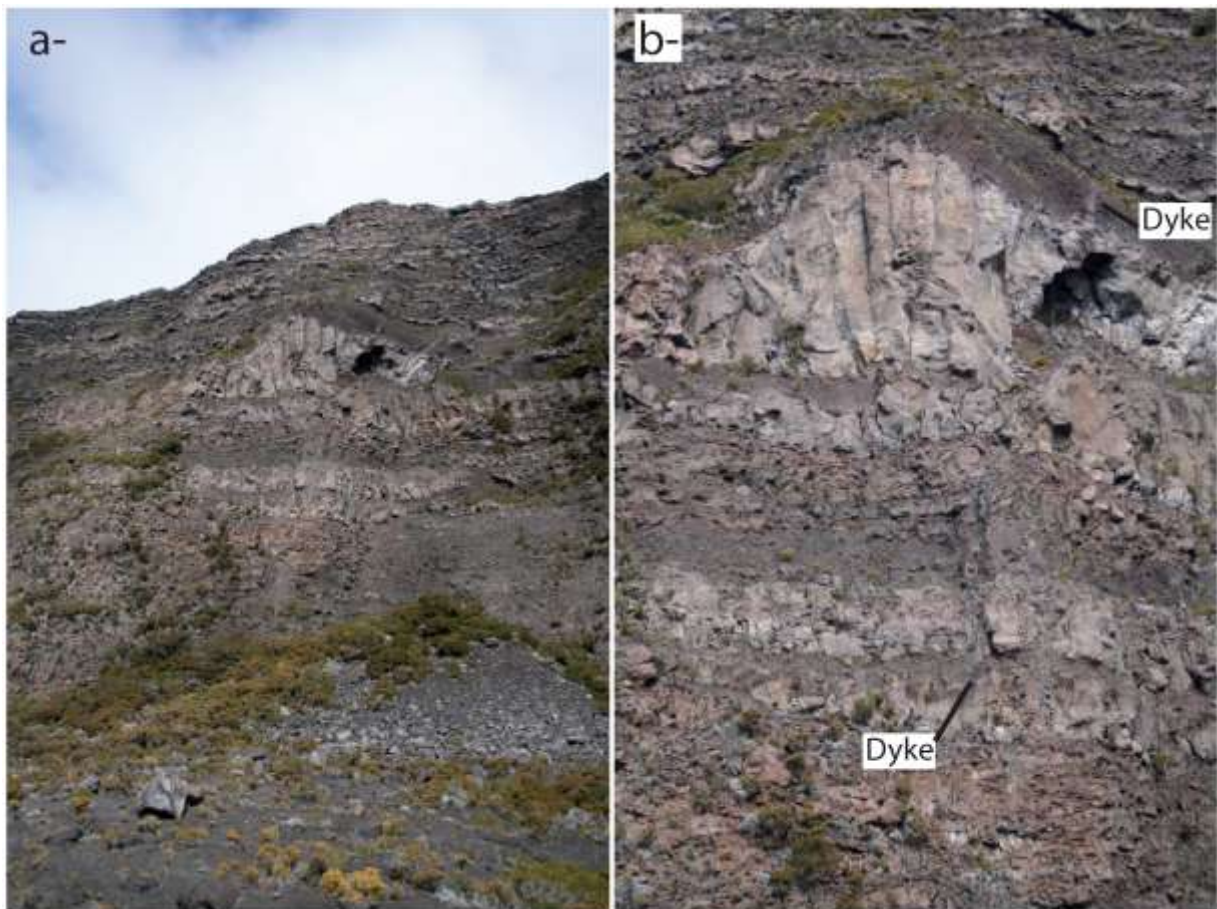


**Figure 3.4-3: Laccolith intruded in the cliff surrounding of the Enclos Fouqué caldera, west of the actual central cone.** *The intrusion has uplifted the upper deposits, and is fed by a dyke which appears divided in several branches. A dyke-like structure can be observed at the top of the laccolith. Absence of down-bending does not support a tumulus origin for this structure. The cliff is about 200 m high.*

### 3.5 Summary and conclusions

This section was focused on Piton des Neiges. The erosion that affected the volcano has created three vast depressions, and several deeply eroded valleys. It offers a good overview of the internal structure of the volcano. The feeding system is organised along three identified main rift zones, N30°, N120° and N160°. These rift zones create the main injection axes, but



did not confer any specific shape to the volcano, which displays a sub-circular shape. All rift zones are created by similar structures, broader at the base and close to the eruptive centre, yet thinner with altitude and distance. The intrusions vary in a wide range of dip, from sub-horizontal sills to sub-vertical dykes, and a limited range of lithology, restricted to basaltic rocks, from picritic basalts to aphyric basalts. More evolved terms are constrained to the central plumbing system, with only rare intrusions observed further than 3-4 km from the eruptive centre. Most of the intrusions are constituted of eruptive rocks, rather than intrusive ones, with only few gabbroic or syenitic intrusions. This organisation suggests that the rift zones were mostly active during the shield building stage (Chevallier, 1979).

Field studies suggest that the rift zones present a common dynamic that is the lateral injection of blade-like dykes from the central plumbing system. However, field evidences also suggest that the stress field at the period of intrusion was extremely different in the rift zones. Two groups can be distinguished, corresponding to at least two different origins for the stress field. The N120° and the N160° appear to be related with a stress field that is observed at a larger scale in the island, with a structural inheritance from the crustal structures. These two rift zones are characterised by steeply dipping intrusions, and sills are rare. Only in the vicinity of the eruptive centre, are intrusions more shallowly dipping, in relation to the magmatic stress field. The N30° rift zone appears to be of a more shallow origin. The presence of a great number of sills suggests that the stress field in this rift zone is highly sensitive to surface stresses, and can be easily blocked, during periods of high injection rates.

Sills are also important features of both Cilaos and Salazie cirques, and less present in Mafate. They correspond, when spread within the lava pile, to the influence of a surface stress field that favours their injection. Field work in Piton de la Fournaise, suggests that the mechanism observed at Piton des Neiges is also valid elsewhere on the island. Alternatively, clusters of sills, as observed at Piton des Neiges suggest that mechanical contrasts favour sill injections, with an importance given to the contrast of toughness between layers. In our case, plastic debris avalanches deposits play the role of tough layers. These layers have been preferentially identified in Cilaos and Salazie, and fit the location of submarine observations (Oehler et al., 2004; Oehler et al., 2008). In both cases, it has been noted that a well defined plane will favour the injection of sills. Observation of only one sill cluster in Mafate suggests that the N120° and the N160° were only rarely affected by debris avalanche.

*4 Growth and Deformation:  
Relationship with the Rift zones*

---

### **Objectives:**

- Study the internal structure of Piton de la Fournaise volcano rift zones.
  
- Study the possible influence of structural heterogeneities on the deformation, and propose a model of deformation that accounts for field evidence and deformation data.
  
- Study the growth of the central cone, propose a model for its shape, and study the interaction between intrusions, deformation and morphology of the cone.

## 4.1 Introduction

Rift zones have been, in the history of Piton des Neiges, present during at least its earlier stage of development, and have seen their activities reduced with time. While the erosion at Piton des Neiges volcano allows us access to the inner structure of the volcano, the active Piton de la Fournaise allows us access to the mechanism of interaction between an active rift zone, the deformation during injection and the growth of the edifice.

As previously seen, injection of magma is accompanied by change of the stress field and deformation. This deformation can be used to obtain the geometry of the source of pressure. At Piton de la Fournaise, deformation during dyke injection shows a particular pattern, with concentration on the east of the N-S trending eruptive fissures and dykes.

Another peculiar aspect of Piton de la Fournaise is its unusual shape. Volcanoes displaying well developed rift zones usually present with a specific morphology that is elongation in the direction of the rift zones. This is the case of most of the volcanoes of the Hawaiian archipelago, Karthala (Comoros), La Palma and Tenerife in the Canary Islands, and other volcanoes. In Réunion, the rift zones identified are not linked with any particular elongated shape. Moreover, despite a N-S trending rift system at the summit, the central cone of Piton de la Fournaise is characterised by an E-W elongation trend. It has been proposed that this morphology was to be linked with the injection of a large quantity of thick and short dykes within the cone, only few of them reaching the surface (Annen et al., 2001).

To answer these two specific aspects of the interaction between rift zones and growth and deformation, we undergone two studies presented here.

## 4.2 Influence of heterogeneities on the deformation: Paper 3

As suggested, deformation at Piton de la Fournaise has been monitored since the opening of the volcanic observatory (OVPF). The pattern of deformation is systematically asymmetric, with higher deformation East of the fissures, commonly trending N-S. When reconstructing the source of pressure, using deformation data, a systematic eastward dipping is revealed. Field study of the rift zone shows that a contradiction exists between field data and numerical modelling results. We propose to answer this problem in the following study published: Letourneur, L., et al., 2008: The effects of rock heterogeneities on dyke paths and asymmetric ground deformation: The example of Piton de la Fournaise (Réunion Island), *Journal of Volcanology and Geothermal Research*, 173:289-302.

## **The effects of rock heterogeneities on dyke paths and asymmetric ground deformation; the example of Piton de la Fournaise (Réunion Island)**

Ludovic Letourneur<sup>a</sup>, Aline Peltier<sup>b, c</sup>, Thomas Staudacher<sup>c</sup>, Agust Gudmundsson<sup>a</sup>

<sup>a</sup> University of Göttingen, Geoscience Center, Department of Structural Geology and Geodynamics, Goldschmidtstrasse 3, 37077, Göttingen, Germany

<sup>b</sup> Université de la Réunion, Laboratoire des Sciences de la Terre de l'Université de la Réunion, UMR 7154, 15 av. René Cassin, 97489 Saint-Denis cedex, La Réunion, France

<sup>c</sup> Observatoire Volcanologique du Piton de la Fournaise, Institut de Physique du Globe de Paris/UMR 7154, 14 RN3, Le 27KM, 97418 La Plaine des Cafres, La Réunion, France

### **Abstract**

During pre-eruptive periods and eruptions, Piton de la Fournaise volcano shows an asymmetric magma-induced pattern of deformation. The origin of this asymmetry is not well constrained and the pre-eruptive deformation does not have a satisfactory explanation. Here we present data on the past history and complex structure of the volcano. We also provide new field data on exposed dykes in the volcano. The field data confirm that the eruptive centre has migrated through time. Our field data indicate average dyke dips of about 80°. By contrast, inferred dips of recent feeder dykes using geodetic data are 53°-75°. We explain this difference as being partly due to the models used to infer the dyke dips from geodetic data, which assume the host rock to be homogeneous and isotropic. When fractures and the other heterogeneities are taken into account in the models, the inferred dyke dips become similar to those of the exposed dykes. New numerical models indicate that when the complex internal structure of the volcano is taken into account, part of the asymmetry of the ground deformation can be explained. Part of the deformation asymmetry, however, is due to the curved structure of the rift system, resulting in the injection of curved dykes, and the dyke dips.

**Keywords:** asymmetric deformation, medium heterogeneity, rift zone.

### **4.2.1 Introduction**

The ground surface deformation of active volcanoes has been observed for a long time (e.g. Murray et al., 1977). The deformation occurs mostly within the short timescale of a magmatic event (eruptive and/or intrusive). More specifically, the deformation reflects stress changes at the surface induced by magmatic processes occurring within the volcano, such as the growth of the magma chamber under internal pressure (e.g. Lundgren et al., 2003; de Zeeuw-van-Dalfsen et al., 2004; Bonaccorso et al., 2005) and the injection of dykes (e.g. Pollard et al., 1983;

Sigmundsson et al., 1999; Fukushima et al., 2005). The deformation intensity and the area affected depend partly on the depth and the shape of the source of pressure (Pollard et al., 1983) and partly on the mechanical properties of the rocks (Gudmundsson, 2003; Gudmundsson, 2006). Another type of deformation can also be observed on active volcanoes, and is interpreted as a more continuous behaviour of the edifice. It is the large-scale deformation induced by volcanic spreading (Borgia, 1994; Delaney and Denlinger, 1999; Owen et al., 2000; Bonforte and Puglisi, 2003; Lundgren et al., 2003), or by the regional stress field (de Zeeuw-van-Dalfsen et al., 2004). As the magma path is determined by the state of stress in the volcano (Gudmundsson, 2006), the regional stress field or volcanic spreading may influence the magma path so as to generate orientated rift zones (Walter et al., 2006).

Usually the regional stress field, volcanic spreading, and distribution of injections responsible for volcanic deformations are mechanically linked. Stresses induced by tectonic or volcano-tectonic events may favour magmatic injections (Neri et al., 2005). Conversely, magma-induced stresses can reactivate volcano-tectonic structures (Ando, 1979; Walter and Amelung, 2006). The result of these interactions is often a complex pattern of deformation (e.g. Lundgren et al., 2003). For example, the pattern of deformation of Etna is interpreted as an eastward motion of the east flank, combined with magmatic deformations (Bonforte and Puglisi, 2003; Lundgren et al., 2003). At Kilauea, the asymmetric pattern of deformation is related to the spreading of the south-eastern flank (Delaney and Denlinger, 1999; Owen et al., 2000).

In other volcanoes, such as Stromboli and Piton de la Fournaise, the asymmetric pattern of deformation observed is supposed to be entirely due to magmatic effects (Zlotnicki et al., 1990; Cayol and Cornet, 1998b; Sigmundsson et al., 1999; Battaglia and Bachèlery, 2003; Froger et al., 2004; Mattia et al., 2004; Fukushima et al., 2005; Peltier et al., 2007). However, for Piton de la Fournaise, some authors suggest that the instability of the eastern flank can lead to overestimate the dip of the modelled dykes (Fukushima et al., 2005; Peltier et al., 2007). Mainly, these authors obtain their results by using a homogeneous, isotropic medium, in which they simulate the injection of dykes. This assumption allows a simplification of the models which, thereby, give quick solutions, but does not reflect the complexity of the volcano.

By contrast, other authors (e.g. Gudmundsson, 2006) suggest that the layering may modify the state of stress in a volcano and thus the observed deformation. Using 2-D numerical models, it can be shown, for examples, that dyke-induced stresses at the free surface of a volcano depend on the mechanical model used: homogeneous or layered (Gudmundsson, 2003). It follows that the inferred geometry of a volcano-deformation source could, because of the

layering, be mistaken. Another implication of these results is the potential effect that all kinds of heterogeneities may have on the stress distribution. Layering in a volcano is mainly the result of exogenous growth processes, which tend to accumulate stiff (high Young's modulus) lava flows and soft (low Young's modulus) pyroclastic and sedimentary layers. Endogenous growth processes, such as dyke injections, create stiff heterogeneities (Gudmundsson, 2006) that may partly control the magma paths in rift zones. Such heterogeneities may modify the state of stress in their surroundings during periods of unrest and thus affect the ground deformation. For example, the evolution of Piton de la Fournaise has been complex and many old intrusions have been identified within the volcano (Bachèlery and Mairine, 1990). The especially strongly asymmetrical west-east structure indicates that the edifice would in any case be subject to asymmetric deformation.

This study is partly based on a field campaign on Piton de la Fournaise volcano and partly on numerical modelling. The main aims are to explore, first, the structure of the plumbing system of the volcano and, second, how the plumbing system as well as fracturing contributes to the asymmetric surface deformation of the volcano observed during most recent eruptions.

#### **4.2.2 Geological settings**

Piton de la Fournaise is the active volcano on Réunion Island, an oceanic island located in the south-western part of the Indian Ocean (*Figure 4.2-1*). Réunion Island is the emerged part of a ~ 7000 m high and ~ 220 km wide edifice composed of 3 volcanoes: Piton des Neiges (PN) and Les Alizés volcano, both inactive, and the active Piton de la Fournaise volcano (PF) (Malengreau et al., 1999). The eruptive history of PF began ~ 530 ka ago (Bachèlery and Mairine, 1990). The growth of the volcano has been affected by several major volcano-tectonic events (Bachèlery and Mairine, 1990); the most recent one led to the creation of a summit collapse, the Enclos Fouqué Caldera (EFC - see the location in *Figure 4.2-1*– Bachèlery and Mairine, 1990), 4.5 ka ago. The Grand Brûlé structure (located in *Figure 4.2-1*) joined the summit caldera to create a single, continuous depression, limited by a 200 to 400 m high scarp, corresponding to the boundary fault, referred to, in this paper, as the Enclos Fouqué Caldera scarp (EFC scarp). The origin of the depression is still debated. Three main hypotheses as to the origin of the depression are discussed by various authors: (1) a landslide (Lénat et al., 1989b; Gillot et al., 1994; Labazuy, 1996; Oehler et al., 2004); (2) a caldera collapse associated with a landslide (Bachèlery, 1981; Bachèlery and Mairine, 1990); and (3) a hybrid event with a caldera-like depression and a landslide (Merle and Lénat, 2003). Recent studies (Bachèlery and

Mairine, 1990; Merle and Lénat, 2003) tend to agree on a vertical collapse of the upper part of the depression.

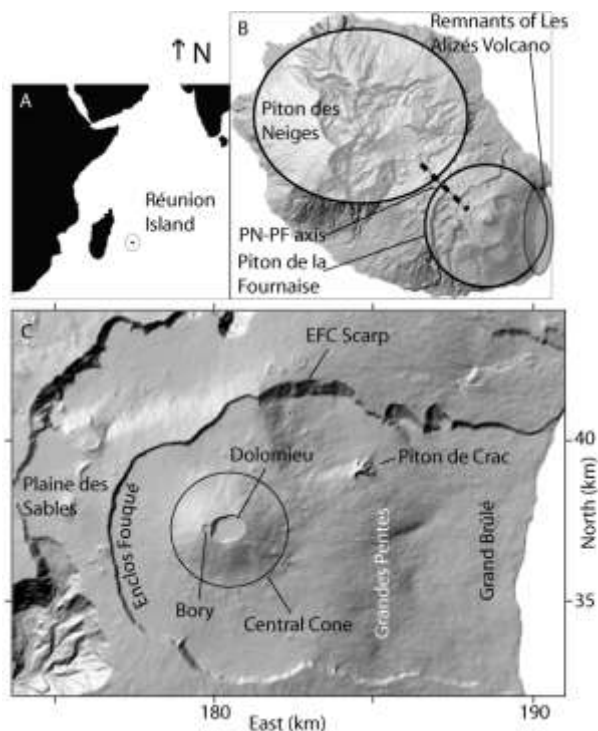


**Figure 4.2-1: (A) Location of Réunion Island, (B) main volcanoes of the island, (C) and main structures of Piton de la Fournaise. Coordinates in Gauss-Laborde Réunion.**

A study of the past eruptive activity reveals that the eruptive centre has gradually migrated from the Plaine des Sables (*Figure 4.2-1*) towards its present location (Bachèlery and Mairine, 1990), which is marked by a steep cone topped by two summit craters, Bory in the west and Dolomieu in the east (*Figure 4.2-1*). The active eruptive centre is fed by two feeding paths: (1) a central plumbing system, allowing the transport of magma from a shallow magma chamber, located at around sea level to the summit crater (Lénat and Bachèlery, 1990; Nercessian et al., 1996; Peltier et al., 2005; Peltier et al., 2006a); and (2) a system of rift zone segments connected to the central plumbing system and allowing the lateral transport of magma (Bachèlery, 1981; Bachèlery and Mairine, 1990; Fukushima, 2005; Peltier et al., 2005). At the edifice scale, mapping of eruptive features, from a set of aerial photographs obtained by the Institut Géographique National (IGN) in August 2003, shows the existence of a NNE-SSE trending main rift zone, confirmed in recent seismic studies (Brenquier et al., 2007), as well as a rift zone trending N120° joining the summit area of both PN and PF (PN-PF axis) (*Figures 4.2-1; 4.2-2*), mentioned by Bachèlery (1981) and rarely active in recent times. At the scale of the central cone, superimposed on the NNE-SSE path, a SW-trending intrusion path is present as well as a N120° intrusion zone south-east of the cone (*Figure 4.2-2*) (Michel and Zlotnicki, 1998; Michon et al., 2007a).



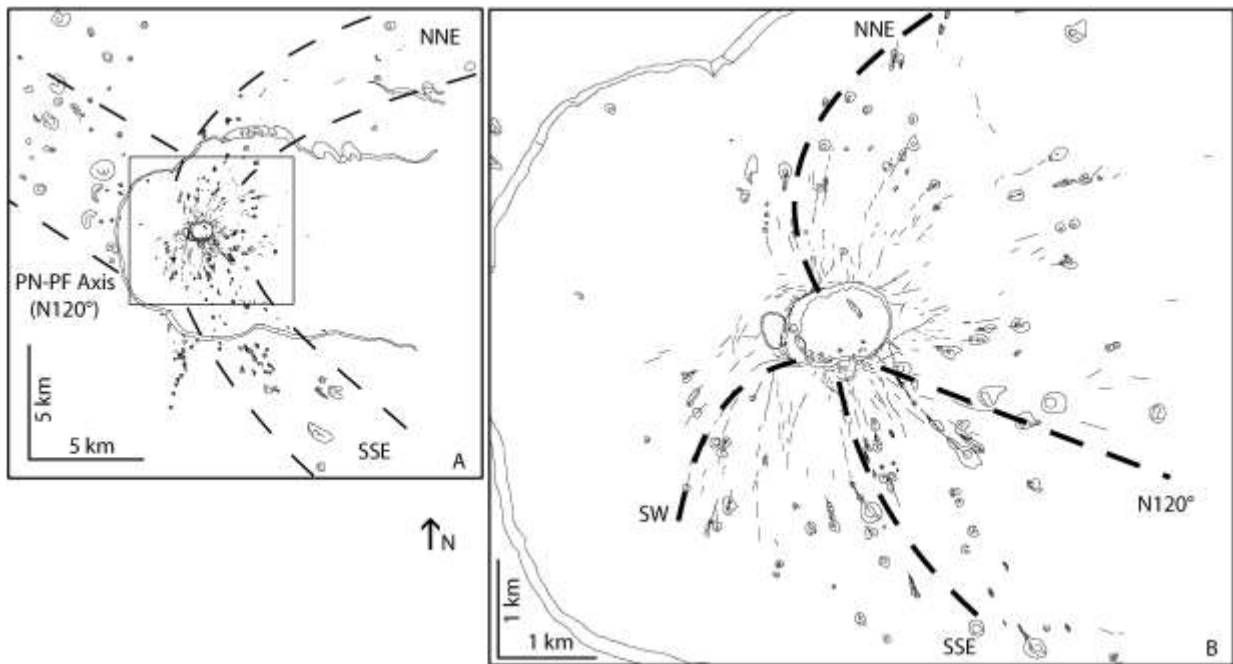


**Figure 4.2-2: Eruptive fissures and cones visible on aerial photographs from August 2003** (provided by the French Institut Géographique National - IGN). The distribution allows the characterisation of the main dyke paths.

Many authors (Briole et al., 1998; Froger et al., 2004; Fukushima et al., 2005; Peltier et al., 2007) have noticed an asymmetric pattern of deformation during recent magma injections and eruptions (*Figure 4.2-3*), as well as during the pre-eruptive inflations (*Figure 4.2-3*), both affecting a limited area close to the summit and along the eruptive fissures. During dyke emplacement, the western part of the volcano shows little surface deformation, except close to the eruptive fissures, while the eastern part shows considerable deformation. The surface deformation is normally interpreted as being attributable to the geometry of the injected dykes (Zlotnicki et al., 1990; Sigmundsson et al., 1999; Battaglia and Bachèlery, 2003; Froger et al., 2004; Fukushima et al., 2005; Peltier et al., 2007).

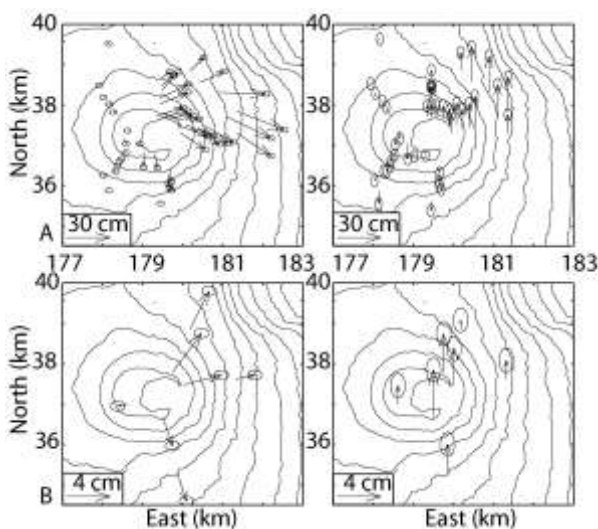


**Figure 4.2-3: A) Cumulative displacements recorded from September 2004 to January 2006.** This period includes 2 eruptions occurring in the Plaine des Osmondes, an eruption on the northern flank of the summit cone and a summit eruption, and B) inter-eruptive displacements recorded between June and October 2005, as detected by the GPS network. On the left are the horizontal displacements, on the right the vertical displacements. Coordinates in Gauss-Laborde Réunion.

### 4.2.3 Field results

#### 4.2.3.1 General description

The EFC scarp provides a natural 200-300 m cross-section through the uppermost products of the volcano, but the vegetation coverage prevents detailed observations in some subsections. The only areas available for observations are the Bellecombe scarp, and the cliff surrounding the Plaine des Osmondes (*Figure 4.2-4*). This cliff shows a tendency to a partial collapse, so we avoided taking measurements in the disturbed areas. Due to inaccessibility of the cliffs, some field measurements had to be made from a great distance and are subject to an error of  $\pm 5^\circ$ .

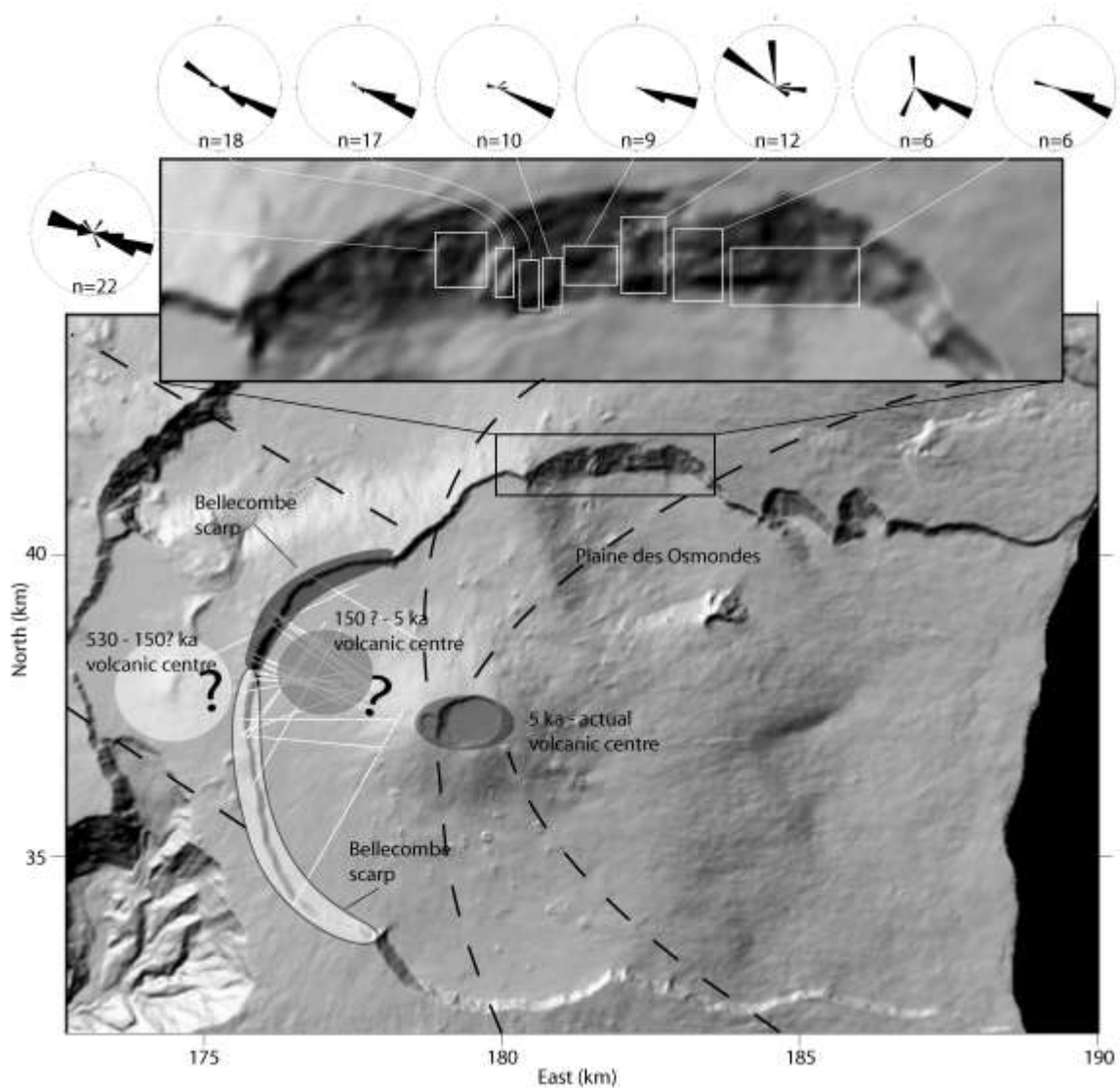


**Figure 4.2-4: Location of the study areas.** In the Plaine des Osmondes area, note that the dip directions are presented through rose diagrams. The shaded circles represent the previous eruptive centre with their period of activity. The actual eruptive centre is located beneath the summit crater. The dashed lines mark the main rift zones. The thin white lines correspond to the strike of the dyke observed in the Bellecombe scarp. The northern part of the Bellecombe scarp is in shaded dark, while the south part is in shaded white. Coordinates in Gauss-Laborde Réunion.

The studied cliffs show a comparatively homogeneous pile of two main lava types, aa and pahoehoe. The variation of thickness among the lava flows is from ~ 1 m in the slopes to 5-10 m in the flat areas and coincides often with change in lava type. A high density of dykes correlates with highly fractured lava flows and pyroclastic layers (*Figure 4.2-5*), mainly due to the creation of small scoria cones along the eruptive fissures.



**E** **Figure 4.2-5: Photograph showing the internal structure of the northern branch of the rift zone.** Photograph taken in the Plaine des Osmondes, facing north. Note dykes, as well as aspects of the lava pile and the abundance of pyroclastic layers. See the person for scale.

#### **4.2.3.2 Dyke studies**

There are two main petrological types of magma emitted recently at PF; (1) largely aphyric basalt with less than 5% of phenocrysts, and (2) more primitive, picritic, olivine-rich basalt with more than 30% of olivine xenocrysts, locally referred to oceanites (Bachèlery, 1981; Albarède and Tamagnan, 1988). We found aphyric basalt dykes in both the areas of study, while olivine-rich dykes were found only in the Plaine des Osmondes. The dyke thicknesses are from 0.5 to 2 m and show no clear relation with the petrology.

The studied areas show different dyke trends. In the northern part of the Bellecombe scarp (*Figure 4.2-4*) the most common trend is N120°-125° (*Figure 4.2-6*), whereas in the southern part of the area dykes have a radial distribution (*Figures 4.2-4; 4.2-6*), with a point of convergence 2-3 km west of the actual summit craters. The dykes observed in the Bellecombe scarp, measured at a maximum depth of 150-200 m beneath the surface, are steeply dipping

(70° to 90°) with a mean values of 77.5° (southward dipping) and 79.9° (northward dipping) (Figure 4.2-7).

In the Plaine des Osmondes, the density of dykes increases on approaching of the rift zone (Figure 4.2-4). Some 90% of the dykes trend N0°-40° (Figure 4.2-6), half of which are eastward (seaward) dipping, and are mostly steep ( $82.1^\circ \pm 12.9^\circ$ ; Figure 4.2-7). One-fourth of these dykes dip westward and are more gently dipping ( $74.8^\circ \pm 15.8^\circ$ ; Figure 4.2-7). The remaining one-fourth of the N0°-40° trending dykes are vertical. A second trend, N85°, is constituted by only 4 % of the dykes (Figure 4.2-6), sub-parallel to the scarp and mainly northward dipping. Some 6% of the dykes do not belong to either of the main trends but strike in various directions without any dominating orientation. The dykes in the Plaine des Osmondes were measured at a depth of 400 m beneath the actual surface.

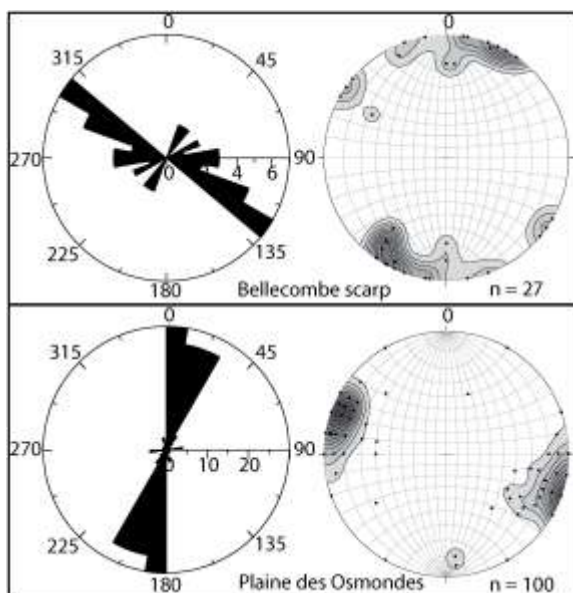


**Figure 4.2-6: Strike direction ( $10^\circ$  class intervals) and pole plot of dykes in the Bellecombe scarp and Plaine des Osmondes (equal area projection, Wulff, lower hemisphere,  $10^\circ$  intervals, density contours of 2%).**

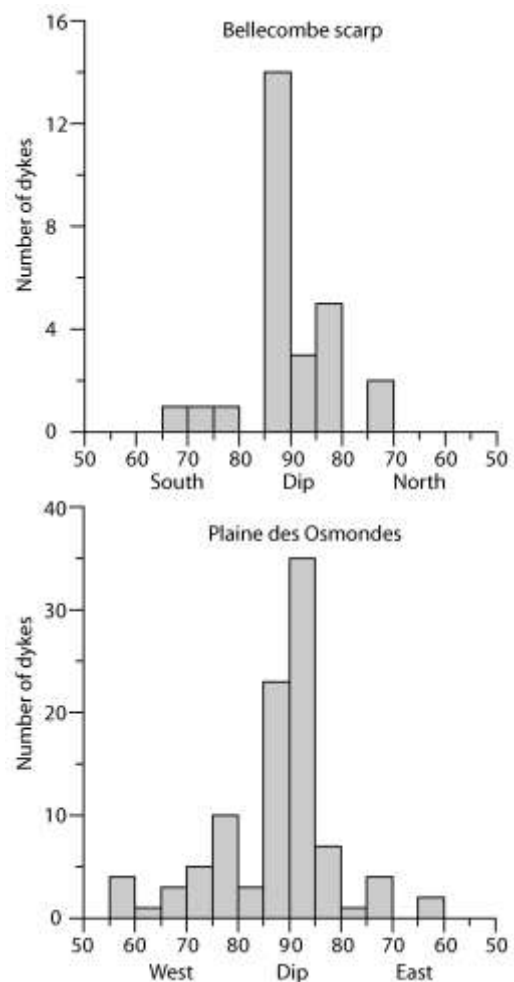


**Figure 4.2-7: Histogram of dip distribution for the Bellecombe scarp and the NE rift zone.**

#### 4.2.3.3 Application to the recent activity

Our field data provide new results as regards the dyke distribution in PF. Various studies have used deformation data to infer the geometry of associated dykes, but do not consider

similar, exposed dykes. The dykes observed in the EFC scarp are clearly older than the event that created the scarp itself ( $> 4.5$  ka) and correspond to a volcanic centre located west of the present one (Bachèlery and Mairine, 1990). Therefore, to allow a comparison between our field data on exposed dykes and the inferred geometries of dykes using recent deformation data, we need to be sure that the state of stress at present is similar to that which existed when the exposed dykes were emplaced.

The age of the EFC collapse is estimated at 4.5 to 5 ka (Bachèlery, 1981; Bachèlery and Mairine, 1990). Gillot et al. (1994) provide dating of  $13 \pm 6$  ka for a lava flow at the base of Piton de Crac (*Figure 4.2-1* for location), a remnant block of the pre-EFC collapse topography (Bachèlery, 1981). Despite an uncertain origin of the Plaine des Osmondes, the consistent altitude between the Plaine des Osmondes and Piton de Crac indicates a similar age. Another dating from Gillot et al. (1994) provides an age for the base of the Bellecombe scarp of  $11 \pm 4$  ka. Thus, intrusions in both areas appear to be older than 4.5 ka and younger than  $13 \pm 6$  ka.

Maintaining a state of stress within the volcano implies maintaining the parameters that can influence the stress. Normally, topography and geometry of the plumbing system, its host rock mechanical properties, as well as the regional stress field, affect the local state of stress. No major plate-scale change has occurred in the past 20 ka around Réunion Island, suggesting that the regional stress field has been essentially constant through this time. The topography, however, has changed in the past due to the creation of the EFC depression and the growth of the central cone. Based on the height of the caldera scarp, there is an elevation difference of  $\sim 200$  m between the present topography and the pre-EFC collapse topography.

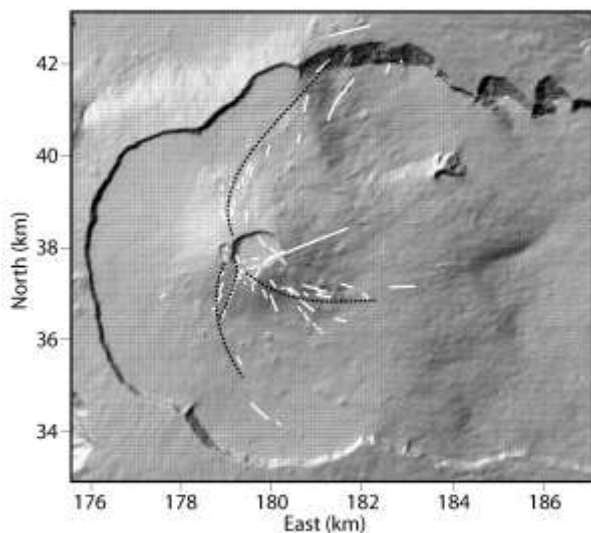


**Figure 4.2-8: Eruptive fissures since 1998 (white).** The dashed black lines correspond to the main trends observed. Coordinates in Gauss-Laborde Réunion.

Furthermore, Bachèlery and Mairine (1990) have shown that the eruptive centre has migrated in the past, from the Plaine des Sables (see *Figure 4.2-1* for location) towards its current position (*Figure 4.2-4*). Our observations confirm that an intermediate stage of migration

occurred (Bachèlery and Mairine, 1990), as is also supported by gravimetric studies (Rousset et al., 1989; Malengreau et al., 1999). The first stage, at around 150 ka (Bachèlery and Mairine, 1990), generated a central plumbing system west of the present summit craters (*Figure 4.2-4*). The present location of the central plumbing system is the result of a migration that probably occurred some 4.5 - 5 ka ago (Bachèlery, 1981) (*Figure 4.2-4*). The present northern branch of the rift zone seems to coincide with the pre-EFC collapse rift zone northern branch. Location of recent eruptions shows that the same path used before the EFC collapse is still used by dykes (*Figures 4.2-4; 4.2-8*). Only the central part of the rift system appears to have been reorganised because of the shifting of the volcanic centre.

Through the time considered, the loading variations affecting the state of stress are at a volcano-scale. The present position of the volcanic centre is closer to the eastern free flank and thus more subject to instabilities. As suggested by Cayol and Cornet (1998), reorientation of stresses may occur in the depth range of a few hundred meters (< 250 m) below the free surface (*Figure 4.2-9*). Such effects on dyke propagation will thus be limited to the summit cone, or close to the eastern flank, and cannot be ruled out for the dyke observed. Thus, the comparison between field data on exposed dykes and recent models on dyke geometries from geodetic data is, despite these variations, justified.

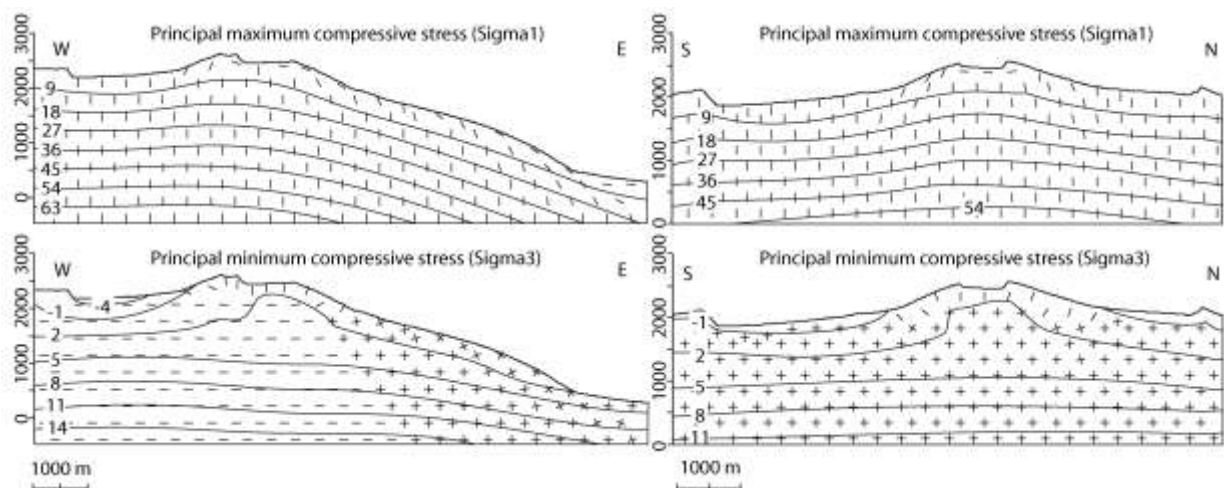


**Figure 4.2-9: Gravity-generated state of stress within the volcano.** We select here S-N and W-E sections through a 3-D representation of the volcano. Both sections cross through the summit craters. The values are in MPa, the negative one representing tension.

The main difference between geodetic and field results concerns the dip values obtained through modelling feeder dykes of recent eruptions and the dyke dips observed in the field. Models give generally shallow seaward dipping dykes on their entire dip dimension ( $53^\circ - 75^\circ$ ) (Cayol and Cornet, 1998b; Froger et al., 2004; Fukushima, 2005; Fukushima et al., 2005;

Peltier et al., 2007) while field results show a mean dyke dip of around  $80^\circ$  at maximum depth of exposure of 400 m (*Figure 4.2-7*).

#### **4.2.4 Modelling**

Several models have been proposed to explain the observed asymmetric deformation (*Figure 4.2-3*), such as shallowly eastward dipping dykes (e.g. Cayol and Cornet, 1998b; Froger et al., 2004; Fukushima et al., 2005; Peltier et al., 2007). These shallow dips are not supported by the field data provided in this study.

We have made many 3-D numerical models, using the code ANSYS ([www.ansys.com](http://www.ansys.com); Logan, 2002) including fractured medium and presence of stiffer rocks within the edifice to test the influence of heterogeneities within the volcano on the asymmetric ground deformation. We have modelled the dyke-induced deformation associated with dykes following the most common path since 1998 (*Figure 4.2-8*). In the models, we also used various models for the dyke-propagation style. Peltier et al. (2005) suggest that a vertical dyke starts from a magma chamber at around 300 m a.s.l. Some dykes propagate laterally, along parts of their paths. However, a lateral injection does not always occur (Peltier et al., 2006a): it may depend on the existence or not of a large-scale level of neutral buoyancy (Ryan, 1987; Pinel and Jaupart, 2004; Fukushima, 2005). The local stress, which depends on the presence of recent intrusions, increasing temporarily the compression, can also influence whether lateral injection occurs, and, so can the magma pressure.

In the models, we take the elevation of 1800 m a.s.l. to be the level of initiation of lateral dyke injections (1600 m a.s.l. in Fukushima, 2005). This altitude coincides with that of the lowest eruptive fissures observed in the surroundings of the cone. Dykes are modelled as vertical fluid-filled cracks, opening with a magma overpressure of 2 MPa (Fukushima, 2005; Peltier et al., 2007) applied horizontally to the dyke walls. The western and bottom boundaries of the models have a zero displacement since PF volcano is buttressed in its western part by the Piton des Neiges volcano (*Figure 4.2-1*).

##### **4.2.4.1 Influence of the superficial fracturing**

To test the influence of pre-existing fractures on dyke-induced ground deformation, we have included vertical fractures. The fractures are modelled as open cracks within a homogeneous medium and extend to a depth of 1400 m a.s.l. (1200 m under the summit craters and 600-800 m under the floor of the caldera). The maximum depth for tension fractures can be obtained

using an equation based on the Griffith criterion (Gudmundsson, 1992). Taking the maximum principal compressive stress to be vertical ( $\sigma_1$ ), the maximum depth is:

$$d_{\max} = \frac{3T_0}{\rho_1 g d} \quad (1)$$

Numerical applications for PF give us a range of 300 to 800 m, while Fukushima (2005) suggests a depth of 1000 m beneath the ground for open fractures. The pressure source is a vertical dyke that stalls at a shallow depth in the northern branch of the rift zone (*Figure 4.2-8*). The *en-échelon* structures of the dyke thought to be present only at a shallow level and correspond to the reorientation of stresses close to and at the surface (Cayol and Cornet, 1998b; Fukushima et al., 2005). Ignoring the *en-échelon* pattern allows us to observe the general pattern of deformation without the short wavelength deformation due to the *en-échelon* structures.

For this set of models, we consider a homogeneous elastic medium with a Young's modulus (elastic stiffness) of 5 GPa and a Poisson's ratio of 0.25 (Fukushima et al., 2005). It also takes into account the topography, which is extracted from a 25 m step Digital Elevation Model (DEM), filtered to a 400 m step. The main structure and topography are kept, the filtering occurring on the small features such as small cones.

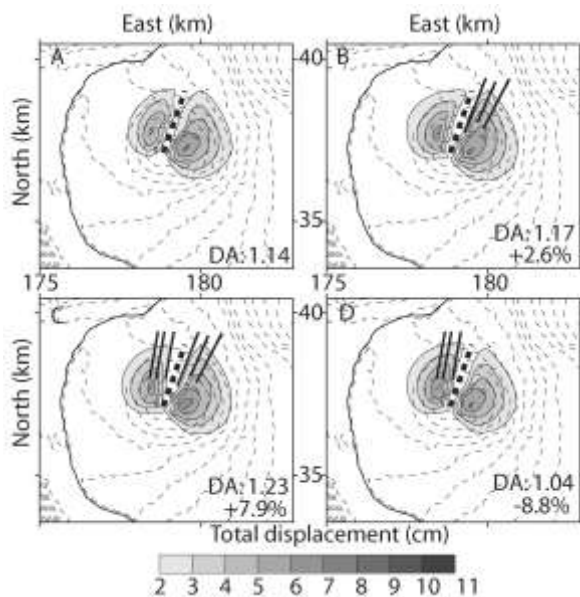


**Figure 4.2-10: Comparison of the deformation induced by a vertical dyke in a: A) homogeneous medium and in a fractured medium with fractures; B) to the east of the dyke; C) to the west of the dyke; and D) with both set of fractures. The trace of the dyke is marked by the black dashed line, and the fractures are marked by the thick white lines. Coordinates in Gauss-Laborde Réunion.**

A degree of asymmetry (DA) for each model is defined by the maximum deformation in the eastern (or northern) side of the dyke, divided by the maximum deformation in the western (or southern) side.

*Figure 4.2-10* compares the total ground displacement for a fully, non-fractured homogeneous medium, and models considering a homogeneous medium including sets of fractures west or east of the intrusion, as well as on both sides. The results show a slight



increase in the asymmetry of deformation by a few percent (8%) between the homogeneous model and the two models including fractures to the east of the intrusion. When fractures are located to the west of the intrusion, the deformation is favoured on the western side of the dyke, reducing the natural asymmetric pattern of deformation.

#### 4.2.4.2 Influence of the rift zone system

Since remnants of the pre-EFC plumbing system could be present in the western part of the volcano as dykes and sills, we tested the influence of stiffer rocks within the volcano (*Figure 4.2-11*) both during the pre-eruptive inflation and the dyke injection. We also tested the influence of the actual rift zone system by including the structural control that it has on the magma injection paths (*Figure 4.2-8*), characterised by curved dykes.

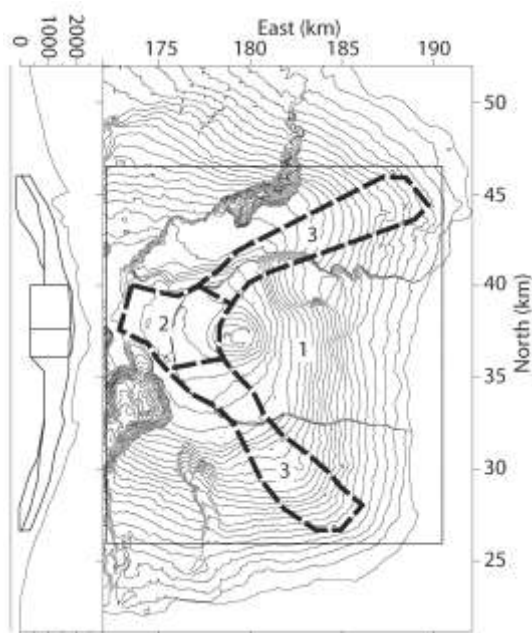


**Figure 4.2-11: Location of the rift zone within the model (dashed line), and limit of the computed area (thin black line) using Ansys.** The numbers correspond to the various medium used. 1 and 2 are elastic isotropic medium of stiffness (Young's modulus) 5 GPa and 8 GPa, respectively. 3 is an orthotropic medium with X and Y = 8 GPa and Z = 4 GPa. The Poisson's ratio is common for all the materials and equal to 0.25. Coordinates in Gauss-Laborde Réunion.

The first set of models presents the resultant total deformation for the injection of vertical and planar dykes in a fully homogeneous medium (*Figure 4.2-12*) along the three main dyke paths observed since 1998 (*Figure 4.2-8*). The second set of models tests separately the effect of the presence of an old plumbing system with vertical and planar dykes. In the third set, the curvature of vertical dykes is tested. We then combine both effects in a last set of models (*Figure 4.2-13*). For the comparison we also use a degree of asymmetry.

For these sets of models, the same program is used, and the dykes considered also stall at shallow depths. Three different media were used to define the different models (*Figure 4.2-11*). Two are elastic isotropic media with a stiffness (Young's modulus) of 5 GPa corresponding to the lava pile constituting the main part of the volcano (Fukushima, 2005), and 8 GPa corresponding to the central part of the old plumbing system. The third medium is an elastic

orthotropic medium with a stiffness of 8 GPa in the X and Y direction and of 4 GPa in the Z direction that corresponds to the branches of the old plumbing system's rift zone.

Results presented in *Figure 4.2-13*, when compared with the homogeneous models (*Figure 4.2-12*), show that in all the cases the presence of the old plumbing system to the west of the actual active part tends to increase slightly the natural asymmetry existing between the east and the west of the intrusion. The curvature of the dyke appears to have a greater effect on the asymmetry of deformation. Both mechanisms combined show a strong increase (by up to 42 %) of the asymmetry, which does not correspond to the simple addition of the effects.

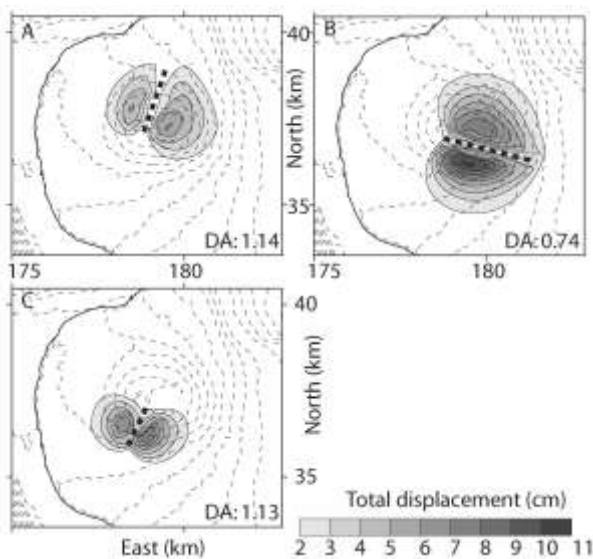


**Figure 4.2-12: Models for the injection of a planar vertical dyke with an overpressure of 2 MPa in a fully homogeneous medium in: A) the northern branch of the rift zone; B) the N120° rift zone; and C) the south-western branch of the rift zone. The DA is included in the figures. Coordinates in Gauss-Laborde Réunion.**

*Figure 4.2-14* shows the deformation triggered by an overpressure of 10 MPa in a shallow magma chamber located at sea level (Nercessian et al., 1996; Peltier et al., 2005). It allows modelling of the pre-eruptive pattern of deformation. The first model is homogeneous with the same characteristics as the other model (stiffness of 5 GPa), while the second model includes the old plumbing system defined above. Its presence leads to a shift of the peak of deformation slightly to the east of the crater, in agreement with the pre-eruptive pattern of deformation observed at PF (*Figure 4.2-3*). The deformation is also 20% larger because of the rift zone.

## 4.2.5 Discussion

### 4.2.5.1 A complex plumbing system

The petrological characteristics of an erupted magma provide information on the path followed by the magma. In our studied areas, olivine-rich basalts have only been observed in the Plaine des Osmondes. Recent eruptions generally support our observations, although olivine-rich basalts can occasionally be observed in other places, along the SSE-trending rift zone (Albarède and Tamagnan, 1988) or in the east of Dolomieu crater, and along the PN-PF

axis, in the Plaine des Sables. According to Bachèlery (1999), olivine-rich basalt magmas are likely to derive from a deep-seated reservoir and are associated with the refilling of the associated shallow magma chamber.

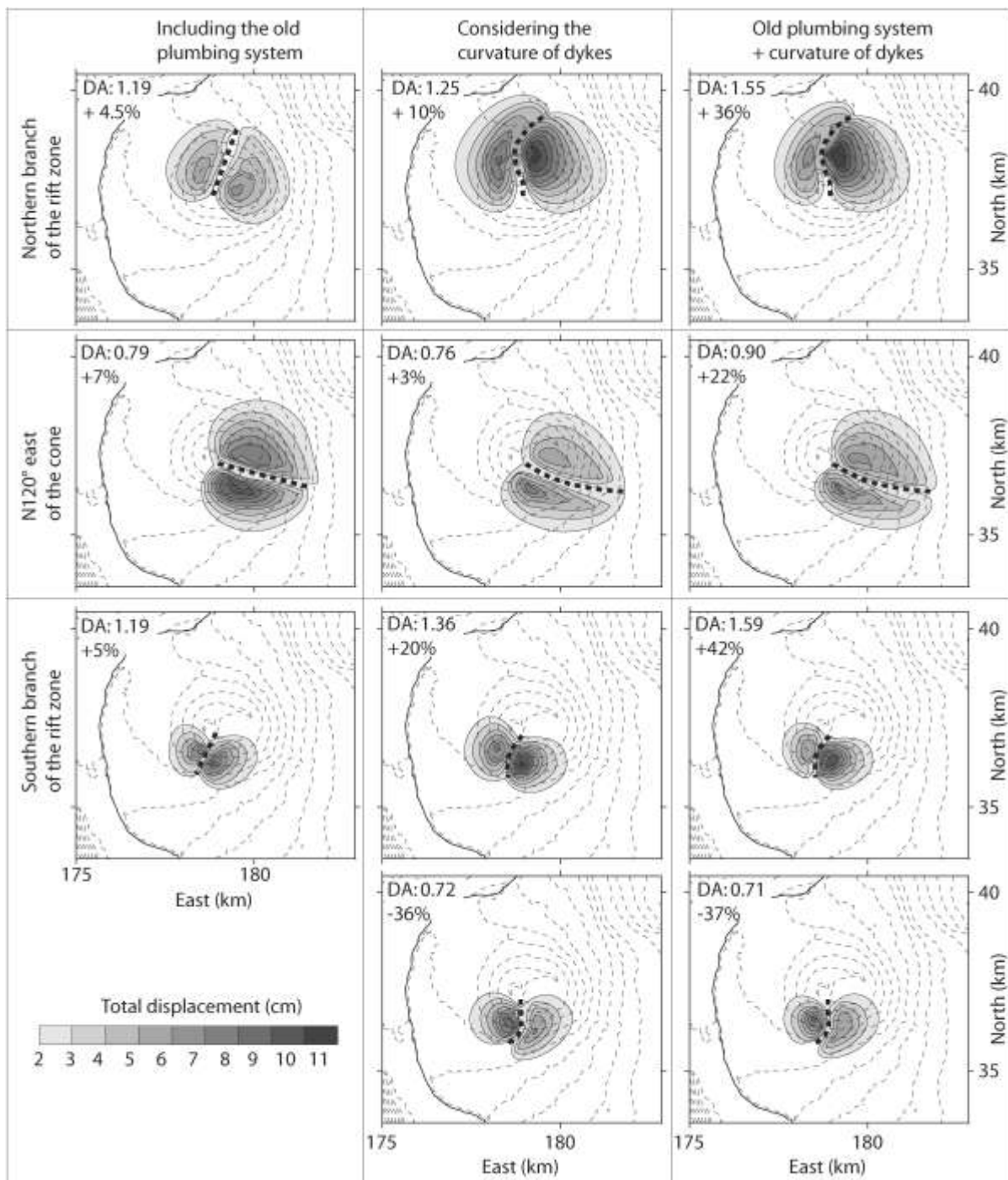


**Figure 4.2-13: Deformation resulting from the injection of dykes along the three main paths used since 1998.** The left column corresponds to vertical planar dykes while the two other correspond to curved vertical dykes. For the injection in the south rift zone, both the curvature to the east and the west are tested. The overpressure in all the models is 2 MPa. The traces of the dykes are represented by the dashed thick black line. Coordinates in Gauss-Laborde Réunion.

As suggested by Peltier et al. (2006), and in the absence of eruptive fissures in the summit area (Figure 4.2-14), olivine-rich basalt eruptions occurring in the Plaine des Osmondes are fed

by lateral dykes propagating at greater depths. The 1998 eruption shows that aphyric dykes can also propagate, at shallow depths, far from the central plug (*Figure 4.2-15*) (Bachèlery, 1999; Peltier et al., 2006a).

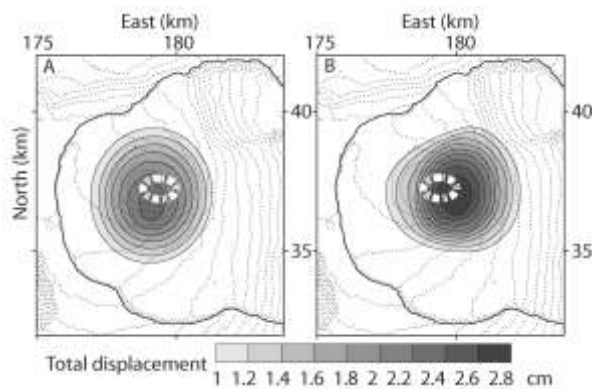


**Figure 4.2-14: Models considering an overpressure of 10 MPa in a shallow magma chamber in a A) homogenous medium and B) in the rift zone. Location of the magma chamber is marked by the white dashed lines with the top located at a depth of 300 m a.s.l. The thickness of the magma chamber is 500 m. Coordinates in Gauss-Laborde Réunion.**

This eruption is considered as a refilling event but does not reflect the common style of an oceanitic eruption (low effusion rate for 1998, while oceanitic eruptions have a high effusion rate, and no olivine crystals) nor aphyric eruptions occurring at PF, because of its duration and the large volume of evolved magma. Aphyric basalts in the recent period are mainly erupted in the summit craters or on the flank of the cone and its close proximity (Peltier et al., 2006a). The PN-PF axis is represented mainly by aphyric basalts or aphyric basalts bearing olivine nodules (Bachèlery, 1981; this study). Bachèlery (1981) suggests that the lavas emitted along the PN-PF axis have a deep origin, the nodules of olivine coming from the ascension of magma through a shallow (partially) crystallised magma chamber.

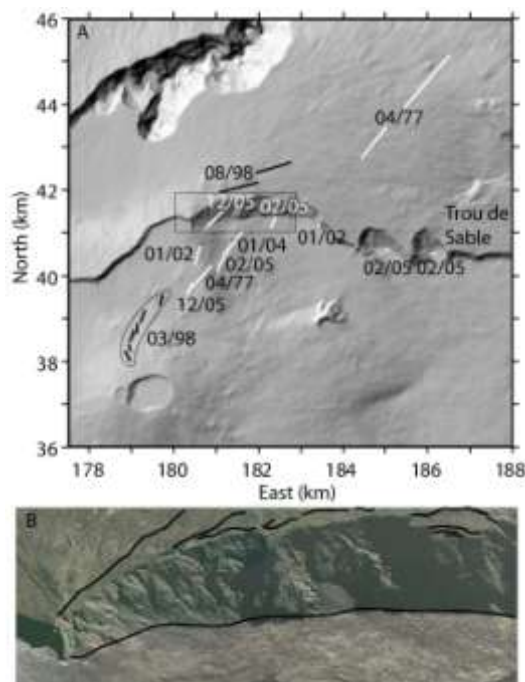


**Figure 4.2-15: A) Location of the April 1977 and the post-1997 eruptive fissures that have propagated in the Plaine des Osmondes or outside Enclos Fouqué. In white, eruptive fissures that emitted olivine-rich lavas. In black, eruptive fissures that emitted aphyric basalt. The dates are in a month/year format. All the fissures that opened in 1998 are related to the same eruption, the opening in 08/98 corresponding to a late propagation of the dyke (Bachèlery, 1999). B) Aerial photograph of August 2003 (IGN) showing the western part of the cliff above the Plaine des Osmondes. In black are the fractures visible on the photograph. Coordinates in Gauss-Laborde Réunion.**

This difference in lithology seems to reflect different magma paths as well as different depths of origin. The N120° direction is found at all scales on the island and the oceanic crust (Michon et al., 2007a), and therefore might control the transport of magmas coming from great depths. The NNE-SSE trending rift zone likely reflects gravitational processes (Walter et al., 2006) and controls the paths of magma at shallow depths, in the active plumbing system. Within the NNE-SSE rift zone, long distance or short distance dyke propagation reflect transport at different depths (Aki and Ferrazzini, 2000; Peltier et al., 2006a). The depth of propagation reflects a difference in overpressure and / or density of the magma; the higher the pressure, the deeper origin of the magma. Existence of a complex storage system can also explain partly the different depths of magma injection (Aki and Ferrazzini, 2000). *Figure 4.2-15* illustrates the various magma/dyke paths within the volcano.

#### **4.2.5.2 Rift zone, fractures and structural control**

Field results confirm that the magma follows some preferential paths in the volcano, such as NNE-SSE-trending, SW-trending, and N120°, marking the rift zones where most of the recent volcanic vents occur (*Figures 4.2-2; 4.2-8*). In the field, rift zones coincide with an increase in the density or intensity of dykes, as well as with an increase in the proportion of pyroclastic (scoria) deposits (*Figure 4.2-5*). The number of tectonic fractures is also much greater within a rift zone than outside the zone. By decreasing the large-scale elastic stiffness and the tensile strength of the host rock, fractures make dyke paths easier to form. This effect on magma paths is observed within the rift zones as well as in association with all the large fractures of the volcano. Field data in the Plaine des Osmondes show a second trend of dykes coinciding with the orientation of the scarp. Recent eruptions demonstrate the structural control that the faults associated with the EFC scarp exert on the magma path.

On 5<sup>th</sup> of January 2002, an eruption began. After a period with a low seismic tremor, the tremor increased. On 12<sup>th</sup> of January 2002, a new eruptive fissure opened at the foot of the EFC scarp, off the apparent axis of propagation of the dyke, suggesting propagation along the EFC scarp following the pre-existing fractures (*Figure 4.2-15*). On 17<sup>th</sup> of February 2005, another eruption occurred in the Plaine des Osmondes. On 25<sup>th</sup> of February, one day before the end of 17<sup>th</sup> February fissure eruption, a new eruptive fissure opened, in the Trou de Sable (*Figure 4.2-15*), at 500 m a.s.l., again along the ECF scarp. The new opening was accompanied by an increase in the seismic tremor, and without any evidence of new magma injection from the summit area, suggesting a further propagation of the initial dyke along the pre-existing fracture boarding the EFC scarp. The lavas emitted in the Trou de Sable are olivine-rich basalts and

strongly degassed. In December 2005, GPS data showed that the dyke, responsible for the opening of a new eruptive fissure within the EFC scarp, propagated further outside the EFC depression. The load difference due to the difference of altitude may have prevented the opening of an eruptive fissure outside the EFC depression as suggested by Acocella et al. (2006) for Vesuvius.

However, in April 1977, an eruption occurred far away from the EFC scarp, outside the EFC depression. Thus, it appears that the EFC scarp and the associated faults did not control all the eruption sites. Injected dykes with a high overpressure, such as the April 1977 dyke (effusion rate of the April 1977 eruption was 3 times higher than the other considered eruptions – Global Volcanism Program website), managed to propagate through the fractures associated with the EFC scarp.

The pre-existing fractures play an essential role in forming the magma path in the rift zone as well as allowing propagation of magma along the EFC scarp. The scarp and associated faults also have an important role as they act as structural barriers, limiting the opening of fractures outside the depression (Acocella et al., 2006) and exert a strong structural control on the magma paths.

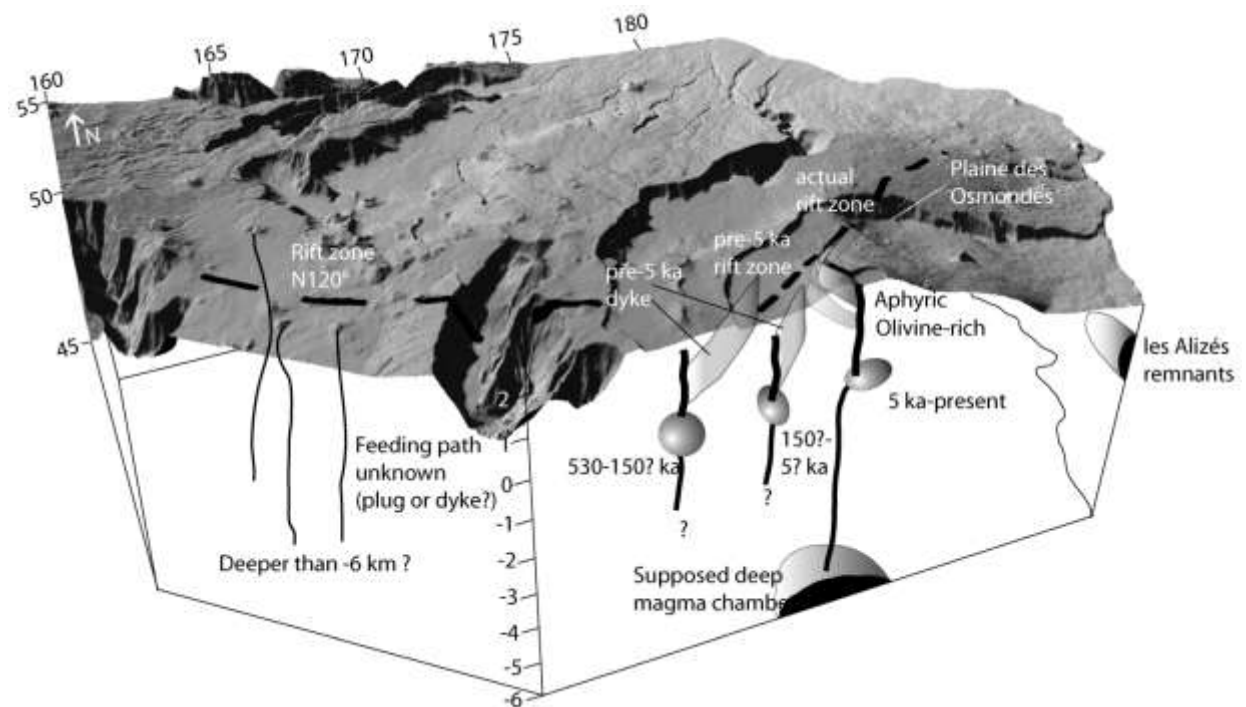


**Figure 4.2-16: Schematic representation of the plumbing system of Piton de la Fournaise.** The depths of shallow magma chamber for the two past volcanic systems (530-150 ka and 150-5 ka) are not well constrained. Thick lines correspond to a plug supposed to be used recurrently to feed eruptions at the summit or on the summit cone. By analogy, we extend the presence of the plug to the two past volcanic systems. At greater depths in the plug, olivine-rich magmas are laterally injected to feed eruptions in the Plaine des Osmondés. The deep magma chamber is inferred from seismic data (Battaglia and Bachèlery, 2003), while the remnants of Les Alizés volcano are based on gravimetric studies (Rousset et al, 1989; Malengreau et al, 1999). Coordinates in Gauss-Laborde Réunion.

### **4.2.5.3 Influence of rift system on deformation**

Our field results, especially from the northern branch of the NNE-SSE rift zone, and the computed dykes (Froger et al., 2004; Fukushima, 2005; Peltier et al., 2007), show a marked difference. The calculated dyke dips, characterising the entire dip dimension of each dyke, are too shallow in comparison with our field observations of dykes propagating at shallow depths (< 400 m). Moreover, although calculated dykes may explain the asymmetric deformation during the injection, they offer no satisfactory explanation for the asymmetric deformation occurring prior to dyke injection (*Figure 4.2-3*). We have explored the influence of various heterogeneities on the ground deformation.

The fully homogeneous models show that a natural asymmetry exists as the deformation in the east is greater than that in the west, demonstrating the influence of the topography on the deformation. In a first set of models, we show that few tectonic fractures within the rift zone have a limited influence on the ground deformation, increasing it by a maximum of 8 % the DA (*Figure 4.2-10*). By decreasing the elastic stiffness of the rocks (Bell, 2000), fractures make the medium more easily deformed and increase the natural asymmetry of deformation that exists. As suggested by *Figure 4.2-2*, the extension of fractures is much greater than in the models. Increasing the number of fractures tends to reduce further the elastic stiffness and thus increase their influence on the ground deformation.

We have also considered the influence of an old plumbing system, located to the west of the actual volcanic centre, on dyke paths (*Figure 4.2-11*). Studies (Rousset et al., 1989; Malengreau et al., 1999) suggest that this old plumbing system was possibly preserved during the vertical collapse of the EFC (Bachèlery, 1981; Merle and Lénat, 2003). The results of numerical modelling indicate that the presence of heterogeneities (old plumbing system) increase, somewhat (< 7 %) the asymmetric deformation both during dyke injection (*Figure 4.2-13*) and pre-eruptive inflation (*Figure 4.2-14*).

We have also tested the effects of curvature of dykes on the surface deformation. The complex evolution of the rift system through time, associated with the gradual migration of the eruptive centre, has resulted in a curved rift system (*Figures 4.2-2; 4.2-8*). Magma paths follow this curvature (Michon et al., 2007a). Our models show that the dykes curvature has potential effects on deformation in some cases (*Figure 4.2-13*), but is far less than actually observed (e.g. Fukushima, 2005). However, the combination of both the curvature of dykes and the presence of the old plumbing system west of the actual intrusion zone have great effects on the ground deformation and make it closer to what is observed.

The presence of the old plumbing system (dense and stiff rocks) west of the actual plumbing system tends to limit the deformation in this direction. The stiff rocks create a barrier and isolate the eastern flank from the rest of the edifice. A similar model has been proposed for Kilauea in Hawaii (Delaney and Denlinger, 1999). However, in the case of Hawaii, the existence of a basal *décollement* allows a more efficient decoupling between the two sides of the rift zone. Curvature of a dyke tends to have two effects. First, it increases the area affected by the loading variation on the convex part of the dykes, and thus dissipates the stress. Second, it concentrates the stresses in the concave part of the dyke, increasing the compression (Walter et al., 2005) and thus the deformation.

For dyke injections to the east of Dolomieu crater along a direction N120°, our models explain the kind of asymmetry observed during some but not all the eruptions. The maximum deformation observed in this area is not always on the same side of the eruptive fissures (Fukushima, 2005). The irregular pattern of deformation along this direction seems to reflect mainly variation in dyke dip that can be partly the effect of the topography of the summit cone (*Figure 4.2-9*). However, a more complex structure in the eastern part of Dolomieu at depth, linked with older intrusive system, cannot be ruled out. In the other two cases studied, the asymmetry obtained in our models does not properly fit the deformation data. A complex internal structure, or the variation in the dyke dip are parameters that allow a better fit of the models and observed deformation. Our models consider vertical dykes, while the stress field associated with the free flank is likely to interfere with the propagating dykes (*Figure 4.2-9*). However, the dyke dip needed to explain the asymmetry will be less in a heterogeneous medium and thus in a better agreement with our field observations of exposed dykes and the inferred stress field (*Figure 4.2-9*).

#### **4.2.6 Conclusions**

In this study we provide new data on the magmatic plumbing system of Piton de la Fournaise, and new results on the deformation of the volcano before and during an eruption. Our main conclusions may be summarised as follows:

➤ The distribution of exposed dykes confirms that the volcanic centre has migrated in the past, its current position being the result of gradual migration from the Plaine des Sables, to close to the Bellecombe scarp (*Figure 4.2-4*), and then towards its current location. The first migration occurred ~ 150 ka ago (Bachèlery and Mairine, 1990), followed by the second migration which was contemporaneous with the formation of Enclos Fouqué Caldera.



➤ The lithology of dykes, observed along the rift zone outside the central cone, indicates a complex plumbing system. Multiple paths are dependent on the depth of origin of the magma as well as the location within the volcano. The PN-PF axis reflects a deep structure (Michon et al., 2007a) and controls the transport of magma from deep-seated sources. The NNE-SSE-trending rift zone, perhaps of gravitational origin (Walter et al., 2006), controls the magma paths at shallower depths (*Figure 4.2-16*).

➤ Fractures induced by recurrent intrusions and long-term deformation of the volcano influence the magma paths. Fractures linked with volcano-tectonic processes such as collapse or landslide influence the propagation of magma along the Enclos Fouqué Caldera scar. The effects of fractures and topographic load variations have a direct impact on the assessment of volcanic hazards as it prevents the opening of fractures outside the Enclos Fouqué Caldera (*Figure 4.2-15*). Propagation and opening outside the Enclos Fouqué Caldera are linked with highly overpressured magma.

➤ Our field data (*Figure 4.2-7*) indicate much steeper dyke dips than geodetic models previously published to explain the asymmetric deformation (*Figure 4.2-3*; e.g. Zlotnicki et al., 1990; Cayol and Cornet, 1998b; Sigmundsson et al., 1999; Battaglia and Bachèlery, 2003; Froger et al., 2004; Fukushima et al., 2005; Peltier et al., 2007). We provide new numerical models that take into account existing fractures and intrusions (*Figures 4.2-10; 4.2-13*). These new models allow an explanation of the asymmetric deformation (*Figures 4.2-10; 4.2-12; 4.2-13; 4.2-14*) and provide a better fit with the field data.

➤ Our models show that complex structure, fracturing and structural control of magma paths allow to explain part of the asymmetric pattern of deformation observed at PF. The same kind of behaviour and influence can be expected in many volcanoes that have a long and complex eruptive history. A better understanding of the past history and internal structures of volcanoes is essential for reaching a better understanding of their present deformation.

### **Acknowledgements**

We thank Ruth Andrew for helpful comments on an earlier version of the manuscript. We also gratefully thank the two anonymous reviewers for their useful comments and the staff of the Volcanological Observatory of Piton de la Fournaise (OVPF) for technical maintenance of the GPS network.

### 4.2.7 Lava pile characterisation

As mentioned in the publication, the lava pile varies according to the location. In flat area, outside rift zones, thick lava flows, accompanied by thin auto-breccia layers can be observed (*Figure 4.2-17*). In rift zones, and steep slopes, lava flows are much thinner, and auto-breccias are replaced by pyroclastic layers that constitute the major part of the lava pile (*Figure 4.2-17*).

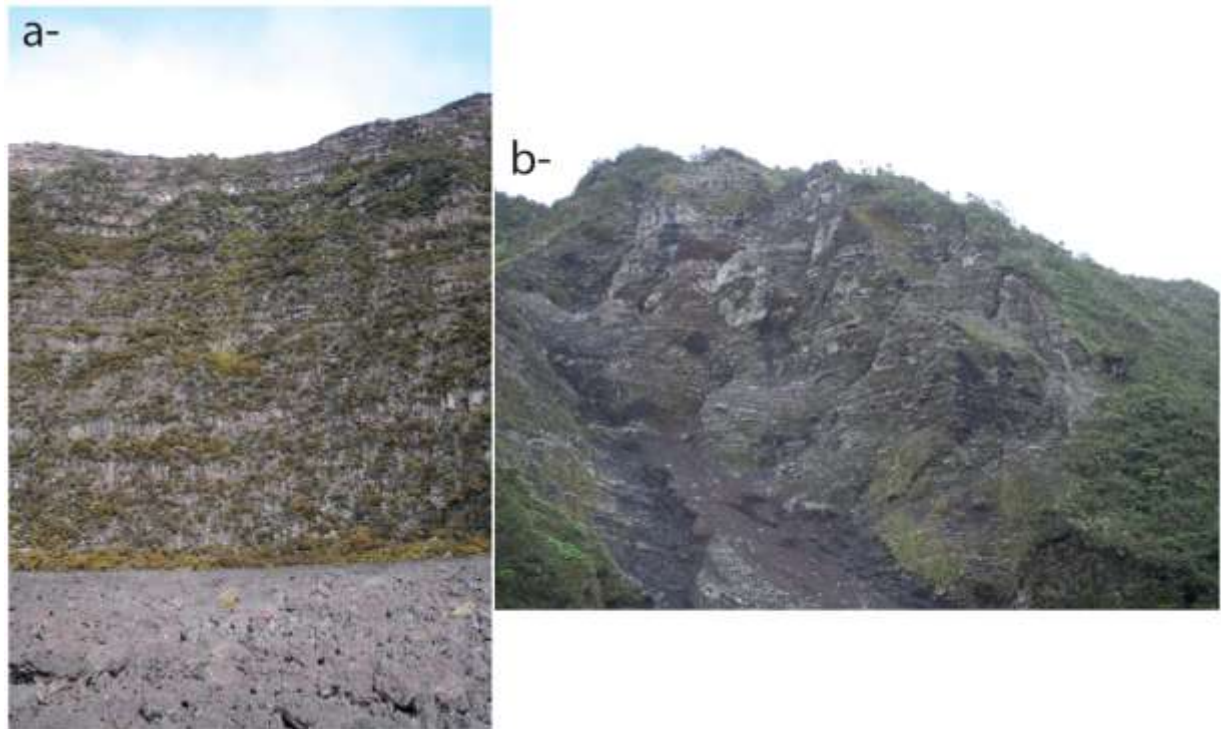


**Figure 4.2-17:** a- lava pile in a flat area, outside feeding structures; b- lava pile in ‘les Grandes Pentes’, along the rift zone. On the left the height of the cliff is about 200 m and on the right the height is about 300 m.

### 4.3 Growth and deformation of Piton de la Fournaise summit cone: Paper 4

In this study, we try to answer the problem outlined by the E-W trending elongation of the summit cone, while related with a feeding system of N-S trending orientation in this part of the volcano. We answer this contradiction, with regards to the deformation linked with magma injection within the edifice as well as its previous history. We also highlight the processes of deformation that affect the central cone, creating a complex network of fractures at its surface. The study presented here has been accepted with minor revisions in the *Journal of Volcanology and Geothermal Research*.

## **Morphology, structure and deformation of the steep central cone of Piton de la Fournaise shield volcano (Réunion Island, Indian Ocean)**

Laurent Michon<sup>1</sup>, Ludovic Letourneur<sup>2</sup>, Aline Peltier<sup>1,3</sup>, Nicolas Villeneuve<sup>4</sup>, Thomas Staudacher<sup>3</sup>

<sup>1</sup> Laboratoire GéoSciences Réunion, Université de la Réunion, Institut de Physique du Globe de Paris, CNRS, UMR 7154 – Géologie des Systèmes Volcaniques, 15 avenue René Cassin, 97715 Saint Denis, France.

<sup>2</sup> Department of Structural Geology and Geodynamics, Geoscience Centre, University of Göttingen, Goldschmidtstrasse 3, D-37077 Göttingen, Germany.

<sup>3</sup> Observatoire Volcanologique du Piton de la Fournaise (OVPF), Institut de Physique du Globe de Paris, CNRS, UMR 7154 – Géologie des Systèmes Volcaniques, 97418 La Plaine des Cafres, France.

<sup>4</sup> Institut de Recherche pour le Développement, US 140, BP172, 97492 Sainte-Clotilde cedex, France.

### **Abstract**

The overall morphology of basaltic volcanoes mainly depends on their eruptive activity (effusive vs. explosive), the geometry of the rift zones and the characteristics of both endogenous and exogenous growth processes. The origin of the steep geometry of the central cone of Piton de la Fournaise volcano, which is unusual for a basaltic effusive volcano, and its deformation are examined with a combination of a detailed morphological analysis, field observations and GPS data from the Piton de la Fournaise Volcano Observatory. The new caldera walls formed during the April 2007 summit collapse reveal that the steep cone is composed of a pyroclastic core, inherited from an earlier explosive phase, overlapped by a pile of thin lava flows. This suggests that exogenous processes played a major role in the building of the steep central cone. Magma injections into the cone, which mainly occur along the N25°-30° and N120° rift zones, lead to an asymmetric outward inflation concentrated in the cone's eastern half. This endogenous growth progressively tilts the south-eastern and eastern flanks of the cone, and induces the development of a dense network of flank fractures. Finally, it is proposed that intrusions along the N120° rift zone are encouraged by a stress accumulation during magma injections along the N25°-30° rift zone.

**Keywords:** Piton de la Fournaise, morphology, volcano fractures, growth process, rift zone.

### **4.3.1 Introduction**

Basaltic shield volcanoes grow by the combined effect of endogenous and exogenous processes (e.g., Annen et al., 2001). Endogenous growth is mainly related to dyke intrusions, which preferentially propagate along the existing rift zones. The volcano shape consequently depends on the intensity of their activity and may vary from elongated, e.g., Karthala in Grande

Comore, and Mona Loa and Kilauea in Hawaii (*Figure 4.3-1*), to sub-circular, e.g. volcanoes of Western Galapagos (*Figure 4.3-1*). Exogenous growth results from the accumulation of lava flows and pyroclastic cones (Naumann and Geist, 2000; Rowland and Garbeil, 2000). Long lava flows tend to flatten the volcano morphology, whereas short and thick ones may encourage the development of steep edifices (*Figure 4.3-1*; Naumann and Geist, 2000; Annen et al., 2001).

At Piton de la Fournaise (PdF), Réunion Island, however, the magmatic activity led to the development of a steep central cone in the Enclos caldera despite the predominance of fissure eruptions that feed fluid basaltic lava flows. Moreover the cone is almost circular whereas most of the eruptions develop along the N25°-30° and N120° rift zones (*Figure 4.3-2*; Michon et al., 2007a). To answer these paradoxes, Annen et al. (2001) proposed, using numerical models, that the geometry of the cone was resulting from a predominant endogenous growth with only 30% of the edifice volume directly related to short lava flows. Although the models roughly fit the current cone geometry, the input and natural data partly disagree. First, the simulated dykes (mean thickness of 3 m) are not as thick in nature as in the models. Indeed, recent works showed that the mean dyke thickness related to the post-1997 eruptions was around 0.5-0.7 m (Fukushima et al., 2005; Peltier et al., 2007). Second, the model of Annen et al. (2001) simulates 10000 dyke intrusions, 7% of them leading to an eruption. Such an intrusion/eruption ratio is the opposite of that observed since 1972, 81 eruptions (92%) and 7 intrusions (8%). Models with more realistic parameters show that the central cone should be much flatter (Annen et al., 2001).

This paper aims at understanding the origin of the atypical geometry of the central cone of PdF. It examines the morphology and inner structure of the cone. It also considers the role of the magmatic and volcano-tectonic structures in both the growth and the deformation of the cone, by combining field data and GPS data. Such a multi-disciplinary approach highlights the existing links between the deformation observed in the field, the displacement measured by GPS, and the recurrent intrusions of the dykes along preferential paths. The origin of the central cone and its deformation are interpreted in the light of both endogenous and exogenous growths.

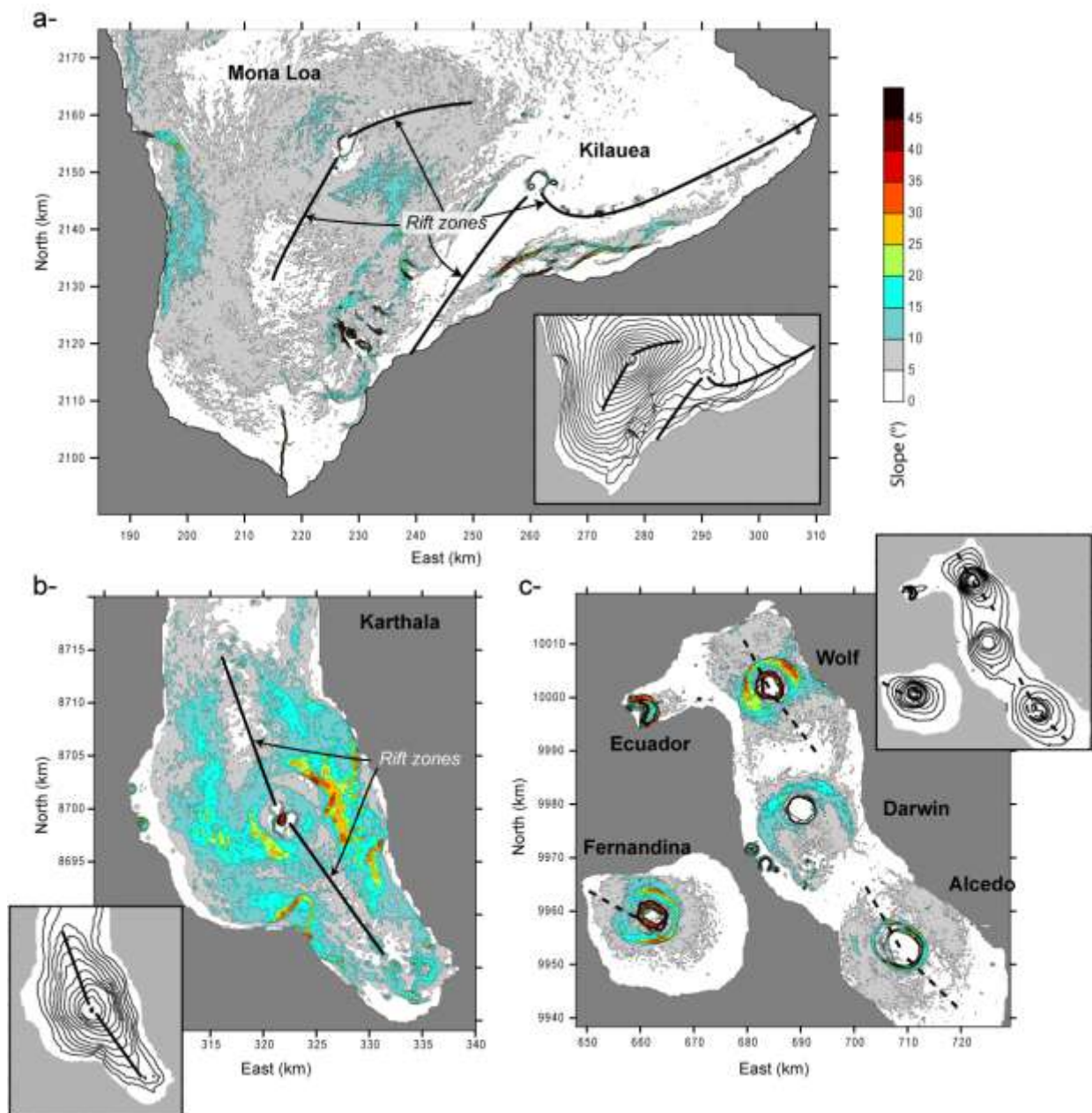


**Figure 4.3-1:** Slope maps of Hawaiian volcanoes (a), Karthala in Grandes Comores (b) and volcanoes in Western Galapagos (c), illustrating the contrasted geometries of the volcanic edifices. Coordinates in UTM WGS84 (a. Zone 5N, b. Zone 38S and c. Zone 15S). DEM from the SRTM mission (Jarvis et al., 2006).

### 4.3.2 Morphology and inner structure of the central cone of PdF

PdF is the active volcano of Réunion Island (Figure 4.3-2). The eruptive centre is located in the upper part of a large U-shaped caldera, the Enclos-Grand Brûlé structure, where most of the eruptions have occurred in the past 4.5 ka (Bachèlery, 1981). The concentration of the activity in the upper part of the caldera led to the construction of a c.400 m high cone. The magma intrusions, which originate from a magma chamber located at about sea level below the cone (Peltier et al., 2007), are concentrated along two N25°-30° and N120° rift zones (Figure 4.3-2; Michon et al., 2007a). Outside the Enclos caldera, the magma intrusions may continue along the

NE and SE-trending rift zones. The present day cone summit shows two collapse structures: Bory crater in the West, which is currently inactive, and Dolomieu in the east, which recently experienced a caldera collapse during the large April 2007 eruption (Figure 4.3-2; Michon et al., 2007b). Before this collapse, the elongated shape of the pre-existing Dolomieu was the result of the coalescence of several pit craters (Lénat and Bachèlery, 1990; Carter et al., 2007). As a whole, Bory and Dolomieu confer a global E-W trending elongation to the summit of the central cone.

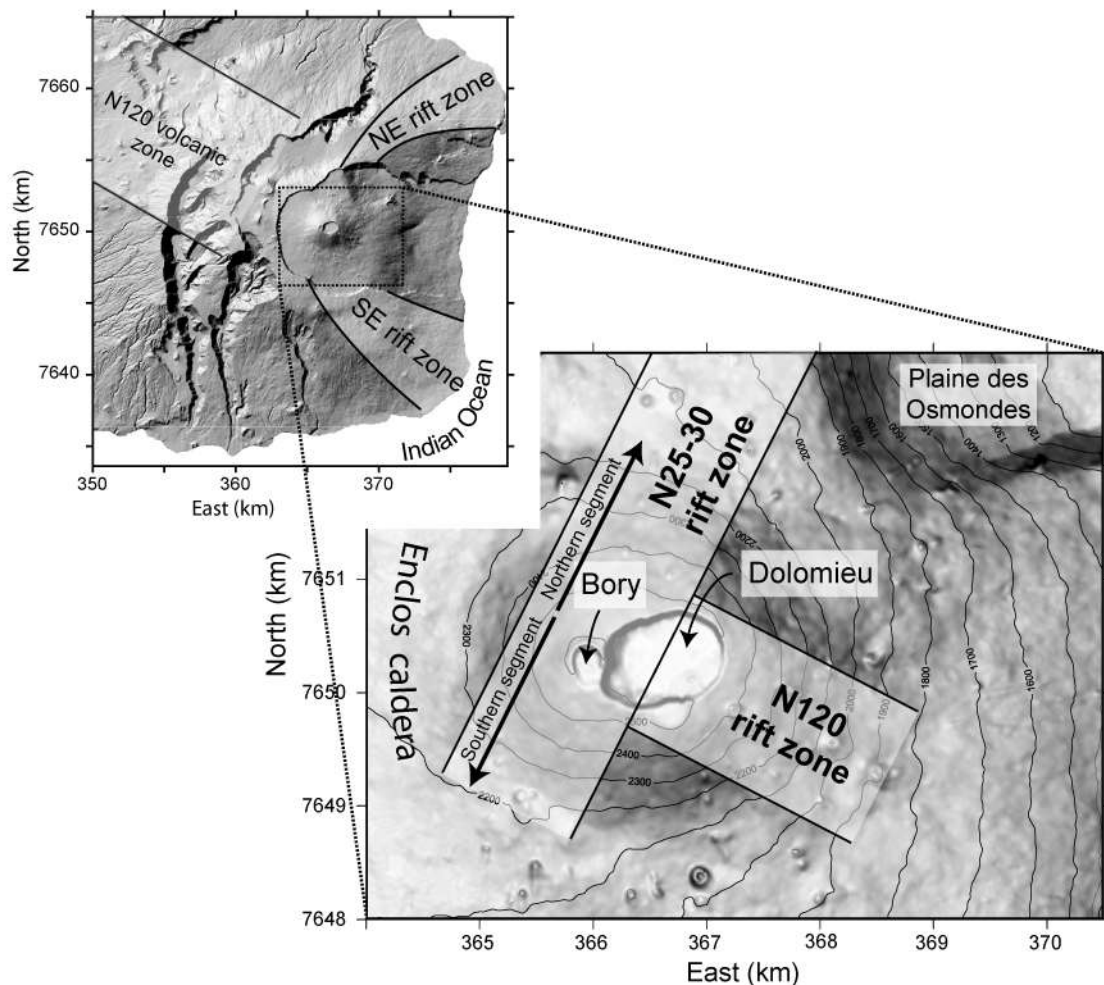


**Figure 4.3-2: 25 m step Digital Elevation Model of Piton de la Fournaise.** *The edifice is characterised by two NE and SE rift zones outside the Enclos caldera. In the Enclos caldera, the recent eruptions are concentrated along two N25°-30° and N120° rift zones (Michon et al., 2007a). The central cone is cut by two summit collapse structures, Bory and Dolomieu. Coordinates in UTM WGS84 (zone 40S).*

The use of a 25 m step digital elevation model (DEM) provided by the Institut Géographique National allows a precise description of the limits of the cone, the distribution of the slopes and the structure of the summit zone. The cone's lower limit corresponds to an almost continuous sharp break-in-slope that separates the caldera floor and the steep flanks of the cone (Figure 4.3-3). The local outline discontinuities are due to the Puy Mi-Côte parasitic cone in the North, and the N120° topographic ridge in the south-east, which is formed by the alignment of large

pyroclastic cones along the N120° rift zone. These two structures disregarded, the base of the cone presents a sub-circular shape with a radius of about 1.6 km (*Figure 4.3-3*). The flanks of the cone present steep slopes, which contrast with the classical view of a basaltic effusive edifice. The western part of the cone, i.e., west of a N15° trending line centred on Dolomieu, is characterised by relatively homogeneous slopes ranging between 15° and 25°. East of the N15° boundary, the cone shows steeper slopes (25°-30°), which locally reach 35°. Although the N120° topographic ridge gives to the south-east flank a complex slope distribution, the low-pass filtered DEM strikingly shows that the steep slopes of the cone's eastern half are not circumferentially distributed, but present two linear trends in the N150° and N55° directions (*Figure 4.3-3*). It is noteworthy that the N55° trend is aligned with a 500 m wide and 700 m long zone characterised by a network of parallel lineaments (*Figure 4.3-3*). Field observations and aerial photographs reveal that the lineaments correspond neither to the limit of lava flows, nor to eruptive fissures. Finally, the summit morphology of the cone is characterised by present collapse structures, Bory and Dolomieu, surrounded by relatively flat areas which were interpreted as totally filled pit craters (*Figure 4.3-3*; Bachèlery, 1981; Lénat and Bachèlery, 1990). Past and present collapse structures are restricted to a slightly elongated zone, the centre of which is nearly superimposed to that of the 3.2 km-across circle marking the base of the cone (*Figure 4.3-3*).

The April 2007 caldera, which deeply cut the central cone, formed new scarps that reveal its internal structure (*Figure 4.3-4*). The northern and southern caldera walls exhibit three main structural features.

➤ The north-western part of the cone built up above a pre-Bory pit crater, the existence of which was already hypothesised by Lénat and Bachèlery (1990) from the occurrence of gentle slopes north of Bory (*Figures 4.3-3*; *4.3-4*). The limits of this collapse structure are underlined in the caldera wall by a strong lithological contrast characterised by thick lava units, and the succession of thin lava flows and scoria layers, inside and outside the pit respectively.

➤ The volcanic units cut by the pre-Bory pit crater are sub-horizontal and parallel to the present day surface, suggesting that the current geometry of the cone is inherited from a stage predating the development of the pre-Bory pit crater. This evolution disagrees with the historical reports of the 18<sup>th</sup> and 19<sup>th</sup> centuries in which the cone is considered to be symmetric and centred on the Bory pit crater until 1760, and becoming asymmetric when the activity shifted to the east flank of the cone in 1766 (Bory de Saint-Vincent, 1804).

➤ The caldera walls reveal a relatively constant lithological pile with a succession of scoria and scoria-rich units underneath a pile of thin lava flows (*Figure 4.3-4*). The scoria

materials suggest a period of predominantly explosive activity, which probably led to the construction of a large pyroclastic cone.

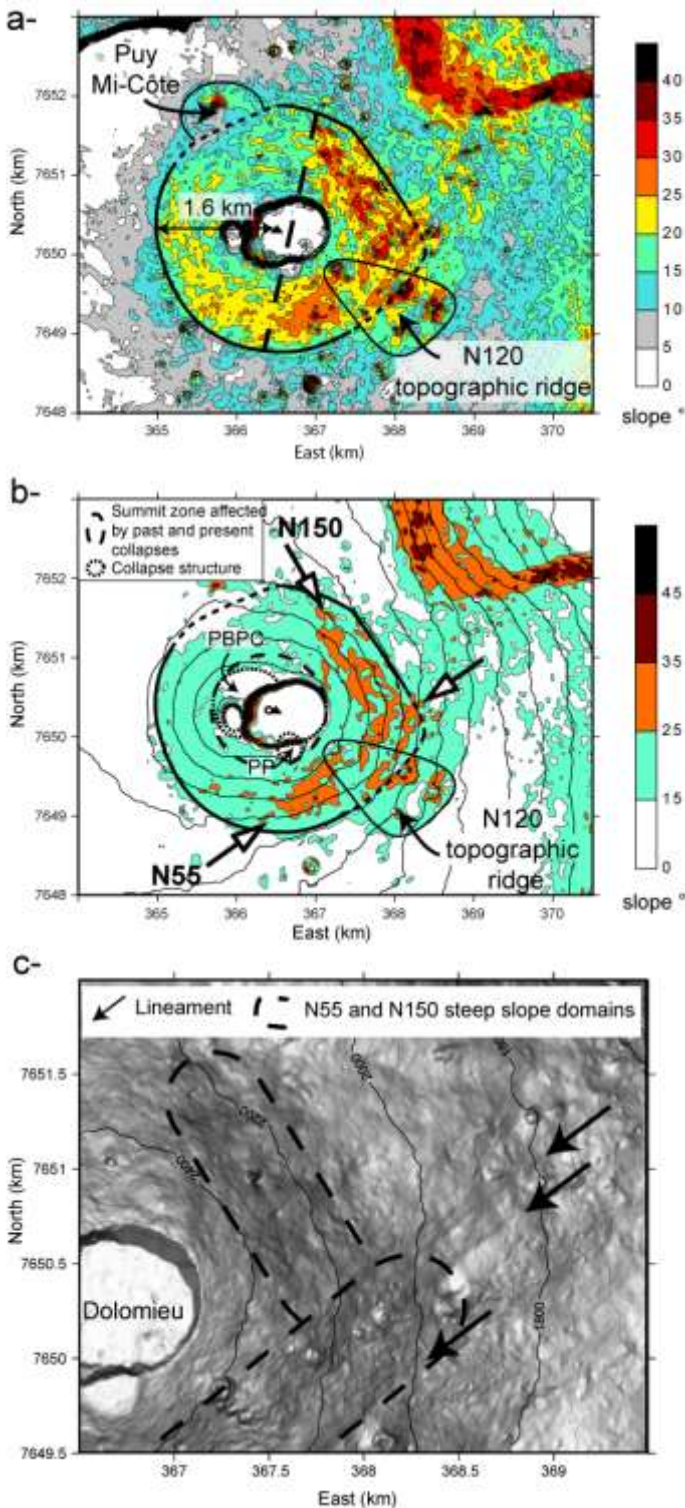


**Figure 4.3-3: a- Slope map of the central cone calculated from the 25 m step DEM.** The cone, which is sub-circular with a radius of 1.6 km, is coalescent to a parasitic cone in the north and a N120° topographic ridge in the NE, formed by several pyroclastic cones. The western and eastern parts of the cone present different slope values. **b-** Slope map of the calculated from a low-pass filtered DEM in order to determine the main characteristics of the morphology. The very steep slopes of the cone's eastern half are distributed in two linear steep slope zones trending in the N55° and N150 directions. PP: Petit Plateau; PBPC: Pre Bory pit crater. **c-** Shaded relief representation of a 7 m step DEM calculated by stereophotogrammetry from a set of aerial photographs performed in 1989. This high resolution DEM highlights clear, parallel lineaments in the northeastern continuity of the N55° steep slope zone. Coordinates in UTM WGS84 (zone 40S).



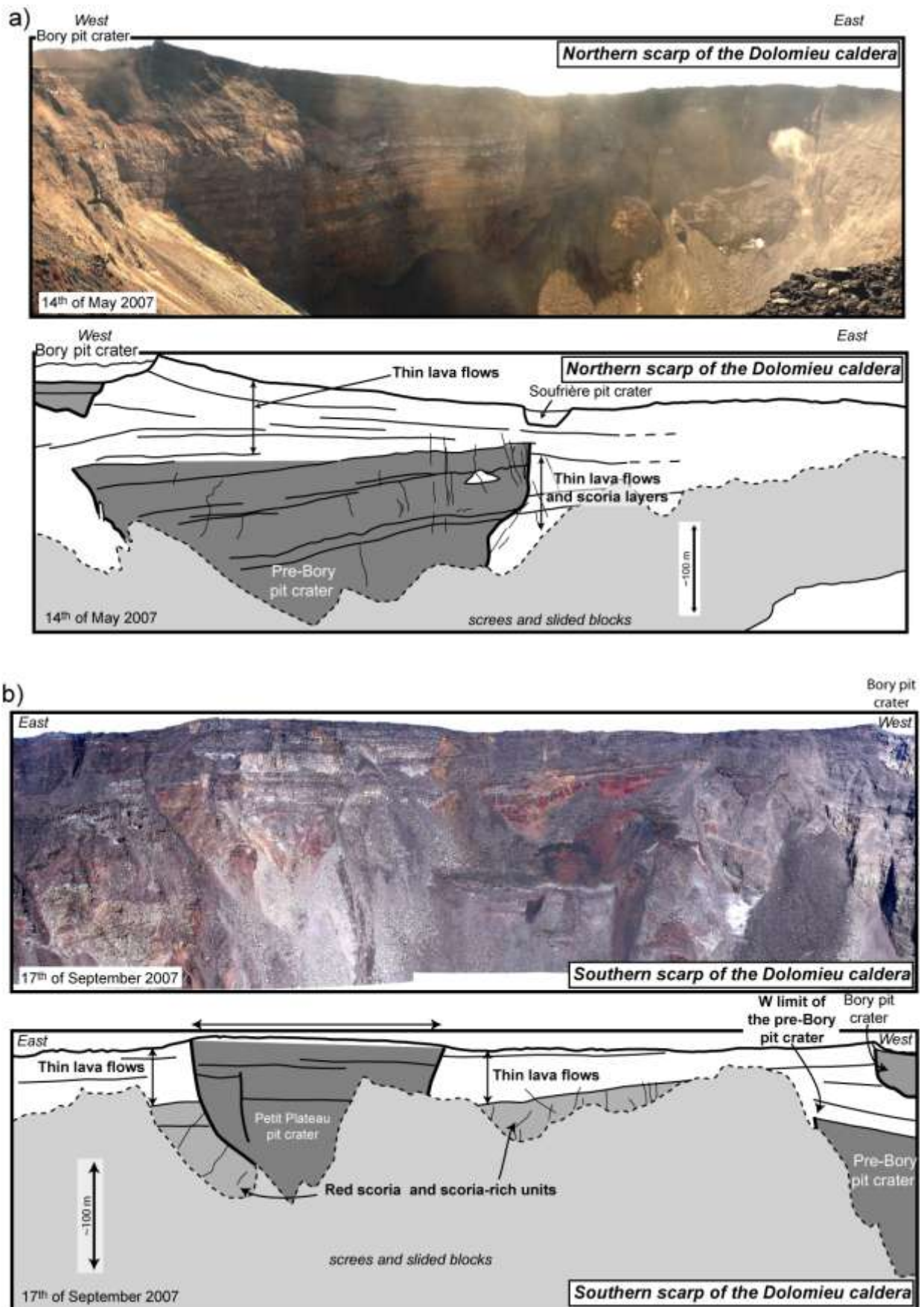
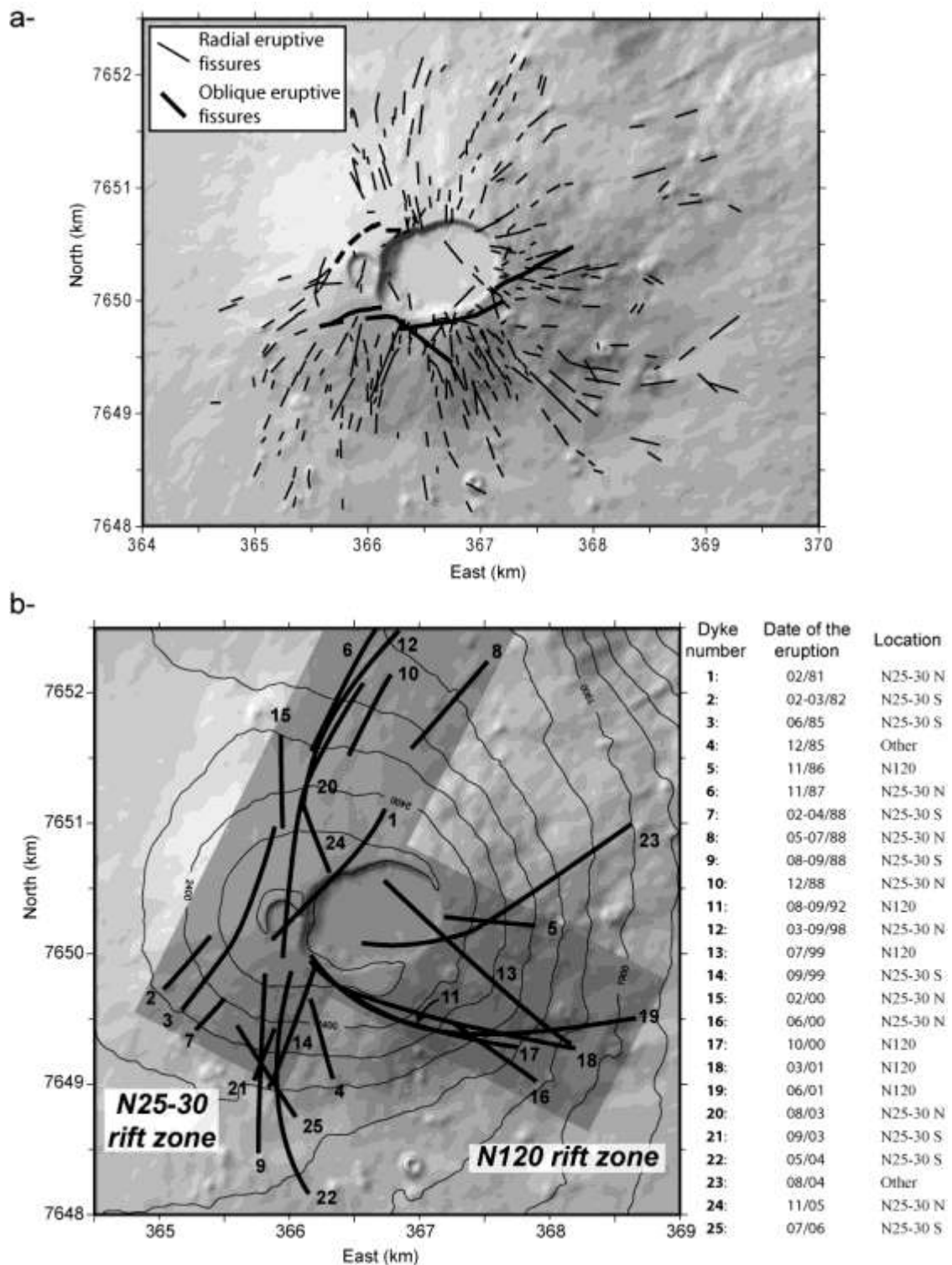


Figure 4.3-4: Panoramas and interpretations of the northern (a) and southern (b) scarps of the April 2007 caldera (photo b: Frederic Massin).

### 4.3.3 Fractures of the central cone

During the last decades, several works have addressed the origin of the tectonic structures of the central cone (Bachèlery, 1981; Bachèlery et al., 1983; Lénat and Bachèlery, 1990; Carter et al., 2007). The different analyses, which were essentially or strictly restricted to the summit of the central cone, revealed the coexistence of concentric and radial volcano-tectonic structures, consisting mainly of extensional fractures and eruptive fissures, respectively. The concentric fractures are restricted within the first tens of meters of the rim of Dolomieu and Bory. Their formation is interpreted as to be related to both the current and paleo pit crater development, and the dynamics of the superficial magma chamber. Only one fracture network which trends obliquely to the north-east rim of Dolomieu, is linked to another process, i.e., the slumping of the east flank (Carter et al., 2007). The volcano-tectonic structures described on the flanks of the central cone correspond to eruptive fissures, which usually present a radial strike and open *en-échelon* during dyke injection. This distribution locally changes in the east flank where the eruptive fissures mimic conjugate systems (Carter et al., 2007). The *en-échelon* distribution on the northern and southern flanks of the central cone was initially interpreted as indicative of co-intrusive left-lateral and right-lateral displacements in the respective flanks, causing the eastward motion of the east flank of PdF (Bachèlery et al., 1983). However, Michon et al. (2007a) recently showed that the *en-échelon* pattern most likely resulted from a reorientation of the magma intrusion close to the surface due to the rotation of the main principle stress  $\sigma_1$  from vertical to downslope, rather than a shear deformation during dyke intrusion.

Since 1990, the date of the last structural work at the cone scale, PdF underwent 27 eruptions and 3 intrusions, each of them leading to the deformation of the summit zone. A new structural analysis was realised on the central cone and the adjacent Enclos floor in order to determine if tectonic structures developed and accommodated the deformation measured from GPS and interferometry (Briole et al., 1998; Sigmundsson et al., 1999; Froger et al., 2004; Fukushima et al., 2005). Our field observations reveal a wide range of fractures affecting the eruptive system. In a way similar to Carter et al. (2007), the present work considers only the fractures cutting at least two adjacent geological units. The fractures restricted to single lava flows or cones, and related to their own dynamics, such as the syn-cooling subsidence or collapse, were disregarded. According to the fracture geometry, size and relationship with the geological formations, three different types of volcano-tectonic structures were distinguished, among which the two first correspond to the radial and concentric fractures already described by Bachèlery et al. (1983) and Carter et al. (2007).



**Figure 4.3-5: a- Distribution of the eruptive fissures. b- List and location of the dykes associated to proximal eruptions since 1981. Coordinates in UTM WGS84 (zone 40S).**

➤ The eruptive fissures mainly open perpendicular to the slope (*Figure 4.3-5*). Their mean length inferred from 68 post-1997 eruptive fissures is 180 m. Only few eruptive fissures are oblique to the slope. Their length is significantly higher (i.e., 2.5 to 11 times longer) than that of the downslope eruptive fissures. They are located in the south-south-east and east flanks of the cone, where they strike N20°-25° and N65° respectively. In the east flank, the recent N65°

trending eruptive fissure of the August 2004 eruption is connected to the south-east corner of Dolomieu.

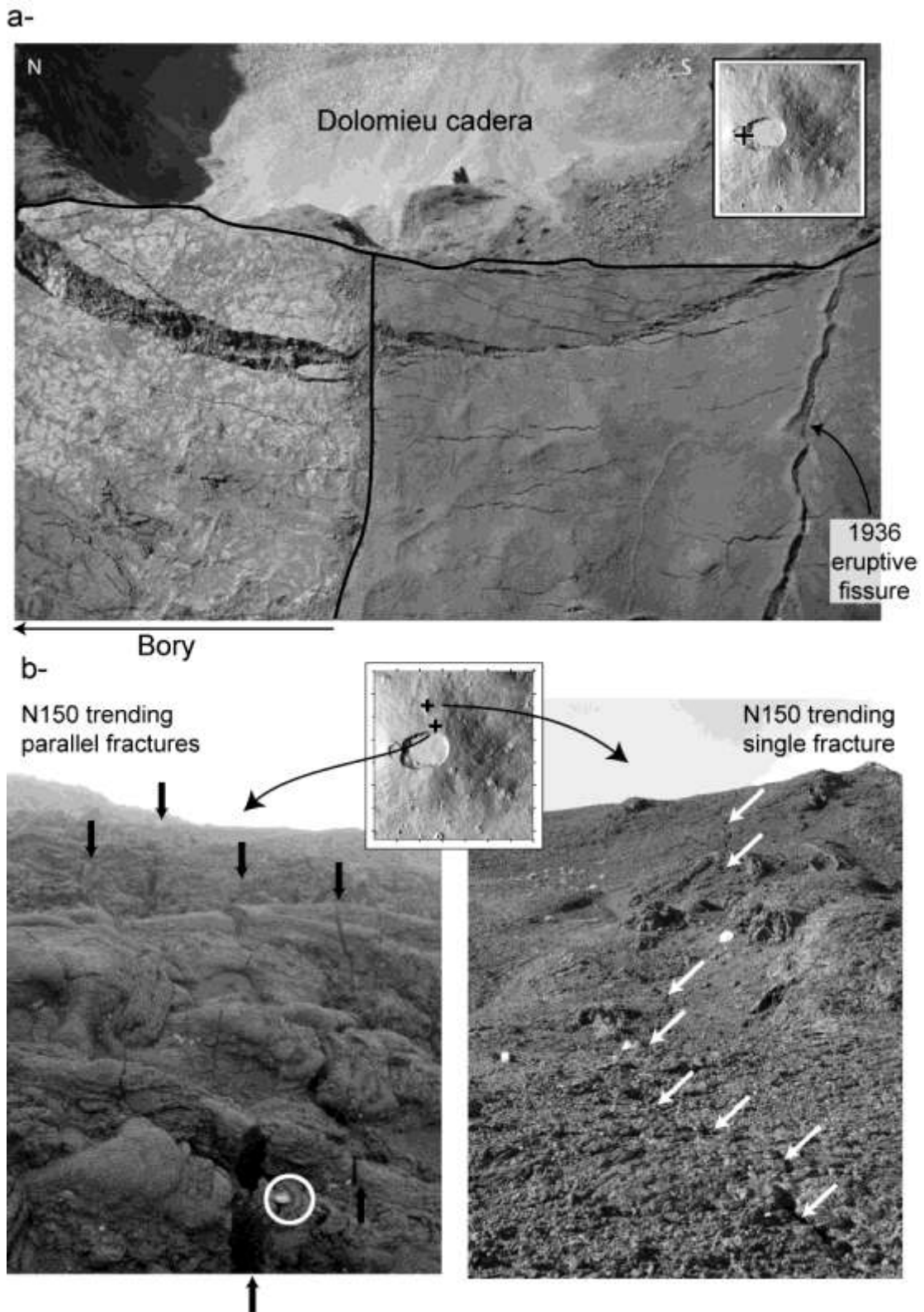


**Figure 4.3-6: a- Picture of the concentric fractures associated to the collapse structures. b- Pictures of the flank fractures that affect the eastern half of the central cone. Here, the N150 deformation zone.**

Aerial photographs of 1936 reveal that older eruptive fissures developed at the same location with a similar geometry. The geometric association of the N65° eruptive fissures with the radial

ones forms the conjugate-like systems described by Carter et al. (2007). The occurrence of long and oblique eruptive fissures in the flanks suggests that besides the sub-surface downslope  $\sigma_1$ , which controls the orientation of most of the eruptive fissures (Michon et al., 2007a), local stress fields or structures may influence the magma migration through the East flank. The local structural control is corroborated by the development of N80° and N50° eruptive fissures close to the southern rim of Dolomieu and north-west of Bory, respectively. Indeed, their orientation is parallel to the southern fault of Dolomieu and at the limit of the pre-Bory pit-crater.

➤ The concentric fractures consist in tens to hundreds of metres long extensional fractures either parallel to the scarps of Bory and Dolomieu (*Figure 4.3-6*), or at the limit of paleo pit craters. The fracture width evolves from few centimetres to 1-2 m close to the pit-crater limits. The maximum fracture density is observed in Bory, south-west and north of Dolomieu and at the limit of Petit Plateau. Carter et al. (2007) recently proposed that these concentric fractures result from the annular extension related to the pit-crater collapse. The analysis of the fractures before and after the April 2007 caldera reveals that most of the fractures form during the collapse events and are reactivated by radial extension stresses during the filling of the collapse structure (Catry et al., Special publication Piton de la Fournaise).

➤ The third type of fractures corresponds to linear structures that usually affect several geological units, i.e., lava flows or pyroclastic cones. They differ from the concentric fractures either by the distance to the collapse structures or by their obliquity with respect to the concentric faults. Here they are named flank fractures even though some of them are located close to the summit or in the Enclos caldera floor. Two distinct geometries were observed in the field. They correspond to (i) several tens of meters long single linear structures or (ii) 10-50 m wide tectonic corridors in which parallel fractures are concentrated (*Figure 4.3-6*). Whatever their geometry, all the fractures are extensive structures showing a slight lateral component in few cases. The systematic mapping of the fractures on both the central cone and the proximal part of the Enclos caldera floor shows a strongly heterogeneous spatial distribution (*Figure 4.3-7*). Most of the fractures are located in the eastern half of the central cone. They are characterised by three main orientations trending in the N20°-30°, N55°-65° and N150°-160° directions. It is remarkable that each trend presents a specific spatial distribution (*Figure 4.3-7*). All the N20°-30° trending fractures are situated east of the N25°-30° rift zone. The N55°-65° fracture network is concentrated along a main axis, which corresponds to the locus of the clear north-east trending lineaments north-east of the N55° steep slope zone (*Figure 4.3-3*). The continuity of the fractures affecting the old lava units in the August 2004 pahoehoe lava flow, and the decreasing opening of the fractures as a function of the age of the lava flow, suggest a

continuous deformation process. Finally, the N150°-160° fractures are mainly located in the north-eastern part of the summit (*Figure 4.3-7*). The fractures are concentrated between the eastern rim of Dolomieu and the top of the N150° trending steep slope zone in the north-east flank. Most of the deformation is restricted to two parallel tectonic corridors of c.450 and 640 m long in which fractures indicate an almost exclusive extension. Only a small part of these deformation zones corresponds to the N150° *R'* shear network described by Carter et al (2007). Contrary to these authors, here it is believed that the shear indicators and the lava tube offsets, which suggest minor opposite lateral displacements, result from slightly differential movements between the lava blocks during a general extension rather than a succession of opposite senses of shear.

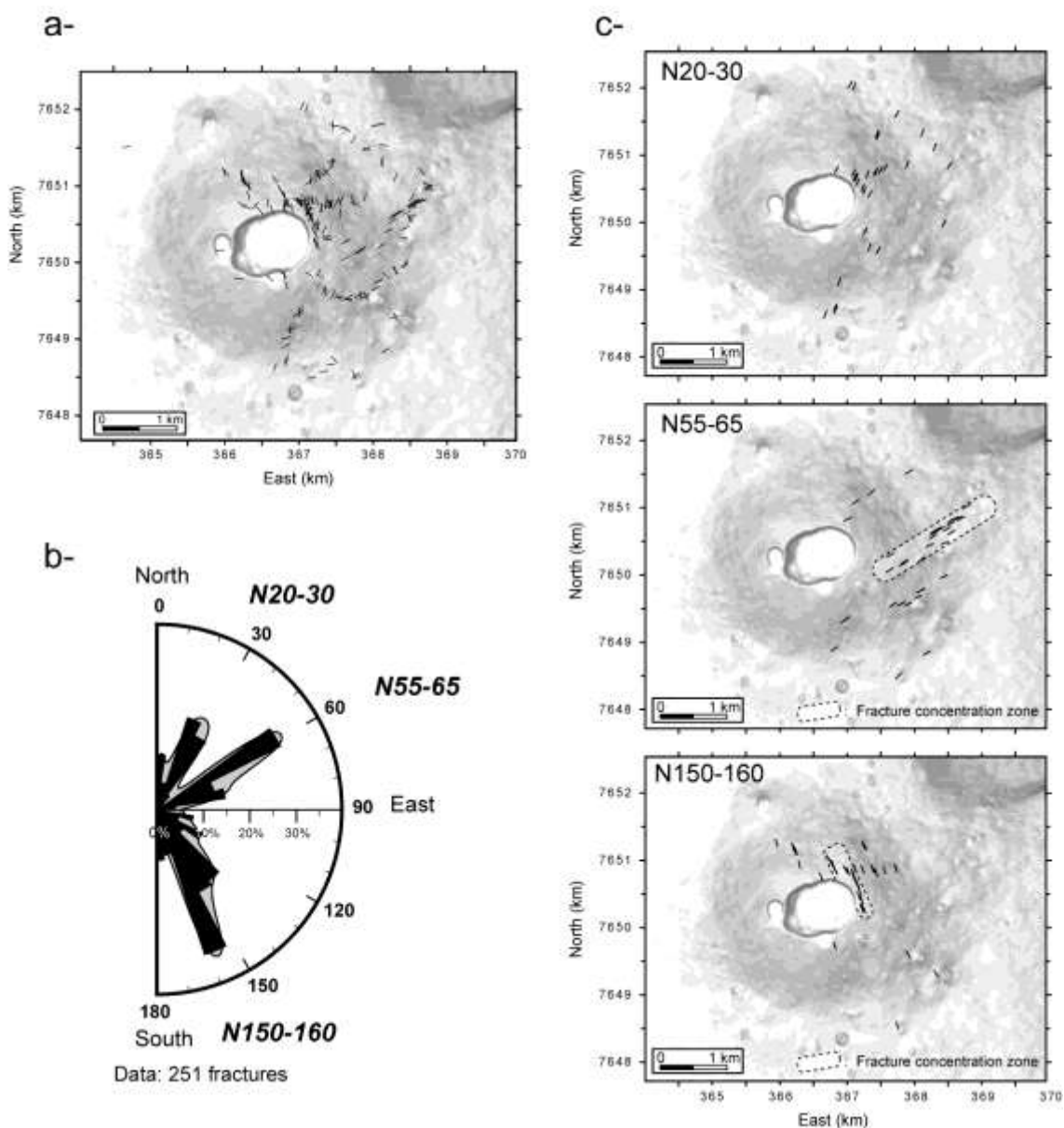


**Figure 4.3-7:** a- Spatial distribution of the flank fractures. b- Rose diagram illustrating the three main fracture trends: N20°-30°, N55°-65° and N150°-160°. c- Spatial distribution of the three main fracture trends. Coordinates in UTM WGS84 (zone 40S).

### **4.3.4 Co-intrusive deformation**

#### ***4.3.4.1 Types of eruptions and the related magmatic paths***

The activity of PdF is characterised by fissure eruptions fed by a magma reservoir located at about sea level (Nercessian et al., 1996; Fukushima et al., 2005; Peltier et al., 2007). Considering the location of the eruption site, three types of eruptions can be distinguished (Peltier et al., 2007). 1- Summit eruptions that start and remain in Dolomieu. 2- Proximal eruptions, which may start in the summit but progress to the flanks of the central cone and usually propagate downslope to the Enclos caldera floor. 3- Distal eruptions that develop away from the central cone, starting in the Enclos caldera floor. Numerical models suggest that the elevation of the first eruptive fissure, which opens during an eruption corresponds to the maximum elevation reached by the feeding dyke (Fukushima, 2005; Peltier et al., 2007). Then, only the dykes related to summit and proximal eruptions (68% of the total eruptions) intrude into the central cone. We determined the dyke orientations related to the 25 proximal eruptions from the distribution of the related eruptive fissures for the period between 1981 and 2007 (*Figure 4.3-5*). Note that the summit eruptions were disregarded since their dyke orientation cannot be accurately determined. Our compilation shows that 92% of the proximal dykes follow the N25°-30° and N120° rift zones described by Michon et al (2007a). 74% of them occur along the N25°-30° axis with an equal distribution on each segment of the rift zone, and 26% of the eruptions developed on the south-east flank along the N120° rift zone (*Figure 4.3-5*).

#### ***4.3.4.2 The co-intrusive displacements inferred from GPS***

At PdF, the dyke intrusions usually lead to an asymmetric deformation of the volcano characterised by a concentration of the displacements east of the dykes (Lénat et al., 1989a; Sigmundsson et al., 1999; Froger et al., 2004; Fukushima et al., 2005). GPS measurements carried out in 1981 and 1995 indicate that the eastern part of the cone summit experienced a 1.5-2 m eastward displacement during this period, whereas the western half remained stable (Briole et al., 1998). A denser GPS network composed of about 80 stainless steel benchmarks cemented around the crater, on the flanks and at the base of the summit cone was installed by the Piton de la Fournaise Volcano Observatory in order to better constrain the co-intrusive deformation of the edifice. Since 2002, this network was repeatedly measured after each eruption. The location of each benchmark was determined with respect to a reference receiver situated north of the Enclos caldera. The sampling-rate of both receivers was of one second and the benchmarks were recorded during a 7-min stop on each.

a- April 2003 - November 2003				b- March 2002 - January 2006				c- 01-2004 eruption									
	Data point	Horizontal (cm)	Vertical (cm)	Total (cm)		Data point	Horizontal (cm)	Vertical (cm)	Total (cm)		Data point	Horizontal (cm)	Vertical (cm)	Total (cm)			
East profile	E. Flank	1a	49.2	39.5	63.1	East	E. Flank	1b	107.4	99.6	146.5	E. Flank	1c	10.2	18.3	21	
		2a	46.8	36.8	59.5			2b	133.1	62.0	146.8			2c	12.6	14.9	19.5
		3a	45.7	34.9	57.5			3b	116.4	113.9	162.9			3c	24.2	17.6	29.9
		4a	44.7	34.2	56.3			4b	114.9	126.8	171.1			4c	26.8	21.8	34.5
Enclos		5a	42.8	25.4	49.8	Enclos		5b	132.5	109.5	171.9	Enclos		5c	25.5	21.9	33.6
		6a	37.5	13.2	39.8			6b	141.7	111.6	180.4			6c	32.2	33.4	46.4
		7a	34.0	(3.3)	34.2			7b	144.2	79.3	164.6			7c	39.8	33.0	51.7
		8a	39.8	(4.4)	40			8b	100.4	75.9	125.9			8c	43.2	39.6	58.6
NE p.		9a	45.5	41.3	60.4	NE		9b	84.7	76.4	114.1	NE		9c	39.6	18.7	43.8
		10a	21.5	(-2.3)	21.6			10b	182.2	123.0	219.8			10c	20.2	28.6	35
South p.		11a	34.8	54.7	64.8	South		11b	73.1	48.4	87.7	South					
		12a	35.2	29.7	46.1			12b	51.9	37.1	63.8						
		13a	19.1	5.5	19.9			13b	11.5	(2.7)	11.8						
NW p.		14a	19.1	10.6	21.8	NW		14b	(3.1)	(0.1)	3.1	NW					
		15a	3.9	(-0.1)	3.9												

(3.3): data smaller than the instrumental error

← N55 fracture zone

**Table 4.3-1: Displacements measured by GPS for periods between April and November 2003 (a), March 2002 and January 2006 (b) and caused by the magma migration linked to the January 2004 distal eruption (c). See figure 8 for the location of the data points.**

It was demonstrated above that between 1981 and 2007 the dykes that intruded the central cone followed the N120° rift zone, and the northern and southern segments of the N25°-30° rift zone, in roughly the same proportion. Between April 2003 and November 2003, three eruptions and one intrusion occurred at the summit and along each rift zone, making the co-intrusive deformation of this period representative of the general behaviour during summit and proximal eruptions. The GPS data clearly show the deformation decoupling between the eastern and western parts of the cone (*Figure 4.3-8*). West of a N-S decoupling axis located between Bory and Dolomieu, displacements are small at the summit (< 22 cm) and almost non-existent at the base of the cone and in the Enclos (*Table 4.3-1*). East of the axis, displacements rotate from a north-eastward to a south-eastward motion from North to South, showing an average eastward motion of the eastern half of the central cone. The total displacement values of the summit are three times larger than in the west. GPS data reveal that the vertical displacements are restricted to the cone and are maximal at the summit. In contrast, both the cone and the proximal part of the Enclos caldera floor experience significant outward horizontal displacements. Finally, it is interesting to note that the north and west flanks present a steady decrease of the displacement values, whereas the south-east and east flanks are characterised by a segmented decrease, which is correlated with the variations of the topography. For the east flank, the GPS data located in the steepest part (data points 1a to 4a in *Table 4.3-1* and *Figure 4.3-8*) indicate a slight decrease of the vertical displacements, i.e., between 39.5 and 34.2 cm, whereas they sharply decrease from 24.2 to 3.3 cm in the same distance in the Enclos floor (data points 5a to 7a).



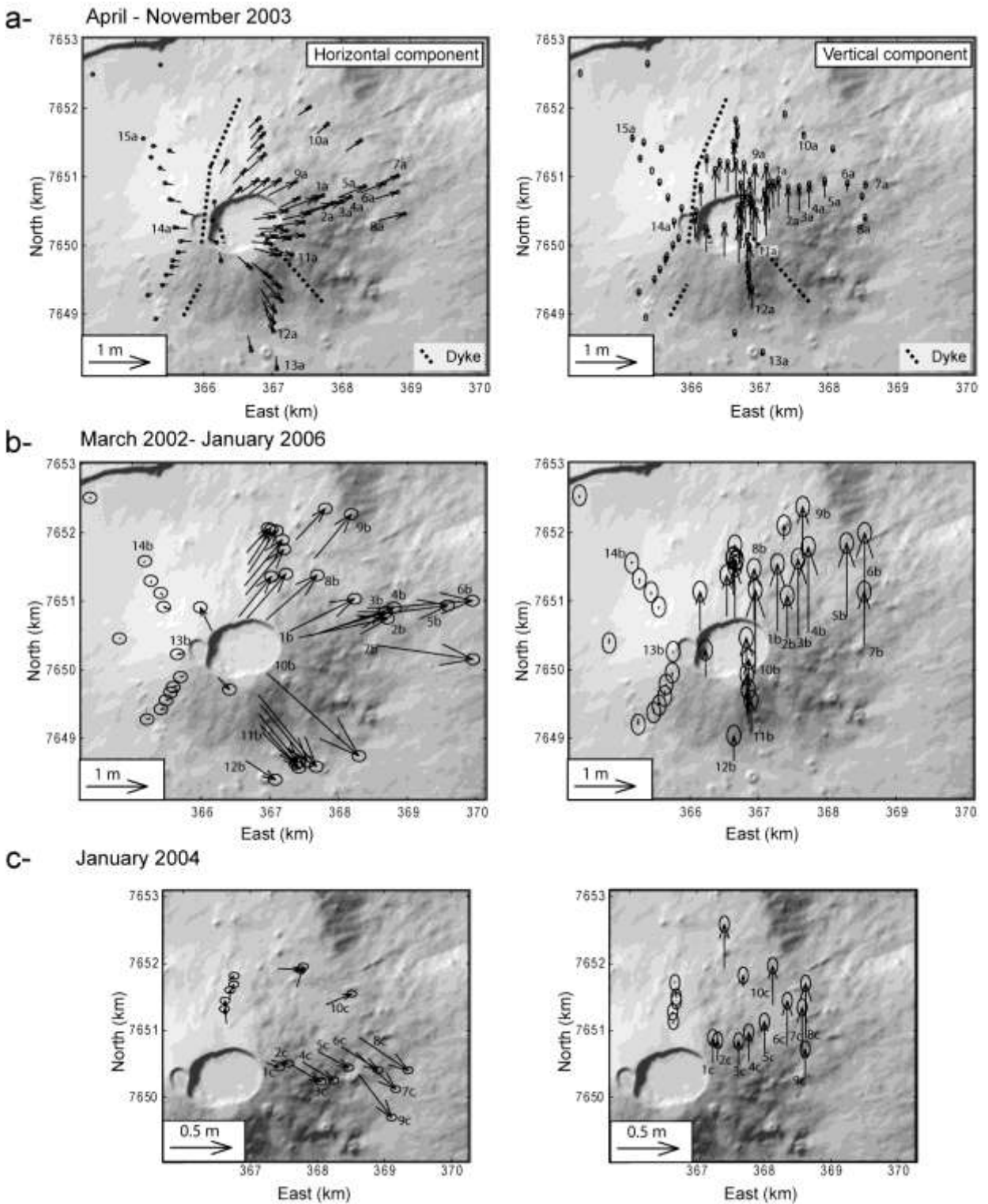


**Figure 4.3-8: Horizontal (left) and vertical (right) co-intrusive displacements recorded by GPS. a- Between April and November 2003. The dashed lines indicate the location of the dykes. b- Between March 2002 and January 2006. c- During the January 2004 eruption. Coordinates in UTM WGS84 (zone 40S).**

In consequence, the recurrent dyke intrusions up to the summit and along the intra-cone segments of the N25°-30° and N120° rift zones lead to a heterogeneous growth of the central cone. Between April and November 2003, the cone underwent a very slight steepening of the west flank (c.4 10<sup>-3</sup>/yr), and a significant inflation of the eastern part, leading to a steepening

of the South and East flanks (c.1.5  $10^{-2}$ °/yr). Moreover, GPS data suggest that each N55° and N150° trending steep slope zone suffers a homogeneous deformation. This overall deformation pattern inferred for the period between April 2003 – November 2003 fully agrees with the slope change determined by Fukushima (2005) between March 1998 and June 2000 (*Figure 4.3-9*), during which five eruptions occurred along the south and north segments of the N25°-30° rift zone and along the N120° rift zone. The striking similarities between the two different periods suggest a relatively constant mode of deformation of the cone when summit and proximal eruptions occur.

Most of the deformation determined for the period between March 2002 and January 2006 is similar to that of April to November 2003 in terms of (i) decoupling between the western and eastern parts and (ii) and steady decrease of the displacement values from the top to the base of the cone in the north, south-west and west flanks (*Figure 4.3-8*). It differs in only one point, which is the regular increase of the total displacement values from 146.5 to 180.4 cm between the eastern top and the Enclos floor (*Table 4.3-1*). Contrary to the periods between March 1998 and June 2000 and between April 2003 and November 2003, during which only summit and proximal eruptions occurred, the period between March 2002 and January 2006 was characterised by summit, proximal and also three distal eruptions in the Plaine des Osmondes (see *Figure 4.3-2* for its location). The displacement pattern related to one of these eruptions, in January 2004, suggests that the downward progressive increase of the displacements in the East flank is induced by distal intrusions toward the Plaine des Osmondes (*Figure 4.3-8* and *Table 4.3-1*). Moreover, GPS data related to the January 2004 distal eruption indicate the existence of different displacement domains separated by the N55° deformation zone described above. The N55° fracture zone limits a differential uplift, which is twice as high in the west of the fracture zone as in the east.

In summary, our data clearly show two different co-intrusive modes of deformation. The cumulated deformation related to both summit and proximal intrusions is centred on the summit craters and is mostly restricted to the central cone. In contrast, the distal intrusions led to a widespread deformation, the limits of which cannot be determined with the current GPS network.

### **4.3.5 Discussion**

#### ***4.3.5.1 Origin of the general steep slopes of the central cone***

The central cone of PdF presents abnormally steep flanks for a basaltic volcano characterised by fissure eruptions and fluid lava flows. Annen et al. (2001) proposed that this morphology

mainly results from predominant endogenous processes with recurrent thick and short intrusions originating from a small and shallow magma chamber, i.e., 200 m in diameter and located 500 m below the summit. Besides the disagreement between the input and natural data concerning the intrusion vs. eruption ratio (see the description in section 1), the existence of a small shallow magma chamber is questionable. Indeed, the present deformation and seismic data suggest that the feeding dykes originate from a relatively deep magma chamber located at about sea level (Fukushima et al., 2005; Peltier et al., 2007). Furthermore, a small magma reservoir cannot explain the development of collapse structures such as the pre-Bory pit crater and the recent Dolomieu caldera that are much larger than the hypothesized magma chamber. Hence, we consider that the geometry of the central cone of PdF does not result from the predominant endogenous processes described by Annen et al. (2001).

The April 2007 caldera collapse, which was coeval to the largest historical eruption deeply cut the central cone of PdF (Michon et al., 2007b; Urai et al., 2007). Observations of the caldera walls reveal that the cone predating the pre-Bory pit crater was essentially made of red scoria. It was subsequently overlapped by several tens of metres of thin lava flows. We propose that the scoria formations are evidences of the occurrence of a hidden strombolian pyroclastic cone below the upper thin lava flows. Strombolian cinder cones are usually characterised by slopes between  $25^{\circ}$  to  $30^{\circ}$  that correspond to the repose angle of the material (Porter, 1972; Wood, 1980). At PdF, the east and south-east flanks of the central cone present such slope values. However, our GPS data, which clearly show their progressive tilting during the recurrent intra-cone intrusions suggest that part of their present slope values result from deformation processes. In the cone's western half, where the intrusion-related deformation is limited, slope values are  $10^{\circ}$  less than that of a classical cinder cone. We consequently interpret the present cone's geometry as resulting from a twofold evolution: a first period during which a cinder cone built up in the Enclos caldera floor, and a second period of predominant effusive activity overlapping and smoothing the initial cone geometry. A similar scenario was proposed to explain the steep morphology of Nyiragongo (Democratic Republic of Congo), where an initial explosive phase built up a steep cone and a lava lake activity with periodic overflowing veneered over the pyroclastic core (McDonald, 1972; Demant et al., 1994).

#### ***4.3.5.2 Tectonic structures, co-intrusive deformation and rift zones***

Since 1981, all the structural analyses and geodetic measurements have shown that the eastern part of the central cone of PdF was affected by an eastward motion (Bachèlery, 1981; Bachèlery et al., 1983; Delorme et al., 1989; Lénat et al., 1989a; Zlotnicki et al., 1990; Briole et

al., 1998; Sigmundsson et al., 1999; Froger et al., 2004; Fukushima et al., 2005; Carter et al., 2007; Peltier et al., 2007; Tinard et al., Special publication Piton de la Fournaise). It has been first proposed that the entire eastern flank of PdF was involved in the deformation process (e.g., Bachèlery, 1981; Lénat et al., 1989a). The NE and SE rift zones were then considered as sinistral and dextral shear zones accommodating the lateral displacements of the volcano flank. However, the recent GPS and radar interferometry data do not confirm such a general process and reveal that the deformation is directly related to dyke intrusions and concentrated around the central cone (Sigmundsson et al., 1999; Froger et al., 2004; Fukushima et al., 2005; Peltier et al., 2007; Tinard et al., Special publication Piton de la Fournaise). If the deformation pattern is well constrained with these types of data, little is known about the effect of the recurrent intrusions in the development, or the interaction with tectonic structures. Using field data collected around the summit collapse structures, i.e., the break-in-slope in the upper east flank, the fractures in the northern part of the N150°-160° fracture zone and the conjugate-like geometry of the eruptive fissures, Carter et al. (2007) proposed an additional deformation process. According to these authors, the east flank of the central cone undergoes a progressive slump above a low strength layer, which is favoured by the recurrent intrusions along the N10° and N170° rift zones. We disagree with this model for the following reasons:

- The fractures used to interpret the northern limit of the slump as a dextral shear zone do indicate a predominant extension, and correspond to a small part of a much longer extension structure, i.e., the N150°-160° fracture zone.
- The conjugate-like geometry of the eruptive fissures results from two sets of eruptive fissures that are the common radial fissures and the long N55° trending fissures which develop in the East flank only.
- The eastern base of the cone lacks any thrust fault or concentric compressive structures which would result from the slump.
- The summit collapses disregarded, the deformation of the cone is exclusively due to the dyke intrusions (Froger et al., 2004; Fukushima et al., 2005) and to a minor pre-eruptive inflation centred on the cone (Peltier et al., 2007).

This brief review reveals a lack of any global model in which both field observations and GPS or radar interferometry data are integrated. In the following, we propose to combine our multi-disciplinary data in order to determine (i) the origin of the different tectonic structures (except for the summit collapses and the concentric fractures that are clearly linked to the magma withdrawal; Hirn et al., 1991; Longpre et al., 2007; Michon et al., 2007b; Catry et al., Special publication Piton de la Fournaise), (ii) the role of the recurrent dyke intrusions in the

morphology of the central cone and (iii) the origin of the N25°-30° and N120° rift zones and their consequences in the cone's evolution.

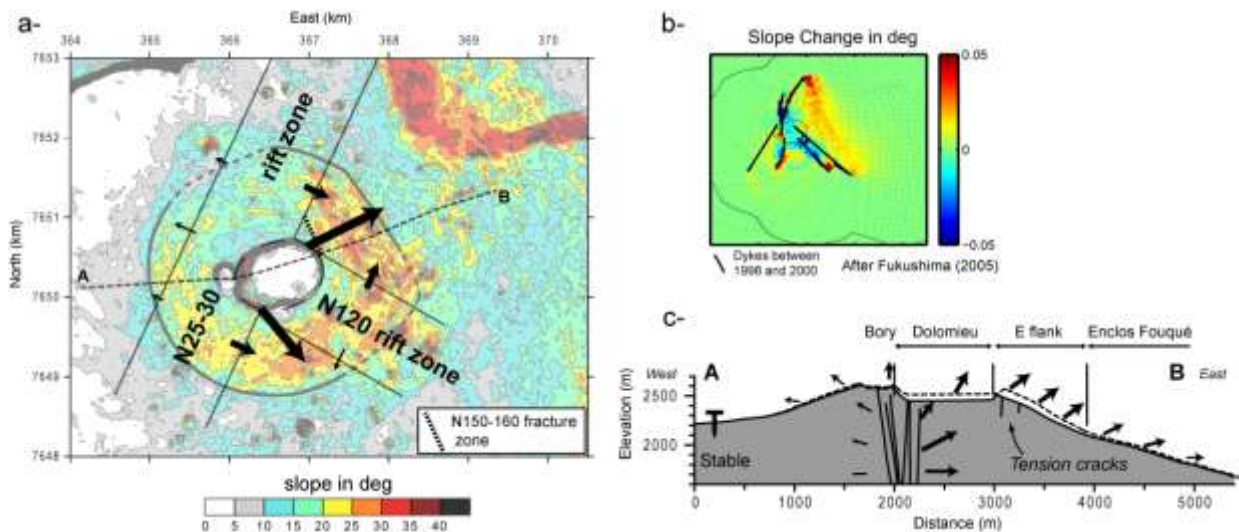


**Figure 4.3-9: Synthesis of the co-intrusive deformation related to summit and proximal intrusions.** *a-* Intrusions along the northern and southern segments of the N25°-30° rift zone and along the N120° rift zone induce the north-eastward and south-eastward tilting of the East and South-East flanks. *b-* Slope changes related to 5 summit and proximal eruptions between 1998 and 2000 (Fukushima, 2005). *c-* E-W cross section presenting the outward inflation of the cone's eastern half.

Our structural analysis of the central cone allows the identification of two sets of tectonic structures. First, the different spatial distributions of the flank fractures, the eruptive fissures and the dykes, especially in the western part of the cone (*Figures 4.3-5; 4.3-7*), confirm that the development of the flank fractures does not correspond to the dyke-induced proximal deformation. In contrast, the superposition of the areas affected by these fractures and the co-intrusive deformation (*Figures 4.3-7; 4.3-8*) suggests that the flank fractures are linked to the outward inflating tilting of the eastern part of the cone. Hence, we propose that the flank fractures, which are essentially characterised by extension, correspond to relatively shallow (maximum depth of few hundreds of metres) tension cracks that accommodate the endogenous growth during summit and proximal injections. The N20°-30° trending fractures may result from the recurrent intrusions along the N25°-30° rift zone whereas the N150°-160° fractures may originate from the combined effect of intrusions along the N120° rift zone and the northern segment of the N25°-30° rift zone (*Figure 4.3-9*). The N55° fracture zone represents the second set of fractures. The N55° fracture zone is underlined by (i) long, oblique eruptive fissures in the east flank of the cone (*Figure 4.3-5*), (ii) a dense fracture network (*Figure 4.3-7*), (iii) striking lineaments on the DEM (*Figure 4.3-3*), and (iv) linear very steep slopes in the SE flank (*Figure 4.3-3*). As a whole, it corresponds to a 3 km-long structure, which is parallel to a larger tectonic structure that accommodated the collapse of the southern part of the Enclos caldera (Michon and Saint-Ange, 2008). Given the characteristics of the N55° fracture zone, we

interpret it as a fault zone punctually reactivated during the north-eastward distal eruptions and controlling both the magma intrusion in the eastern part of the cone and the co-intrusive tilting of the south-east flank. The occurrence of volcano-tectonic events along or close to the fault trace (Sapin et al., 1996) corroborates the fault zone interpretation. Assuming that the dyke's lateral propagation in the East flank is controlled by the fault zone, a minimum fault depth of 1000-1500 m a.s.l. is indirectly determined from the usual depth at which the proximal dykes initiate their lateral propagation (Fukushima et al., 2005; Peltier et al., 2007).

The GPS data indicate that the recurrent intrusions along the rift zones induce a heterogeneous deformation of the cone with (i) a significant inflation of the eastern part of the summit, (ii) the steepening of the south-east and east flanks, and (iii) very slight tilting of the western part (*Figure 4.3-9*). These results strikingly agree the total deformation related to five successive intrusions between 1998 and 2000, during which the east flank and, to a lesser extent, the south-east flank underwent an increase of the slope (Fukushima, 2005). The superposition of the tilted zones and the N55° and N150° very steep slope zones strongly suggests that the slope value difference of about 5°-10° between the east and south-east flanks, and the west and north flanks results from the endogenous growth associated with intra-cone intrusions along the N25°-30° and N120° rift zones (*Figure 4.3-9*). Hence, if most of the present morphology of the central cone results from an exogenous growth, the specific morphology of the cone's eastern part is clearly due to endogenous processes.

The absence of any elongation along the N25°-30° rift zone despite the substantial concentration of the intrusions along this structure contrasts with the morphologies of Hawaiian volcanoes and Karthala (*Figure 4.3-1*). Annen et al. (2001) showed that the geometry of the volcanoes was sensitive to the dyke length/source depth ratio. Volcanoes with ratios lower than one present an elongation perpendicular to the rift zones, whereas the elongation is parallel to the rift zones for ratios greater than one. For ratios close to one, the edifice remains circular despite the presence of radial rift zones. At PdF, the mean dyke length along the northern and southern segments of the N25°-30° rift zone and the source depth are of the same range (about 2000 m). Then, the development of short dykes along the N25°-30° and N120° rift zones may explain the sub-circular geometry of the central cone.

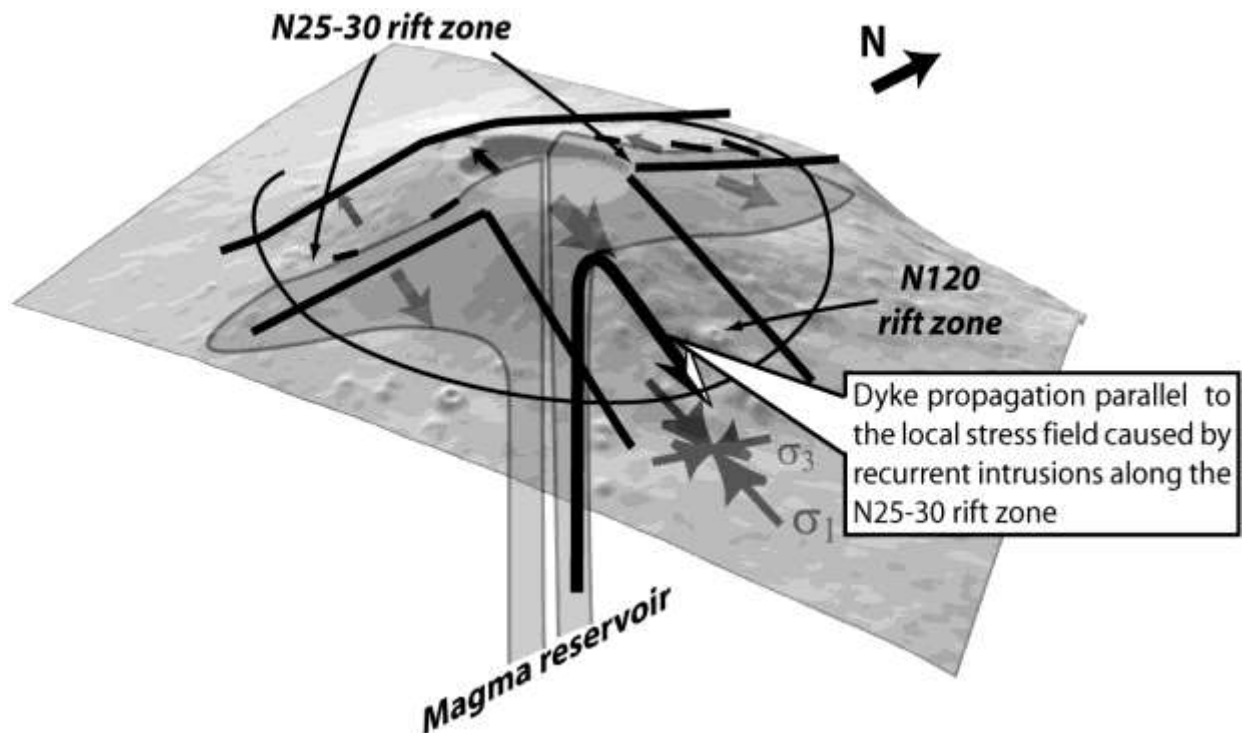


**Figure 4.3-10: Interpretation of the short, narrow N120° rift zone as resulting from the stress accumulation induced by recurrent intrusion along the N25°-30° rift zone. See text for explanation.**

The N25°-30° and N120° rift zones were determined from the orientation and location of the dykes intruded since 1981. Michon et al. (2007a) proposed that the N25°-30° rift zone, on which the cone built up, results from recurrent magma intrusions along a large, 10 km-long structure in the Enclos caldera floor. The origin of the N120° rift zone is less constrained. It could be related to the regional N120° trending volcanic zone between Piton des Neiges and Piton de la Fournaise, the development of which has been interpreted as to be controlled by N120° crustal faults (*Figure 4.3-2*; Chevallier and Vatin-Perignon, 1982; Michel and Zlotnicki, 1998; Michon et al., 2007a). However, the lack of any N120° trending intrusions in the Enclos caldera, west of the N25°-30° rift zone, and the contrasted geometries between the narrow rift zone east of the cone and the wide volcanic zone between PdF and Piton des Neiges suggest a different origin of both structures. The intrusions of PdF propagate first vertically below the western part of Dolomieu and then, in many cases, laterally when the level of neutral buoyancy is reached (Fukushima et al., 2005; Peltier et al., 2005). The recurrent magma intrusions along the N25°-30° rift zone (74% of the proximal eruptions) increase the orthogonal stress. We propose that this dynamics creates a perpendicular sub-horizontal local main principal stress  $\sigma_1$ , which subsequently controls the N120° trending lateral propagation below the south-east flank of the central cone (*Figure 4.3-10*). Such an interpretation may explain the lack of any N120° intrusions in the buttressed western part of the Enclos caldera and the small length of the N120° rift zone by a rapid decrease of the local  $\sigma_1$  away from the plumbing system. This rift system,

which has been determined from the summit and proximal intrusions, is not fully connected with the NE and SE rift zones outside the Enclos caldera. Indeed, recent geophysical data (Brenquier et al., 2007) suggest that the NE and SE rift zones along which the distal eruptions occur are related to tectonic structures that are located below the magma chamber that feeds the summit and proximal eruptions.

#### **4.3.6 Conclusion**

Our work corresponds to the first analysis of the central cone of PdF, which combines structural and GPS data. The main results can be summarised as follows:

- Similarly to Nyiragongo (Demant et al., 1994), the central cone is formed by a pyroclastic core overlapped by few tens of metres of lava flows. The general steep geometry of the cone does consequently not result from endogenous processes but from an initial phase during which a pyroclastic cone formed.
- The cone undergoes a contrasted co-intrusive deformation during summit and proximal eruptions along two N25°-30° and N120° rift zones. Most of the co-intrusive displacements are concentrated in its eastern half where they induce a progressive outward inflation and the tilting of the East and South-East flanks. A dense network of flank fractures, which differs from the eruptive fissures and the concentric fractures linked to the summit collapses, accommodate the progressive endogenous growth.
- The dynamics of the plumbing system also reactivates a N55° fault zone, which mainly controls magma intrusions in the East flank and decouples the deformation of the Enclos caldera floor during the north-eastward distal eruptions.
- The N25°-30° rift zone of PdF is related to a large, 10 km-long fracture zone, whereas the short, narrow N120° rift zone results from a N120° trending stress accumulation west of the N25°-30° rift zone, which guides magma intrusions.

#### **Acknowledgments**

The authors thank Ruth Andrew for improving an initial version of the manuscript. This is an IPGP contribution.



## 4.4 Conclusions

While the previous part was dealing with the internal structure of Piton des Neiges intrusive system, in this section, the attention is focused on the active Piton de la Fournaise volcano. Scarps of past volcano-tectonic events, as well as recent events have allowed access into the upper part of the intrusive system. Field data have suggested that previous models of evolution could be reconsidered.

The morphology of the cone, previously associated with a mainly endogenous growth, provides an answer. It appears that the central cone has been, in the past the source of more explosive eruptions, causing the accumulation of pyroclastic cones, at its base. This is also associated with the tilt of the eastern flank of the volcano under the injection of magma, with deformation concentrated to the east of the eruptive features. This mechanism has led to the development of a large network of tectonic fractures, in the area of maximum deformation, east of the cone. These fractures suggest that deeper structures might have been reactivated, leading to the appearance of large lineaments.

The origin of this specific deformation, during an eruptive or intrusive event, localised mostly on the eastern part of eruptive structures oriented along a NNE or SSE trend, also provides an answer. Modelling by other authors of the source of pressure for recent eruptions had lead to the conclusion that part of the asymmetric deformation was due to the asymmetric topography, but the deformation was mainly due to the eastward dipping dykes (Cayol and Cornet, 1998b; Battaglia and Bachèlery, 2003; Froger et al., 2004; Fukushima et al., 2005; Peltier et al., 2005; de Michele and Briole, 2007). Observations within the rift zone and the Dolomieu pit-crater suggest otherwise. Structural data suggests that the rift system is not straight but rather curved, and is collinear with the previous rift system, preserved during a vertical volcano-tectonic event. Use of numerical modelling has shown that the asymmetry observed could be partly linked with both the curvature and the presence of a stiff inclusion west of the actual plumbing system.

## *5 General conclusions*

---

Recent studies on Réunion have focused mostly on the active Piton de la Fournaise volcano, and addressed several points of its activity. Most of the studies have focused on the intrusive dynamics, and tried to infer the plumbing system from both the deformation data (Cayol and Cornet, 1998b; Battaglia and Bachèlery, 2003; Froger et al., 2004; Fukushima et al., 2005; Peltier et al., 2005; de Michele and Briole, 2007), and the use of petrological and geochemical data (Vlastélic et al., 2005; Peltier, 2007). Recent works have also focused on the structure of the volcano, its evolution and potential influence in its deformation (Carter et al., 2007; Michon et al., 2007a; Peltier, 2007; Michon and Saint-Ange, 2008). Finally, recent activity at Piton de la Fournaise has also reopened the discussion on collapse mechanisms of pit-craters (Michon et al., 2007b). However, no interest has been given to the structure of the feeding system as it appears in the field.

Aside from this important focus on Piton de la Fournaise, almost no interest has been brought to the dormant Piton des Neiges. Recent research has been concerned mostly with the erosional processes. Interest has also been focused on the petrologic evolution of the edifice (Gillot and Nativel, 1982; Deniel et al., 1992), as well as its structure (Chevallier, 1979; Chevallier and Vatin-Perignon, 1982). However, structural studies show disagreement on the location of principal feeding structures. Moreover, they describe an extensive sill network, the origin of which is not satisfactorily explained.

This study had several goals, concerning both Piton des Neiges and Piton de la Fournaise. The knowledge of the dormant volcano can be used to better understand the active one, and inversely, current dynamics can be used to infer the dynamics of the dormant one. This study, along with its aims for a better understanding of the dynamics in Réunion Island, also brings new models that can be applied in other volcanic domains.

At Piton des Neiges, the rift system has been identified, with several rift zones, organised along the N30°, N120° and N160° directions, each of which presents different characteristics. The former, N30°, appears to be controlled by a much localised stress field, whose origin is, in the central part related to the magmatic stress field, with the injection of inclined sheets. Further away, the rift zone becomes controlled by the surface and gravitational stress field, with a maximum compressive stress shallowly dipping, explaining the origin of the shallowly inclined sheets and sills. It also appears that sill clusters, predominantly observed in this rift zone are the result of a combination of two effects, (1) the presence of well defined contact, and (2) the existence of large amount of plastic

breccias, identified as debris avalanches deposits. The N120° and N160° rift zones are, on the other hand, controlled by a different stress field. While in the central part, the magmatic stress field controls the injection of magma, it becomes apparent that further away, a different stress field controls the magma. This stress field has been identified as the dominant stress field in the island, representing the main axis of magma injection and the main extensional axis, the origin of which is inherited from crustal structures.

It has been identified that Piton de la Fournaise and Piton des Neiges share a common dynamic, with injection of magma from a central magma chamber, and the lateral injection dependant on the density of magma. The rift zones of the two volcanoes present similarities in their configuration, with a large proportion of steeply inclined dykes. These observations are in disagreement with the recent model of deformation, which is reconsidered in this study.

The asymmetry of deformation observed at Piton de la Fournaise can be partly explained by the injection of magma in a complex rift system, inherited from the pre-5 ka edifice that lead to a curved rift system, favouring deformation in the eastern side of the fissures. It can also be proposed that remnants of the previous eruptive system, located west of the current one can influence the deformation. This asymmetric deformation leads to a preferential tilt of the eastern flank of the central cone, which is affected by a large network of tectonic fractures. Finally, the structure of the rift zones, with distance, suggests that the present stress field is well established and is hardly affected by the surface stress field.

The new data presented here give new insights into the dynamics and structure of shield volcanoes, and especially those in Reunion. While we now have a better overview of the structure of the intrusive system of Piton des Neiges, and a better understanding on the origin of sills in volcanic domain, we still lack knowledge about the volcano. It has long been identified that flank collapses occurred in the history of the volcano, and this study shows that these deposits have influenced the later volcanic activity. However, the mechanisms triggering such events remain unclear. Detailed mapping and study of debris avalanche deposits would allow a better understanding of their origin.

Similarly, while our data provide information on the dynamics of the intrusive system, no constraint is given as to the respective period of activity. Dating as well as geochemistry would provide such constraints. It would also allow to better constrain the sources of

magma, and combined with geophysical studies of the area and modelling, the origin of the rift zone could be further understood.

At Piton de la Fournaise, it has been demonstrated that the structure of the volcano can influence its deformation. In the future, we might reach a better understanding of the processes of deformation using more realistic models, both in Réunion and elsewhere. Such considerations would allow revision of the sources of pressure, and *in-fine* providing more realistic models on the potential hazards. In Reunion, such hazards include essentially the risk of flank collapse.

## *Bibliography*

- Acocella, V., Porreca, M., Neri, M. and Mattei, M., 2006. Fissure eruptions at Mount Vesuvius (Italy): Insights on the shallow propagation of dikes at volcanoes. *Geology*, 34: 673-676.
- Aki, K. and Ferrazzini, V., 2000. Seismic monitoring and modeling of an active volcano for prediction. *Journal of Geophysical Research - Solid Earth*, 105: 16617-16640.
- Albarède, F. and Tamagnan, V., 1988. Modelling the recent geochemical evolution of the Piton de la Fournaise Volcano, Réunion Island, 1931-1986. *Journal of Petrology*, 29: 997-1030.
- Ancochea, E., Brandle, J.L., Huertas, M.J., Cubas, C.R. and Hernan, F., 2003. The felsic dikes of La Gomera (Canary Islands): identification of cone sheet and radial dike swarms. *Journal of Volcanology and Geothermal Research*, 120: 197-206.
- Ancochea, E., Hernan, F., Huertas, M.J., Brandle, J.L. and Herrera, R., 2006. A new chronostratigraphical and evolutionary model for La Gomera: Implications for the overall evolution of the Canarian Archipelago. *Journal of Volcanology and Geothermal Research*, 157: 271-293.
- Anderson, E.M., 1937. The dynamics of sheet intrusion. *Proceedings of the Royal Society of Edinburgh*, 58: 242-251.
- Anderson, E.M., 1951. The dynamics of faulting and dyke formation with applications to Britain, 2<sup>nd</sup> ed. Oliver & Boyd, Edinburgh, 206 pp.
- Ando, M., 1979. The Hawaii earthquake of November 29, 1975: Low dip angle faulting due to forceful injection of magma. *Journal of Geophysical Research - Solid Earth*, 84: 7616-7626.
- Annen, C., Lénat, J.-F. and Provost, A., 2001. The long-term growth of volcanic edifices: numerical modelling of the role of dyke intrusion and lava-flow emplacement. *Journal of Volcanology and Geothermal Research*, 105: 263-289.
- Ashby, M.F. and Jones, D.R.H., 1998. *Engineering materials 1: An introduction to properties, applications and design*. Butterworth-Heinemann, 306 pp.
- Bachèlery, P., 1981. Le Piton de la Fournaise (Ile de la Réunion). Etude volcanologique, structurale et pétrologique. Ph.D. Thesis, Université Blaise Pascal, Clermont-Ferrand, 215 pp.
- Bachèlery, P., 1999. Le Fonctionnement des volcans boucliers. HDR Thesis, Université de la Réunion, Saint-Denis.
- Bachèlery, P., Chevallier, L. and Gratier, J.P., 1983. Caractères structuraux des eruptions historiques du Piton de la Fournaise (Ile de la Réunion). *Comptes Rendus Académie Science Paris*, 296: 1345-1350.
- Bachèlery, P. and Mairine, P., 1990. Evolution volcano-structurale du Piton de la Fournaise depuis 0.53 Ma. In: J.-F. Lénat (Ed), *Le volcanisme de la Réunion*. CRV, Clermont-Ferrand, pp. 213-242.
- Bachèlery, P., Robineau, B., Courteaud, M. and Savin, C., 2003. Avalanches de débris sur le flanc occidental du volcan bouclier Piton des Neiges (Réunion). *Bulletin de la Société Géologique de France*, 174: 125-140.
- Barde-Cabusson, S., 2007. Formation de caldera par fluage d'un système hydrothermal volcanique. PhD Thesis, University Blaise Pascal, Clermont-Ferrand, 203 pp.

- Barde-Cabusson, S. and Merle, O., 2007. From steep-slope volcano to flat caldera floor. *Geophysical Research Letters*, 34: L10305, doi:10.1029/12007GL029784.
- Barker, D.S., 2000. Emplacement of a xenolith-rich sill, Lajitas, Texas. *Journal of Volcanology and Geothermal Research*, 104: 153-168.
- Battaglia, J. and Bachèlery, P., 2003. Dynamic dyke propagation deduced from tilt variations preceding the March 9, 1998, eruption of the Piton de la Fournaise volcano. *Journal of Volcanology and Geothermal Research*, 120: 289-310.
- Battaglia, M., Troise, C., Obrizzo, F., Pinguet, F. and de Natale, G., 2006. Evidence for fluid migration as the source of deformation at Campi Flegrei caldera (Italy). *Geophysical Research Letters*, 33: L01307, doi:10.1029/2005GL024904.
- Bell, F.G., 2000. *Engineering Properties of Soils and Rocks*, Fourth Edition, 4<sup>th</sup> Ed. Blackwell Publishing, Oxford, 482 pp.
- Best, M.G., 2002. *Igneous and Metamorphic Petrology*, 2<sup>nd</sup> Ed. Blackwell Publishing, Oxford, 729 pp.
- Bonaccorso, A., Cianetti, S., Giunchi, C., Trasatti, E., Bonafede, M. and Boschi, E., 2005. Analytical and 3-D numerical modelling of Mt. Etna (Italy) volcano inflation. *Geophysical Journal International*, 163: 852-862.
- Bonforte, A., Guglielmino, F., Palano, M. and Puglisi, G., 2004. A syn-eruptive ground deformation episode measured by GPS, during the 2001 eruption on the upper southern flank of Mt Etna. *Bulletin of Volcanology*, 66: 336-341.
- Bonforte, A. and Puglisi, G., 2003. Magma uprising and flank dynamics on Mount Etna volcano, studied using GPS data (1994-1995). *Journal of Geophysical Research - Solid Earth*, 108: 2153, doi:10.1029/2002JB001845.
- Bonneville, A., VonHerzen, R.P. and Lucazeau, F., 1997. Heat flow over Reunion hot spot track: Additional evidence for thermal rejuvenation of oceanic lithosphere. *Journal of Geophysical Research - Solid Earth*, 102: 721-722,747.
- Borgia, A., 1994. Dynamic Basis of Volcanic Spreading. *Journal of Geophysical Research - Solid Earth*, 99: 17791-17804.
- Bory de Saint-Vincent, J.B.G.M., 1804. *Voyage dans les quatres principales iles des Mers d'Afrique*. XIII, Paris, 434 pp.
- Brenguier, F., Shapiro, N.M., Campillo, M., Nercessian, A. and Ferrazzini, V., 2007. 3-D surface wave tomography of the Piton de la Fournaise volcano using seismic noise correlations. *Geophysical Research Letters*, 34: doi:10.1029/2006GL028586.
- Bret, L., Fèvre, Y., Join, J.L., Robineau, B. and Bachèlery, P., 2003. Deposits related to degradation processes on Piton des Neiges Volcano (Réunion Island): overview and geological hazard. *Journal of Volcanology and Geothermal Research*, 123: 25-41.
- Briole, P., Bachèlery, P., McGuire, B., Moss, J., Ruegg, J.C. and Sabourault, P., 1998. Deformation at Piton de la Fournaise: Evolution of the monitoring techniques and knowledge acquired in the last five



- years. In: R. Casal, M. Fytikas, G. Sigvaldasson and G. Vougioukalakis (Eds), *Volcanic risk - the European laboratory volcanoes*. EUR 18161 EN. European Commission, pp. 467-474.
- Burchardt, S., 2008. New insights into the mechanics of sill emplacement provided by field observations of the Njardvik Sill, Northeast Iceland. *Journal of Volcanology and Geothermal Research*, 173: 280-288.
- Carracedo, J.C., 1994. The Canary-Islands - an Example of Structural Control on the Growth of Large Oceanic-Island Volcanos. *Journal of Volcanology and Geothermal Research*, 60: 225-241.
- Carracedo, J.C., 1999. Growth, structure, instability and collapse of Canarian volcanoes and comparisons with Hawaiian volcanoes. *Journal of Volcanology and Geothermal Research*, 94: 1-19.
- Carracedo, J.C., Day, S.J., Guillou, H. and Gravestock, P., 1999a. Later stages of volcanic evolution of La Palma, Canary Islands: Rift evolution, giant landslides, and the genesis of the Caldera de Taburiente. *Geological Society of America Bulletin*, 111: 755-768.
- Carracedo, J.C., Day, S.J., Guillou, H. and Torrado, F.J.P., 1999b. Giant Quaternary landslides in the evolution of La Palma and El Hierro, Canary Islands. *Journal of Volcanology and Geothermal Research*, 94: 169-190.
- Carter, A., de Vries, B.V., Kelfoun, K., Bachèlery, P. and Briole, P., 2007. Pits, rifts and slumps: the summit structure of Piton de la Fournaise. *Bulletin of Volcanology*, 69: 741-756.
- Catry, T., Villeneuve, N., Michon, L. and Peltier, A., 2008. Mode of summit deformation and collapses at Piton de la Fournaise. *Journal of Volcanology and Geothermal Research*.
- Cayol, V. and Cornet, F.H., 1998a. Effects of topography on the interpretation of the deformation field of prominent volcanoes - Application to Etna. *Geophysical Research Letters*, 25: 1979-1962.
- Cayol, V. and Cornet, F.H., 1998b. Three-dimensional modeling of the 1983-1984 eruption at Piton de la Fournaise Volcano, Réunion Island. *Journal of Geophysical Research - Solid Earth*, 103: 18025-18037.
- Chadwick Jr., W.W., Geist, D.J., Jónsson, S., Poland, M., Johnson, D.J. and Meertens, C.M., 2006. A volcano bursting at the seams: Inflation, faulting, and eruption at Sierra Negra volcano, Galápagos. *Geology*, 34: 1025-1028.
- Chadwick, W.W. and Howard, K.A., 1991. The Pattern of Circumferential and Radial Eruptive Fissures on the Volcanos of Fernandina and Isabela Islands, Galapagos. *Bulletin of Volcanology*, 53: 259-275.
- Charvis, P., Laesanpura, A., Gallart, J., Hirn, A., Lepine, J.C., de Voogd, B., Minshull, T.A., Hello, Y. and Pontoise, B., 1999. Spatial distribution of hotspot material added to the lithosphere under La Réunion, from wide-angle seismic data. *Journal of Geophysical Research - Solid Earth*, 104: 2875-2893.
- Chevallier, L., 1979. Structures et évolution du volcan Piton des Neiges, île de la Réunion: Leurs relations avec les structures du Bassin des Mascareignes, Océan Indien occidental. Ph.D. Thesis, Université de Grenoble, Grenoble.

- Chevallier, L. and Vatin-Perignon, N., 1982. Volcano-structural evolution of Piton des Neiges, Reunion Island, Indian Ocean. *Bulletin of Volcanology*, 45: 285-298.
- Dahm, T., 2000. Numerical simulations of the propagation path and the arrest of fluid-filled fractures in the Earth. *Geophysical Journal International*, 141: 623-638.
- de Michele, M. and Briole, P., 2007. Deformation between 1989 and 1997 at Piton de la Fournaise volcano retrieved from correlation of panchromatic airborne images. *Geophysical Journal International*, 169: 357-364.
- de Voogd, B., Palome, S.P., Hirn, A., Charvis, P., Gallart, J., Rousset, D., Danobeitia, J. and Perroud, H., 1999. Vertical movements and material transport during hotspot activity: Seismic reflection profiling offshore La Réunion. *Journal of Geophysical Research - Solid Earth*, 104: 2855-2874.
- de Zeeuw-van-Dalfsen, E., Pedersen, R., Sigmundsson, F. and Pagli, C., 2004. Satellite radar interferometry 1993–1999 suggests deep accumulation of magma near the crust-mantle boundary at the Krafla volcanic system, Iceland. *Geophysical Research Letters*, 31: doi:10.1029/2004GL020059.
- Delaney, P. and Pollard, D.D., 1981. Deformation of host rocks and flow of magma during growth of minette dikes and breccia-bearing intrusions near Ship Rock, New Mexico. U. S. Geological Survey Professional Paper, 1202: 61 p.
- Delaney, P.T. and Denlinger, R.P., 1999. Stabilization of volcanic flanks by dike intrusion: an example from Kilauea. *Bulletin of Volcanology*, 61: 356-362.
- Delorme, H., Bachèlery, P., Blum, P.A., Cheminée, J.-L., Delarue, J.F., Delmond, J.C., Hirn, A., Lepine, J.C., Vincent, P.M. and Zlotnicki, J., 1989. March 1986 Eruptive Episodes at Piton de la Fournaise Volcano (Réunion Island). *Journal of Volcanology and Geothermal Research*, 36: 199-208.
- Demange, J., Chovelon, P. and Puvilland, P., 1989. Geothermal model of the Salazie-Cirque (Réunion Island): Volcanic and structural Implications. *Journal of Volcanology and Geothermal Research*, 36: 153-176.
- Demant, A., Lestrade, P., Lubala, R.T., Kampunzu, A.B. and Durieux, J., 1994. Volcanological and Petrological Evolution of Nyiragongo Volcano, Virunga Volcanic Field, Zaire. *Bulletin of Volcanology*, 56: 47-61.
- Deniel, C., Kieffer, G. and Lecointre, J., 1992. New  $^{230}\text{Th}$ - $^{238}\text{U}$  and  $^{14}\text{C}$  age determinations from Piton des Neiges Volcano, Réunion - a revised chronology for the differentiated Series. *Journal of Volcanology and Geothermal Research*, 51: 253-267.
- Dieterich, J.H., 1988. Growth and persistence of Hawaiian volcanic rift zones. *Journal of Geophysical Research - Solid Earth*, 93: 4258-4270.
- Duncan, R.A. and Richards, M.A., 1991. Hotspots, mantle plumes, flood basalts, and true polar wander. *Reviews of Geophysics*, 29: 31-50.
- Dvorak, J.J. and Okamura, A.T., 1985. Variations in Tilt Rate and Harmonic Tremor Amplitude During the January August 1983 East Rift Eruptions of Kilauea Volcano, Hawaii. *Journal of Volcanology and Geothermal Research*, 25: 249-258.

- Dyment, J., 1991. Structure et évolution de la lithosphère océanique dans l'océan Indien: Apport des anomalies magnétiques. Ph.D Thesis, University of Strasbourg, Strasbourg, 374 pp.
- Dyment, J., 1998. Evolution of the Carlsberg Ridge between 60 and 45 Ma: Ridge propagation, spreading asymmetry, and the Deccan-Reunion hotspot. *Journal of Geophysical Research - Solid Earth*, 103: 24,067-024,084.
- Dzurisin, D., Lisowski, M., Wicks, C.W., Poland, M.P. and Endo, E.T., 2006. Geodetic observations and modeling of magmatic inflation at the Three Sisters volcanic center, central Oregon Cascade Range, USA. *Journal of Volcanology and Geothermal Research*, 150: 35-54.
- Elsworth, D. and Day, S.J., 1999. Flank collapse triggered by intrusion: the Canarian and Cape Verde Archipelagoes. *Journal of Volcanology and Geothermal Research*, 94: 323-340.
- Elsworth, D. and Voight, B., 1995. Dike Intrusion as a Trigger for Large Earthquakes and the Failure of Volcano Flanks. *Journal of Geophysical Research - Solid Earth*, 100: 6005-6024.
- Fernández, C., de la Nuez, J., Casillas, R. and Garcia Navarro, E., 2002. Stress fields associated with the growth of a large shield volcano (La Palma, Canary Islands). *Tectonics*, 21: 1031, 1010.1029/2000TC900038.
- Francis, P., 1993. *Volcanoes: A planetary perspective*. Clarendon Press, Oxford, 456 pp.
- Froger, J.-L., Fukushima, Y., Briole, P., Staudacher, T., Souriot, T. and Villeneuve, N., 2004. The deformation field of the August 2003 eruption at Piton de la Fournaise, Réunion Island, mapped by ASAR interferometry. *Geophysical Research Letters*, 31: doi:10.1029/2004GL020479.
- Froger, J.-L., Merle, O. and Briole, P., 2001. Active spreading and regional extension at Mount Etna imaged by SAR interferometry. *Earth and Planetary Science Letters*, 187: 245-258.
- Froger, J.-L., Remy, D., Bonvalot, S. and Legrand, D., 2007. Two scales of inflation at Lastarria-Cordon del Azufre volcanic complex, central Andes, revealed from ASAR-ENVISAT interferometric data. *Earth and Planetary Science Letters*, 255: 148-163.
- Fukushima, Y., 2005. Transferts de magma au volcan du Piton de la Fournaise déterminés par la modélisation 3D de données d'interférométrie radar entre 1998 et 2000. Ph.D. Thesis, Université Blaise Pascal, Clermont-Ferrand, 182 pp.
- Fukushima, Y., Cayol, V. and Durand, P., 2005. Finding realistic dike models from interferometric synthetic aperture radar data: The February 2000 eruption at Piton de la Fournaise. *Journal of Geophysical Research - Solid Earth*, 110: B03206, doi:03210.01029/02004JB003268.
- Gallart, J., Driad, L., Charvis, P., Sapin, M., Hirn, A., Diaz, J., de Voogd, B. and Sachpazi, M., 1999. Perturbation to the lithosphere along the hotspot track of La Réunion from an offshore-onshore seismic transect. *Journal of Geophysical Research - Solid Earth*, 104: 2895-2908.
- Gautneb, H. and Gudmundsson, A., 1992. Effect of Local and Regional Stress-Fields on Sheet Emplacement in West Iceland. *Journal of Volcanology and Geothermal Research*, 51: 339-356.

- Gillot, P.Y., Lefevre, J.C. and Nativel, P.E., 1994. Model for the structural evolution of the volcanoes of Réunion Island. *Earth and Planetary Science Letters*, 122: 291-302.
- Gillot, P.Y. and Nativel, P., 1982. K-Ar chronology of the ultimate activity of Piton des Neiges Volcano, Réunion Island, Indian Ocean. *Journal of Volcanology and Geothermal Research*, 13: 131-146.
- Gillot, P.Y. and Nativel, P., 1989. Eruptive history of the Piton de la Fournaise Volcano, Réunion Island, Indian Ocean. *Journal of Volcanology and Geothermal Research*, 36: 53-65.
- Glass, J.B., Fornari, D.J., Hall, H.F., Cogan, A.A., Berkenbosch, H.A., Holmes, M.L., White, S.M. and De la Torre, G., 2007. Submarine volcanic morphology of the western Galapagos based on EM300 bathymetry and MR1 side-scan sonar. *Geochemistry Geophysics Geosystems*, 8: Q03010, doi:03010.01029/02006GC001464.
- Goult, N.R., 2005. Emplacement mechanism of the Great Whin and Midland Valley dolerite sills. *Journal of Geological Society, London*, 162: 1047-1056.
- Griffith, A.A., 1920. The phenomena of flow and rupture in solids. *Philosophical Transactions of the Royal Society of London. Series A. Physical Sciences and Engineering*, 221: 163-198.
- Griffith, A.A., 1924. Theory of rupture. In: C.B. Biezano and J.M. Burgers (Eds), 1<sup>st</sup> Int. Cong. Appl. Mech. J. Waltman Jr, Delft, pp. 53-63.
- Gudmundsson, A., 1992. Formation and growth of normal faults at the divergent plate boundary in Iceland. *Terra Nova*, 4: 464-471.
- Gudmundsson, A., 2002. Emplacement and arrest of sheets and dykes in central volcanoes. *Journal of Volcanology and Geothermal Research*, 116: 279-298.
- Gudmundsson, A., 2003. Surface stresses associated with arrested dykes in rift zones. *Bulletin of Volcanology*, 65: 606-619.
- Gudmundsson, A., 2006. How local stresses control magma-chamber ruptures, dykes injections, and eruptions in composite volcanoes. *Earth Science Reviews*, 79: 1-31.
- Hirn, A., Lepine, J.C., Sapin, M. and Delorme, H., 1991. Episodes of Pit-Crater Collapse Documented by Seismology at Piton de la Fournaise. *Journal of Volcanology and Geothermal Research*, 47: 89-104.
- Holmes, A., 1965. *Principle of physical geology*, 2<sup>nd</sup> ed. Ronald Press, New York, 1303 pp.
- Houlié, N., Briole, P., Bonforte, A. and Puglisi, G., 2006. Large scale ground deformation of Etna observed by GPS between 1994 and 2001. *Geophysical Research Letters*, 33: doi:10.1029/2005GL024414.
- Huertas, M.J., Arnaud, N.O., Ancochea, E., Cantagrel, J.M. and Fuster, J.M., 2002. Ar-40/Ar-39 stratigraphy of pyroclastic units from the Canadas Volcanic Edifice (Tenerife, Canary Islands) and their bearing on the structural evolution. *Journal of Volcanology and Geothermal Research*, 115: 351-365.

- Hurwitz, S., Christiansen, L.B. and Hsieh, P.A., 2007. Hydrothermal fluid flow and deformation in large calderas: Inferences from numerical simulations. *Journal of Geophysical Research - Solid Earth*, 112: B02206, doi:02210.01029/02006JB004689.
- Irwin, G.R., 1958. Fracture. In: S. Flügge (Ed), *Handbuch der Physik*. Vol. 6. Springer-Verlag, Berlin, pp. 551-590.
- Jaeger, J.C., Cook, N.G.W. and Zimmerman, R., 2007. *Fundamentals of Rock Mechanics*, Fourth Edition. Blackwell Publishing Ltd., 475 pp.
- Jarvis, A., Reuter, H.I., Nelson, A. and Guevara, E., 2006. Hole-filled seamless SRTM data V3, International Centre for Tropical Agriculture (CIAT), available from <http://srtm.csi.cgiar.org>.
- Johnson, A.M. and Pollard, D.D., 1973. Mechanics of growth of some laccolithic intrusions in the Henry Mountains, Utah, I: Field observations, Gilbert's model, physical properties and flow of the magma. *Tectonophysics*, 18: 261-309.
- Kanninen, M.F. and Popelar, C.H., 1986. *Advanced Fracture Mechanics*. Oxford University Press, Oxford, 584 pp.
- Kavanagh, J.L., Menand, T. and Sparks, R.S.J., 2006. An experimental investigation of sill formation and propagation in layered elastic media. *Earth and Planetary Science Letters*, 245: 799-813.
- Klausen, M.B., 2004. Geometry and mode of emplacement of the Thverartindur cone sheet swarm, SE Iceland. *Journal of Volcanology and Geothermal Research*, 138: 185-204.
- Klausen, M.B., 2006. Geometry and mode of emplacement of dike swarms around the Birnudalstindur igneous centre, SE Iceland. *Journal of Volcanology and Geothermal Research*, 151: 340-356.
- Klugel, A., Hansteen, T.H. and Galipp, K., 2005. Magma storage and underplating beneath Cumbre Vieja Volcano, La Palma (Canary Islands). *Earth and Planetary Science Letters*, 236: 211-226.
- Labazuy, P., 1996. Recurrent landslides events on the submarine flank of Piton de la Fournaise volcano (Réunion Island). In: W.J. McGuire, A.P. Jones and J. Neuberg (Eds), *Volcano Instability on the Earth and other Planets*. Geological Society Special Publication 110, pp. 293-305.
- Lawn, B.R. and Wilshaw, T.R., 1975. *Fracture of Brittle solids*, 1<sup>st</sup> Ed. Cambridge University Press, Cambridge and New York, 213 pp.
- Lénat, J.-F. and Bachèlery, P., 1990. Structure et fonctionnement de la zone centrale du Piton de La Fournaise. In: J.-F. Lénat (Ed), *Le volcanisme de la Réunion*. CRV, Clermont-Ferrand, pp. 257-296.
- Lénat, J.-F., Bachèlery, P., Bonneville, A. and Hirn, A., 1989a. The Beginning of the 1985-1987 Eruptive Cycle at Piton de la Fournaise (La Réunion) - New Insights in the Magmatic and Volcano-Tectonic Systems. *Journal of Volcanology and Geothermal Research*, 36: 209-232.
- Lénat, J.-F., Fitterman, D., Jackson, D.B. and Labazuy, P., 2000. Geoelectrical structure of the central zone of Piton de la Fournaise volcano (Reunion). *Bulletin of Volcanology*, 62: 75-89.

- Lénat, J.-F., Gibert-Malengreau, B. and Galdeano, A., 2001. A new model for the evolution of the volcanic island of Reunion (Indian Ocean). *Journal of Geophysical Research - Solid Earth*, 106: 8649-8663.
- Lénat, J.-F., Vincent, P. and Bachèlery, P., 1989b. The Off-Shore Continuation of an Active Basaltic Volcano - Piton de la Fournaise (Réunion Island, Indian Ocean) - Structural and Geomorphological Interpretation from Sea Beam Mapping. *Journal of Volcanology and Geothermal Research*, 36: 1-36.
- Letourneur, L., Peltier, A., Staudacher, T. and Gudmundsson, A., 2008. The effects of rock heterogeneities on dyke paths and asymmetric ground deformation; the example of Piton de la Fournaise (Réunion Island). *Journal of Volcanology and Geothermal Research*, 173: 289-302.
- Lipman, P.W. and Coombs, M.L., 2006. North Kona slump: Submarine flank failure during the early(?) tholeiitic shield stage of Hualalai Volcano. *Journal of Volcanology and Geothermal Research*, 151: 189-216.
- Lister, J.R. and Kerr, R.C., 1991. Fluid-mechanical models of crack propagation and their application to magma transport in dykes. *Journal of Geophysical Research - Solid Earth*, 96: 10049-10077.
- Logan, D., 2002. *A First Course in the Finite Element Method*. Brooks/Cole, Pacific Grove, USA, 720 pp.
- Longpre, M.A., Staudacher, T. and Stix, J., 2007. The November 2002 eruption at Piton de la Fournaise volcano, La Réunion Island: ground deformation, seismicity, and pit crater collapse. *Bulletin of Volcanology*, 69: 511-525.
- Louvat, P. and Allègre, C.J., 1997. Present denudation rates on the island of Réunion determined by river geochemistry: Basalt weathering and mass budget between chemical and mechanical erosions. *Geochimica et Cosmochimica Acta*, 61: 3645-3669.
- Lu, Z., Wicks, C., Dzurisin, D., Power, J.A., Moran, S.C. and Thatcher, W., 2002. Magmatic inflation at a dormant stratovolcano: 1996-1998 activity at Mount Peulik volcano, Alaska, revealed by satellite radar interferometry. *Journal of Geophysical Research - Solid Earth*, 107: 2134.
- Lundgren, P., Berardino, P., Coltelli, M., Fornaro, G., Lanari, R., Puglisi, G., Sansosti, E. and Tesauro, M., 2003. Coupled magma chamber inflation and sector collapse slip observed with synthetic aperture radar interferometry on Mt. Etna volcano. *Journal of Geophysical Research - Solid Earth*, 108: 2247, doi:2210.1029/2001JB000657.
- Lundgren, P., Casu, F., Manzo, M., Pepe, A., Berardino, P., Sansosti, E. and Lanari, R., 2004. Gravity and magma induced spreading of Mount Etna volcano revealed by satellite radar interferometry. *Geophysical Research Letters*, 31: doi:10.1029/2003GL018736.
- Mahoney, J.J., Duncan, R.A., Khan, W., Gnos, E. and McCormick, G.R., 2002. Cretaceous volcanic rocks of the South Tethyan suture zone, Pakistan: implications for the Reunion hotspot and Deccan Traps. *Earth and Planetary Science Letters*, 203: 295-310.
- Maillot, E., 1999. *Les systèmes intrusifs des volcans boucliers océaniques: Ile de la Réunion (Océan Indien)*. Approche structurale et expérimentale. PhD Thesis, Université de la Réunion, Saint-Denis.

- Malengreau, B., Lénat, J.-F. and Froger, J.-L., 1999. Structure of Réunion Island (Indian Ocean) inferred from the interpretation of gravity anomalies. *Journal of Volcanology and Geothermal Research*, 88: 131-146.
- Marinoni, L.B., 2001. Crustal extension from exposed sheet intrusions: review and method proposal. *Journal of Volcanology and Geothermal Research*, 107: 27-46.
- Marinoni, L.B. and Gudmundsson, A., 2000. Dykes, faults and palaeostresses in the Teno and Anaga massifs of Tenerife (Canary Islands). *Journal of Volcanology and Geothermal Research*, 103: 83-103.
- Mattia, M., Rossi, M., Guglielmino, F., Aloisi, M. and Bock, Y., 2004. The shallow plumbing system of Stromboli Island as imaged from 1 Hz instantaneous GPS positions. *Geophysical Research Letters*, 31: doi:10.1029/2004GL021281.
- McDonald, G., 1972. *Volcanoes*. Prentice-Hall inc., Englewood Cliffs, New Jersey, 510 pp.
- McDougall, I., 1971. The geochronology and evolution of the young volcanic island of Réunion, Indian Ocean. *Geochimica et Cosmochimica Acta*, 35: 261-288.
- McGuire, W.J., Pullen, A.D. and Saunders, S.J., 1990. Recent dyke-induced large-scale block movement at Mount Etna and potential slope failure. *Nature*, 343: 357-359.
- Merle, O. and Borgia, A., 1996. Scaled experiments of volcanic spreading. *Journal of Geophysical Research - Solid Earth*, 101: 13805-13817.
- Merle, O. and Lénat, J.-F., 2003. Hybrid collapse mechanism at Piton de la Fournaise volcano, Réunion Island, Indian Ocean. *Journal of Geophysical Research - Solid Earth*, 108: 2166, doi:10.1029/2002JB002014.
- Michel, S. and Zlotnicki, J., 1998. Self-potential and magnetic surveying of La Fournaise volcano (Réunion Island): Correlations with faulting, fluid circulation, and eruption. *Journal of Geophysical Research - Solid Earth*, 103: 17845-17857.
- Michon, L., Letourneur, L., Peltier, A., Villeneuve, N. and Staudacher, T., in press. Morphology, structure and deformation of the steep central cone of Piton de la Fournaise shield volcano (Réunion Island, Indian Ocean). *Journal of Volcanology and Geothermal Research*.
- Michon, L. and Saint-Ange, F., 2008. Morphology of Piton de la Fournaise basaltic shield volcano (La Réunion Island): Characterization and implication in the volcano evolution. *Journal of Geophysical Research-Solid Earth - Solid Earth*, 113: B03203.
- Michon, L., Saint-Ange, F., Bachèlery, P., Villeneuve, N. and Staudacher, T., 2007a. Role of the structural inheritance of the oceanic lithosphere in the magmato-tectonic evolution of Piton de la Fournaise volcano (La Réunion Island). *Journal of Geophysical Research - Solid Earth*, 112: B04205, doi:10.1029/2006JB004598.
- Michon, L., Staudacher, T., Ferrazzini, V., Bachèlery, P. and Marti, J., 2007b. April 2007 collapse of Piton de la Fournaise: A new example of caldera formation. *Geophysical Research Letters*, 34: doi:10.1029/2007GL031248.

- Mogi, K., 1958. Relations between the eruptions of various volcanoes and the deformation of the ground surfaces around them. *Bulletin of the Earthquake Research Institute, University of Tokyo*, 36: 99-134.
- Moore, J.G., Clague, D.A., Holcomb, R.T., Lipman, P.W., Normark, W.R. and Torresan, M.E., 1989. Prodigious submarine landslides on the Hawaiian Ridge. *Journal of Geophysical Research - Solid Earth*, 94: 17465-17484.
- Moore, J.G., Normark, W.R. and Holcomb, R.T., 1994. Giant hawaiian landslides. *Annual Review of Earth Planetary Science*, 22: 119-144.
- Mudge, M.R., 1968. Depth Control of Some Concordant Intrusions. *Geological Society of America Bulletin*, 79: 315-332.
- Murray, J.B., Guest, J.E. and Butterworth, P.S., 1977. Large ground deformation on Mount Etna volcano. *Nature*, 266: 338-340.
- Naumann, T. and Geist, D., 2000. Physical volcanology and structural development of Cerro Azul Volcano, Isabela Island, Galapagos: implications for the development of Galapagos-type shield volcanoes. *Bulletin of Volcanology*, 61: 497-514.
- Nehlig, P., Quinquis, J.-P., Bucelle, M. and Odon, O., 2006. Carte Géologique de la Réunion. BRGM.
- Nercessian, A., Hirn, A., Lepine, J.C. and Sapin, M., 1996. Internal structure of Piton de la Fournaise volcano from seismic wave propagation and earthquake distribution. *Journal of Volcanology and Geothermal Research*, 70: 123-143.
- Neri, M., Acocella, V., Behncke, B., Maiolino, V., Ursino, A. and Velardita, R., 2005. Contrasting triggering mechanisms of the 2001 and 2002-2003 eruptions of Mount Etna (Italy). *Journal of Volcanology and Geothermal Research*, 144: 235-255.
- Nunes, J.C., Camacho, A., Franca, Z., Montesinos, F.G., Alves, M., Vieira, R., Velez, E. and Ortiz, E., 2006. Gravity anomalies and crustal signature of volcano-tectonic structures of Pico Island (Azores). *Journal of Volcanology and Geothermal Research*, 156: 55-70.
- O'Neill, C., Muller, D. and Steinberger, B., 2003. Geodynamic implications of moving Indian Ocean hotspots. *Earth and Planetary Science Letters*, 215: 151-168.
- Oehler, J.-F., 2005. Les déstabilisations de flanc des volcans de l'île de La Réunion (Océan Indien): Mise en évidence, implications et origines. PhD Thesis, Université Blaise Pascal, Clermont-Ferrand, 478 pp.
- Oehler, J.F., de Vries, B.V. and Labazuy, P., 2005. Landslides and spreading of oceanic hot-spot and arc shield volcanoes on Low Strength Layers (LSLs): an analogue modeling approach. *Journal of Volcanology and Geothermal Research*, 144: 169-189.
- Oehler, J.F., Labazuy, P. and Lénat, J.-F., 2004. Recurrence of major flank landslides during the last 2-Ma-history of Réunion Island. *Bulletin of Volcanology*, 66: 585-598.



- Oehler, J.F., Lénat, J.F. and Labazuy, P., 2008. Growth and collapse of the Reunion Island volcanoes. *Bulletin of Volcanology*, 70: 717-742.
- Okada, Y., 1985. Surface deformation due to shear and tensile faults in a half-space. *Bulletin of the Seismological Society of America*, 75: 1135-1154.
- Okubo, C.H., 2004. Rock mass strength and slope stability of the Hilina slump, Kilauea volcano, Hawai'i. *Journal of Volcanology and Geothermal Research*, 138: 43-76.
- Owen, S., Segall, P., Lisowski, M., Miklius, A., Denlinger, R. and Sako, M., 2000. Rapid deformation of Kilauea Volcano: Global positioning system measurements between 1990 and 1996. *Journal of Geophysical Research - Solid Earth*, 105: 18983-18998.
- Pagli, C., Sigmundsson, F., Arnadóttir, T., Einarsson, P. and Sturkell, E., 2006. Deflation of the Askja volcanic system: Constraints on the deformation source from combined inversion of satellite radar interferograms and GPS measurements. *Journal of Volcanology and Geothermal Research*, 152: 97-108.
- Pagli, C., Sigmundsson, F., Pedersen, R., Einarsson, P., Arnadóttir, T. and Feigl, K.L., 2007. Crustal deformation associated with the 1996 Gjalp subglacial eruption, Iceland: InSAR studies in affected areas adjacent to the Vatnajökull ice cap. *Earth and Planetary Science Letters*, 259: 24-33.
- Peltier, A., 2007. Suivi, modélisation et évolution des processus d'injections magmatiques au Piton de La Fournaise (Réunion) à partir d'une analyse croisée des données de déformation, géochimiques et structurales. Ph.D. Thesis, Université de la Réunion, Saint-Denis, 347 pp.
- Peltier, A., Bachèlery, P., Semet, M. and Staudacher, T., 2006a. Geophysical and geochemical evidences of three levels of dyke initiation in the shallower reservoir of Piton de La Fournaise volcano, American Geophysical Union Fall Meeting, San Francisco.
- Peltier, A., Ferrazzini, V., Staudacher, T. and Bachèlery, P., 2005. Imaging the dynamics of dyke propagation prior to the 2000–2003 flank eruptions at Piton de La Fournaise, Réunion Island. *Geophysical Research Letters*, 32: doi:10.1029/2005GL023720.
- Peltier, A., Staudacher, T. and Bachèlery, P., 2007. Constraints on magma transfers and structures involved in the 2003 activity at Piton de La Fournaise from displacement data. *Journal of Geophysical Research - Solid Earth*, 112: B03207, doi:03210.01029/02006JB004379.
- Peltier, A., Staudacher, T., Catherine, P., Ricard, L.-P., Kowalski, P. and Bachèlery, P., 2006b. Subtle precursors of volcanic eruptions at Piton de la Fournaise detected by extensometers. *Geophysical Research Letters*, 33: doi:10.1029/2005GL025495.
- Peterson, D.W. and Moore, R.B., 1987. Geologic history and evolution of geologic concepts, Island of Hawaii. U. S. Geological Survey Professional Paper, 1350: 149-189.
- Pinel, V. and Jaupart, C., 2000. The effect of edifice load on magma ascent beneath a volcano. *Philosophical Transactions of the Royal Society of London. Series A. Physical Sciences and Engineering*, 358: 1515-1532.

- Pinel, V. and Jaupart, C., 2004. Magma storage and horizontal dyke injection beneath a volcanic edifice. *Earth and Planetary Science Letters*, 221: 245-262.
- Pollard, D.D., Delaney, P.T., Duffield, W.A., Endo, E.T. and Okamura, A.T., 1983. Surface deformation in volcanic rift zones. *Tectonophysics*, 94: 541-584.
- Pollard, D.D. and Fletcher, R.C., 2005. *Fundamentals of Structural Geology*. University Press, Cambridge, 510 pp.
- Pollard, D.D. and Johnson, A.M., 1973. Mechanics of growth of some laccolithic intrusions in the Henry Mountains, Utah, II: Bending and failure of overburden layers and sill formation. *Tectonophysics*, 18: 311-354.
- Porter, S.C., 1972. Distribution, morphology and size frequency of cinder cones on Mauna Kea volcano, Hawaii. *Geological Society of America Bulletin*, 83: 3607-3612.
- Rançon, J.P., Lerebour, P. and Augé, T., 1989. The Grand Brûlé Exploration Drilling - New Data on the Deep Framework of the Piton de la Fournaise Volcano .1. Lithostratigraphic Units and Volcanostructural Implications. *Journal of Volcanology and Geothermal Research*, 36: 113-127.
- Rivalta, E., Bottinger, M. and Dahm, T., 2005. Buoyancy-driven fracture ascent: Experiments in layered gelatine. *Journal of Volcanology and Geothermal Research*, 144: 273-285.
- Rodriguez-Losada, J.A. and Martinez-Frias, J., 2004. The felsic complex of the Vallehermoso Caldera: interior of an ancient volcanic system (La Gomera, Canary Islands). *Journal of Volcanology and Geothermal Research*, 137: 261-284.
- Rousset, D., Lesquer, A., Bonneville, A. and Lénat, J.-F., 1989. Complete Gravity Study of Piton de la Fournaise Volcano, Réunion Island. *Journal of Volcanology and Geothermal Research*, 36: 37-52.
- Rowland, S.K. and Garbeil, H., 2000. Slopes of Oceanic Basalt Volcanoes. In: P.J. Mouginiis-Mark, J.A. Crisp and J.H. Fink (Eds), *Remote sensing of active volcanism*. Geophysical Monograph, Vol. 116. 116, pp. 223-246.
- Rubin, A.M., 1990. A Comparison of Rift-Zone Tectonics in Iceland and Hawaii. *Bulletin of Volcanology*, 52: 302-319.
- Rubin, A.M., 1995. Propagation of magma-filled cracks. *Annual Review of Earth Planetary Science*, 23: 287-336.
- Rubin, A.M. and Pollard, D.D., 1987. Origins of blade-like dikes in volcanic rift zones. *U. S. Geological Survey Professional Paper*, 1350: 1449-1470.
- Ryan, M.P., 1987. Neutral buoyancy and the mechanical evolution of magmatic systems. In: B.O. Mysen (Ed), *Magmatic Processes: Physicochemical Principles*. Geochemical Society, Special Publication No. 1, pp. 259-287.
- Ryan, M.P., Blevins, J.Y.K., Okamura, A.T. and Koyanagi, R.Y., 1983. Magma reservoir subsidence mechanics: Theoretical summary and application to Kilauea Volcano, Hawaii. *Journal of Geophysical Research - Solid Earth*, 88: 4147-4181.

- Sapin, M., Hirn, A., Lepine, J.C. and Necessian, A., 1996. Stress, failure and fluid flow deduced from earthquakes accompanying eruptions at Piton de la Fournaise volcano. *Journal of Volcanology and Geothermal Research*, 70: 145-167.
- Schwarz, S., Klugel, A., van den Bogaard, P. and Geldmacher, J., 2005. Internal structure and evolution of a volcanic rift system in the eastern North Atlantic: the Desertas rift zone, Madeira archipelago. *Journal of Volcanology and Geothermal Research*, 141: 123-155.
- Sigmundsson, F., Durand, P. and Massonnet, D., 1999. Opening of an eruptive fissure and seaward displacement at Piton de la Fournaise volcano measured by RADARSAT satellite radar interferometry. *Geophysical Research Letters*, 26: 533-536.
- Smith, J.R., Malahoff, A. and Shor, A.N., 1999. Submarine geology of the Hilina slump and morpho-structural evolution of Kilauea volcano, Hawaii. *Journal of Volcanology and Geothermal Research*, 94: 59-88.
- Smith, W.H.F. and Sandwell, D.T., 1997. Global seafloor topography from satellite altimetry and ship depth soundings. *Science*, 277: 1957-1962.
- Staudigel, H., Feraud, G. and Giannerini, G., 1986. The history of intrusive activity on the Island of La Palma (Canary Islands). *Journal of Volcanology and Geothermal Research*, 27: 299-322.
- Sturkell, E., Sigmundsson, F. and Slunga, R., 2006. 1983-2003 decaying rate of deflation at Askja caldera: Pressure decrease in an extensive magma plumbing system at a spreading plate boundary. *Bulletin of Volcanology*, 68: 727-735.
- Tinard, P., Froger, J.-L., Cayol, V., Fukushima, Y., Souriot, T., Staudacher, T. and Briole, P., 2008. Continuous InSAR monitoring of Piton de la Fournaise volcano (La Reunion Island): four years of magmatic transfers revealed. *Journal of Volcanology and Geothermal Research*.
- Tryggvason, E., 1994. Observed Ground Deformation at Hekla, Iceland Prior to and During the Eruptions of 1970, 1980-1981 and 1991. *Journal of Volcanology and Geothermal Research*, 61: 281-291.
- Upton, B.G.J. and Wadsworth, W.J., 1965. Geology of Réunion Island, Indian Ocean. *Nature*, 207: 151-154.
- Upton, B.G.J. and Wadsworth, W.J., 1972. Peridotitic and gabbroic rocks associated with the shield-forming lavas of Réunion. *Contribution to Mineralogy and Petrology*, 35: 139-158.
- Urai, M., Geshi, N. and Staudacher, T., 2007. Size and volume evaluation of the caldera collapse on Piton de la Fournaise volcano during the April 2007 eruption using ASTER stereo imagery. *Geophysical Research Letters*, 34: doi:10.1029/2007GL031551.
- Valko, P. and Economides, M.J., 1995. *Hydraulic fracture Mechanics*. Wiley, 318 pp.

- Vlastélic, I., Staudacher, T. and Semet, M., 2005. Rapid change of lava composition from 1998 to 2002 at Piton de la Fournaise (Réunion) inferred from Pb isotopes and trace elements: Evidence for variable crustal contamination. *Journal of Petrology*, 46: 79-107.
- Walker, G.P.L., 1987. The dike complex of Koolau volcano, Oahu: internal structure of a hawaiian rift zone. U. S. Geological Survey Professional Paper, 1350: 961-994.
- Walker, G.P.L., 1992. Coherent Intrusion Complexes in Large Basaltic Volcanos - a New Structural Model. *Journal of Volcanology and Geothermal Research*, 50: 41-54.
- Walker, G.P.L., 1999. Volcanic rift zones and their intrusion swarms. *Journal of Volcanology and Geothermal Research*, 94: 21-34.
- Walker, G.P.L. and Eyre, P.R., 1995. Dike complexes in American Samoa. *Journal of Volcanology and Geothermal Research*, 69: 241-254.
- Walter, T.R., 2003. Buttressing and fractional spreading of Tenerife, an experimental approach on the formation of rift zones. *Geophysical Research Letters*, 30: 1296, doi:1210.1029/2002GL016610.
- Walter, T.R. and Amelung, F., 2006. Volcano-earthquake interaction at Mauna Loa Volcano, Hawaii. *Journal of Geophysical Research - Solid Earth*, 111: B05204, doi:05210.01029/02005JB003861.
- Walter, T.R., Klügel, A. and Münn, S., 2006. Gravitational spreading and formation of new rift zones on overlapping volcanoes. *Terra Nova*, 18: 26-33.
- Walter, T.R. and Schmincke, H.U., 2002. Rifting, recurrent landsliding and Miocene structural reorganization on NW-Tenerife (Canary Islands). *International Journal of Earth Sciences*, 91: 615-628.
- Walter, T.R., Troll, V.R., Cailleau, B., Belousov, A., Schmincke, H.U., Amelung, F. and Von der Bogaard, P., 2005. Rift zone reorganization through flank instability in ocean island volcanoes: an example from Tenerife, Canary Islands. *Bulletin of Volcanology*, 67: 281-291.
- Watson, S. and McKenzie, D., 1991. Melt generation by plumes: A study of Hawaiian volcanism. *Journal of Petrology*, 32: 763-783.
- Wolfe, C.J., McNutt, M.K. and Detrick, R.S., 1994. The Marquesas Archipelagic Apron - Seismic Stratigraphy and Implications for Volcano Growth, Mass-Wasting, and Crustal Underplating. *Journal of Geophysical Research - Solid Earth*, 99: 13591-13608.
- Wood, C.A., 1980. Morphometric Evolution of Cinder Cones. *Journal of Volcanology and Geothermal Research*, 7: 387-413.
- Zlotnicki, J., Ruegg, J.C., Bachèlery, P. and Blum, P.A., 1990. Eruptive Mechanism on Piton de la Fournaise Volcano Associated with the December 4, 1983, and January 18, 1984 Eruptions from Ground Deformation Monitoring and Photogrammetric Surveys. *Journal of Volcanology and Geothermal Research*, 40: 197-217.

**Name:** Ludovic Letourneur  
**Geburtstag:** 28. Dezember 1982  
**Geburtsort:** Annecy (Haute-Savoie), Frankreich  
**Staatsangehörigkeit:** Französisch

### **Ausbildung und Berufstätigkeit**

10/2005-07/2008 Wissenschaftlicher Mitarbeiter am Geowissenschaftlichen Zentrum der Georg-August-Universität Göttingen (GZG).

09/2004-06/2005 Master in “Magmatischen und metamorphen Prozessen - Vulkanologie” an der Blaise Pascal Universität, Clermont-Ferrand, Frankreich / Thema der Masterarbeit: “*Study of the volcano-tectonic relationship in the dynamics of Piton de la Fournaise volcano, Réunion Island*”.

09/2003-06/2004 Maîtrise Geowissenschaften an der Blaise Pascal Universität, Clermont-Ferrand, Frankreich / Thema der Maîtrisearbeit: “*Self-potential study of Yasur volcano and its relation with the Yenkahe horst (Vanuatu)*”.

09/2002-06/2003 License (*äquivalent Bachelor*) Geowissenschaften an der Blaise Pascal Universität, Clermont-Ferrand, Frankreich

09/2000-06/2002 DEUG (*äquivalent Vordiplom*) Geowissenschaften an der Université de Savoie, Chambéry, Frankreich

07/2000 Baccalaureat (Allgemeine Hochschulreife), Annecy, Frankreich

### **Rezensierte Artikel und Buchkapitel:**

Letourneur, L., Peltier, A., Staudacher, T. und Gudmundsson, A., 2008. The effects of rock heterogeneities on dyke paths and asymmetric ground deformation: The example of Piton de la Fournaise (Réunion Island), *Journal of Volcanology and Geothermal Research* (2008), doi:10.1016/j.jvolgeores.2008.01.018

Gudmundsson, A., Friese, N., Andrew, R., Philipp, S.L., Ertl, G. und Letourneur, L. (2008): Effects of dyke emplacement and plate pull on mechanical interaction between volcanic systems and central Volcanoes in Iceland. In: Hoskuldsson, A., Sparks, R. S. J. & Thordarson, T (Hrsg.): *Volcanic Processes: The Legacy of G.P.L. Walker* (the “Walker Volume”). Geological Society London, Special Publications (im Druck).

Michon, L., Letourneur, L., Peltier, A., Villeneuve, N. und Staudacher, T., 2008. Morphology, structure and deformation of the steep central cone of Piton de la Fournaise shield volcano (Réunion Island, Indian Ocean). Zur Publikation angenommen für einen Sonderband zum Vulkan Piton de la Fournaise, *Journal of Volcanology and Geothermal Research*.

### **Kurzfassungen und Beiträge :**

Andrew, R. E. B., Gudmundsson, A. und Letourneur, L., 2008. *Kurzfassung und Poster*. Mechanical interaction between the fissure and graben of the 1783 Sakftareldar Eruption and the hyaloclastite Laki mountain. EGU General Assembly, Wien, Österreich, 14.-18. April 2008. Geophysical Research Abstracts, 10, EGU2008-A-10304.

Gudmundsson, A., Andrew, R. E. B. und Letourneur, L. 2007. *Kurzfassung und Vortrag*. Tectonics of the 1783 Laki crater row and the associated graben, South Iceland. *Eos Trans. AGU*, 88(52), Fall Meet. Suppl., Abstract V52B-05

Letourneur, L. und Gudmundsson, A. 2006. *Kurzfassung und Poster*. A double magma chamber explains the high eruption frequency at Piton de la Fournaise Volcano (Réunion Island). George Walker Memorial Meeting, Reykholt, Iceland. 12 - 17 June, 2006.

Letourneur, L. und Gudmundsson, A. 2006. *Kurzfassung und Poster*. Asymmetrical deformation of the summit cone of Piton de la Fournaise (Reunion Island). EGU General Assembly, Wien, Österreich, 02 - 07 April 2006. Geophysical Research Abstracts, 8, EGU06-J-02703.

Letourneur, L. und Gudmundsson, A. 2006. *Kurzfassung und Poster*. Asymmetrical deformation of the Piton de la Fournaise (Réunion Island) summit cone. In: Philipp, S.L., Leiss, B., Vollbrecht, A., Tanner, D. & Gudmundsson, A. (eds): 11. Symposium 'Tektonik, Struktur- und Kristallingeologie', Zusammenfassungen der Tagungsbeiträge, Göttingen 22.-24.03., 130-132.